



# 2nd G-EVER International Symposium and the 1st IUGS & SCJ International Workshop on Natural Hazards

Hazard and Risk Management in Asia-Pacific Region: Earthquake,  
Tsunami, Volcanic Eruption and Landslide in Subduction Zones

## Abstracts Volume

Oct. 19-20, 2013

Sendai City Information & Industrial Plaza, Sendai, Tohoku, Japan

### Organizers:

G-EVER Consortium

Geological Survey of Japan, National Institute of Advanced Industrial Science and  
Technology (AIST)

The International Union of Geological Sciences (IUGS)

Science Council of Japan (SCJ)

### Co-Organizers:

The Geological Society of Japan

Coordinating Committee for Geoscience Programmes in East and Southeast Asia  
(CCOP)

## Supported by:

Tohoku University

Disaster Prevention Research Institute (DPRI), Kyoto University

National Research Institute for Earth Science and Disaster Prevention (NIED)

GNS Science

Philippine Institute of Volcanology & Seismology (PHIVOLCS)

The Seismological Society of Japan

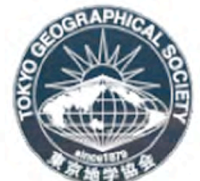
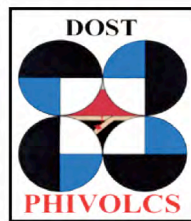
The Volcanological Society of Japan

Japan Association for Quaternary Research

Japanese Society for Active Fault Studies

Japan Society of Engineering Geology

Tokyo Geographical Society



## 2nd G-EVER International Symposium and the 1st IUGS & SCJ International Workshop on Natural Hazards

### Abstracts Volume

**Editor:** G-EVER Promotion Team

Shinji Takarada, Yuzo Ishikawa, Naoji Koizumi, Toshihiro Uchida, Yasuto Kuwahara, Akira Takada, Norio Shigematsu, Tadashi Maruyama, Ryosuke Ando, Ryuta Furukawa and Eikichi Tsukuda

Published by G-EVER Consortium and Geological Survey of Japan (GSJ), National Institute of Advanced Industrial Science and Technology (AIST), 1-1-1 Higashi, Tsukuba, 305-8567, Japan.

Pages: 187, Oct 19, 2013

Copyright 2013 by G-EVER Consortium and Geological Survey of Japan, AIST

**Contact information:** [g-ever-ml@aist.go.jp](mailto:g-ever-ml@aist.go.jp)

## Preface

Large-scale earthquakes and volcanic eruptions are very rare natural disasters. However, once a disaster occurs in today's highly globalized economy, it can create unpredictable turmoil all over the world, not just in the affected area. Global-scale disaster mitigation activities are crucial for the sustainable development of the global economy to ensure human security. Global scale natural hazards are not the fire on the other side of riverbank.

This is the second Asia-Pacific Region Global Earthquake and Volcanic Eruption Risk Management (G-EVER) Symposium. The International Union of Geological Sciences (IUGS) and Science Council of Japan (SCJ) co-hosted this symposium. Hence, the “2nd G-EVER International Symposium and the 1st IUGS & SCJ International Workshop on Natural Hazards” is held in Sendai, Tohoku, Japan. The first G-EVER International Symposium was held in Tsukuba on March 11, 2013 as a follow up activity of the first Workshop of Asia-Pacific Region Global Earthquake and Volcanic Eruption Risk Management (G-EVER1) in February 2012. It was a commemoration of the devastating 2011 earthquake off the Pacific coast of Tohoku, Japan.

G-EVER1 focused on the formulation of strategies to reduce the risks of disasters worldwide caused by the occurrence of earthquakes, tsunamis and volcanic eruptions. More than 150 participants attended the workshop. During the workshop, the G-EVER1 Accord was approved by all participants. The Accord consists of 10 recommendations including the following:

1. Establishment of a framework for cooperation of research institutes and related organizations in the Asia-Pacific region working on seismic and volcanic disaster prevention.
2. Enhancement of exchange and sharing of various information on seismic and volcanic disaster prevention.
3. Building an international standard for database, data exchange and disaster risk assessment.

The G-EVER Consortium among the Asia-Pacific geohazard research institutes was established after the workshop in 2012. The G-EVER Hub website (<http://g-ever.org>) was setup to promote the exchange of information and knowledge about volcanic and seismic hazards among Asia-Pacific countries. Establishing or endorsing data interchange standards and standardized analytical methods for geohazard institutes of the world are important to promote data sharing and comparative analyses. G-EVER International Conference is scheduled every 2 years in the Asia-Pacific countries. Several G-EVER working groups and projects were proposed such as the following: (1) risk mitigation of large-scale earthquakes WG, (2) risk mitigation of large-scale volcanic eruptions WG, (3) next-generation volcanic hazard assessment system WG, and (4) Asia-Pacific region natural hazard mapping project.

The major activities of G-EVER include participation in global risk reduction efforts such as the Integrated Research on Disaster Risk (IRDR) Program, Global Earthquake Model (GEM) and Global Volcanic Model (GVM). G-EVER will be an active player in the new project Future Earth: Research for Global Sustainability. Our knowledge will help build a better future of Earth. Recently, it was announced that the 3<sup>rd</sup> United Nations (UN) world conference on disaster reduction will be held in Japan in 2015. I hope our efforts will be recognized during the UN conference.

After the Tohoku earthquake, many initiatives for risk prevention and reduction of natural disasters were made all over the world. The 2nd G-EVER International Symposium and the 1st IUGS&SCJ International Workshop on Natural Hazards aim to encourage extensive discussions on the present situation of natural disaster mitigation for earthquake, tsunami, volcanic eruption and landslide in Asia-Pacific region. These include (1) discussion on important research works and priorities to develop a strong and resilient society, (2) ideal hazard maps essential in a society and Asia-Pacific scale hazard assessment activities, and (3) importance of contributions to solid earth science. We hope that through these discussions a clear direction for mitigation measures can be determined in order to reduce the risks of global scale earthquakes and volcanic eruptions.

Eikichi TSUKUDA

*President of the G-EVER Consortium  
Director-General of the Geological Survey of Japan, AIST*



The first workshop of Asia-Pacific Region Global Earthquake and Volcanic Eruption Risk Management (G-EVER1) at AIST, Tsukuba, February 22-24, 2012



The 1st Asia-Pacific Region Global Earthquake and Volcanic Eruption Risk Management (G-EVER) International Symposium at AIST, Tsukuba, March 11, 2013

# The 2nd G-EVER International Symposium and the 1st IUGS & SCJ International Workshop on Natural Hazards

## Program

### Oct. 19 (Sat)

Opening addresses:

*Chair: Naoji Koizumi*

- 9:30-9:45        Eikichi Tsukuda (Director General, GSJ, AIST, G-EVER Consortium President)
- 9:45-9:50        Roland Oberhaensli (IUGS President)
- 9:50-9:55        Ryo Matsumoto (SCJ-IUGS Japanese Branch)
- 9:55-10:00      Adichat Surinkum (Director, CCOP Technical Secretariat)

### Session 1: Scientific challenges for risk reduction of natural disasters: Overview

*Chair: Ryo Matsumoto, Yujiro Ogawa and Shinji Takarada*

- 10:00-10:25      Catastrophic earthquakes and tsunamis: Towards more effective risk reduction..... 7  
                         Ian Lambert (IUGS Secretary General) and Roland Oberhaensli (IUGS)
- 10:25-10:50      Response of the damaged scientists to the Tohoku earthquake-tsunami catastrophe..... 9  
                         Akira Ishiwatari (Tohoku Univ.)
- 10:50-11:15      Geo-sciences for post-2015 challenges of disaster risk reduction..... 13  
                         Kuniyoshi Takeuchi (ICHARM, PWRI)
- 11:15-11:35      [Coffee Break] (Group Photo)
- 11:35-12:00      Is satellite monitoring of remote volcanoes good enough for aviation safety?..... 17  
                         John Eichelberger (Alaska Univ., G-EVER Consortium Vice-President)
- 12:00-12:25      Scientific and social challenges of forecasting a VEI  $\geq 7$  eruption..... 20  
                         Chris Newhall and Annie Winson (Earth Observatory of Singapore)
- 12:25-12:50      Global earthquake and volcanic eruption risk management (G-EVER), next-generation  
                         volcanic hazard assessment system and Asia-Pacific region hazard mapping project..... 24  
                         Shinji Takarada, Joel Bandibas and G-EVER Promotion Team (Geological Survey  
                         of Japan, AIST)
- 12:50-14:30      [Lunch]  
                         Poster Session Core Time  
                         SCJ-IUGS Japanese Branch Meeting

## Session 2: Volcanic eruption, landslides and seismic hazards

*Chair: James Goff, Yasuto Kuwahara and Akira Takada*

14:30-14:55	Complexity of the Shinmoe-dake eruption in 2011.....	28
	<u>Setsuya Nakada</u> (ERI, Univ. of Tokyo)	
14:55-15:20	From landslides to civil unrest: the implications of subduction zone earthquakes.....	31
	<u>Peter Bobrowsky</u> (Simon Fraser Univ.)	
15:20-15:45	Submarine landslides and marine geohazards.....	35
	<u>Kiichiro Kawamura</u> (Yamaguchi University)	
15:45-16:10	Landslides in tectonically active countries.....	37
	<u>Masahiro Chigira</u> and <u>Toshitaka Kamai</u> (Kyoto Univ.)	
16:10-16:35	Landslide detection by broadband seismic network.....	39
	<u>Cheng-Horng Lin</u> (Academia Sinica)	
16:35-16:55	[Coffee Break]	
<u>Cancelled</u>	Preliminary study on the seismotectonics of the 2013 Lushan Ms7.0 earthquake, West Sichuan, China.....	40
	<u>Dong Shuwen</u> (Chinese Academy of Geological Sciences)	
16:55-17:20	Strong motion observation in April 20, 2013 Lushan, China, Earthquake and its damage implication.....	41
	<u>Ruizhi Wen</u> (China Earthquake Administration)	
17:20-17:45	Proposals to revise ISC-GEM earthquake catalog.....	45
	<u>Yuzo Ishikawa</u> (Geological Survey of Japan, AIST)	
17:45-18:10	Scenario-based tsunami hazard assessment for the coast of Vietnam from the Manila Trench source.....	47
	<u>Nguyen Hong Phuong</u> , <u>Vu Ha Phuonga</u> and <u>Pham The Truyen</u> a (VAST)	

**Oct. 20 (Sun)**

## Session 3: Hazard assessment, 2011 Tohoku-oki earthquake and subduction tectonics

*Chair: John Eichelberger, Ronald Harris and Kazuhisa Goto*

9:00-9:25	GEM-Faulted Earth: Towards a global active fault database.....	51
	<u>Pilar Villamor</u> (GEM-Faulted Earth team, GNS Science)	
9:25-9:50	Toward a harmonized map of seismic hazard assessment (SHA) in the East Asia	

	region.....	54
	<u>Ken Xiansheng Hao</u> and Hiroyuki Fujiwara (NIED)	
9:50-10:15	What occurred in the Japan trench region before and after the Tohoku-oki earthquake?: Seismological aspects.....	58
	<u>Toru Matsuzawa</u> (Tohoku Univ.)	
10:15-10:40	Tsunami generation mechanism due to the 2011 Tohoku-oki earthquake and a new method for the real-time tsunami inundation prediction.....	62
	<u>Yuichiro Tanioka</u> and Aditya Gusman (Hokkaido Univ.)	
10:40-11:00	[Coffee Break]	
11:00-11:25	Subduction zone tectonics: Subduction accretion versus erosion and the nature of the plate interface.....	66
	<u>Mark Cloos</u> (Univ. Texas, Austin)	
11:25-11:50	Crustal deformation of northeastern Japan clarified by geodetic observation over the past century.....	70
	<u>Takuya Nishimura</u> (Kyoto Univ.)	
11:50-12:15	Strain buildup and release in the Northeast Japan orogen over geologic and geodetic time scales with implications for gigantic subduction earthquakes.....	73
	<u>Yasutaka Ikeda</u> (Univ. Tokyo)	
12:15-13:30	[Lunch]	

#### **Session 4: 2011 Tohoku-oki earthquake and tsunamis**

*Chair: Pilar Villamor, Masahiro Chigira and Yuzo Ishikawa*

13:30-13:55	The 2011 Tohoku-oki tsunami and paleotsunami deposits at the Pacific coast of Tohoku.....	77
	<u>Kazuhisa Goto</u> (Tohoku Univ.)	
13:55-14:20	Sediment transport by the 2011 Tohoku-oki tsunami at Sendai Plain: implications from numerical simulation.....	80
	<u>Daisuke Sugawara</u> , Tomoyuki Takahashi and Fumihiko Imamura (Tohoku Univ.)	
14:20-14:45	Tsunamis and tsunami deposits: Looking beyond the sand.....	83
	<u>James Goff</u> (Univ. NSW)	
14:45-15:05	[Coffee Break]	
15:05-15:30	Did earthquake science reduce causalities of the Mw 9.0 Tohoku-oki earthquake?.....	87
	<u>Masataka Ando</u> (Shizuoka University)	

15:30-15:55	Implications of the 2011 Tohoku Earthquake for other subduction zones elsewhere.....	89
	<u>Phil Cummins</u> (ANU)	
15:55-16:20	Who's next? History of tsunami disasters in Indonesia.....	92
	<u>Ronald Harris</u> , John Major and Yung-Chun Liu (Brigham Young University)	
16:20-16:45	Geopolitics and earth's future: Natural disasters and related geoscientific research.....	95
	<u>Yildirim Dilek</u> (Miami University)	
16:45-17:00	[Coffee Break]	

## General Discussion

*Chair: Chris Newhall, Yildirim Dilek, Yujiro Ogawa and Shinji Takarada*

17:00-18:25	Discussion	
18:25-18:30	Closing Remarks	
	<u>Hirokazu Kato</u> (Emeritus Professor, Former Director General, GSJ, AIST)	

## Poster Session: Oct. 19 (Sat) 9:30 – Oct. 20 (Sun) 18:30

[Core time: Oct. 19 12:50-14:30 and Oct. 20 12:15-13:30]

P1. Quiescence in aftershock activity of the 2008 Iwate-Miyagi inland earthquake caused by the 2011 Tohoku-oki earthquake.....	96
<u>Yuhei Suzuki</u> and Shinji Toda (Tohoku University)	
P2. Characteristic thickness distribution of the 2011 Tohoku-oki tsunami deposits in a narrow valley at the southern end of Sendai Plain.....	99
<u>Tomoya Abe</u> (Nagoya University), Kazuhisa Goto (Tohoku University), Daisuke Sugawara (Tohoku University)	
P3. Tsunami deposits distribution in Sendai Plain evaluated by Sediment transport model.....	103
<u>Kohei Hashimoto</u> (Tohoku University), Kazuhisa Goto (Tohoku University), Daisuke Sugawara (Tohoku University), Fumihiko Imamura (Tohoku University)	
P4. Geochemical characteristics of paleotsunami deposits.....	107
<u>Tetsuya Shinozaki</u> , Shigehiro Fujino (University of Tsukuba) and Minoru Ikehara (Kochi University)	
P5. Distribution and age of the possible paleo-tsunami deposit at a coastal lowland, southeastern Kyushu	110
<u>Masaki Yamada</u> , Shigehiro Fujino, Takashi Chiba (University of Tsukuba), Kazuhisa Goto (Tohoku Univ.) and James Goff (University of New South Wales)	
P6. Estimation of the sizes of paleotsunamis using tsunami boulders at Ishigaki Island, Japan.....	114
<u>Akifumi Hisamatsu</u> , Kazuhisa Goto and Fumihiko Imamura (Tohoku University)	

P7. The combination of anisotropy of anhysteretic remanent magnetization (AARM) and grain size data provide information about the hydrodynamic conditions of the tsunami deposits.....	118
<u>Shusaku Kon</u> , Norihiro Nakamura, Daisuke Sugawara, Kazuhisa Goto and Yasutaka Iijima (Tohoku University)	
P8. Deep structure of the seismic dangers regions in the Sea of Okhotsk.....	121
<u>Alexander Rodnikov</u> (Russian Academy of Sciences)	
P9. Repeating earthquake activity along the Izu-Bonin trench.....	125
<u>Kota Hibino</u> , Naoki Uchida (Tohoku University), Takeshi Matsushima (Kyushu University) and Toru Matsuzawa (Tohoku University)	
P10. Japan trench and Nankai trough: New scope of the two contrasting features of subduction zones and geo-hazardous aspect.....	125
<u>Yujiro Ogawa</u> (Tsukuba University), Kiichiro Kawamura (Yamaguchi University), and Tomoyuki Sasaki (Ocean Engineering & Development Co. Ltd)	
P11. Sanriku-oki large slump deposits and feasibility studies for future scientific drilling accounting for submarine landslide mechanism.....	131
<u>Sumito Morita</u> (GSJ, AIST), Shusaku Goto (GSJ, AIST), Yuichiro Miyata (Yamaguchi University), Yuki Nakamura (University of Tokyo), Yu Kitahara (Kochi University) and Yasuhiro Yamada (Kyoto University)	
P12. Structural characteristics of large-scale submarine landslides on a very gentle continental slope from 3D seismic data off Shimokita Peninsula, Northeast Japan.....	134
<u>Yuki Nakamura</u> (University of Tokyo), Sumito Morita (GSJ, AIST), Juichiro Ashi (University of Tokyo)	
P13. The estimation of the low-velocity subducting crust of the Pacific slab beneath Hokkaido, northern Japan.....	134
<u>Takahiro Shiina</u> , Junichi Nakajima, Genti Toyokuni, and Toru Matsuzawa (Tohoku University)	
P14. A study of earthquake location by artificial explosive data.....	138
<u>Chien-Hsin Chang</u> , Peih-Lin Leu and Tzay-Chyn Shin (Department of Seismological Center, Central Weather Bureau, Taiwan)	
P15. Cooperative hydrological and geochemical research for earthquake forecasting in Taiwan between Disas.Prev.Res.Center, NCKU, Taiwan and Geological Survey of Japan, AIST.....	139
<u>Naoji Koizumi</u> , Norio Matsumoto (GSJ, AIST), Wen-Chi Lai (National Cheng Kung University) and Mamoru Nakamura (University of the Ryukyus)	
P16. Experimental analysis on Rowe's stress-dilatancy relation and frictional instability of fault Gouges.....	141
<u>Momoko Hirata</u> , Jun Muto, Hiroyuki Nagahama and Kenshiro Otsuki (Tohoku University)	
P17. Self-affinities Analysis of Fault-related Folding.....	145
<u>Kazuhei Kikuchi</u> (Tohoku University), Kazutoshi Abiko (Yamagata Prefectural Government), Hiroyuki Nagahama and Jun Muto (Tohoku University)	

P18. Application of GIS Technology in heavy metal source analysis of river water in mining area.....	149
<u>Qingqing Lu</u> , Noriyoshi Tsuchiya, Takahiro Watanabe, Ryo Yamada and Shinichi Yamasaki (Tohoku University)	
P19. Inhomogeneity of fractal property in rock minerals using 3D X-ray CT measurement.....	153
<u>Junko Yamaki</u> , Jun Mutoa, Hiroyuki Nagahama, Osamu Sasaki, and Harumasa Kano (Tohoku University)	
P20. Seismic luminous phenomena and VHF electromagnetic emission originated from radon Emanation.....	157
<u>Asuka Seki</u> (Tohoku University), Izumi Tohbo (Mitsubishi Research Institute), Yasutaka Omori (National Institute of Radiological Science), Jun Muto and Hiroyuki Nagahama (Tohoku University)	
P21. Electromagnetic radiations from semiconductor minerals.....	161
<u>Mitsuyuki Ozawa</u> , Jun Muto, Hiroyuki Nagahama, Toshiro Nagase (Tohoku University)	
P22. Sinusoidal model for the annual variation of atmospheric radon concentration in Japan.....	165
<u>Saki Nakamura</u> , Koseki Hayashi, <u>Yumi Yasuoka</u> (Kobe Pharmaceutical University), Hiroyuki Nagahama, Jun Muto (Tohoku University), Yasutaka Omori (National Institute of Radiological Sciences), Tetsuo Ishikawa, Toshiyuki Suzuki, Yoshimi Homma (Fukushima Medical University), Hayato Ihara (Wakayama Medical University), Takahiro Mukai (Kobe Pharmaceutical University)	
P23. Hazard mitigation of a caldera-forming eruption: From past experience in Indonesia to modern society.....	169
<u>Akira Takada</u> , Ryuta Furukawa (GSJ, AIST), Kiyoshi Toshida (CRIEPI), Supriyati Andreastuti and Nugraha Kartadinata (CVGHM)	
P24. Rainfall induced disasters in India with special reference to Uttarakhand calamity.....	172
<u>Ravi Kumar Umrao</u> , Rajesh Singh and Trilok Nath Singh (Indian Institute of Technology)	
P25. Web Based Rapid Mapping of Disaster Areas using Satellite Images, Web Processing Service, Web Mapping Service, Frequency Based Change Detection Algorithm and J-iView.....	176
<u>Joel Bandibas</u> and Shinji Takarada (Geological Survey of Japan, AIST)	
P26. Geoethical elements in risk communication.....	180
<u>Jose Luis González García</u> (Complejo de la Moncloa), Jesús Martínez-Frías (Geosciences Institute, CSIC-UCM) and Niichi Nishiwaki (Nara University)	

# Catastrophic earthquakes and tsunami: Towards more effective risk reduction

Ian Lambert<sup>a</sup> and Roland Oberhaensli<sup>b</sup>

<sup>a</sup>Secretary General IUGS; Senior Advisor Australian Geoscience Council. [ian.lambert7@gmail.com.au](mailto:ian.lambert7@gmail.com)

<sup>b</sup>Department of Earth and Environmental Science, University of Potsdam; President IUGS, [r.oberhaensli.iugs@geo.uni-potsdam.de](mailto:r.oberhaensli.iugs@geo.uni-potsdam.de)

The International Union of Geological Sciences (IUGS) was formed in 1961 as the umbrella organisation to represent the geosciences globally. With 120 member countries, it:

- Promotes development of the geosciences through the support of international, broad-based, and interdisciplinary scientific studies relevant to the entire System Earth;
- Applies the results of these and other studies to preserving Earth's natural environment, using all natural resources wisely and improving the prosperity of nations and the quality of human life;
- Strengthens public awareness of geology and advances geological education in the widest sense;
- Develops and promulgates geoscience standards, including for information management and chronostratigraphy;
- Through its membership of the International Council for Science (ICSU), has good links to a wide range of scientific and technical expertise.

The Executive Committee has decided that IUGS should scope new initiatives dealing with major global challenges. One is related to major earthquakes and tsunami, with particular reference to addressing any gaps in geological information that are limiting the effectiveness of scientific advice on risks and risk reduction. That is the reason IUGS is sponsoring this IUGS and SCJ International Workshop on Natural Hazards.

Since the disastrous Boxing Day tsunami of 2004, the amount of breadth of research into the

processes and complexity of the lithosphere and related issues that lead to catastrophic tsunamigenic events have increased considerably. But it is timely to critically appraise whether more action is needed, including in relation to coordination of research and monitoring activities, systematic field observations, integration of all relevant data, and developing mechanisms to ensure the best possible scientific advice is marshalled and presented in a timely manner to key government decision makers.

While academic research is vital for understanding processes, it is often government agencies that are responsible for ensuring systematic and widespread observations, monitoring and advice. The International Council for Science (ICSU) is well placed to provide leadership and coordination roles through its Integrated Research on Disaster Risk (IRDR) program.

It is submitted that there is scope for:

- Systematic, internationally coordinated geological inputs, particularly identifying paleo-tsunami deposits in the Quaternary geological record to establish the occurrence, magnitude and frequency of previous tsunami in all regions with significant populations at risk;
- Improved coverage and coordination of geodetic and seismic monitoring networks;
- More coordination of research, analyses and modelling of data;
- Systems analysis to understand concatenated events;

- Developing formal mechanisms for gathering and communicating timely, authoritative scientific and technical advice to governments and other decision makers;
- Consideration whether international guidelines would be beneficial
- Need to ensure no conflicts of interest for advisors or decision makers.

It is hoped that this workshop will facilitate a broad consensus, and action, on:

- Additional activities and programs that are most important for increasing our capability to predict and mitigate the impacts of tsunami;
- Appropriate mechanisms for managing and communicating authoritative information to underpin short to longer term decision making at international and national levels; and
- Funding opportunities for the most important additional activities.

# Response of the damaged scientists to the Tohoku earthquake-tsunami catastrophe

Akira Ishiwatari<sup>a</sup>

<sup>a</sup>*Center for Northeast Asian Studies, Tohoku University, Kawauchi 41, Aoba-ku, Sendai 980-8576 JAPAN  
Email: geoishw@cneas.tohoku.ac.jp.*

*President of the Geological Society of Japan (JGS)*

*Japan Drilling Earth Science Consortium (J-DESC) IODP Section Chair*

## 1. Preface

As the president of the Geological Society of Japan and a Professor of Tohoku University that co-sponsor this 2<sup>nd</sup> G-EVER meeting, I wish to address a welcome message to all who have come here for learning and discussing about “Hazard and Risk Management in Asia-Pacific Region: Earthquake, Tsunami, Volcanic Eruption and Landslide in Subduction Zones”. It is very timely to have this meeting 2.5 years after the Tohoku earthquake here in Sendai that is located at the center of the damaged area.

## 2. The 2011 Tohoku Earthquake

The earthquake and tsunami on March 11, 2011 took 18,550 lives, including 2,667 people who are still missing, along the 500 km-long Pacific coastal area of Northeast Japan. Sendai is the largest city with more than one million populations in the area, and death toll of the City counted 737. Ishinomaki, Rikuzen Takada, Otsuchi, Kesenuma, Kamaishi and Higashi Matsushima are the cities counted more than 1,000 deaths (including missing people). Most of the deaths were caused by tsunamis, which were higher than 20 meters in some places. Seismic tremor was not so strong in spite of the very large magnitude of the earthquake (M=9.0, Mw=9.1), but caused some collapses of houses and buildings as well as landslide and liquefaction of the ground in the wide area from Tokyo to Hokkaido. Another important damage caused

by this earthquake-tsunami event is the explosion of Fukushima Daiichi reactors and resulted radioactive pollutions. About 84,000 people are still evacuated from the polluted area, and more than 25,000 people lived in the highly polluted area cannot go home at all. The incident is still going on in the power plant from where highly polluted groundwater is flowing into the ocean. Thus the damages of this earthquake are three-fold; Earthquake, tsunami and nuclear incident.

As a local citizen living in the damaged area, I would like to appreciate great helps for us that were provided by many countries of the world such as rescue teams, medical and food supplies, and monetary donations. They have been really helpful. Thank you.

## 3. Personal studies after the earthquake

As local scientists trained in field geology, we started to run around the Sendai area immediately after the earthquake to count number of fallen tombstones in cemeteries. Japanese tombstones are relatively homogenous in shape and size throughout the country, and their fall-down rate (percentage of fallen-down stones in a cemetery) has been taken by geologists as a useful parameter for seismic intensity of the area. We found that the tombstone fall-down rates due to the March 11, 2011 earthquake (av. 8%, max. 68%, Fig. 1) were lower than those of the M7.4 earthquake of June 12,

1978 (av. 34%, max. 100%, Fig. 2), the last big one in Sendai. Our survey finished before April 7, when the biggest aftershock pushed down more tombstones.

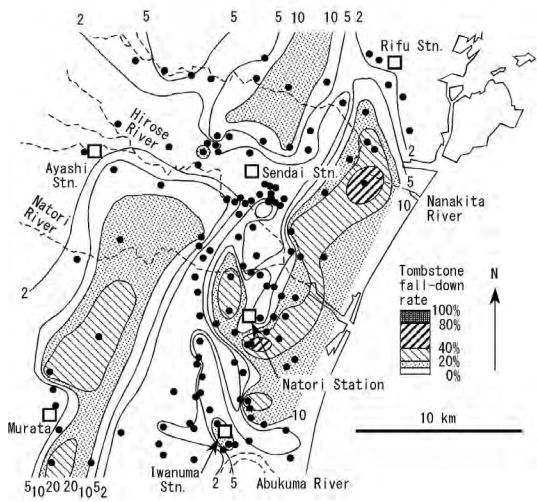


**Fig. 1.** Tombstone fall-down rates in the cemeteries around Sendai counted after the M9.0 Tohoku earthquake on March 11, 2011 (after Ishiwatari, Miyamoto and Hirano (2011) *Geol. Soc. Japan News*, **14**(4), 9-11.)

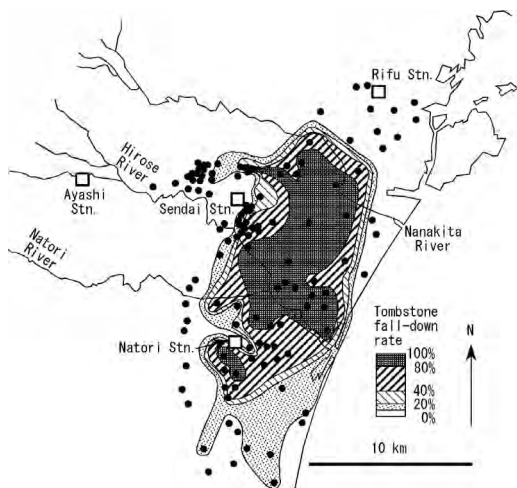


**Fig. 2.** Tombstone fall-down rates in the cemeteries around Sendai counted after the M7.4 Miyagiken-oki earthquake on June 12, 1978. (after *Contrib. Inst. Geol. Paleont., Tohoku Univ.* No. 80 (1979), redrawn by Ishiwatari)

I also measured environmental radioactivity in Sendai just after the explosion of the Fukushima Daiichi reactors. As Sendai was out of the main stream of the radioactive plumes, which went to a northwestern direction toward Fukushima City, the environmental radioactivity in Sendai never exceeded 0.6  $\mu\text{Sv/h}$  (Fig. 3). Now the environmental radioactivity resumed its natural level at 0.06  $\mu\text{Sv/h}$  in Sendai, but it still counts 0.34  $\mu\text{Sv/h}$  in Fukushima. If you travel from Sendai to Tokyo by a Shinkansen train with checking beeps of a Geiger counter, you can easily work out a convex upward pattern with a peak between Fukushima and Koriyama. Mr. Shigeki Chiba, a school teacher in Fukushima Prefecture, made detailed radioactive measurements in the polluted areas, and found some hot spots, “hot materials”, and unusual changes in plants and animals. You can see his results in the homepage of the Geological Society of Japan (<http://www.geosociety.jp/english/content0025.html>).

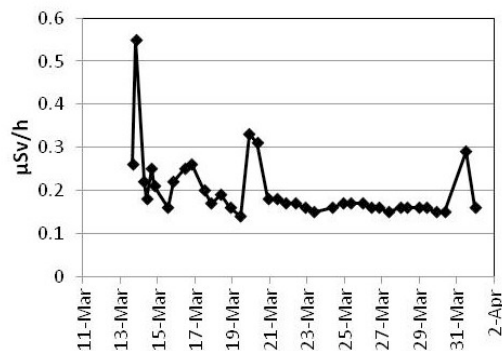


**Fig. 3.** Variation of environmental radioactivity (at 1 m above the ground) in Sendai City directly after the explosions of the Fukushima Daiichi reactors on March 12, 13 and 14, 2011. Measured by Ishiwatari using a Geiger counter “Inspector+” produced by S. E. International Inc., USA. The current radioactive level is 0.06 micro Sv/h that is almost equal to the level of natural radioactivity of the area.

#### 4. Geological Society's actions

The Geological Society of Japan announced a public comment on April 5, 2011, stressing that the society should pay much more attention to the geological records of low-frequency, catastrophic hazards such as big earthquake-tsunamis and volcanic eruptions, pointing out that geologists already presented sedimentary evidences for destructive tsunamis that have attacked the Tohoku coast in every few hundred years (for example, Jogan tsunami in 869 AD) and the necessity of developing education of earth sciences for students and general public. The Society launched some projects in response to the tsunami such as museum "rescue" activities for the tsunami-damaged museums and its important samples, studying methods to process toxic tsunami soils, providing natural radioactivity map of whole country to the public, etc.

#### 5. Tohoku University and the earthquake

In Tohoku University, the government installed a new institute called International Research Institute for Disaster Science (IRIDeS), and launched several scientific, technological, social and medical programs in response to the disaster. It is important to notice that the preceding organization of this institute had been active in our University for many years before 2011. We expected coming of a big earthquake in near future, because such earthquakes of M7 size have hit the Sendai area periodically every 30 years, and it had passed more than 30 years after the last one in 1978. The university professors gave lectures to the local people for warning and preparing, but no one expected such a large earthquake would come next. The word "unexpected" is the most spoken in these years, but the earthquake itself was really "expected" with confidence, and we were prepared for that. I think these preceding activities of our

University resulted in the quick organization of the IRIDeS and our vital research activities.

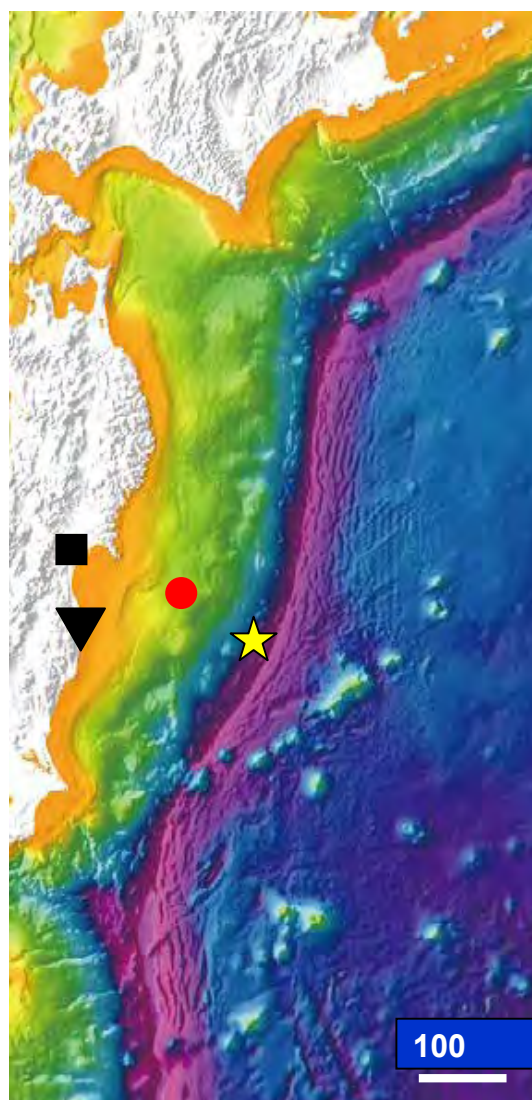


**Fig. 4.** Position of the epicenter (circle) of the Tohoku earthquake on March 11, 2011 and the Exp. 343 drilling site (star) by "Chikyu" in 2012. The topographic map is provided by the courtesy of JAMSTEC. Locations of Sendai (square) and Fukushima Daiichi (triangle) are also shown.

#### 6. Quick response of IODP

The Integrated Ocean Drilling Program (IODP), for which I am participating in its scientific planning and management, executed a very challenging, quickly responding drilling mission called JFAST (Expedition 343) using the Japanese

drilling ship “Chikyu” last year (2012). The drilling site is located in the Japan Trench at about 250 km to the southeast of Sendai (Fig. 4), and this cutting-edge scientific mission turned out to be very successful. The international team could drill more than 800 m beneath the 7,000 m-deep ocean floor in the Japan Trench, and obtained important drill cores penetrating the fault zones that may have moved during the Tohoku earthquake event. The ocean floor of 7,000 m depth has never been drillable by the American drill ship JOIDES Resolution, whose maximum drillable depth is about 5,000 m. The core sample should give an answer why such a big tsunami happened by that earthquake. The team was also successful in measuring the temperature profile through the drill hole to detect remaining frictional heat that was generated during the fault movement.

#### **7. Nuclear debate after the earthquake**

The explosions of the Fukushima Daiichi nuclear reactors caused serious debate and re-evaluation on the safety of the other nuclear power plants in Japan (51 reactors in 18 sites). Only two of them are working in August 2013, and all will be stopped in October. The Nuclear Regulation Authority of the Government asked four academic societies of related fields, namely the Geological Society of Japan, the Seismological Society of Japan, Japanese Society for Active Fault Studies, and Japan Association for Quaternary Research to recommend evaluation committee members to assess activity of fault zones beneath the power plants. In recommendation, the government asked us to keep a condition that the member should not have engaged in the evaluation tasks in the past. The selected geologists are now examining outcrops, drill cores, and acoustic profiles to check whether the fault zones have been activated within

the recent 120-130 thousand years or not, in other words matching the current definition of active fault in Japan or not. The Japanese law prohibits constructing a nuclear reactor or its important facilities directly above an active fault.

#### **8. Conclusions**

We hope our experiences can give some new knowledge and scientific merits to your study, and we also hope to learn a lot from your scientific expertise through this meeting. I also hope that all of you visit the tsunami-flooded area to see the magnitude of the hazard and to observe the response of our society, for example, to provide temporary houses for evacuated people, to repair anti-wave dikes, to prepare piled-up grounds for reconstructing houses, and to plant pine trees along the uprooted shorelines.

I wish you a comfortable stay in Sendai without encountering a big aftershock, which can happen in an unfortunate case, and I ask you to bring big scientific souvenirs back home for your future activity. Thank you for your kind attention.

# Geosciences for post-2015 challenges in disaster risk reduction

Kuniyoshi Takeuchi<sup>a</sup>

<sup>a</sup>*International Centre for Water Hazard and Risk Management (ICHARM), Public Works Research Institute (PWRI), Minamihara 1-6, Tsukuba 305-8516, Japan, kuni.t@pwri.go.jp*

## 1. Importance of year 2015

The year 2015 is of paramount importance in promoting disaster risk reduction. The current Hyogo Framework for Action (HFA) 2005-2015 endorsed at the second World Conference on Disaster Reduction in Kobe on 18-22 January 2005 comes to an end and the post-HFA or HFA2 will be set forth at the third UN World Conference on Disaster Risk Reduction to be held in Sendai on 14-18 March 2015. The agenda and action plans to be discussed and launched are now under discussion in various regions and levels under the leadership of UNISDR.

The Millennium Development Goals (MDGs) are included in the United Nations Millennium Declaration adopted as the UN General Assembly Resolution at the 55<sup>th</sup> UN General Assembly on 18 September 2000 (A/RES/55/2). The most goals are targeted in 2015 and their renewals, the post-MDGs or now called as Sustainable Development Goals (SDGs) are under consideration to set forth also in 2015.

Still more, the Kyoto Protocol to the United Nations Framework Convention on Climate Change (UNFCCC) was adopted at the COP3 meeting in Kyoto by the parties to UNFCCC in December 1997. The Protocol is now extended from 2012 to 2020 in Doha, 2012 and the successor is planned to be agreed upon in 2015 to be implemented in 2020.

Thus all those renewals are going to take place in 2015 which is very important for disaster risk communities to properly direct disaster risk reduction for the next decade.

## 2. Preparation for post-2015

### *Targets in MDGs*

In the Millennium Declaration there are 8 sections where disasters are mentioned in sections 4 and 6 as below:

1. Values and principles
2. Peace, security and disarmament
3. Development and poverty eradication
4. Protecting our common environment  
Together with Kyoto Protocol, forests, bio-diversity & desertification, water resources and free access to the information on human genome, it lists “to intensify cooperation to reduce the number and effects of natural and manmade disasters.”
5. Human rights, democracy and good governance
6. Protecting vulnerable  
“ensure that children and all civilian populations that suffer disproportionately the consequences of natural disasters, genocide, armed conflicts and other humanitarian emergencies are given every assistance and protection so that they can resume normal life as soon as possible.”
7. Meeting the special needs of Africa
8. Strengthening the United Nations

The MDGs are stated in “3. Development and poverty eradication” as follows:

- To halve, by the year 2015, the proportion of the world’s people whose income is less than one dollar a day and the proportion of people who suffer from hunger and, by the same date, to halve the proportion of people who are unable to reach or to afford safe drinking water.
- To ensure that, by the same date, children

everywhere, boys and girls alike, will be able to complete a full course of primary schooling and that girls and boys will have equal access to all levels of education.

- By the same date, to have reduced maternal mortality by three quarters, and under-five child mortality by two thirds, of their current rates.
- To have, by then, halted, and begun to reverse, the spread of HIV/AIDS, the scourge of malaria and other major diseases that afflict humanity.
- By 2020, to have achieved a significant improvement in the lives of at least 100 million slum dwellers as proposed in the “Cities Without Slums” initiative.

It also resolved gender equality, work for young people, partnerships with the private sector and civil society and benefits of new technologies, especially information and communication technologies available to all.

#### *Needs of disaster targets in SDGs*

But unfortunately there were no disaster reduction targets appeared in MDGs. Thus considering a high political implication of goal setting in the UN General Assembly level, it has been strongly sought to include a disaster reduction target this time in the Sustainable Development Goals.

In order to make it realized, clear, simple and measurable targets should be proposed and appealed. Along this line, many attempts have been on the way. For example in Rio+20 held in Brazil in June 2012, Science, Technology and Innovation Forum was held and in both Water and Disaster sessions, disaster targets were stated in recommendations such as:

- Halve the population exposed to high disaster risk under natural hazards.
- Provide universal access to basic early warning for extreme natural hazards.

In the final Rio+20 Outcomes statement, unlike the Rio declaration in 1992, importance of disaster reduction has been mentioned in many paragraphs.

Some major preparation processes towards SDGs are as follows:

- (1) The Secretary-General's High-Level Panel on the Post-2015 Development Agenda established in July 2012. The eminent 27 members include co-chairs: President Yudoyono of Indonesia, President Johnson Sirleaf of Liberia and Prime Minister Cameron of the UK and among members, former Prime Minister Naoto Kan.

The Panel report was submitted to the UN Secretary General in May 2013 (UN, 2013). The report proposes to include disaster reduction target within the poverty eradication goal (one of 12 goals) as among many others “Build resilience and reduce deaths from natural disasters by x%”

- (2) UN Sustainable Development Solutions Network August 2012 led by Professor Jeffrey D. Sachs, Director of The Earth Institute, Columbia University which hosts the Secretariat of the network.

Their draft report was publicized for consultation in May 2013 (SDSN, 2013). In this draft, disaster reduction is included in the productive and resilient city goal (one of 10 goals) as “Sustainable cities will ensure clean air and water, use land and resources efficiently, reduce greenhouse gas emissions, and increase disaster and climate resilience.”

- (3) UN General Assembly Open Working Group on SDGs was established in July 2012 following Rio+20 recommendations in June 2012. This is the official UN function responsible to synthesize all different proposals from different sectors to be agreed by the General Assembly.

In both High Level Panel and Solutions Network, the disaster reduction targets are mentioned but not eminent especially in the latter.

#### *Post-Hyogo Framework for Action (HFA2)*

Hyogo Framework for Action agreed at WCDR in 2005 on the priority areas of governmental commitments:

1. Ensure that disaster risk reduction is a

national and a local priority with a strong institutional basis for implementation.

2. Identify, assess and monitor disaster risks and enhance early warning.
3. Use knowledge, innovation and education to build a culture of safety and resilience at all levels.
4. Reduce the underlying risk factors.
5. Strengthen disaster preparedness for effective response at all levels.

Those priority areas have been well taken in many nations and disaster management has been shifting from humanitarian responses after disaster happens to disaster risk reduction before it happens. This disaster risk reduction process is still progressing and HFA2 is not completed yet in any nations. Therefore it should continue rather than be replaced by other actions. In order to accelerate actions, its progress should be monitored and assessed. The promotion of monitoring risk and reducing risk where increasing risk is identified should be declared in the HFA2. It is a tragic reality that a vicious cycle of disaster management such as below is still prevailing.

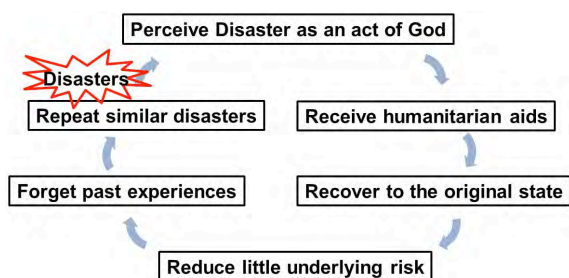


**Fig. 1.** Vicious cycle of disaster management

This vicious cycle should be replaced by a proactive disaster risk reduction defined as:

- (1) Perception: There's no such thing as a natural disaster. Disaster occurs as a result of societal actions and not by the nature.
- (2) Action: Reduce disaster risk before disasters happen by properly choosing where to live and how to live.

### 3. Geosciences for post-2015

In order to support the HFA2, geosciences are expected to play a key role. There would be

at least three categories of roles: One is to obtain the basic knowledge of geophysical and biochemical mechanism of the Planet Earth which forms the basis of all geoscientific services.

Based on such knowledge, they are expected to provide useful information for risk monitoring, assessment and early warning. Monitoring is a continuous observation of geoscientific processes. Risk assessment needs long term statistical and probabilistic, if not deterministic, information that serve for planning and design of infrastructure and system of disaster risk reduction. Early warning needs short term forecasts, as much deterministic as possible, for emergency preparedness and responses including evacuation.

The other is geoscientific literacy building which forms the basis of individual and societal resiliency against disaster and also societal supports for disaster risk reduction. Disaster risk reduction needs political commitment which is only possible by societal support based on societal disaster literacy. The best example of geoscientists who played an irreplaceable role in literacy building would be "Torahiko Terada".

In order to support the monitoring needs of HFA2, disaster risk should be measured and assessed for which geoscientific technology needs to be developed. There are quite a few such efforts by many researchers and research institutes.

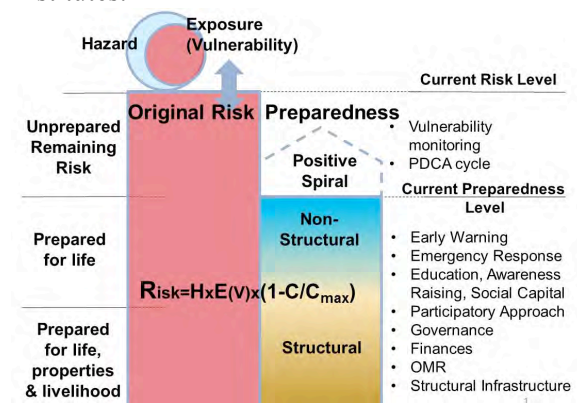


**Fig. 2.** Original Risk and Preparedness

Disaster Risk is conceptually expressed as an integration of probability of hazard and its

consequences. Consequences are a function of hazard severity, exposure of vulnerability and prepared counter measures or coping capacity. This concept is schematically expressed as  $R=H \times E(V) \times (1-C/C_{max})$  where H is hazard, E(V) is exposure of vulnerable objects to hazard H, C is coping capacity, both structural and non-structural, such as early warning, preparedness, engineering infrastructure, rehabilitation supports etc. and  $C_{max}$  is a hypothetical maximum coping capacity.

Assessment of hazard (probability of occurrence, time, place, intensity and duration) and geographical extent of exposure is the responsibility of geoscientists. Some assessments are available in such as GAR2009 report (UNISDR, 2009) but their resolution and accuracy are not necessarily useful for local risk assessment and monitoring. It is because historical data are sparse, inconsistent and often inaccurate and, above all, they are not uniformly and universally available in nations, regions and localities. This is why the technology to monitor and assess risk in seamless manner is important.

#### **4. Seamless monitoring of vulnerability and disaster risk**

ICHARM has been developing the flood risk monitoring technology that can cover the area where ground observation data are missing or poorly available.

The basic procedure is the use of globally available precipitation and radiation data and globally available topographical, geological and land cover data in the public domain. Based on those data, hydrological model BTOPMC and topographical model FID are used to simulate flood discharges and inundation levels for a certain frequency level such as 50 years return period or 2% probability of occurrence in a year. In this stage the effect of risk reduction efforts are not included. Then the number of population and assets in the inundated areas are counted and damages are estimated in relation to inundation depth (Kwak et al., 2012).

Based on this original risk without risk

reduction efforts, the next step is to assess the effect of risk reduction first by structural means such as diversion canals, dams, levees etc. and then by nonstructural means such as early warning, hazard maps, evacuation etc. The assessment of the effect of structural means is more tractable than non-structural means but various indices to measure the effect of non-structural means are under development.

#### **5. Final remarks**

Considering the importance of SDGs and HFA2, ICSU-ISSC-ISDR research program Integrated Research on Disaster Risk (IRDR) (chaired by Prof. David Johnston, Massey University, New Zealand) started 2008 is organizing IRDR Conference 2014 promoting disaster risk reduction in SDGs and scientific contribution to HFA2. IRDR Conference 2014 meeting will be held in Beijing 7-9 June 2014. <http://www.irdrinternational.org/irdr-conference/>  
IRDR Japan National Committee IRDR-Japan (Chaired by Prof. Toshio Koike, University of Tokyo) is also organizing a conference in 2015, the exact date to be decided.

#### **References**

- UN (2013) A new global partnership: eradicate poverty and transform economies through sustainable development, the Report of the High-Level Panel of Eminent Persons on the Post-2015 Development Agenda, May 2013.
- SDSN (2013) An action agenda for sustainable development - draft for public consultation, Sustainable Development Solutions Network, 7 May 2013.
- ISDR (2009) ISDR (2009) Global Assessment Report on Disaster Risk Reduction. United Nations, Geneva, Switzerland.
- Kwak, Y, K Takeuchi, K Fukami and J Magome (2012) A new approach to flood risk assessment in Asia-Pacific region based on MRI-AGCM outputs, Hydrological Research Letters 6, 70–75.

## **Is satellite monitoring of remote volcanoes good enough for aviation safety?**

John C. Eichelberger<sup>a</sup>

<sup>a</sup> *Graduate School, University of Alaska Fairbanks, Fairbanks, Alaska, USA 99775, jceichelberger@alaska.edu*

Few people question the wisdom of maintaining real-time geophysical networks on active and potentially active volcanoes that are located near population centers. Such networks provide warning in advance of eruptive activity, most commonly by detecting increasing micro-seismicity beneath the volcano and/or inflation of the volcano. Relatively few eruptions on well-monitored come as a “surprise”. Such surprises tend to occur at frequently active systems where there is already a high level of preparedness. Presumably, high temperatures and open pathways in such systems allow a new batch of magma to arrive at the surface with minimal perturbation to the shallow volcanic environment. Ground-based geophysical observations are invariably supplemented with satellite remote sensing. Satellite observations are most often used to confirm that a geophysically detected eruption is beginning, although occasionally satellite-based evidence of increasing gas and/or heat emission has been successfully interpreted as a sign of impending activity. Synthetic aperture radar (SAR) satellites could in theory be used to help forecast eruptions by interferometric detection of inflation, but in practice there is not adequate temporal and spatial coverage at present for InSAR to be more than an early guide for focusing attention.

Ever since the phenomenon of ingestion of ash causing in-flight failure of jet aircraft engines was recognized some three decades ago, there has been discussion of instrumenting volcanoes that pose no threat to people or property on the ground, solely for the purpose of

warning pilots of imminent eruption. Despite horrific accounts of large passenger aircraft losing power in all engines in flight, in every case thus far pilots have been able to restore some power and avert a crash. No fatalities have occurred. Given that the cost of placing and maintaining ground networks on remote volcanoes is high, and that many other natural and human phenomena do cause fatal accidents, the majority of remote active volcanoes remain unmonitored.

This issue has been much discussed by the International Civil Aviation Organization (ICAO), a treaty organization under the United Nations that sets international standards for aviation. ICAO has worked with the World Meteorological Organization (WMO) to establish Volcanic Ash Advisory Centers (VAACs), of which there are now 9 distributed around the world. These centers use weather satellites to detect ash clouds 24/7 and forecast their trajectories in order to warn pilots of potential encounters. The North Pacific, where busy eastern Asia – North America air routes coincide with some 100 active but mostly unmonitored volcanoes of the Kuril, Kamchatka, and Aleutian Arcs, is covered by VAACs in Anchorage and Washington, DC operated by the National Oceanic and Atmospheric Administration (NOAA) and in Tokyo by the Japan Meteorological Agency (JMA). Globally, the system has worked well, with the exception of the Eyjafjallajökull, Iceland eruption of 2010 when over-reliance on inadequate ash dispersion models led to shutting down of aviation over most of Europe for days.

The problem with relying on satellite imagery alone for detection of ash eruptions is that much of the coverage is discontinuous in time and detection requires that the eruption column rise above the local cloud layer. Thus, an obstacle to safe flight is already present when a warning is given. A warning within 5 minutes of ash reaching flight levels, as desired by the aviation industry, is not achievable using satellite imagery alone. Given that modern jet aircraft travel at about 1000 km/h, it is clear why quick warnings are necessary. Prior warning of the likelihood of activity, which is possible only with ground stations, allows pilots to take on extra fuel and plan for possible diversions. This can be the difference between having to turn back or simply taking a somewhat longer route to the destination. A country that operates a VAAC but has no active volcanoes of its own may advocate that countries with volcanoes monitor even remote ones. A country with many remote volcanoes for which installation of ground networks would be expensive is more likely to take the position that satellite-only monitoring is adequate.

The situation is further complicated by internal governmental structures. Although every fully functional nation has a federal agency that oversees aviation and a meteorological organization, ground monitoring of natural hazards are conducted in different ways. This may be through a geological survey (US and Chile), a weather organization (Japan and Iceland), or a hybrid scientific – government - academic organization (France, Russia, Italy). One reason for choosing a weather service is that such organizations are already set up to conduct monitoring around the clock.

The Aleutian Volcanic Arc of the United States is illustrative of the challenge to placing ground networks on remote volcanoes. Prior to the late 1980s, there was no organized volcano

monitoring in Alaska although there was a considerable volcanological research effort. Disruptions caused by the 1986 eruption of Augustine Volcano motivated planning by leaders of the US Geological Survey (USGS) in Alaska, the University of Alaska Fairbanks, and the Alaska Division of Geological and Geophysical Surveys. Interest and guidance on the part of Ted Stevens, an influential US Senator and a pilot himself with a concern for aviation safety, led to modest funding of the Alaska Volcano Observatory (AVO) as a three-way partnership, based on an agreement in 1988.

Soon after work began to upgrade existing research networks to operational monitoring, seismicity began to increase rapidly at Redoubt Volcano. A powerful explosive eruption occurred on December 14, 1989. Although warnings were issued, a KLM 747 passenger aircraft nevertheless entered the eruption cloud between Anchorage and Fairbanks, lost power in all four engines, and fell some 6000 m of altitude before the pilot managed to restart two engines and land at Anchorage.

This triggered the first of many large federal appropriations added to the budget of the USGS by Senator Stevens. AVO built up rapidly in staff and in instrumentation. In 1995, Senator Stevens began directing funds to the Federal Aviation Administration (FAA) budget as well to extend AVO monitoring beyond the populated Cook Inlet area westward out the Aleutian chain. Most of these volcanoes represent a hazard to aviation alone.

AVO went from real-time monitoring of 4 volcanoes to 33 by the mid '00s. AVO succeeded in providing early warning of many explosive eruptions, in one case demonstrably saving lives on the ground. However, the system was not sustainable. Special appropriations were required every year. Although common practice in the US Congress at the time, such

appropriations were increasingly despised as “pork” because they did not go through the normal budget process. To much of Congress, instrumenting volcanoes in Alaska appears to be a “special” one-state issue, not a matter with international implications. In contrast, the State of Alaska saw it as a federal issue. When Senator Stevens was not re-elected to Congress in 2008, support through FAA ceased. Meanwhile the USGS did not receive budget increases commensurate with the rising cost of operations. Through lack of maintenance, the number of volcanoes reliably monitored has now declined to 28 and is in danger of declining further.

Besides the question of whether ground monitoring is really necessary is the question of who should pay for it: The airlines who fly these routes? The FAA which already receives tax funds for aviation safety? The USGS where the monitoring expertise resides and which is the traditional US agency for geo-hazards? Or should monitoring of remote volcanoes be left to NOAA’s VAACs?

There has never been a rigorous cost-benefit analysis and perhaps one is not possible. Given the absence of fatalities due to aircraft encountering ash, the argument for improved monitoring has shifted from safety to route efficiency. The current situation is not likely to change in the near term unless there is another Redoubt-like incident. However that incident occurred not because of inadequate monitoring but because the aviation industry was not yet aware of the problem and the lines of warning messaging had not been well prepared. That condition no longer exists, thanks to the efforts of many scientists, government agencies, the aircraft and aviation industries, and ICAO.

What is likely to change over the next few decades, however, is a huge increase in shipping and commercial activity as the Arctic Ocean shortcut between the Atlantic and Pacific opens.

Whether this causes a reassessment of volcano monitoring in the Aleutians as they become less remote remains to be seen. This is only part of a broader problem of natural hazards, including earthquakes and tsunamis, that can impact the support facilities needed for commercialization of the Arctic.

# Scientific and social challenges of forecasting a VEI $\geq 7$ eruption

Chris Newhall<sup>a</sup> and Annie Winson<sup>a</sup>

<sup>a</sup>*Earth Observatory of Singapore, Nanyang Technological University, 50 Nanyang Ave., Block N2-01a-10, Singapore 639798, cnewhall@ntu.edu.sg or cgnewhall@gmail.com*

## 1. What is known of VEI $\geq 7$ eruptions

A VEI  $\geq 7$  eruption has a deposit volume of more than  $10^8 \text{ m}^3$  and has the potential to send pyroclastic flows 10's or even up to 100 km from source. Tephra fall may be several meters thick near source and several cm thick even 1000 km downwind. A caldera of at least 5 km in diameter will form. Ten such eruptions are known from the past 10,000 y, so the nominal return time, worldwide, is 1000 y. Because many calderas and their products are as yet undated, the actual return period is probably less.

The timescale and character of precursors to an eruption of VEI  $\geq 7$  are largely unknown. The latest VEI 7 eruption was that of Tambora in 1815, long before the era of instrumental volcano monitoring.

At least five things can be gleaned from geologic and historical records. First, there are a few historical and archaeological accounts of precursors to VEI 7 eruptions of Tambora and Santorini. We know, for example, that Tambora began to have small phreatomagmatic eruptions and increased steaming in 1812. There was also a report from a ship's captain who described 'a dense column of immense circumference' rising from the volcano in 1814. Then moderate size eruptions began from April 5 until the climax on April 10-11, 1815. At Santorini, earthquakes damaged houses in Akrotiri long enough before the Minoan eruption to allow people to make repairs, and again just before the eruption in enough time for people to flee.

Second, at several of the ten Holocene examples of VEI  $\geq 7$  eruptions, there is a geologic record of small precursory eruptions, including eruption of a silicic lava at Crater Lake (Mazama) so soon before the climactic eruption that the lava was still fluid and spilled slightly into and down the wall of the newly created caldera (Bacon, 1985; Bacon and Lanphere, 2006). The precursory phreatomagmatic eruptions at Tambora appear in tephra layer F1 (Self et al, 1984; Sigurdsson and Carey, 1989; Sutawidjaja et al., 2006).

Third, there are petrologic clues about time between disequilibrium events (e.g., magma mixing) and eruption. For example, at Santorini, Druitt et al. (2012) found evidence for three episodes of magma mixing, one  $< 100$  y, one  $\sim 10$  y, and one just months before the climatic Minoan eruption  $\sim 1600$  BC. Similar study at Pinatubo suggested magma mixing as early as March 1991 (M. Coombs, pers. commun.).

Fourth, there is a large body of information about precursors to VEI 1-5 eruptions and a few case examples of precursors to VEI 6 eruptions (e.g., Krakatau, 1883; Pinatubo, 1991). A tectonic earthquake occurred near Krakatau on 1 September 1880, more earthquakes were felt from March to May 1882, and steam and ash emissions began 20 May 1883. From Pinatubo, we know that events were triggered by a M7.8 regional earthquake on 16 July 1990, followed by the abovementioned magma mixing and by felt local earthquakes from March 1991 onward,

and steam explosions on 2 April 1991. Most of the precursors were unremarkable – giving little clue to the size of the impending eruption – until onset of strong shallow LP seismicity just 24 hours before the climatic phase and already several days into the precursory VEI 3 eruptions (Harlow et al., 1996).

A fifth lesson comes from El Chichon and Pinatubo – that exceptionally large explosive eruptions often release large masses of SO<sub>2</sub>, well in excess of what could have been dissolved in the erupted volume of melt (Gerlach et al., 1996). It now appears that accumulation of a large volume of gas in excess of saturation – in a discrete bubble phase in magma even at depth – is a common and possibly a necessary precondition for an eruption to escalate and be sustained as a plinian eruption. It is impossible to sample pre-eruption magma from depth to check for such an excess gas phase, but petrologic studies and rough calculations of the balance between magma and gas supply vs. eruptions and degassing can indicate whether such an accumulation seems likely.

Several new technologies have been developed since the time of the 1991 Pinatubo eruption. One of the most useful will be InSAR, which now shows many volcanoes receiving magma recharge (e.g., Pritchard and Simons, 2004; Fournier et al., 2010). Less than half of these erupt, so an InSAR anomaly tells us when recharge is occurring, and thus that an eruption MIGHT follow.

Monitoring of diffuse CO<sub>2</sub> also offers potential to spot deep magma intrusion before it is shallow enough to trigger seismicity and sometimes even before a deformation signal is evident. Of the major gases in magma, CO<sub>2</sub> is the least

soluble and begins to exsolve when rising magma is still 10-20 km below the surface. At this depth, country rock is ductile and magma intrusion can be largely aseismic, so CO<sub>2</sub> leakage to the surface can be the first apparent precursor (e.g., Hernandez et al., 2001; Padrón et al., 2008; Aiuppa et al., 2011)

## **2. What can be forecast, and how?**

The most general forecast is a 30-year or similarly long probability of eruption. This can be based on known recurrence intervals of large eruptions at the volcano in question. Because it appears that there is a certain time required for recharge and re-accumulation of an excess gas phase, the probability of a large eruption will be low within the early part of an average repose period, typically for the first few centuries after the last one. After sufficient time for gas re-accumulation, then the probability of large eruption will depend on other factors, e.g., rates and volumes of recharge, magma mixing, etc.

If geophysical and geochemical monitoring confirms continued or repeated magma resupply, but still no definite, accelerating trend toward eruption, the probability of eruption within a year or a decade is increasing, but little more can be said.

Any short-term forecast will probably look for an escalating, accelerating pattern of seismicity and deformation rates, and/or a decreasing interval between small, precursory magmatic eruptions. Repeated InSAR, coupled with another post-Pinatubo technology (GPS) will be able to show shallowing and acceleration of deformation, and seismic networks can show shallowing (rare) or shifts toward lower spectral frequency (common). The keys are evidence of accelerating magma ascent rate

and/or rate of pressurization of the magma reservoir, causing deformation and brittle fracture of country rock to accelerate, and escape of gas under high pressure. That is, evidence of a runaway process.

Each of the VEI 3 eruptions of Pinatubo between June 12 and June 15, 1991, opened the conduit a little more and brought increasingly gas-rich dacite magma to the surface, on the heels of the vanguard, hybrid andesite (mixed basalt + dacite) magma. The latter was largely degassed before it reached the surface because it was degassing as it prepared the conduit. The intervals between these precursory VEI 3 eruptions – and the column heights -- decreased from June 12 to June 15, as the conduit was progressively opened. A very sharp escalation in shallow LP earthquakes on June 14 probably reflected dacite magma, loaded with excess gas, rising faster and faster into shallow depth where that gas was expanding and either building pressure or forcing its way out of the magma. Unfortunately, no SO<sub>2</sub> measurements could be made on June 12-14 because the pilot of the light plane we were using flew off, with the COSPEC, as soon as he saw the June 12 eruption!

### **3. Social considerations for forecasts of a VEI $\geq$ 7 eruption**

Forecasting will be a particular challenge if there is a large population nearby. Long-range forecasts will be sensitive because they could cause anxiety, negatively impact financing for business and residential construction, perhaps require costly insurance, and perhaps discourage new economic investment in the area. There is already a tendency in the news media to sensationalize any eruption forecast, and it will be especially difficult to let the public know of a low-probability, high-consequence VEI  $\geq$ 7 eruption without

causing immediate overreaction. Information must be released, but thoughtfully to minimize overreaction.

Short-range forecasts (weeks to days in advance) can potentially allow for evacuations of people and moveable property, but there is little room for either a premature forecast (false alarm) or one that is too late to allow evacuation. The dilemma for scientists is that – based on Pinatubo and other experience – the certainty of a forecast made weeks in advance will be low. Historical but smaller eruptions in two caldera settings – Campi Flegrei and Rabaul – confirm that unmistakable, unequivocal indicators of a runaway process toward eruption appear just a day or two before the eruption begins. High certainty in short-range forecasts will not be possible until just days to hours in advance, when it is already very late for evacuations. If the public wants to be safe, it will need to accept some possibility of false alarms, and be prepared to make and stay in precautionary evacuation for as much as several weeks, possibly more than once! In public conversations regarding volcanic risk tolerance and mitigation, it may be helpful to highlight the abovementioned dilemma of timing and the need for a social compact that accepts tradeoffs between early warning and certainty.

### **References**

- Aiuppa, A., Burton, M., Allard, P., Caltabiano, T., Giudice, G., Gurrieri, S., Liuzzo, M., Salerno, G. (2011) First experimental evidence for the CO<sub>2</sub>-driven origin of Stromboli's major explosions. *Solid Earth Discussions* 3, 411-430.
- Bacon, C.R. (1985) Implications of silicic vent patterns for the presence of large crustal magma chambers. *J Geophys Res*, 90:B13, 11243-11252  
(DOI: 10.1029/JB090iB13p11243)

- Bacon, C.R., Lanphere, M.A. (2006) Eruptive history and geochronology of Mount Mazama and the Crater Lake region, Oregon. *Geol Soc Am Bull*, 118, 1331-1359.
- Druitt, T.H., Costa, F., Deloule, E., Dungan, M., Scaillet, B. (2012) Decadal to monthly timescales of magma transfer and reservoir growth at a caldera volcano. *Nature*, 482, 77-80.
- Fournier, T.J., Pritchard, M.E., Riddick, S.N. (2010) Duration, magnitude, and frequency of subaerial volcano deformation events: New results from Latin America using InSAR and a global synthesis. *Geochemistry, Geophysics, Geosystems* 11:1 (DOI: 10.1029/2009GC002558)
- Gerlach, T.M., Westrich, H.R., Symonds, R.B. (1996) Preruption vapor in the magma of the climactic Mount Pinatubo eruption: Source of the giant stratospheric sulfur dioxide cloud. *In* Newhall, C.G., Punongbayan, R.S. (eds), *Fire and Mud: Eruptions and Lahars of Mount Pinatubo, Philippines*. PHIVOLCS and Univ. of Washington Press, 415-433.
- Harlow, D.H., Power, J.A., Laguerta, E.P., Ambubuyog, G., White, R.A., Hoblitt, R.P. (1996) Precursory seismicity and forecasting of the June 15, 1991, eruption of Mount Pinatubo. *In* Newhall, C.G., Punongbayan, R.S. (eds), *Fire and Mud: Eruptions and Lahars of Mount Pinatubo, Philippines*. PHIVOLCS and Univ. of Washington Press, 285-305.
- Hernández, P.A., Notsu, K., Salazar J.M., Mori, T., Natale, G., Okada, H., Virgili, G., Shimoike, Y., Sato, M., Pérez, N.M. (2001) Carbon dioxide degassing by advective flow from Usu Volcano, Japan. *Science*, 292, 83-86.
- Padrón, E., Melián, G., Marrero, R., Nolasto, D., Barrancos, J., Padilla, G., Hernández, P.A., Pérez, N.M. (2008), Changes in the diffuse CO<sub>2</sub> emission and relation to seismic activity in and around El Hierro, Canary Islands. *Pure Appl Geophys* 165, 95-114.
- Pritchard, M.E., Simons, M. (2004) An InSAR-based survey of volcanic deformation in the central Andes. *Geophysics, Geochemistry, Geosystems (G<sup>3</sup>)* 5:2 (DOI: 10.1029/2003GC000610)
- Self, S., Rampino, M., Newton, M., Wolff, J. (1984) Volcanological study of the great Tambora eruption of 1815. *Geology* 12, 659-663.
- Sigurdsson, H., Carey, S. (1989) Plinian and co-ignimbrite tephra fall from the 1815 eruption of Tambora Volcano. *Bull Volcanol*, 51:4, 243-270.
- Sutawidjaja, I.S., Sigurdsson, H., Abrams, L. (2006) Characterization of volcanic deposits and geoarchaeological studies from the 1815 eruption of Tambora volcano. *J Geologi Indonesia*, 1, 49-57.
- Werner, C., Evans, W.C., Poland, M., Tucker, D.S., Doukas, M.P. (2009) Long-term changes in quiescent degassing at Mount Baker Volcano, Washington, USA; Evidence for a stalled intrusion in 1975 and connection to a deep magma source. *J Volcanol Geotherm Res*, 186, 379-386.

# Global earthquake and volcanic eruption risk management (G-EVER), next-generation volcanic hazard assessment system and Asia-Pacific region hazard mapping project

Shinji Takarada<sup>a</sup>, Joel C. Bandibas<sup>a</sup>, and G-EVER Promotion Team<sup>a</sup>

<sup>a</sup>Geological Survey of Japan, AIST, 1-1-1 Higashi, Tsukuba, Ibaraki 305-8567, Japan, s-takarada@aist.go.jp

## 1. G-EVER Activities

The Asia-Pacific Region Global Earthquake and Volcanic Eruption Risk Management (G-EVER) Consortium among the geohazard research institutes in the Asia-Pacific region was established in 2012. G-EVER aims to formulate strategies to reduce the risks caused by the occurrence of earthquakes, tsunamis and volcanic eruptions worldwide.

The First Workshop on Asia-Pacific Region Global Earthquake and Volcanic Eruption Risk Management (G-EVER1) was held in Tsukuba, Japan from February 22 to 24, 2012. During the workshop, the G-EVER1 accord was approved by the participants. The Accord consists of 10 recommendations like enhancing collaboration, sharing of resources, and making information about the risks of earthquakes and volcanic eruptions freely available and understandable.

The G-EVER Promotion Team of GSJ was formed in November 2012. The G-EVER Hub website (Fig. 1; <http://g-ever.org>) was setup to promote the exchange of information and knowledge about volcanic and seismic hazards among the Asia-Pacific countries. Establishing or endorsing standards on data sharing and analytical methods is important to promote data and analyses results sharing. The major activities of G-EVER include participation in global risk reduction efforts such as the Integrated Research on Disaster Risk (IRDR) Program, Global Earthquake Model (GEM) and Global Volcanic Model (GVM).

The G-EVER international conference will be held every 2 years in the Asia-Pacific region. On the other hand, one to two days G-EVER international symposium will be held annually. The 1st G-EVER International Symposium was held in Tsukuba, Japan on March 11, 2013. The 2nd G-EVER Symposium is held in Sendai, Tohoku Japan, on October 19-20, 2013 (this volume).

Several G-EVER Working Groups and projects were proposed such as the following: (1) Risk mitigation of large-scale earthquakes WG, (2) Risk mitigation of large-scale volcanic eruptions WG, (3) Next-generation volcanic hazard assessment WG, and (4) Asia-Pacific region earthquake and volcanic hazard mapping project.

## 2. Next-generation volcanic hazard assessment system

The next-generation volcano hazard assessment WG is developing a useful system for volcanic eruption prediction, risk assessment,



Fig. 1. G-EVER Hubsite (<http://g-ever.org>)

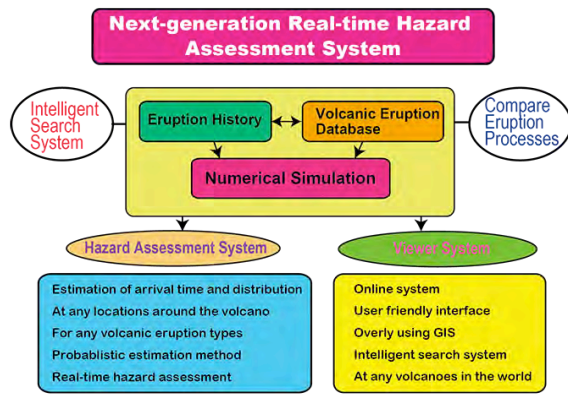


**Fig. 2.** Concept diagram of the next-generation real-time volcanic hazard assessment system

and evacuation strategy at various eruption stages. The assessment system is based on volcanic eruption history datasets, volcanic eruption database and numerical simulations (Fig. 2). Volcanic eruption histories including precursor phenomena leading to major eruptions are important for the prediction of future volcanic eruptions. A high quality volcanic eruption database, which contains compilations of eruption dates, volumes, and styles, is

important for the next-generation volcano hazard assessment system. Formulating international standards on how to estimate the volume of volcanic materials are important to make a high quality volcanic eruption database. GIS based spatial distribution database of volcanic materials (eg. Tephra and pyroclastic flow distributions) is important for accurate area and volume estimation and risk assessments.

The volcanic eruption database is developed based on past eruption results, which only represent a subset of possible future scenarios. Therefore, numerical simulations with controlled parameters are needed for more precise volcanic eruption predictions. The "best-fit" parameters of the past major eruptions in the world have to be estimated and the simulation results database should be made.

The use of the next-generation system should enable the visualization of past volcanic eruptions datasets such as distributions, eruption volumes and eruption rates, on maps and diagrams using timeline and GIS software. Similar volcanic eruptions types should be easily

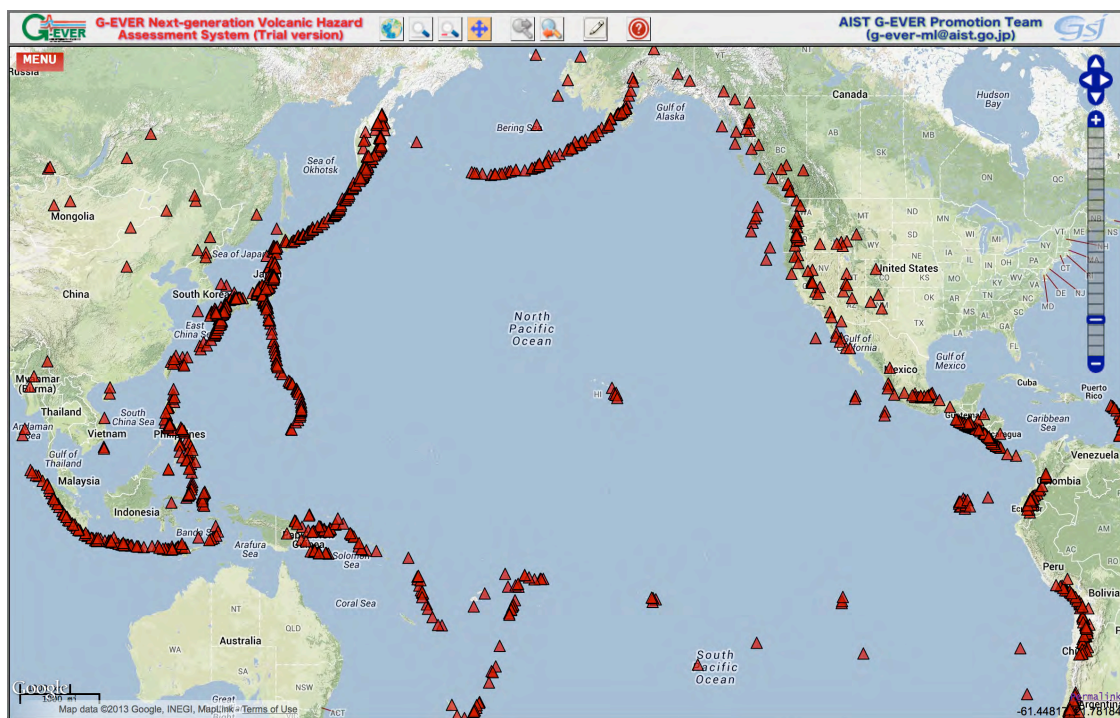


**Fig. 3.** G-EVER next-generation volcanic hazard assessment system (Trial version).

<http://volcano.g-ever1.org/vhazard/HazardAssessment/>

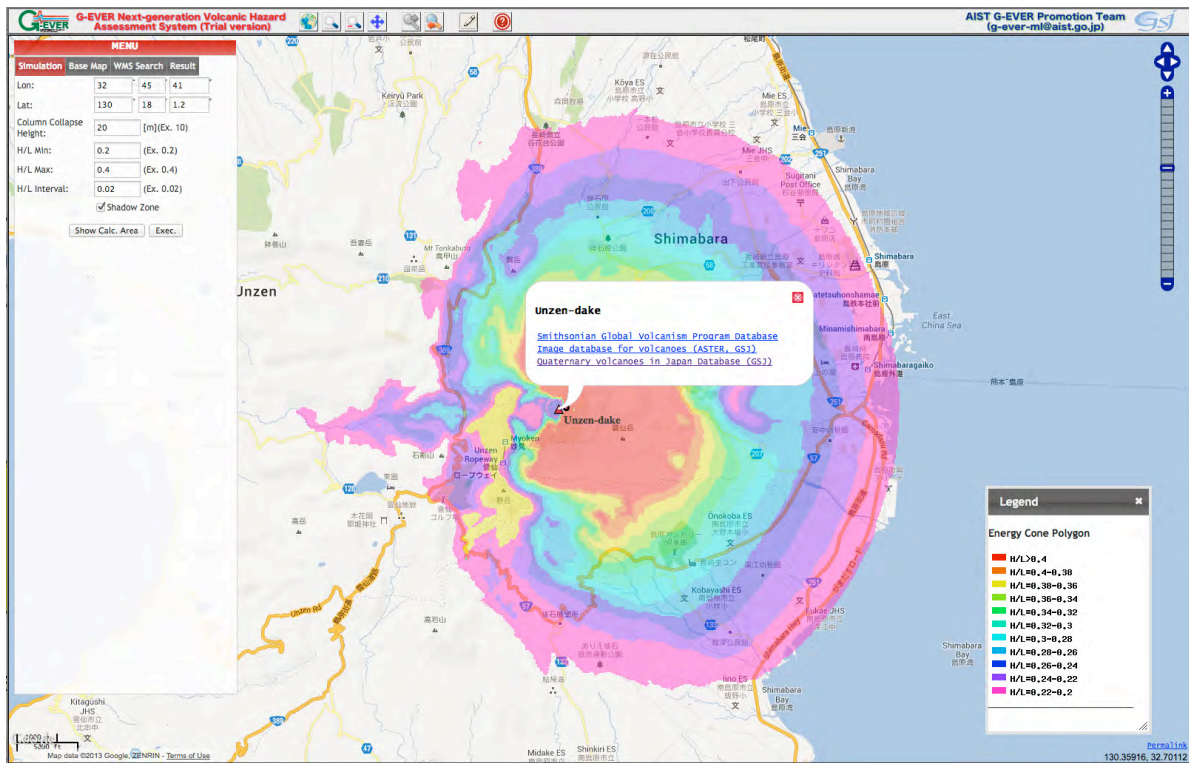


**Fig. 4.** An energy-cone simulation result at Unzen Volcano, western Japan, using G-EVER next-generation volcanic hazard assessment system. Almost all volcanoes in the world can be evaluated on this system because of the wide coverage of ASTER Global DEM.

searchable from the eruption database. Using the volcano hazard assessment system, prediction of the time and area that would be affected by volcanic eruptions at any locations near the volcano should be possible, using numerical simulations. The system should estimate volcanic hazard risks by overlaying the distributions of volcanic deposits on major roads, houses and evacuation areas using a GIS enabled systems. The next-generation real-time hazard assessment system would be implemented with user-friendly interface, making the risk assessment system easily usable and accessible online.

Preliminary version of the next-generation volcanic hazard assessment system, which can run energy cone simulations at any volcano in the world, using ASTER Global DEM, and the links to major volcanic databases, such as Smithsonian, VOGRIPA and Quaternary volcanoes, is available since June 2013 (Figs. 3 and 4). Previous GEO Grid volcanic gravity simulation system covers only 14 major

volcanoes in the world. On the other hand, almost all volcanoes in the world can be evaluated using this volcanic hazard assessment system. Currently, the system covers more than 3200 Quaternary volcanoes worldwide. Links to major volcanic databases in the world are useful to examine eruption history in detail. Using Google and Bing maps as base maps provide more information for hazard evaluations.

### 3. Asia-Pacific region earthquake and volcanic hazard mapping project

The Asia-Pacific region earthquake and volcanic hazard mapping project aims to make an advanced online information system that provides past and recent earthquake and volcanic eruption information (eg. age, location, scale, affected areas and fatalities) and risk assessment tools for earthquake and volcanic eruption hazards. A printed map version will also be published as the new version of the Eastern Asia Geological Hazard Map of

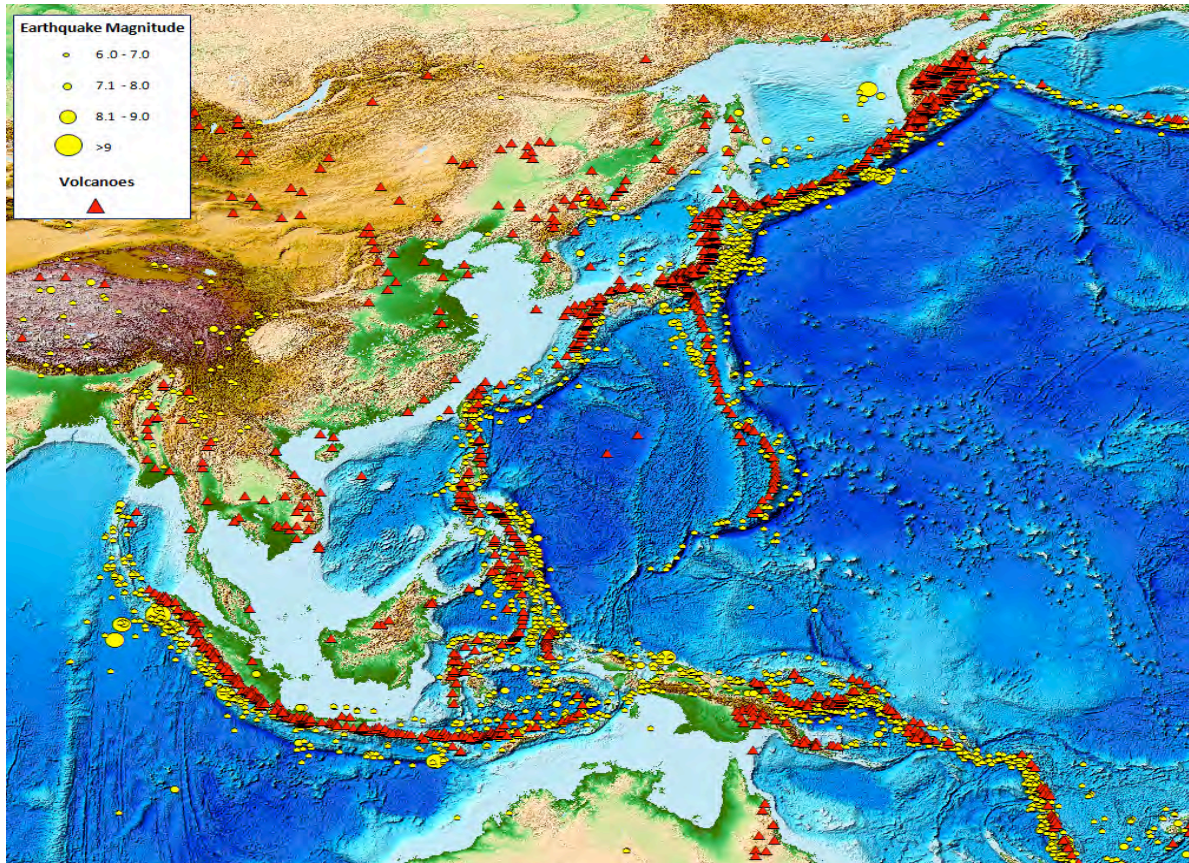


**Fig. 5.** Preliminary version of Asia-Pacific region earthquake and volcanic hazard assessment system. Distribution of epicenter of large-scale earthquakes ( $M > 6$ ) since 1971 (USGS) and Quaternary volcanoes (Smithsonian, VOGRIPA and Japanese Quaternary volcanoes databases) are shown. Etopo1 (NOAA) is used as a topographic map. Detailed information is available to click each volcanoes and earthquake epicenters.

the Commission for the Geological Map of the World (CGMW). The online hazard mapping system will provide useful information about earthquake and volcanic hazards in an interactive and user-friendly interface (Fig. 5). Past and recent large-scale earthquakes ( $>M7$ ) and volcanic eruptions ( $>VEI 5$ ), tsunami inundation areas, active faults distributions, major landslides will be shown on the map. Links to major earthquakes and volcanic eruptions databases will be available in the system. The earthquake and volcanic eruption hazard mapping project will be implemented with the cooperation of major research institutes and organization in the Asia-Pacific region such

as PHIVOLCS, CVGHM, GNS Science, EOS, USGS and CCOP.

## References

- Takarada, S. (2013) Asia-Pacific Region Global Earthquake and Volcanic Eruption Risk Management (G-EVER) Consortium: the new hazard mitigation activities, abstract of IAVCEI 2013, Kagoshima, 4A1\_4H-O4.
- Takarada, S. (2013) The next-generation real-time volcanic hazard assessment system in G-EVER, abstract of IAVCEI 2013, Kagoshima, 4P1\_4D-O21.

# Complexity of the Shinmoe-dake eruption in 2011

Setsuya Nakada<sup>a</sup>

<sup>a</sup>*Volcano Research Center, Earthquake Research Institute, University of Tokyo, Yayoi, Bunkyo-ku, Tokyo 113-0032, Japan, nakada@eri.u-tokyo.ac.jp*

## 1. Introduction

The eruption at Shinmoe-dake volcano, Kirishima, in Kyushu, Japan, which began in January 2011, is a well-monitored example. This eruption took place about 300 years after the last magmatic eruption. The main phase is represented by subplinian/vulcanian events and successive lava accumulation, which was followed by repeated vulcanian events (Fig. 1). Subplinian eruptions may be transitional between vulcanian explosions and plinian eruptions in terms of magnitude and intensity (Cashman, 2004). The transition between two phenomena is common in several recent eruptions. Therefore, it is expected that the eruption process of the 2011 eruption at Shinmoe-dake may give the valuable information to illustrate the transition between vulcanian and subplinian eruptions.

Multi-purpose observational research was carried out on this eruption. Satellite SAR was very effective for monitoring the eruption



**Fig. 1.** Subplinian event at Shinmoedake (Kirishima volcano) on the afternoon of 26 January 2011. Abundant pumiceous blocks showered on the southern slope of the Shinmoe-dake summit crater. Taken by K. Shimousuki.

conditions and for issuing alerts to the public. Unmanned autonomous aerial vehicles were employed to get information on physical and chemical conditions of cooling lava which filled the summit crater. Details of the eruption story, magma system under the ground, and mechanisms of eruption phenomena were deciphered. This paper is the review of the 2011 eruption at Shinmoe-dake summarized in the Earth Planets and Space (EPS) special issue (vol. 65, no. 6, 2013) and Nakada et al. (2013).

## 2. Outline of the eruption

The 2011 eruption began with three subplinian explosive events, followed by lava accumulation at the summit crater and then vulcanian explosions. Precursory phreatic events took place first in 2008 and often in 2010. Seismic activity around the Kirishima region had increased since 2006 and escalated in 2010. As well, ground deformation by GPS measurements suggested inflation of the region in the same time scale. The direct precursory phenomenon of the climactic phenomena (subplinian eruptive events), however, are involvement of juvenile materials in the tephra which was issued a week before the climactic eruption events. We could not forecast the climactic events timely, though the above abnormal condition had been observed.

The first two subplinian events were relatively long but included periods with a low eruption column, and each event ended with the highest eruption column (~7 km above the crater). Duration of the third subplinian event was short and preceded by the first vulcanian event. When the eruption column was highest,

**Table 1.** Chronology of the 2013 eruption at Shinmoe-dake.

<i>Phreatic Stage</i>	
22 Aug. 2008	Phreatic event
31 Mar., 17 Apr., 6 & 27 May, 27 & 28 Jun., 5 & 10 Jul. 2010	Phreatic events
<i>Subplinian Stage</i>	
19 Jan. 2011	Phreatomagmatic event
26-27 Jan. 2011	Continuous activity including three subplinian events
27 Jan. 2011	Vulcanian event just prior to the third subplinian event
<i>Lava-accumulation Stage</i>	
28-29 Jan. 2011	Continuous emission of fine ash (phreatomagmatic)
28-31 Jan. 2011	Continuous lava accumulation event in the crater
28 & 30 Jan. 2011	Vulcanian events during lava accumulation
<i>Vulcanian Stage</i>	
1, 2, 3, 4, 6, 7, 9, 10, 11, 14, 18, 24 & 28 Feb., 1 Mar. 2011	Vulcanian events
7 to 9 Feb., 28 Feb. to 1 Mar., 3 to 4 Mar. 2011	Continuous ash emission events (phreatomagmatic)
8, 13, 23, & 29 Mar., 3 & 18 Apr. 2011	Vulcanian events
<i>Phreatomagmatic Stage</i>	
16, 23 & 29 Jun. to 1 Jul., 6 Aug., Aug. 31 to 6&7 Sep. 2011	Continuous ash emission events (phreatomagmatic)

the crater was widened to the north and ash clouds flowed outside the crater.

The eruptive events following the subplinian



**Fig. 2.** (Top) Vigorous ash emission and dome growth near the explosive vent in the summit crater on 28 January 2011. (Bottom) Growing dome filled the summit crater by the morning of 31 January. Taken by T. Kobayashi.

events are beyond our expectation. A lava dome appeared close to the vent of subplinian events within the crater, growing at a high effusion rate (see below). During the dome growth, vulcanian events occurred at the subplinian vent. Degassing may have occurred effectively without destruction of the growing dome. The lava dome grew, swelling and extending for four days, and covered the subplinian vent. Based on the information of dome growth including that from SAR images, the town officials of Takaharu Town, east of and nearest to Shinmoe-dake, decided by themselves to recommend evacuation of about 1100 people living in the area close to the volcano at the night of 30 January, because of the danger of pyroclastic flow. There was a high risk of intense vulcanian event due to insufficient degassing.

When an intense vulcanian event occurred on 1 February, the lava dome was deflated, and the vulcanian stage started. The eruption ended with phreatomagmatic events during June-September.

### 3. Discussion

The 1716-17 eruption was more explosive

than the 2011 eruption, and at least 5 subplinian events occurred being associated with pyroclastic flows of the scale larger than in 2011. The main phase of the 1716-17 eruption had continued for about three months, including multiple subplinian and vulcanian events (Imura and Kobayashi, 1991). It was preceded by a phreatic event 8 months before, and followed by the large subplinian event about 7 months after. During the subplinian events small-scale pyroclastic flows reached about 2 km from the crater. The total volume of the tephra (about  $0.07 \text{ km}^3$ ) is about 7 times larger than that of the 2011 eruption ( $0.7\text{-}1.2 \times 10^7 \text{ m}^3$ ). The sequence of the 2011 eruption was simpler than that of the 1716-17 eruption. However, it was more complex than that documented and geologically readable story of the 1716-17 eruption.

In the last eruption, the magma discharge rates were  $0.6\text{-}1.4 \times 10^6 \text{ kg/s}$  ( $240\text{-}560 \text{ m}^3/\text{s}$ ) for the first and second subplinian events and  $0.2\text{-}1.1 \times 10^6 \text{ kg/s}$  ( $80\text{-}440 \text{ m}^3/\text{s}$ ) for the first vulcanian and the third subplinian event. The rate for lava accumulation was one order of magnitude lower ( $1.0\text{-}1.3 \times 10^5 \text{ kg/s}$  or  $41\text{-}52 \text{ m}^3/\text{s}$ ), but as high as the rate that elsewhere has led to subplinian and vulcanian eruptions (Cashman, 2004; Pallister et al., 2013). The reason that rapid dome growth continued without transition to more explosive eruption is probably that degassing from the underlying

magma was effective through the vents of the subplinian events and fine-ash emission events. However, the second and third vulcanian events which occurred during the dome growth may have reflected insufficient degassing.

## References

- Cashman, K.V. (2004) Volatile controls on magma ascent and eruption, In Sparks, R.S.J. and C.J. Hawkesworth, Eds). “*The state of the planet: frontiers and challenges in geophysics*”, Geophysical Monograph, Amer. Geophys. Union, 109-124.
- Imura, R. and Kobayashi, T. (1991) Eruptions of Shinmoedake Volcano, Kirishima Volcano Group, in the last 300 years, *Bull. Volcanol. Soc. Japan*, 36, 135-148 (in Japanese with English abstract).
- Pallister, J.S., Schneider, D.J., Griswold, J.P., Keeler, R.H., Burton, W.C., Nyles, C., Newhall, C.G., Ratdonopurbo, A. (2013) Merapi 2010 eruption-Chronology and extrusion rates monitored with satellite radar and used in eruption forecasting. *J. Volcanol. Geotherm. Res.*, 261, 144-152.
- Nakada, S., Nagai, M., Kaneko, T., Suzuki, Y. and Maeno, F. (2013) The outline of the 2011 eruption at Shinmoe-dake (Kirishima), Japan, *Earth Planets Space*, 65, 475-488.

# From landslides to civil unrest: the implications of subduction zone earthquakes

Peter Bobrowsky<sup>a</sup>

<sup>a</sup>*Past Secretary General-IUGS, Adjunct Professor, Simon Fraser University, Burnaby, BC, Canada, V5A1S6  
ptbobrow@sfu.ca*

## 1. Background

It is clear that subduction zones have played an integral part in the collective history of the Earth's natural hazards for millennia. Like super-volcanoes and large comet/asteroids, subduction zones fall into the class of low frequency/high magnitude hazards (LF/HM). Events in this group of hazards tend to have recurrence intervals that range from centuries to millions of years. See for example the recent summary of recurrence intervals for paleotsunamis based on records associated with the Cascadia Subduction Zone (CSZ) of the Pacific Northwest of North America (Fig. 1; from Peterson et al. 2013). This infrequency in turn relegates these hazards to lesser prominence in the consciousness of human thought. Although the hazards are significant when they

do occur, and although they have long lasting repercussions, their infrequency provides us with a challenge with respect to raising awareness amongst the general populace.

The direct threats associated with such events, for example the eruption blast effects associated with a super-volcano or the shaking generated in a subduction zone earthquake, can be catastrophic since they tend to occur suddenly and simultaneously affect very large geographic areas. Some secondary hazards and effects are often given equal attention, for instance, the threat to aviation from volcanic ash-clouds or the threat of coastal damage associated with great-earthquake generated tsunamis. In most cases, damages to both the social and natural environments can be substantial.

Equally important but even less prominent is the multitude of secondary and tertiary ancillary threats, hazards and effects that accompany and follow the primary hazard. Few of these are appreciated or discussed, but all warrant due attention by the scientific community. In the long-term the intensity and magnitude of the ongoing effects diminishes progressively, much like the oscillation associated with the vibrating string of an instrument (Fig. 2). The illustration shown here taken from de Boer and Sanders (2002) highlights the far-reaching effects of a major eruption but applies equally well to subduction zone hazards.

Herein I propose that the critical assessment of subduction zones should extend beyond the primary effects of a large earthquake and associated tsunami. This essay gives brief consideration to the threats, hazards, and impacts linked to terrestrial slope instability arising from subduction zone earthquakes.



Fig. 1. CSZ tsunamis sites (Peterson et al. 2013).



Fig. 2. Vibrating string theory of far reaching effects taken from de Boer and Sanders (2002).

## 2. Subduction Zone hazards

In the minutes to days that follow any large earthquake generated along a subduction zone the primary focus is on the obvious: the energy released at the source, severity (intensity and magnitude), seismotectonics, peak acceleration at the surface, distance to source, travel path and near surface materials relative to infrastructure, response of structures to amplitude and duration of ground motion, fault ruptures, tsunami generation and propagation paths, inundation and run-up estimates, etc. These are important pieces of information that must be observed, compiled and interpreted to better characterize and understand the nature of the earthquake event.

In the chaos that immediately follows such an event the clearly visible are the easiest to comprehend: liquefaction, collapsed buildings, damaged infrastructure, subaerial landslides, secondary fires are a few of the common features observed in the aftermath. Less clear immediately would be the subaqueous landslides triggered by the earthquake including some of their effects or the pending damage which can result several months later from prominent aftershocks (cf. Stein and Toda, 2013).

Terrestrial landslides triggered by earthquakes are well documented around the world (Rodriguez et al. 1999). Those triggered by great earthquakes, although more difficult to confirm, have also been shown to exist. For example, Schulz et al. (2012) provided good

geochronological control linking two large rockslides to the January 1700 Cascadia great earthquake (Fig. 3).

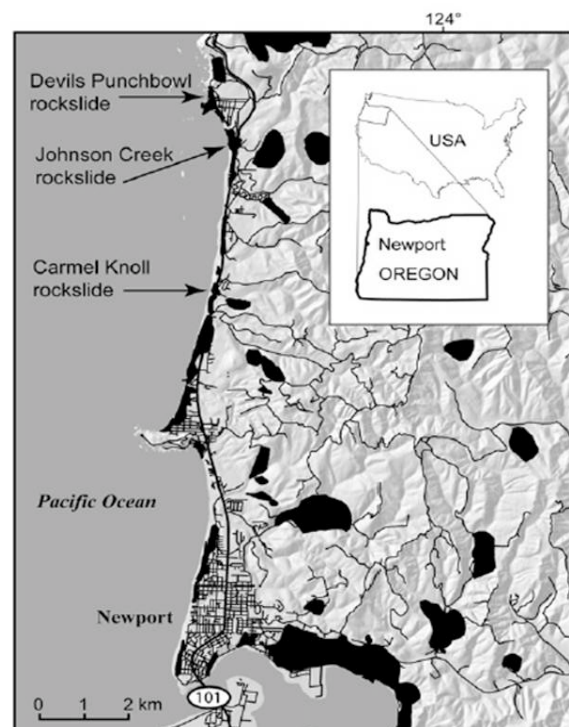
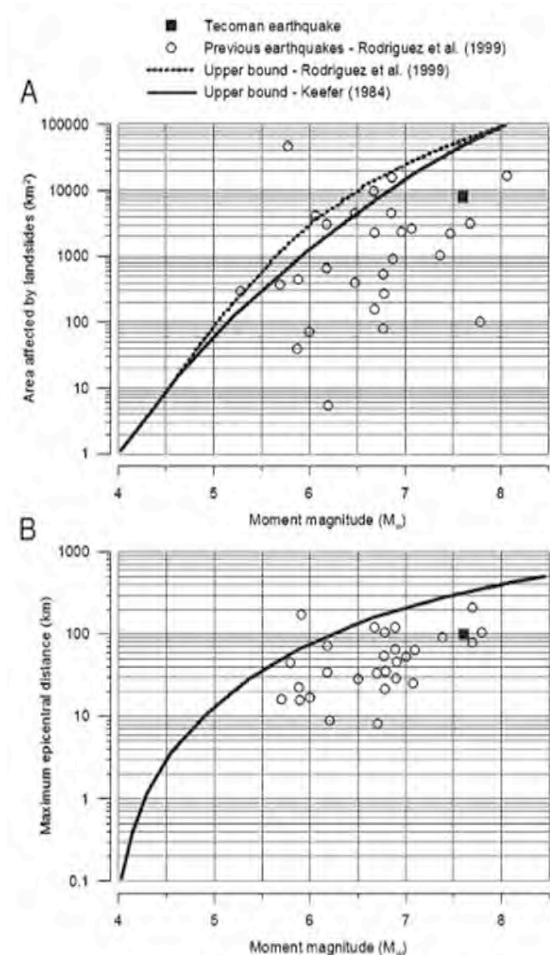


Fig. 3. Rockslides generated by 1700 great earthquake in Oregon, USA (from Schulz et al. 2012).

The 12 May 2008  $M_w$  7.9 Wenchuan, China earthquake generated thousands of damaging landslides. Indeed the slope instabilities triggered by this catastrophe are some of the best studied and documented associations recorded to

date (Qi et al. 2010).

The important point here is that landslides of much smaller magnitude are capable of generating landslides. Obviously site conditions (surficial materials, bedrock type, slope angle, vegetation), previous activity, distance to epicenter, etc. are factors that will control the presence and extent of earthquake triggered landslides. Keefer et al. (2006) looked at 100s of landslides triggered by the 21 January 2003 M 7.6 Tecoman, Mexico earthquake. Comparisons to other historic data shows landslides can be confidently linked to a range of earthquake magnitudes as low as about  $M_w$  5.5 (Fig. 4).



**Fig. 4.** Moment magnitude of earthquake vs. area affected landslides and landslide distance from epicenter (from Keefer et al. 2006).

Work by Collins et al. (2012) illustrated interesting spatial patterns in the in situ characteristics for the 100s of landslides generated in Japan by the 2007  $M_w$  6.6 Niigata

Chuetsu-Oki earthquake. Whereas Bommer and Rodriguez (2002) provided detailed and convincing far-reaching characterizations of landslides associated with two earthquakes in El Salvador.

Although not the focus of attention in this discussion, submarine landslides generated by landslides pose an equal problem. The study of such failures is complicated by difficulty of access especially when trying to link to particular earthquake events, nonetheless several successful studies completed examining this hazard (see for example Yamada et al. 2010)

### 3. Summary Comments

The impact of earthquake generated landslides is clear. Many and often most fatalities associated with earthquakes are the result of coeval slope failures (see for instance the death toll associated with the Wenchuan earthquake). Landslides can damage, destroy and bury homes, buildings, other types of structures, roads, railways, and so on. As a result they severely affect post-disaster emergency response efforts usually by disabling key transportation routes and other access. Large tracts of terrain that do not fail during the actual shaking often become metastable following an earthquake and thus becomes more prone to failure in the future due to other triggering mechanisms. Subaerial landslides triggered by earthquakes have been shown to generate tsunamis and seiches (Lastras et al. 2013).

The economic costs associated with earthquake triggered landslides have never been properly quantified. Total costs attributed to earthquakes rarely distinguish between direct and indirect costs and rarely distinguish between the affiliated damage causing factors: shaking, subsidence, slope failure, flooding, fires, etc.

In particular the hazard associated with mega-quake earthquake triggered landslides should be given greater attention, in particular as they pertain to societal and environmental vulnerabilities under the threat of future large  $M_w$  9 earthquakes.

## References

- Bommer, J.J. and C.E. Rodriguez (2002) Earthquake-induced landslides in Central America. *Engineering Geology* 63:189-220.
- Collins, B.D., Kayen, R. and Y. Tanaka (2012) Spatial distribution of landslides triggered from the 2007 Niigata Chuetsu-Oki Japan Earthquake. *Engineering Geology* 127:14-26.
- De Boer, J.Z. and D.T. Sanders (2002) *Volcanoes in Human History*. Princeton University Press, Princeton, 295 pages
- Keefer, D.K., Wartman, J., Ochoa, C.N., Rodriguez-Marek, A. and G.F. Wiczorek (2006). Landslides caused by the M 7.6 Tecoman, Mexico earthquake of January 21, 2003. *Engineering Geology* 86:183-197.
- Lastras, G. et al. (2013) Landslides Cause Tsunami Waves: Insights from Aysen Fjord, Chile. *EOS* 94(34):297-298.
- McAdoo, B.G., Pratson, L.F. and D.L. Orange (2000) Submarine landslide geomorphology, US continental slope. *Marine Geology* 169:103-136.
- Peterson, C.D., Clague, J.J., Carver, G.A. and K.M. Cruikshank (2013) Recurrence intervals of major paleotsunamis as calibrated by historic tsunami deposits in three localities: Port Alberni, Cannon Beach, and Crescent City, along the Cascadia margin, Canada and USA. *Natural Hazards* 68:321-336.
- Qi, S., Xu, Q., Lan, H., Zhang, B. and J. Liu (2010) Spatial distribution analysis of landslides triggered by 2008.5.12 Wenchuan Earthquake, China. *Engineering Geology* 116:95-108.
- Rodriguez, C.E., Bommer, J.J. and R.J. Chandler (1999) Earthquake-induced landslides: 1980-1997. *Soil Dynamics and Earthquake Engineering* 18:325-346.
- Schulz, W.H., Galloway, S.L. and J.D. Higgins (2012) Evidence for earthquake triggering of large landslides in coastal Oregon, USA. *Geomorphology* 141-142:88-98.
- Stein, R.S. and S. Toda (2013) Megacity Megaquakes – Two Near Misses. *Science*, 341:850-852.
- ten Brink, U.S., Barkan, R., Andrews, B.D. and J.D. Chaytor (2009) Size distributions and failure initiation of submarine and subaerial landslides. *Earth and Planetary Science Letters* 287:31-42.
- Yamada, Y., Yamashita, Y. and Y. Yamamoto (2010) Submarine landslides at subduction margins: Insights from physical models. *Tectonophysics* 484:156-167.

# Submarine landslides and marine geohazards

Kiichiro Kawamura<sup>abc</sup>

<sup>a</sup>*Graduate School of Science and Engineering, Yamaguchi University, 1677-1 Yoshida, Yamaguchi 753-8512, Japan, kiichiro@yamaguchi-u.ac.jp*

<sup>b</sup>*IFREE, JAMSTEC, 2-15 Natsushima, Yokosuka 237-0061, Japan*

<sup>c</sup>*ERI, University of Tokyo, 1-1-1 Yayoi, Bunkyo, Tokyo 113-0032, Japan*

## 1. Why submarine landslides now?

The submarine landslides are indirectly visible, but they affect directly our society. For example, tsunamis might be excited mostly by an active fault movement on a seafloor, but some of the tsunamis could be excited by large submarine landslides in coastal areas in the 1952 Alaska Earthquake and the 2010 Haiti Earthquake and in deep-sea in the 1896 Meiji Sanriku Earthquake as shown in Kawamura et al. (2011) (Fig. 1).

Underwater cables are cut suddenly by submarine landslides and related bottom currents. Such a cable cut accident damages economics as shown by Hsu et al. (2008) (Fig. 1). These submarine landslides are historical events. We have various observation data in the events, but we can not understand its mechanism yet.

In contrast to the historical events, we have disclosed submarine landslide topography using Echo sounder system. The Storegga Slide in Norwegian Sea is one of the famous submarine landslides as a geological events (Fig. 1). This slide of about 800 km long and about 200 km width is the largest slide in Quaternary. The slide has been formed since about 8100 yr BP. The trigger mechanism of this slide might be related to methane hydrate decomposition, but it is not well understood. At this area, natural gas is exploited and produced carefully and also safely on the basis of the marine geological and geotechnical studies.

Thus, we need further submarine landslide studies for marine geo-hazards and marine

exploitation.

## 2. Can we predict submarine landslides?

Basically, we do not know the formation mechanisms and also processes of submarine landslides. The mechanism of submarine landsliding is thought to be earthquake shaking, pore pressure increment, slope steepening and so on. Most of the previous studies calculated simply slope instability on each marine slope to evaluate the probability for the submarine landslides. This calculation is based on a case that submarine landslides are formed by earthquake shaking. But the trigger mechanism in various natural examples might be complicated. Some of the researchers challenged to understand the formation mechanisms using soil mechanics experiments (Sultan et al., 2004). We would need more descriptive and also experimental studies to understand the formation mechanism. This is the first step for a prediction of the submarine landslides.

## 3. Future for submarine landslide studies

We have an international community for the submarine landslide study; IGCP585 E-MARSHAL ([www.igcp585.org](http://www.igcp585.org)). Aim of our community is to understand various submarine landslide problems of all around the world.

## References

Kawamura, K., Sasaki, T., Kanamatsu, T., Sakaguchi, A. and Ogawa, Y., 2012, Large submarine landslides in the Japan Trench: A new scenario for additional tsunami generation, *Geophys. Res. Lett.*, 39, L05308, doi:10.1029/2011GL050661.

Hsu, S.-K., Kuo, J., Lo, C.-L., Tsai, C.-H., Doo, W.-B., Ku, C.-Y., Sibuet, J.-C., 2008. Turbidity currents, submarine landslides and the 2006 Pingtung earthquake off SW Taiwan. *J. Terre. Atmos. Ocean Sci.* 19 (6), 767–772.

Sultan, N. et al. (2004) Triggering mechanisms of slope instability processes and sediment failures on continental margins: a geotechnical approach. *Mar. Geol.*, 213, 291-321.

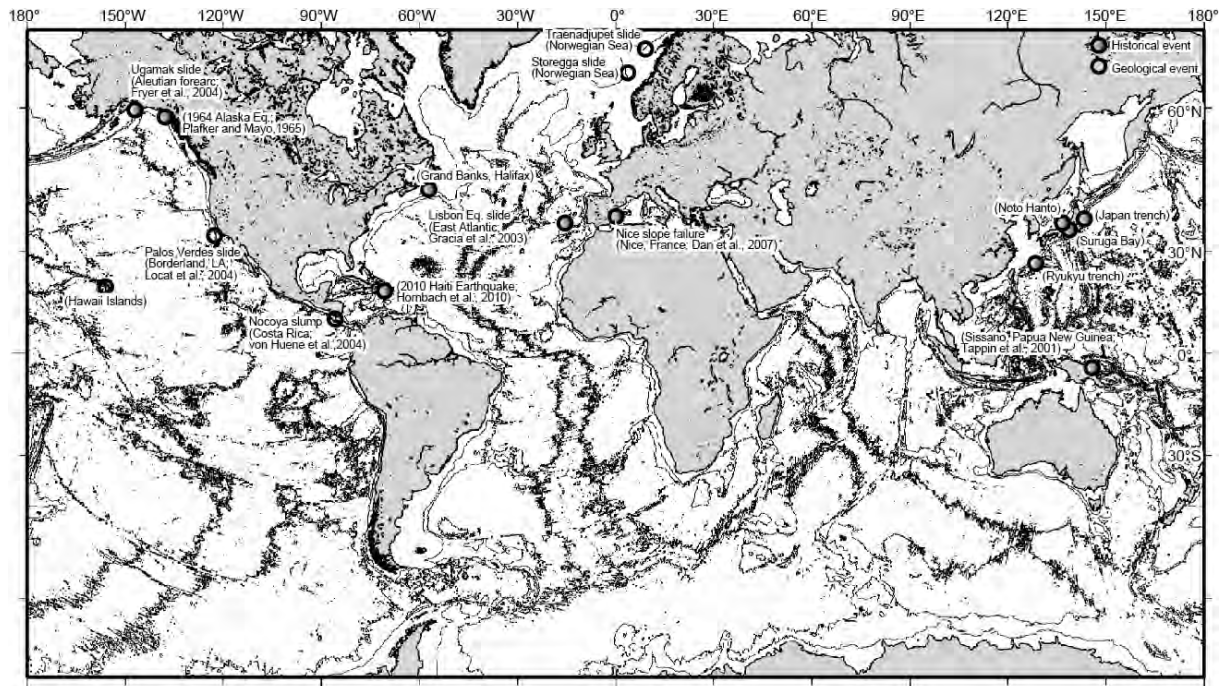


**Fig. 1.** Major submarine landslides identified from historical and geological records.

# Landslides in tectonically active countries

Masahiro Chigira<sup>a</sup> and Toshitaka Kamai<sup>a</sup>

<sup>a</sup>*Disaster Prevention Research Institute, Kyoto University, Gokasho, Uji 611-001, Japan, chigira@slope.dpri.kyoto-u.ac.jp*

## 1. Introduction

Landslide is one of the most fatal hazards in tectonically active countries, although earthquake or volcanic eruption itself has been paid big attention as causes of fatal natural hazards. Asia is the most landslide-susceptible area in the world, and every year we have been experiencing devastating landslides, which have been induced by rainstorms, earthquakes, and snowmelt alongside of other complicating factors. Recent triggers include 2011 typhoon Talas and the Tohoku earthquake in Japan, 2009 typhoon Molakot in Taiwan, 2009 Padang earthquake in Indonesia, and 2008 Wenchuan earthquake and following rainstorms in China. Important thing is that even a landslide induced by rainfall may have been the cumulative result of repeated earthquakes and rainfalls.

In order to mitigate landslide-induced disasters, one of the most effective ways, is to know where and when landslides occur and to keep away from those susceptible areas or evacuate from there in appropriate timing. Rock or debris-slide avalanches, in particular, are very hazardous and must be predicted and considered to be prepared for, because they commonly occur suddenly and rapidly travel long distance, devastating wide areas.

We have been studying geological and geomorphological features of catastrophic rock and debris-slide avalanches in Asian countries and reached to the conclusions that they could be predicted at least as potential sites. Most of the catastrophic rockslide-avalanches induced by either rainstorms or earthquakes are preceded by a certain type of gravitational slope deformation, but debris slide-avalanches of pyroclastic fall deposits are not. The latter is induced by

earthquakes in areas of a particular type of successions of pyroclastics, which involve heavily weathered pyroclastics or paleosol in the depths. The features as above could be used as criteria for the prediction of potential sites of catastrophic landslides.

## 2. Earthquake induced landslides

Earthquakes induce landslides not only on natural slopes but also on man-made valley fillings for residential houses. Those landslides occurred in many locations in 1978 Miyagiken-oki earthquake in Japan, and thereafter during 1995 Kobe and 2011 Tohoku earthquakes. Earthquake tremors are amplified on higher slopes and also in valley filling loose materials, which is one of the major reasons why landslides are induced by earthquakes. However, such amplification phenomena have not been studied enough. We are now monitoring seismic behavior in mountains and man-made valley fills and analyzing its effects on landslide initiation.

Recent earthquakes, the 2011 Tohoku earthquake, the 2009 Padang earthquake, the 2008 Wenchuan earthquake, the 2008 Iwate-Miyagi Inland earthquake, the 2005 northern Pakistan earthquake, and the 2004 Mid-Niigata-Prefecture earthquake, gave us lessons about where and why large, catastrophic landslides are induced by earthquakes: those landslides had specific preparatory processes, mechanical or chemical, to be induced by earthquakes.

The 2011 Tohoku earthquake induced long run out catastrophic landslides in pyroclastic fall deposits with a sliding surface in halloysite-rich paleosol, which once was made by chemical weathering and has been resiltified so that

gibbsite changed to halloysite. Halloysite is very fragile against shaking and has been a major component of sliding surface materials of landslides during many earthquakes including the 2009 Padang earthquake. Dissolution of carbonate by groundwater was another chemical preparatory process of landslides induced by the 2008 Wenchuan earthquake.

Mechanical preparation for earthquake-induced large landslides is deep-seated gravitational slope deformation, which preceded many landslides involving the Daganbao landslides by the Wenchuan earthquake and the Chiu-fen-erh-shan and the Tsaoling landslides during the Chi-Chi earthquake. Deep-seated gravitational slope deformation deteriorates rocks, which would become more susceptible to earthquake tremor. River erosion that undercut previous landslides, once collided to the opposite slope, is another important mechanical preparation for the landslides reactivated by earthquakes. There occurred many such catastrophic landslides during the Mid Niigata prefecture earthquake and the northern Pakistan earthquake.

Rainfalls that precede an earthquake could strongly affect the occurrence of landslide. 2004 Mid-Niigata-Prefecture earthquake, Japan induced many landslides, but 2007 Noto-hanto, and 2007 Off-Mid-Niigata-Prefecture earthquakes induced very limited number of landslides even though they caused similar earthquake tremor in the areas with the similar geologic and geomorphic settings with those of 2004 Mid-Niigata-Prefecture earthquake. The difference landslide occurrence may be due to the preceding rainfalls of these earthquakes; 2004 Mid-Niigata-Prefecture earthquake had been preceded by more than 100-mm rainfall within three days before the earthquake, but the other earthquakes had been preceded much less amounts of rainfall.

### **3. Rainfall-induced landslides**

In addition to earthquakes, most of the Asian

countries are located in monsoon area, where large amounts of precipitation increase the risk of landslides. To predict potential sites of shallow landslides by rainstorms were studied deterministically using physical models. However, such a modeling needs geometrical data and mechanical properties, which vary widely and could not be estimated appropriately. Potential sites of shallow landslides may thus not be easily identified. Instead, deep-seated landslides occur with very site-specific geologic and geomorphic conditions; many of them are preceded by gravitational slope deformation, which recently has been found to be very characteristic. Deep-seated gravitational slope deformation that preceded catastrophic failures induced by typhoon Talas 2011 Japan, had been surveyed with airborne laser scanner beforehand, of which high-resolution DEMs gave us an important clue to identify which type of topographic features of gravitational slope deformation is susceptible to catastrophic failure. We found that 26 of 39 deep-seated catastrophic landslides had small scarps along the heads of future landslides. These scarps were caused by gravitational slope deformation that preceded the catastrophic failure. Although the scarps may have been enlarged by degradation, their sizes relative to the whole slopes suggest that minimal slope deformation had occurred in the period immediately before the catastrophic failure. The scarp ratio, defined as the ratio of length of a scarp to that of the whole slope both measured along the slope line, ranged from 1% to 23%. 38% of the landslides with small scarps had scarp ratios less than 4%, and a half less than 8%. This fact suggests that the gravitational slope deformation preceded catastrophic failure was relatively small and may suggest that those slopes were under critical conditions just before catastrophic failure. The other landslides also had been preceded by gravitational deformation, which could have been identified using high-resolution DEMs by LiDAR.

# Landslide Detection by Broadband Seismic Network

Cheng-Horng Lin<sup>a</sup>

<sup>a</sup>*Institute of Earth Sciences, Academia Sinica, P O Box 1-55, Nankang, Taipei, Taiwan, lin@earth.sinica.edu.tw*

Fatal disasters caused by landslides have significantly increased recently as the frequency of extreme rainfalls associated with climate change has increased in the world. The situation in Asia is becoming worse due to typhoons in eastern Asia and the southwest monsoon along the southern edge of the Himalayas. For example, one of the most recent fatal disasters by landslides occurred in Taiwan during Typhoon Morakot in 2009 killed 474 residents in the Hsiaolin village. Thus, landslide disasters have become an important issue in global natural hazards.

In fact, landslides may generate extremely long-period (>10 s) seismic signals that propagate over long distances (Lin et al., 2010). Thus, it is important to develop a seismic monitoring system for detecting extremely long-period signals generated by landslides using a regional broadband seismic network.

A band-pass filter with periods between 20 and 50 s can efficiently enhance the signal from the seismic energy generated by the landslide. The arrivals of the first peaks in the extremely long period seismic signals were measured to identify the source location. Using the arrival times of the seismic signals measured at the individual stations, we have located the source of the landslide using the traditional hypocenter determination method (HYPO77). For the Hsiaolin landslide, the estimated source was about 8 km away from the verified location in the field. This difference may be due to errors in the arrival time measurements or the simplified 1-D velocity model.

Based on careful examination of seismic records from BATS and F-net, we have identified a number of large landslides or submarine slumps on 8 August (Fig. 1). Most of landslide earthquakes were located in mountainous terrain where the accumulated

rainfall totals were extremely high (> 2000 mm). In addition to these landslide earthquakes, we also found sources located off the southern coast of Taiwan. Most of the offshore events were located around canyons and steep continental slopes. Thus, these offshore events might have been associated with submarine slumping and/or debris flows caused by huge amounts of sediments that were carried into this region by rivers during the significant floods in southern Taiwan. In particular, several offshore events clustered along Kaoping Canyon (Figure 1). In fact, during Typhoon Morakot, some submarine cables were also damaged in the area offshore southern Taiwan. Thus, our detection of offshore landslide earthquakes suggests that the damage to these submarine cables off the southern coast of Taiwan were due to slumping or debris flow along the canyons or bathymetric slopes.

Our results showed that inland landslides and submarine slumps were successfully detected using data from broadband seismic networks. A dense broadband seismic network will play a new role in monitoring landslides and mitigating their hazards in the future.

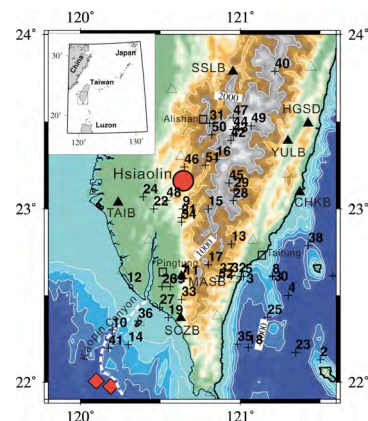


**Fig. 1.** Locations of large landslides (cross), broadband seismic stations (triangles), the Hsiaolin village (red circle), Kaoping canyon (heavy dashed line) and the previously damaged submarine cables (red diamonds) in the southern Taiwan area

# Preliminary Study on the Seismotectonics of the 2013, Lushan Ms7.0 Earthquake, West Sichuan

Dong Shuwen<sup>a</sup>, Zhang Yueqiao<sup>b</sup>, Hou Chuntang<sup>b</sup>, Shi Jusong<sup>b</sup>, Wu Zhonghai<sup>b</sup>,  
Li Hailong<sup>b</sup>, Sun Ping<sup>b</sup>, Liu Gang<sup>a</sup> and Li Jian<sup>a</sup>

<sup>a</sup> Chinese Academy of Geological Sciences, Beijing, 100037 China, dic@cags.ac.cn

<sup>b</sup> Institute of Geomechanics, Chinese Academy of Geological Sciences, Beijing, 100081 China

On April, 20, 2013, an earthquake with a magnitude of Ms7.0 shocked the region of Lushan County, Yaan City, west Sichuan. The epicenter is located in zone between Shuangshi and Taiping Townships, with the focal depth of about 13-14 km. The maximum intensity degree attained IX. Although severe destruction of buildings in the shocked area, field investigation did not find obvious co-seismic surface rupture, except a small quantity of grand fissures with sand liquidation. Integrate analysis of high resolution satellite images, main-and-after shock distribution and focal mechanism shows that this earthquake is an independent reverse faulting event possibly rupturing the southern segment of the Shuangshi-Dachuan fault, along the SW segment of the Longmenshan fault zone. We infer that the main shock may have occurred on a west-dipping ramp (with dipping angle of 33-43°) of a sole décollement beneath the SW Longmenshan, a similar seismotectonic setting of the Wenchuan earthquake. Historically, there recorded at least two earthquakes with magnitude of Ms6-6.5 along the Shuangshi-Dachuan fault, together with the Lushan earthquake, they characterize the fault activity behavior of this fault zone. In-situ stress measurement results show that this earthquake resulted from the brutal release of accumulated crustal stress within the SW segment of the Longmenshan fault zone.

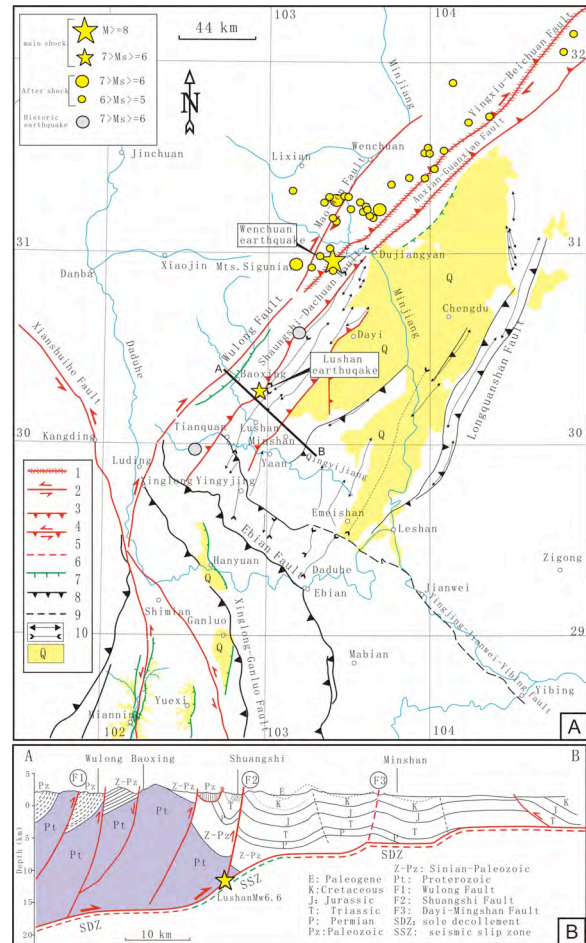


**Fig.1. (A)** Map showing the neotectonic and active faults in the south-central segment of the Longmenshan structural zone and locations of the epicenters of the Wenchuan earthquake and Lushan earthquake. 1-surface rupture of the Wenchuan earthquake; 2- active strike-slip fault; 3- active reverse fault; 4- active strike-slip and reverse fault; 5- inferred fault; 6- Late Quaternary normal fault; 7- late Cenozoic reverse fault; 8- inferred Late Cenozoic fault; 9- Late Cenozoic fold; 10- Quaternary sediments; **(B)** Structural cross-section of the southwestern segment of the Longmen Mountains.

# Strong motion records from the April 20, 2013 Lushan Earthquake, China

Ruizhi WEN<sup>a</sup>, Yefei REN<sup>a</sup> and Xutao HUANG<sup>a</sup>

<sup>a</sup> Institute of Engineering Mechanics, China Earthquake Administration, Harbin 150080, China, ruizhi@iem.ac.cn

## 1. Introduction

On April 20, 2013, at 08:02am local time, a strong  $M_s7.0$  earthquake hit Lushan, a county of southwest of Sichuan Province in China. (<http://www.csndmc.ac.cn/newweb/index.jsp>). Most of the rural dwelling suffered a significant level of damage near the epicenter area and several small cities and village suffered severe damage, causing 196 death, 1000 injured and 10000 homeless.

National Strong Motion Observation Network System (NSMONS) of China managed by the China Earthquake Administration recorded the acceleration data in Lushan earthquake sequences. The main shock was recorded by 126 digital strong motion instruments. For the local network, Chengdu rapid earthquake intensity system, built by the local municipality after 2008 Wenchuan earthquake, 65 strong motion station triggered in this event. It is the first time in China that the local network could provide such high quality observation data to the public. Locations of those triggered free-field stations for main shock recordings are shown in Fig.1. It shows the distribution of the stations in local areas including parts of Sichuan, Yunan and Sanxi Province. The strong-motion records from Lushan earthquake have filled a gap for near-fault records from medium earthquake in China mainland.

## 2. Comparison with GMPEs

Table 1 shows the locations of the strong motion stations closest to the epicenter together with surface projected rupture. According to the

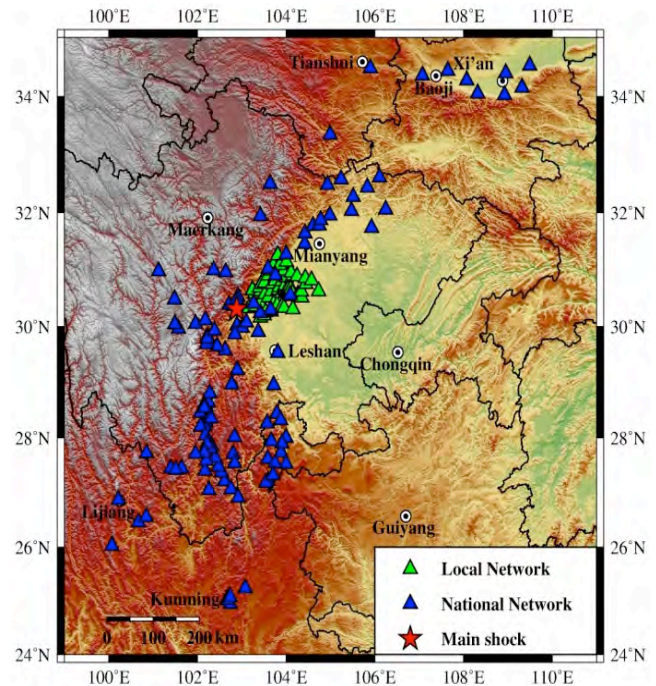


**Fig.1.** Triggered strong motion stations in Lushan  $M_s7.0$  Earthquake

Chinese seismic code, the borehole profile is usually to 20 m depth and the average shear-wave velocity is calculated from the top soil layer of 20 m depth ( $V_s20$ ). The average shear-wave velocity from the surface to 30 m depth ( $V_s30$ ) is now usually adopted as an international standard for site classification. For NSMONS, some stations do not have adequate borehole information and the depth usually less than 20m. To obtain  $V_s30$ , the extrapolation method was used assuming a constant velocity from the ensuing depth to 30m, as the shear wave velocity should not have much variation at depth (Boore, 2001). Wen et al. (2011) provided

the site classifications of 77 near-fault stations by using the HVSR method and the response spectral shapes (RSS) method. When employing the GMPEs, required input parameters are calculated by the parameters by the finite fault mode using far field body wave records (Wang et al, 2013). Joyner-Boore distance,  $R_{JB}$ , the rupture distance,  $R_{RUP}$ , and epicenter distance  $R_{epi}$ , are also calculated. It could remarked that four stations fall inside the hanging wall of the fault, that is 51BXY, 51BXZ, 51BXD and 51LSF.

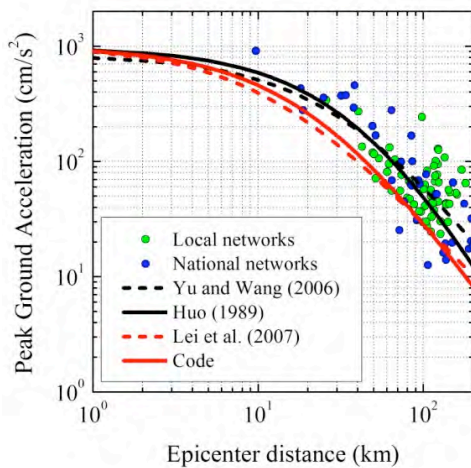


**Fig.2.** Comparison with Chinese GMPEs by geometrical horizontal PGA recorded from national and local network

### 3. Observed near-field strong motion records

Typical strong motion records and some related parameters are shown in Fig.3 and Table 1. Among the acceleration records from the main shock, the largest PGA was recorded at 51BXD station in Baoxing Wenchuan County. PGAs recorded in the EW, NS, and UD directions are -1005 Gal, 824 Gal and 478 Gal, respectively. It is the first record that PGA exceeded 1g in Chinese strong motion history. Even in 2008 Wenchuan Earthquake, the maximum PGAs recorded at Woulong Station did not exceeded 1g, that is the EW, NS and UD directions are 824.1 Gal, 802.7 Gal and 622.9 Gal, respectively. It should be a milestone in Chinese strong motion history. The 51BXD record is followed by the record obtained at 51BXZ station in Baoxing Country, PGAs recorded in EW, NS and UD directions are 583gal, 316gal and

387gal. Both 51BXD and 51BXZ are sitting on the outcropping and could be classified to the rock station which contains the high frequency and amplitude for the near field.

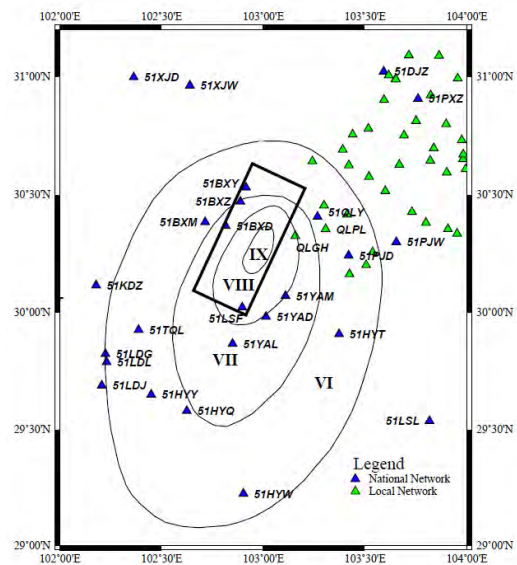


**Fig. 3.** Macro Intensity map and triggered strong motion stations

**Table. 1.** Typical strong motion records

Code	Site	$R_{epi}$ (km)	PGA (cm/s <sup>2</sup> )		
			EW	NS	UD
51BXD	Rock	9.7	-1005.3	823.6	478.1
51BXZ	Rock	18.2	583.2	316.4	-387.2
51BXY	Soil	24.9	429.2	-298.6	244.4
51BXM	Soil	18.7	-387.2	199.8	132.1
51LSF	Soil	31.9	387.4	357.0	-267.4
51YAD	Soil	38.4	-524.4	398.6	196.3
QLGH	Soil	25.9	375.8	-308.0	222.1
QLPL	Rock	40.4	318.3	230.6	84.5

### 4. Observed far-field strong motion records

In the far field, many records were also obtained. Although the epicenter distance of the station is nearly 600 km. Those 7 stations which about 500km away form the epicenter and the maximum PGA are less then 4gal, but still enough to show site effect. We chose 53CHA as the reference site since it shows a flat H/V ratio over the available frequency band of engineering. By the traditional H/V method, the amplification factors of high frequency components are

smaller than those of low frequency components. The amplification factors is higher when the period greater then 1s. During 2008 Wenchuan earthquake, the abnormal macro intensity along basin edge from Baoji to Meixian in the Weihe basin induced from combined amplification effects of both soil sites and basin edge effects on ground motions.

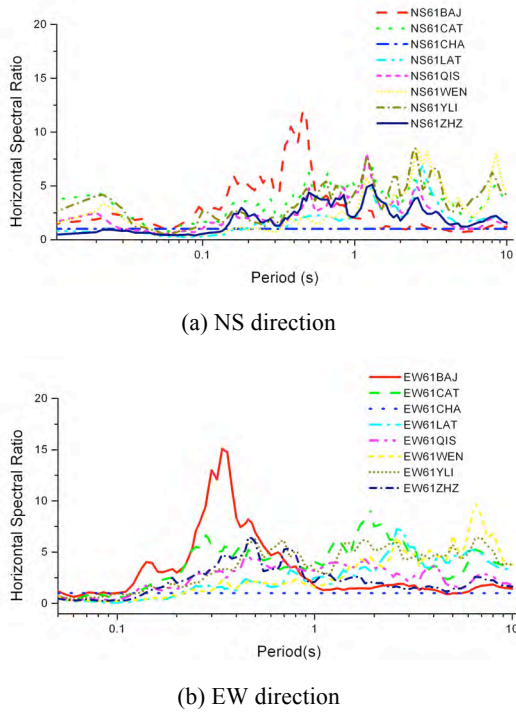


Fig.4. Horizontal spectral ratios

### 5. Strong motion with surveyed macroseismic intensity

Historical seismicity regarding Longmenshan area and the surrounding area had caused heavy and extensive damage. This earthquake shows a striking similarity with the 2008 sequence available historical data accounts for heavy damage. Housner Intensity  $I_H$  (Housner 1952) can be an effective parameter to correlate the severity of seismic motions to structural damage, particularly in cases of existing non-ductile Reinforced Concrete (RC) buildings

$$I_H = \int_{T_1}^{T_2} S_v(T, \xi) dT$$

where  $T$  is the fundamental period of the structure under examination,  $\xi$  is the damping ratio (assumed equal to 5% in the analyses

developed in this article),  $T_1$  and  $T_2$  define the interval of period values where ordinary buildings can be mostly placed. Whit regard to the computation of  $I_H$ , it is worth noting that it is usually computed in the period range [0.1–2.5] s, while period range [0.2–2]s has been used in accordance.EMS-98.A comparison between the recorded data in terms of  $I_H$  values corresponding to different macroseismic intensity scales are shown in Fig 5. It also shows the step relationship between  $I_H$  values and the ordinal macro seismic intensity according to EMS-98. The same  $I_H$  value could be classified to different macroseismic intensity. Although  $I_H$  value calculated from [0.2–2]s is much better than from [0.1–2.5]s, but still does not good enough. Comparisons in terms of  $I_H$  show that the values computed using code spectra are generally comparable with the ones from recorded data. Furthermore, code values are generally higher than those observed when considering. When integral parameters are considered, the results achieved in the present study show that the difference is great when using Housner Intensity as reference parameter of ground motion to map the Chinese macroseismic intensity.

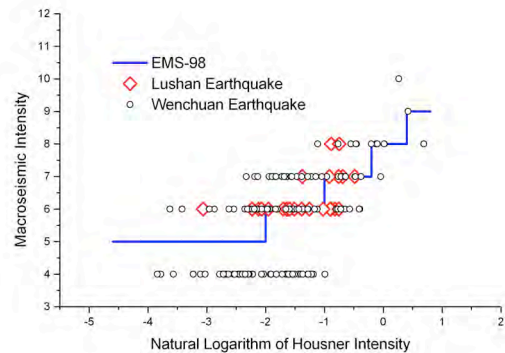


Fig.5. Macroseismic intensity respect to  $I_H$  for Lushan and Wenchuan data, period range [0.2–2]s

### 6. Couclusion

The Lushan earthquake occurred on April 20, 2013 is another destructive event after Wenchuan Earthquake in 2008. The preliminary characteristics of these recordings were given

including the station spatial locations. The analyzed results show the characteristics of predominant high-frequency components and short duration for this event. The observed PGAs and spectral accelerations were also compared with the ground motion prediction equation commonly used in China, which shows the observed PGAs and high-frequency spectral accelerations have a good agreement with the empirical predicted ones but the moderate and long-period components are remarkably higher.

Journal Geophysics, 56(4): 1412-1417. (in Chinese)

WEN Ruizhi, REN Yefei, QI Wenhao, et al. (2013) The maximum acceleration recording from Lushan Earthquake on April 20, 2013[J]. Journal of Southwest Jiaotong University. (in Chinese).

## References

- BOORE Dave (2001) Effect of baseline corrections on displacements and response spectra for several recordings of the 1999 Chi-Chi, Taiwan[J]. Bulletin of the Seismological Society of America, 91(5): 1199-1211
- HOUSNER Geogre (1952) Intensity of ground motion during strong earthquakes. Second technical report. California Institute of Technology, Pasadena, California.
- LEI Jiancheng, GAO Mengtan and YU Yanxiang (2007) Seismic motion attenuation relations in Sichuan and adjacent areas[J]. Acta Seismologica Sinica, 29(5): 500-511.
- HUO Junrong (1989) Study on the attenuation laws of strong earthquake ground motion near the source[D]. Ph.D. Dissertation, Institute of Engineering Mechanics, China Earthquake Administration.
- Standard of Peoples Republic of China. The Chinese Seismic Intensity Scale (GB/T 17742-2008)[S]. 2008. (in Chinese)
- YU Yanxiang and WANG Suyun (2006) Attenuation relations for horizontal peak ground acceleration and response spectrum in Eastern and Western China[J]. Technology for Earthquake Disaster Prevention, 1(3): 206-217.
- WANG Weimin, HAO Jinlai, YAO Zhenxing (2013) Preliminary result for rupture process of Apr. 20, 2013, Lushan Earthquake, Sichuan, China[J]. Chinese

# Proposals to revise ISC-GEM earthquake catalog

Yuzo Ishikawa<sup>a</sup>

<sup>a</sup>*G-EVER Promotion Team, Geological Survey of Japan, AIST, 1-1-1 Higashi, Tsukuba, Ibaraki 305-8567, Japan, catfish@wa2.so-net.ne.jp*

## 1. Introduction

It is important to edit the accurate earthquake catalogue for evaluating realistic disaster in the world. Many seismologists presented earthquake catalogues. For example, catalogues by Abe (1981), Abe & Noguchi (1983), Engdahl & Villaseñor (2002), and Utsu (2002) were famous. Recently, ISC released ISC-GEM Global Instrumental catalogue (Version 1) in 31 Jan, 2013 (Version 1.03 on 11 June). It is much better than The Centennial Catalog (Engdahl and Villaseñor, 2002). ISC used Abe's catalogue (1900-1903), Gutenberg Notepads (Abe's adaptation) (1904-1917), BAAS Bulletin (1913-1917) and ISS Bulletin (1918-1963). But, in the early 20 century not all seismic stations in Japan and Taiwan were reported to BAAS Bulletin and ISS Bulletin. We will be able to add new hypocenters to ISC-GEM using these seismological reports. And ISC-GEM catalog adopted the cut-off magnitudes like 1900-1917:  $M_s \geq 7.5$  (worldwide + smaller shallow events in stable continental areas), 1918-1959:  $M_s \geq 6\frac{1}{4}$ , 1960-2009:  $M_s \geq 5.5$ . In this case, everyone thought that most of the deep events would not be included. The catalogue of damaging earthquakes in the world by Utsu (2002) was used to check ISC-GEM catalogue.

## 2. Deep and intermediate deep earthquakes

Figure 1 shows the depth—time distribution. The upper one is from ISC-GEM and shows dense distribution after 1960, but sparse before 1940. The lower one is from Utsu catalogue and showed more events before 1920 than the It is difficult to follow the move history of the station, now. But correct values were needed It

upper one. Several events in and around Taiwan and Japan were selected to determine hypocenters. The software HYPOSAT (Schweitzer, 2003) and new station coordinates were used to determine hypocenters in and around Japan and Taiwan.

## 3. The coordinate of station locations

The other important data is station locations. Locations of seismic stations must be unified by the WGS84 coordinate system. For example, in Taiwan, two stations were compared by my new observation as followed,

TAI, TAI, 22.99520, 120.19700, 14.0 ISC  
TAINAN, 22.99372, 120.20522, 13 new  
Difference 0.00148 -0.00822

TAP, TAP, 25.03930, 121.50600, 6.0 ISC  
TAIPEI, 25.03755, 121.51472, new  
Difference 0.00175 -0.00872

The distances from ISC location to new value are about 1km and it is mainly caused by the change of coordinate system from Tokyo Datum or TWD67 to TWD97 (WGS84). So, it is very important that the same coordinate system should be used to determine hypocenters.

The other important information is the history of the station movement. For example, the Shanghai station named Zikawei in China was listed in the station listing of ISC as followed,

ZKW, 31.18330, 121.43300, 7.0

But this station moved twice as followed  
ZKW1, 31.19250, 121.42361: 1904/01/22  
-1910/05/

ZKW2, 31.19250, 121.43055: 1910/05/ -1912/01/  
ZKW3, 31.19222, 121.43000: 1912/01/ -1951

It is difficult to follow the move history of the station, now. But correct values of station

locations were needed to re-determine hypocenter accurately.

### References

- Abe, K. (1981) Magnitudes of large shallow earthquakes from 1904 to 1980, *Physics of the Earth and Planetary Interiors*, 27, 72-92.
- Abe, K. and S. Noguchi (1983) Determination of magnitude for large shallow earthquakes 1898-1917, *Physics of the Earth and Planetary Interiors*, 32, 45-59.

Engdahl, E. R. and A. Villasenor(2002) : Global seismicity : 1900-1999, *International handbook of earthquake and engineering seismology*, ed. W. H. K. Lee et al., Academic Press, 665-690.

Utsu, T., 2002, A list of deadly earthquakes in the World: 1500-2000, in *International Handbook of Earthquake and Engineering Seismology Part A*, edited by Lee, W.K., Kanamori, H., Jennings, P.C., and Kisslinger, C., pp. 691-717, Academic Press.

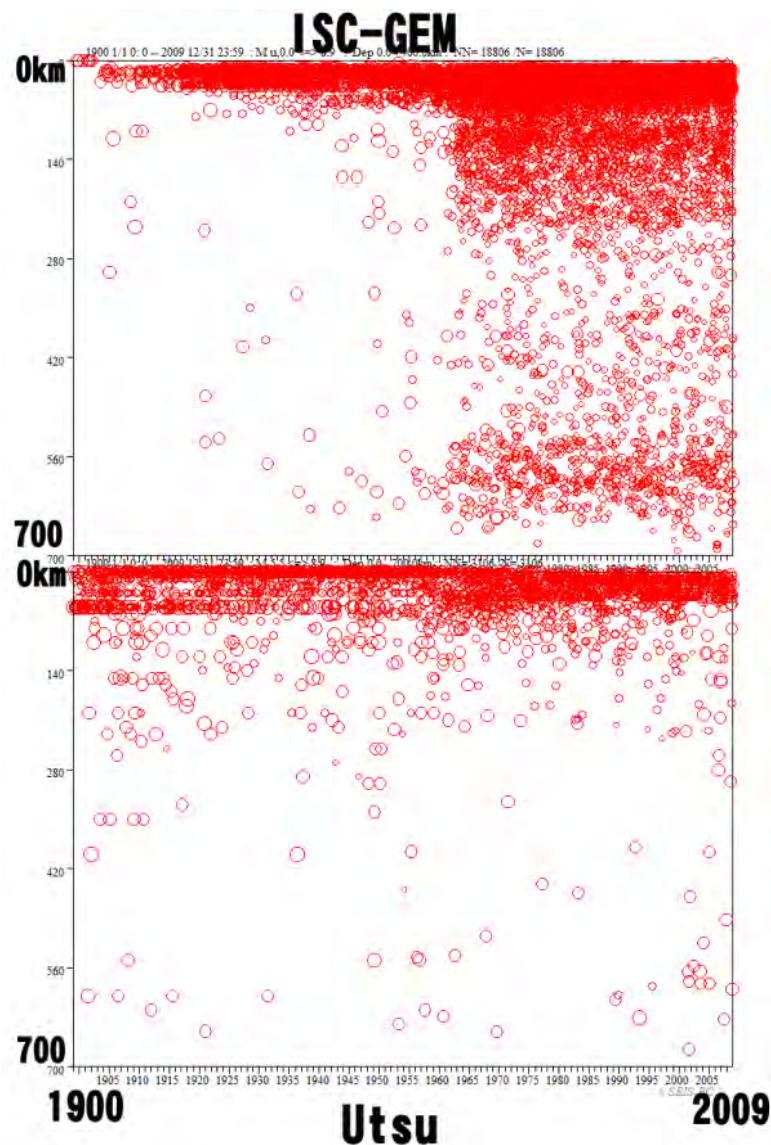


Fig. 1. Depth changes of hypocenters in ISC-GEM and Utsu's catalogues.

# Scenario-based Tsunami Hazard Assessment for the coast of Vietnam from the Manila Trench source

Nguyen Hong Phuong<sup>a</sup>, Vu Ha Phuong<sup>a</sup> and Pham The Truyen<sup>a</sup>

<sup>a</sup>*Institute of Geophysics, Vietnam Academy of Science and technology, 18 Hoang Quoc Viet street, Cau Giay District, Hanoi, Vietnam, phuong.dongdat@gmail.com*

## 1. Introduction

Although no historical records of the occurrence of tsunamis in the past are available in the country up to now, there is no denying the fact that the Vietnamese coast can be threaten by tsunamis generating from the sources inside the East Vietnam sea. Based on the analysis of tectonic feature and geodynamic characteristics of regional faults systems in the southeast Asia, 9 source zones capable of generating tsunamis affecting Vietnamese coast were delineated in the South China Sea and adjacent sea areas. Among the tsunami source zones defined in the East Vietnam sea region, the Manila trench, west of the Philippines is considered as the most dangerous for the Vietnamese coast. The recent research results show that the maximum expected earthquake magnitude for the Manila Trench source zone may reach to the value of  $M_w = 8.7$ , and it takes approximately 2 hours for a tsunami from this source zone to hit the Vietnamese coast at the earliest.

## 2. Seismotectonic characteristics of the Manila trench source zone

Tectonic and geodynamic characteristics of the Manila trench has been studied by many investigators. The Manila Trench is the 1200 km-long submarine expression of the east-dipping South China Sea subduction zone, which initiated in the early Miocene (22–25 Ma) and remains active to the present day.

Along this subduction zone, the oceanic crust of the South China Sea descends eastward beneath the Philippines, southernmost Taiwan and the intervening ocean floor. The broadly

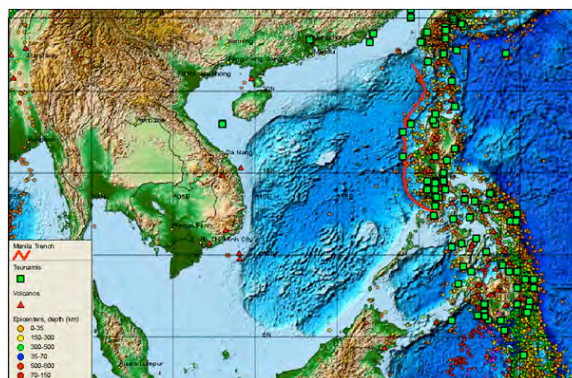


**Fig. 1.** Location of the Manila trench and distribution of earthquakes, volcanoes and tsunamis events in the South China sea. The data is in the time period from 1975 up to now and taken from 2010 are taken from NEIC. The moment magnitude is in the range from 5.0 up.

convex-westward shape of the Manila Trench is due to the westward migration of Luzon over the subducting oceanic slab, while the southern and northern ends of the trench are pinned at collisions at the latitudes of Palawan Island ( $12^{\circ}\text{N} - 120^{\circ}\text{E}$ ) and southern Taiwan ( $23^{\circ}\text{N} - 120^{\circ}\text{E}$ ).

Using a catalogue of earthquakes and focal mechanism data in northern Luzon, the Philippines, Bautista C. et al (2001) studied the tectonic characteristics of the Manila Trench subduction zone and proposed a model of the subducted slab of the Eurasian plate beneath the Manila Trench. The authors developed 9 seismicity profiles across the Manila megathrust to give a 3-D imagination of the geometry and mechanism of the source zone.

Hsu et al (2012) summarized the earthquake focal mechanism data in the Manila Trench subduction zone and classified the events by the mechanism types. The normal type earthquakes

are concentrated in the northern part of the megathrust between the 22°N latitude and the 18°N latitude, while the thrust type events are concentrated in the rest of the megathrust, mostly in segment located between the 16°N latitude and the 12°N latitude. This is an important fact for the prediction of the tsunami occurrence, as most tsunamis are known to be originated by thrust faults.

### 3. The Manila trench source modeling

A worst case source model of the Manila trench was created for this study, incorporating all advantages of the two models proposed by Tso-RenWu et al (2009) and Megawati et al (2009). Geometrically, the model imitates a 6-segments shape of the Manila trench, but with the parameters modified to fit the size and shape of each segment in the map. In addition, the dislocation of each segment is assigned in accordance with the slide values defined by the Megawati's model. This model corresponds to a worst case scenario caused by a 9.3 magnitude earthquake.

### 4. Development of tsunami scenarios

In order to assess the tsunami threats from the Manila trench source zone to the coasts and islands of Vietnam, a database of tsunami scenarios was developed. The modeling of the Manila trench source zone provides a basis for construction of tsunami generating earthquake scenarios. The following initial assumptions are adopted:

- 1) The whole source zone is a megathrust that consists of 6 fault segments. As the megathrust dips eastward to the Philippines's continent, the left hanging wall is assumed to have shallower depth comparing to the right foot wall.
- 2) The magnitudes of tsunami generating earthquakes are known values ranging from  $M_0$  to  $M_{max}$ , where  $M_0 = 6.5$  and  $M_{max} = 9.3$  are lower and upper magnitude thresholds of scenario earthquakes, respectively.

- 3) The focal depths of tsunami generating earthquakes are known values, which can be one of the three values of 15, 30 and 55 km.

The empirical relationships proposed by Well and Coppersmith (1994) were used for establishing the fault parameters of tsunami sources.

### 5. Numerical simulation of tsunami scenarios from the Manila trench source

The well validated open source code, COMCOT (Cornell Multi-grid Coupled Tsunami Model), is chosen to perform the simulation. The COMCOT model is capable of solving both linear and nonlinear shallow water equations (SWE) in the spherical and Cartesian coordinate systems. The nested grid system can provide tsunami simulations in both deep-water and near-shore coastal regions. The COMCOT model also provides the moving boundary algorithm to simulate the tsunami inundation (Philip L. – F. Liu et al, 1998).

The COMCOT model was applied for simulation of 100 tsunami scenarios originated from the Manila source zone.

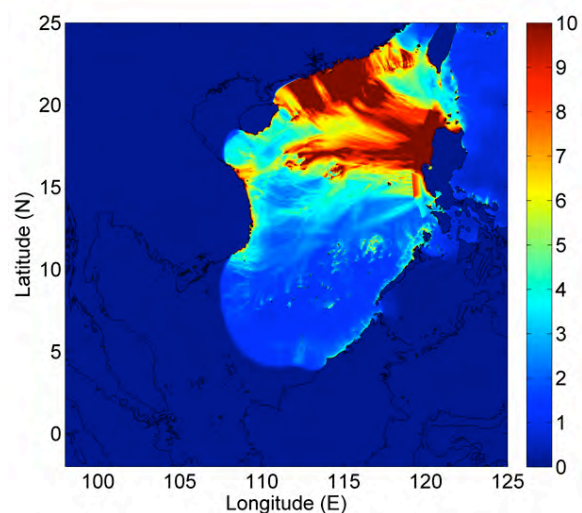


**Fig. 2.** Maximum free-surface elevation in the East Vietnam Sea according to the  $M_w=9.3$  scenario.

### 6. Results and Discussion

In this paper, only results of three extreme

scenarios with magnitudes of  $M_w9.3$ ,  $M_w9.0$  and  $M_w8.7$  are presented. For the worst case scenario, the highest tsunami hazards is observed along the Central Vietnam coast, between the Quang Ngai and Ba Ria – Vung Tau provinces, with maximum wave height of 20 m observed at the coast of Quang Ngai province (Fig.2). The maximum wave heights reduce to 11m for the  $M_w9.0$  scenario and 4.2 m for the  $M_w8.7$  scenario.

Detail assessment was conducted for three coastal cities including Hai Phong (North Vietnam) and Da Nang and Nha Trang (Central Vietnam). Figures 3a and 3b show the sea level data at the Hon Dau monitoring station at the coast of Hai Phong caused by the  $M_w8.7$  and  $M_w9.3$  scenarios, respectively. As can be seen from the figures, the tsunami will hit the coast of Hai Phong approximately 8 hours and a half after occurrence of the scenario earthquake.

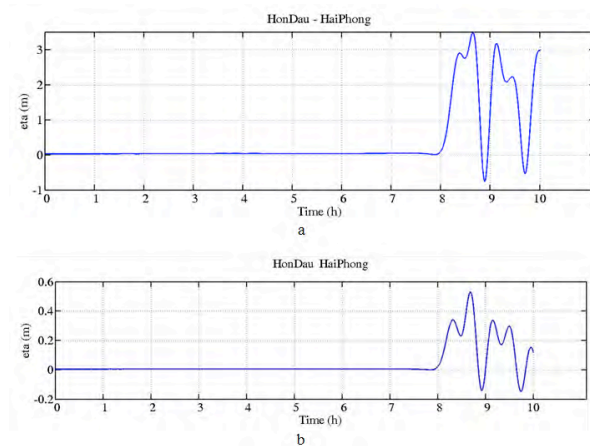


**Fig. 3.** Time-history free-surface elevation at the Hon Dau monitoring station according to the  $M_w9.3$  (a) and  $M_w8.7$  (b) scenarios.

Results of detail tsunami hazard assessment for Da Nang city are shown in Figure 4. As can be seen in these figures, the maximum wave heights can reach to 11, 8 m at Da Nang coast and 11,2 m at Nha Trang coast according to the worst case scenario  $M_w9.3$ .

## 7. Conclusion

In this study, a database of tsunami scenarios

excited by Manila Trench megathrust was established, with an initial source model

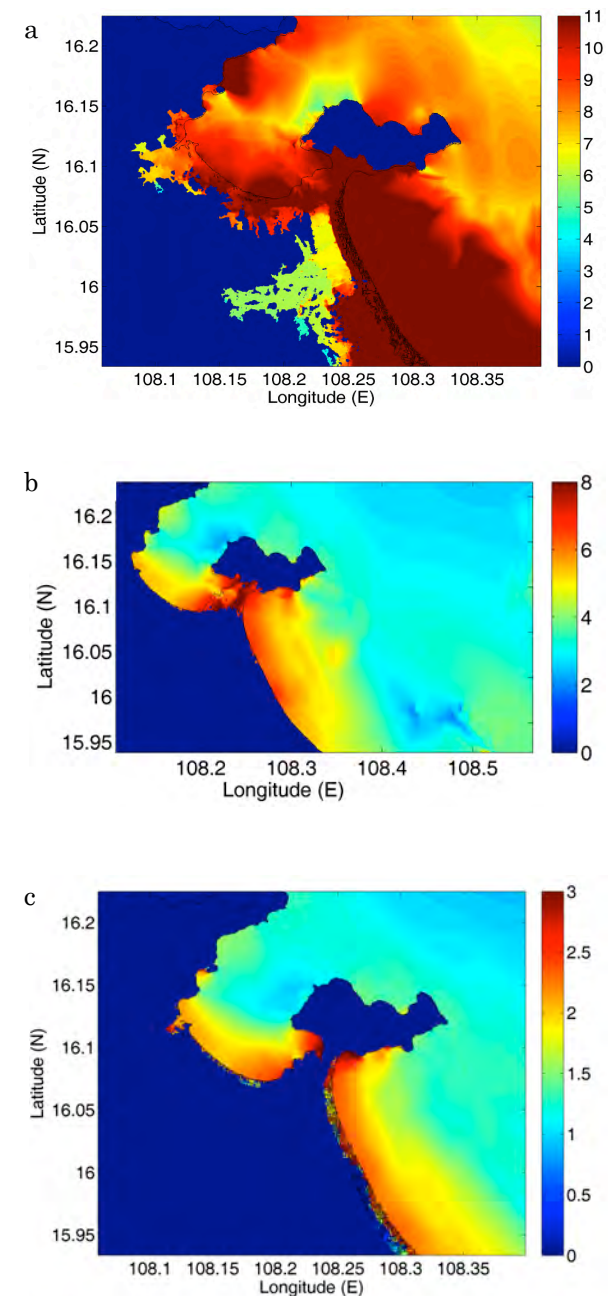


**Fig. 4.** Tsunami wave heights at Da Nang coast according to  $M_w9.3$  (a)  $M_w9.0$  and  $M_w8.7$  (b) scenarios.

developed referring to the models proposed by Tso-RenWu et al (2009) and Megawati et al (2009). The tsunami propagation and runup are numerically computed by using the COMCOT open source code. We focus the discussion in Central Vietnam coastal regions,

and carefully describe the tsunami impact to several coastal cities, Hai Phong, Da Nang and Nha Trang.

In Central Vietnam coast, the maximum tsunami wave high of 21 m is observed at the Quang Ngai province coast. The maximum wave height is 11.8 m recorded at the coast of Da Nang city and is 11.2 m at the coast of Nha Trang city. It might be concluded that the tsunami hazards from Manila Trench source are devastating to Vietnamese coast, especially to the Central Vietnam coast.

## References

- Bautista, C.B., Bautista, M.L.P., Oike, K., Wu, F.T., Punongbayan, R.S., 2001. A new insight on the geometry of subducting slabs in northern Luzon, Philippines. *Tectonophysics* 339, 279–310.
- Kusnowidjaja Megawati, Felicia Shaw, Kerry Sieh, Zhenhua Huang, Tso-Ren Wu, Yunung Lin, Soon Keat Tan, Tso-Chien Pan, 2009. Tsunami hazard from the subduction megathrust of the South China Sea: Part I. Source characterization and the resulting tsunami. *Journal of Asian Earth Sciences* 36, 13–20.
- Philip L. -F. Liu, Seung-Buhm Woo and Yong-Sik Cho, 1998. Computer Program for Tsunami Propagation and Inundation. School of Civil and Environmental Engineering, Cornell University, Ithaca, NY 14853, USA.
- Phuong Hong Nguyen, Que Cong Bui, Xuyen Dinh Nguyen. Investigation of tsunami sources, capable of affecting the Vietnamese coast. *Natural Hazards*, 64(1) pp 311-327. DOI: 10.1007/s11069-012-0240-3, October 2012.
- Tso-Ren Wu, Hui-Chuan Huang, 2009. Modeling tsunami hazards from Manila trench to Taiwan. *Journal of Asian Earth Sciences* 36, 21–28.
- Ya-Ju Hsu, Shui Ben Yu, Teh-Ru Alex Song, Teresito Bacolcol, 2012. Plate coupling

along the Manila subduction zone between Taiwan and northern Luzon. *Journal of Asian Earth Sciences* 51, 98–108.

# GEM Faulted Earth: Towards a Global Active Fault Database

Pilar Villamor<sup>a</sup> on behalf of the GEM-Faulted Earth team

<sup>a</sup>*GNS Science, PO Box 30368, Lower Hutt 5040, New Zealand, P.Villamor@gns.cri.nz*

The Faulted Earth Project is one of the global seismic hazard components of the Global Earthquake Model (GEM) Project. The GEM Foundation was established in early 2009, as a public/private partnership initiated and approved by the Global Science Forum of the Organisation for Economic Co-operation and Development (OECD-GSF). GEM aims to establish a uniform, independent standard to calculate and communicate earthquake risk worldwide. With committed backing from academia, governments, and industry, GEM will contribute to achieving profound, lasting reductions in earthquake risk worldwide.

The motivation for GEM stems from the observation that over half a million people died in the last decade due to earthquakes and tsunamis, most of these in the developing world, where the risk is increasing due to rapid population growth and urbanization. But in many earthquake-prone regions no hazard models exist, and even where models do exist, they are often inaccessible. Better risk awareness can reduce the toll that earthquakes take by leading to better construction, improved emergency response, and greater access to insurance. By functioning as a true community effort, the GEM initiative aims to produce a state-of-the-art, dynamic and open-source model for the assessment of seismic risk worldwide; a model that is based on the probabilistic assessment of earthquake occurrence, the resulting ground motions, and the impact these have on structures and populations in terms of damage, social and economic loss. GEM will set a uniform, independent standard for earthquake hazard, risk and loss assessment.

The construction of the GEM model is based on a combination of regional and global components. GEM Faulted Earth (hereafter referred to as GFE) is one of the global components, together with the Instrumental Earthquake Catalogue (1900-2009), Historical Earthquake Catalogue and Archive (100-1903), Ground Motion Prediction Equations, and Geodetic Strain Rate Model. Major aims of GEF were: i) to build a database structure which can

host the global active fault, fold and fault source data; ii) develop active web-based fault compilation tool (on the GEM OpenQuake Platform, developed in collaboration with the GEM model facility); and iii) compile a Global Active Fault Database. Over the last three years nearly 100 individuals from 43 institutions in 21 countries contributed to the GEM Faulted Earth (GFE) Project. The project has now finished and most goals are achieved.

The highlights of GFE are and its six work packages (WPs) are:

## **WP1: Data Specification**

This WP critically reviewed existing active fault databases for use in the design of the GEM Faulted Earth database. The deliverable report contains a description and evaluation of existing online, downloadable, and/or published national, regional, or global fault databases.

## **WP2: Global Fault database development**

The focus of WP2 was to design and build global fault, fold and fault source database. The design philosophies include: 1) the use of multiple levels; 2) compulsory and optional attributes, 3) a hierarchical structure (traces, sections, faults); 4) the conversion of folds to blind faults; 5) the use of automatic calculations of fault sources, 6) data completeness factors and 7) the treatment of uncertainties.

A 'Data Dictionary' provides definitions, formats, and guidelines for compilation of each attribute in the database. Two reports provide technical database design information and data exchange information for the GFE Database. An XML format offers a uniform method of exchange for existing neotectonic fault and fault source databases and datasets.

## **WP3: Global Fault & Source Database**

The focus of WP3 was the upload of existing data. Active fault data uploaded are from Japan, New Zealand, USA (mainland and Hawaii), Alaska and Australia. Fault source databases include New Zealand and global mid-ocean ridge transforms, although the latter also includes some

limited active fault data. Global subduction thrusts and the Himalaya Frontal Thrust are supplied to GEM independently. The deliverables include a report on the bulk-upload. Two further reports describe the new compilation of subduction sources and the database attributes compiled for the Himalayan Frontal Fault System.

#### **WP4: GEM Faulted Earth portal**

The GFE web-based tool for compilation and viewing of active fault data has been design in collaboration with GEM and is fully integrated in the OpenQuake Platform. Fine tuning of the tool is still under progress but a sandbox server and a stand-alone server laptop are available for training and exploring the tool. Guidelines for using the tool have been developed and are available as report including an overview of the GFE neotectonic fault, fold, and fold source database and guidelines for compiling new data.

#### **WP5: New Active Fault Data**

The focus of WP5 was the compilation of new active fault data. We held two regional workshops to train researchers to use the web-based tool and to start compilation. 26 participants from nine countries attended the South East Asia workshop in Bangkok in November 2012. 31 participants from eight countries attended the workshop in Mexico in April 2013. Researchers attending these workshops are trained to incorporate their data into a global active fault database through the Openquake Platform. A report on the workshops is also available.

#### **WP6: Final Report & Dissemination**

WP6 included the publication of the book 'Active Faults of the World' by Robert Yeats and a final report.

#### **List of reports**

##### **WP1**

Litchfield N., Berryman, K., Christophersen, A., Stein, R., Willis, M. (2011) Inventory of existing fault databases and data attributes, GEM Faulted Earth, Available from [www.nexus.globalquakemodel.org/gem-faulted-earth/posts/](http://www.nexus.globalquakemodel.org/gem-faulted-earth/posts/)

##### **WP2**

Litchfield, N., Berryman, K., Thomas, R. (2013) Data Dictionary, GEM Faulted Earth, available from

[www.nexus.globalquakemodel.org/gem-faulted-earth/posts/](http://www.nexus.globalquakemodel.org/gem-faulted-earth/posts/)

Thomas R., Litchfield N., Christophersen A. (2012) Database Design, GEM Faulted Earth, Available from [www.nexus.globalquakemodel.org/gem-faulted-earth/posts/](http://www.nexus.globalquakemodel.org/gem-faulted-earth/posts/)

Thomas, R. (2012) Database XML Interchange, GEM Faulted Earth, Available from [www.nexus.globalquakemodel.org/gem-faulted-earth/posts/](http://www.nexus.globalquakemodel.org/gem-faulted-earth/posts/)

##### **WP3**

Litchfield N., Thomas R. (2013) Bulk upload of national and global databases, GEM Faulted Earth, available from [www.nexus.globalquakemodel.org/gem-faulted-earth/posts/](http://www.nexus.globalquakemodel.org/gem-faulted-earth/posts/)

Berryman K., Wallace, L., Hayes, G., Bird, P., Wang, K., Lay, T., Stein, R., Sagiya, T., Basili, R., Rubin, C., Parsons, T., Barrientos, S., Kreemer, C., Litchfield, N., Pagani, M., Gledhill, K., Haller, K., Coasta, C. [2013, in prep]. The GEM Faulted Earth subduction characterisation project. Available shortly from [www.nexus.globalquakemodel.org/gem-faulted-earth/posts/](http://www.nexus.globalquakemodel.org/gem-faulted-earth/posts/)

Berryman K., Wesnousky, S., Reis, W., Litchfield, N. [2013, in prep]. The Himalayan Frontal Fault System: a data attribute compilation project of GEM Faulted Earth. Available shortly from [www.nexus.globalquakemodel.org/gem-faulted-earth/posts/](http://www.nexus.globalquakemodel.org/gem-faulted-earth/posts/)

##### **WP4**

Litchfield N., Wyss B., Christophersen A., Thomas R., Berryman K., Henshaw P., Villamor P (2013) Guidelines for compilation of neotectonic faults, folds and fault sources, GEM Faulted Earth, available from [www.nexus.globalquakemodel.org/gem-faulted-earth/posts/](http://www.nexus.globalquakemodel.org/gem-faulted-earth/posts/)

##### **WP5**

Villamor P., Ornthammarath T., Zúñiga R., Horspool N., Christophersen A., Langridge R. (2013) Towards New Active Fault Data, Version 1.0, July 2013, GEM Faulted Earth Project, available soon from [www.nexus.globalquakemodel.org/gem-faulted-earth/posts/](http://www.nexus.globalquakemodel.org/gem-faulted-earth/posts/).

**WP6**

Yeats, R. (2012) Active Faults of the World,  
Cambridge University Press

**Extra**

Stirling M.W., Godefroy T. (2012) Magnitude  
Scaling Relationships, GEM Faulted Earth  
and Regionalisation Global Components.  
Lower Hutt: GNS Science. GNS Science  
Miscellaneous Series 42. Components,  
Available from  
[www.nexus.globalquakemodel.org/gem-faulted-earth/posts/](http://www.nexus.globalquakemodel.org/gem-faulted-earth/posts/)

# Toward a harmonized map of seismic hazard assessment (SHA) in the East Asia region

Ken Xiansheng Hao<sup>a</sup> and Hiroyuki Fujiwara<sup>a</sup>

<sup>a</sup>National Research Institute for Earth Science and Disaster Prevention (NIED), 3-1 Tennodai, Tsukuba, 305-0006, Japan, hao@bosai.go.jp

## 1. Most of deadliest earthquakes

It looks like very low that annual probability of large earthquake occurrence, for example, 0.0004 or a 2500-year return period that equivalent to a level of 2% probability of exceedance in 50 years, at a given site. However, the probability is dramatic high once sites integrated on a continental scale, or on global scale. It is so surprise that 32 of the top 50 deadliest earthquakes have occurred in Asia by historical records. Of them, we briefly introduce major earthquakes in East Asian region as indicated in Fig. 1.

The 1976 Tangshan earthquake ( $M_s=8.0$ ; focal depth  $H=11$ km) occurred at 3:42AM early morning on July 28. It was ranked the top deadliest earthquake of the 20th century, around 240,000 to 255,000 and 164,000 severely injured. One of authors investigated the epicenter area just three days after the quake. Destroyed buildings were everywhere but stood one was hardly found. The countless bodies had been lying along roads with strong rancidness under the hot summer. The quake was unexpected for the large magnitude and the hypocenter just below a million-population city. There had been no any aseismic measures since the anti-seismic standard was the modified Mercalli intensity (MMI) VI~VII.

The 2008 Wenchuan earthquake ( $M_w=7.9$ ;  $H=19$  km) occurred at 2:28PM afternoon on May 12. It once again shocked world that claimed 90,000 fatalities and devastated huge regions spanning 300 km in Sichuan, western China where has no large earthquake records in near 2000 years of Chinese historiographies.

The two parallel thrust-faults ruptured simultaneously along 220 km in length of Longmenshan fault-zone. One of many lessons raised by the event is the underestimation of seismic hazard assessment in Wenchuan area that estimation was VII but recording was XI. The similar question was also raised during the Tangshan earthquake.

The 1999 Chi-Chi earthquake ( $M_w=7.6$ ;  $H=9.2$  km) is the largest in-land earthquake in Taiwan in the 20th century and it caused 2,444 deaths and missing; over 100,000 buildings were severely damaged. Fortunately, a total of 640 digital accelerographs at the free-field sites deployed in Taiwan in 1996 therefore the rich data acquired especially along the near-field of fault.

The 1995 Kobe earthquake ( $M_j=7.3$ ;  $H=16$  km) claimed 6,400 fatalities and shocked whole societies of Japan that so-called prepared earthquake country. The earthquake became a major wake-up call for Japanese disaster prevention authorities. Headquarters for earthquake research promotion (HERP) was soon established as the government's special agency, with the aim of clarifying the sharing of responsibilities concerning earthquake research which should be directly linked with administrative measures, and promoting such research in a centralized manner.

The 2011 Tohoku earthquake ( $M_w=9.0$ ;  $H=30$  km) claimed about 20,000 people and it was the most powerful known earthquake ever to have hit Japan, and the fifth most powerful earthquake in the world since modern record keeping began in 1900. Most of deaths were

caused by tsunami inundation and only about 100 deaths by the shaking damage related.

Korea has relatively low seismicity but the 1952 earthquake (M=6.5) occurred near

HERP for over 10 years. We operate a platform of Japan seismic hazard information station (J-SHIS) to publish the SHA maps and updated annually.

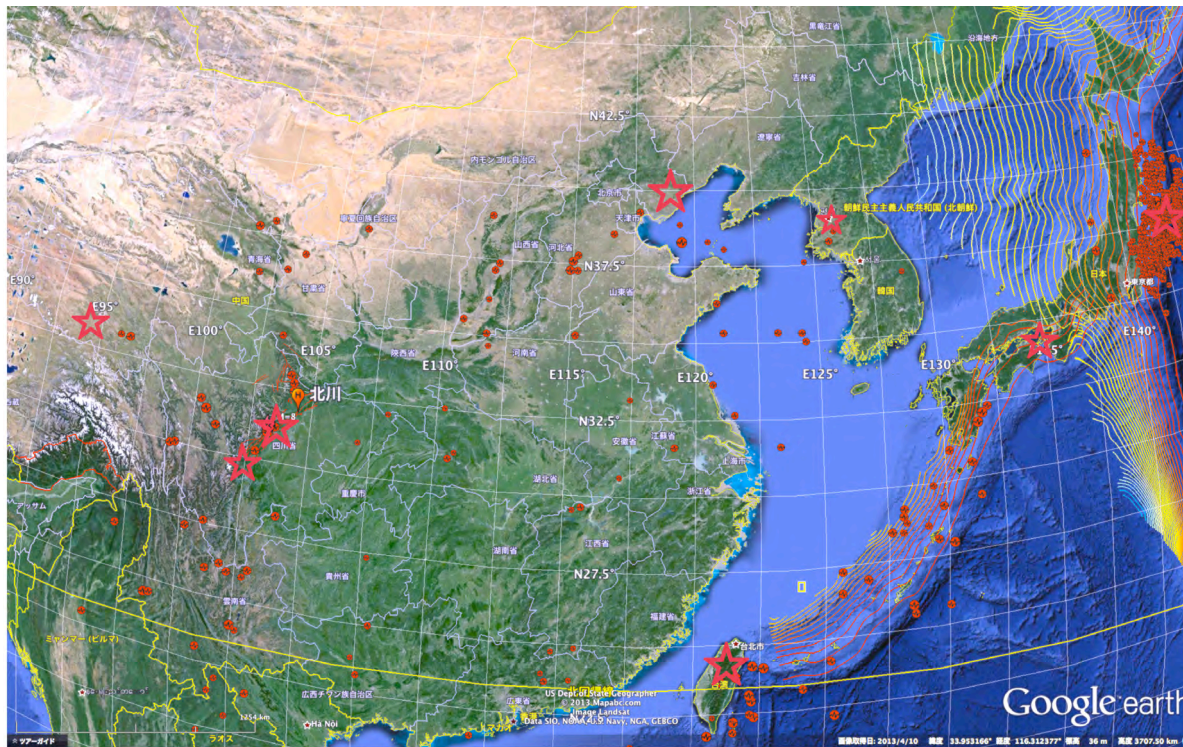


**Fig. 1.** Major earthquakes in East Asian region and slab depth with contoured at 20 km intervals

Pyeongyang, North Korea during the Korean War.

## 2. International collaborations on SHA

The event-based studies are being extremely required for different types of earthquakes but the frequency of earthquakes remains relatively low and its fundamental mechanisms remain still unclarified. To mitigate earthquake disasters, seismic hazard assessment can draw a strategic zoning map based on statistic information of seismicity, geophysical, geodetic data and active faults. The motivations drove us collaborate with China, Korea, Taiwan and the rest of Asia areas, as well as global regions.

### 2.1 SHA in Japan

NIED carries out an on-going national mission of seismic hazard assessment (SHA) of Japan by following the leading scientific results guided by earthquake research committee (ERC)

### 2.2 SHA in China and Korea

A seismic ground motion parameter zonation map of China was issued in 2001 and the coming new map carried out principally by institute of geophysics, China Earthquake Administration (Chief editor: Gao M.).

Korean national project of making an active fault map and seismic hazard map (2009~2012) was carried out principally by Korea institute of geoscience and mineral resources (KIGAM) and National Emergency Management Agency (NEMA).

In collaborative works with leading experts in China, Japan and Korea (CJK), we initiated a strategic cooperative programs (2010~2013) of “seismic hazard assessment for the next generation map”, supported by MOST China, JST Japan and NRF Korea, respectively.

Under the goal of trilateral strategic project, three annual symposiums have been held for reviewing data and discussing methodologies

adopted in the current Probabilistic SHA (PSHA) maps (CJK, 2011).

Meanwhile, the following items are being put to high priority to carry out, such as improving ground motion attenuation relationships, combining PSHA with deterministic approach for potential large earthquake.

### **2.3 SHA in Taiwan**

Taiwan and Japan, stretched by island arcs, located on hanging-wall side thrusts by the Western-Pacific subduction zones as shown in Fig. 1. Moreover, movements of the Philippines Plate, Eurasian Plate, and North-American Plate make much more complex plate boundaries in between. Both of Taiwan and Japan have the highest level of seismicity and suffered the destructive earthquakes recently. The 1999 Chi-Chi Earthquake became a major wake-up call for Taiwanese disaster prevention authorities. Under the common lessons learnt from destructive earthquakes and the urgency of the unexpected earthquake possibly occur in the future, the committee of Taiwan Earthquake Model (TEM) and NIED had consensus of collaborative researches to share data, knowledge and information to mitigate the disasters and two annual workshops have been held since then (TEM, 2012).

### **2.4 Collaboration with Global Earthquake Model**

The Global earthquake model foundation (GEM, 2013) is a collaborative effort devised and launched by the OECD Global science forum, aimed at engaging the global community in the transparent design, development and deployment of uniform open standards and tools for earthquake risk assessment worldwide. Combining the strengths, knowledge and needs, more than 26 public and private organizations have joined GEM. With the common motivations and missions, NIED proudly joined GEM as a representative of Japan to reinforce the public part of GEM's partnership in September 2012, since its SHA's methodologies

and technologies were highly valued.

The OpenQuake engine just released (GEM, 2013) is GEM's core tool for calculating the PSHA and risk, which more than 80 countries where 350 users have tested the open source OpenQuake engine. The interactive works between the J-SHIS and OpenQuake engine are on going.

On the second phase of GEM (2014-2018), GEM intends to expand regional activities and partnerships, with a focus on learning and knowledge exchange around the OpenQuake platform.

### **3. Harmonization of East Asia SHA**

As one of the GEM members, we are contributing on both of GEM global components and regional programs. On the GEM regional programs, our efforts of working with China, Korea, Taiwan, and the rest of East-Asia regions will possibly become one of the GEM regional programs. We have hosted the joint symposium of seismic hazard assessment on Sendai Japan on June 2013 includes 1) the workshop on Ground motion attenuation models, 2) the 3rd CJK annual meeting and 3) the 2nd TEM-NIED workshop. Over 50 presentations presented and about 90 people include professional from Vietnam joined the symposium.

On the symposium, one of the authors has summarized a SHA map in East Asia region (Hao and Fujiwara, 2013) under the collaborative works by Gao (2013), Jeon (2013), Chan et.al. (2013). It attracted much attention that people in different countries can have the same sense to understand the others although the map is with different definitions of contents and maps. The East Asia SHA map could be a blueprint for the coming harmonized map. We call for collaboration and support by public institutions and GEM regional programs to carry on the harmonization map in the East Asia region.

### **4. Summary**

In the East Japan subduction zone, the

maximum potential earthquake magnitude was under-estimated by the previous PSHA map (2011ver. J-SHIS). To deal with this complicated issue, we have been working for the reconsiderations of different seismic models with uncertainties in SHA. Though collaborative works we hope these lessons and experiences will benefit to East Asia regions as well as the world.

## References

- CJK (2011) <http://www.j-shis.bosai.go.jp/intl/cjk/>.
- Chan, C-H., M. Pagani, C.-T. Cheng (2013) Probabilistic seismic hazard assessment for Taiwan: Application of OpenQuake, <http://www.j-shis.bosai.go.jp/intl/tem/workshop/2nd.html>.
- Jeon J.S. (2013) Current status of probabilistic seismic hazard map in Korea, [http://www.j-shis.bosai.go.jp/intl/cjk/3rd\\_annual\\_meeting.html](http://www.j-shis.bosai.go.jp/intl/cjk/3rd_annual_meeting.html).
- J-SHIS (2011) <http://www.j-shis.bosai.go.jp/map/?lang=en>.
- Gao, M. (2013) The new seismic map of China, [http://www.j-shis.bosai.go.jp/intl/cjk/3rd\\_annual\\_meeting.html](http://www.j-shis.bosai.go.jp/intl/cjk/3rd_annual_meeting.html).
- GEM (2013) <http://www.globalquakemodel.org>.
- Hao, K. X. and H. Fujiwara (2013) Recent destructive earthquakes and international collaboration for seismic hazard assessment, *Journal of Disaster Research*, Vol.8 No.5, in press.
- TEM (2012) <http://www.j-shis.bosai.go.jp/intl/tem/>

# What occurred in the Japan trench region before and after the Tohoku-oki earthquake?: Seismological aspects

Toru Matsuzawa<sup>a</sup>

<sup>a</sup>Research Center for Prediction of Earthquakes and Volcanic Eruptions, Graduate School of Science, Tohoku University, Aoba-ku, Sendai 980-8578, Japan, matuzawa@aob.gp.tohoku.ac.jp

## 1. Introduction

The 2011 M9.0 Tohoku-oki earthquake surprised most of the seismologists in the world because Tohoku (northeastern Hoshu, Japan) was located in one of the most investigated subduction zones in the world and interplate coupling was thought to be too weak to generate M9 earthquakes there. I explain here why we seismologists thought M9 earthquakes were unlikely to occur and what were observed before and after the Tohoku-oki earthquake.

## 2. Reasons why the M9 earthquake was not anticipated

### 2.1 Age of the descending plate

Ruff and Kanamori (1980) found a relationship among the maximum magnitude for the events in a subduction zone, convergence rate of the plates and age of the descending plate. According to their results, subduction zones with faster convergence rates and younger descending plates tend to show larger maximum magnitudes. This results seemed to be very reasonable because the coupling between continental plates and younger and faster oceanic plates should become stronger; the plate interfaces should be easily locked then.

Stein and Okal (2007) reinvestigated the relationship and concluded that the correlation between the convergence speed and the maximum magnitude were vague. Their revised data, however, still showed that the M9 events had occurred in subduction zones with descending oceanic plates younger than 80 Ma, while the Pacific plate descending beneath Tohoku is as old as 130 Ma.

### 2.2 Margin type

The northeast subduction zone is known as an 'erosional' margin. Bilek (2010) investigated the relation of margin types and the locations of M9.0 or larger events. Her result clearly showed that the  $M > 9$  events had occurred only along accretionary margins and never along the erosional plate margins. This seemed also reasonable because soft sediments on a oceanic plate would be easily scraped at the trench if the two plates pushed each other strongly.

### 2.3 Seismicity

Small earthquakes had frequently occurred east off Tohoku while the background seismicity had been quite inactive along the Nankai trough. The contrast in the seismicity was explained by the difference in the coupling of the plates: weak along the Japan trench and strong along the Nankai trough. This interpretation explains well the historical large earthquakes:  $M > 8$  events repeatedly occurred with recurrence interval of 150-200 years along the Nankai trough while such huge earthquakes were quite rare along the Japan trench although the convergence rate is three times higher than along the Nankai trough.

Moreover, small repeating earthquakes actively occur along the Japan trench (e.g., Igarashi et al., 2003) while they had been very few along the Nankai trough. Since the small repeating earthquakes were thought to occur in the creeping regions, the existence of them seemed to indicate the weak coupling there.

### 2.4 Strain rate

GPS data after the middle of 1990s show that E-W contraction of  $\sim 10^{-7} \text{ y}^{-1}$  was

predominant in Tohoku (e.g., Sagiya et al., 2000). On the other hand, geodetic data of around 100 years show N-S or NE-SW extension of  $\sim 10^{-7} \text{ y}^{-1}$  was prevailing (e.g., Hashimoto, 1990). Therefore, we thought that strain energy in Tohoku was released every several tens of years by large earthquakes and was not accumulated over 100 years.

### **3. Observations just before the Tohoku-oki earthquake**

According to the GPS and small repeating earthquake data, the source area for the Tohoku-oki earthquake showed large slip deficit during the period from the middle of 1990s to early 2000s (e.g., Igarashi et al., 2003; Suwa et al., 2006; Uchida and Matsuzawa, 2011). After 2008, however, the interplate locking in some areas off southern Tohoku was unfastened (Suito, et al., 2011; Nishimura, 2012; Uchida and Matsuzawa, 2013). In particular, a slow slip event occurred to the east of the epicenter of the Tohoku-oki earthquake in the end of 2008 (Ito et al., 2013).

A slow slip event occurred again in February 2011 there (Kato et al., 2012; Ito et al., 2012), and March 9 M7.3 earthquake occurred to the west of the slow slip region. The afterslip of the M7.3 event was propagated to the south to trigger the March 11 main shock (Kato et al., 2012; Ohta et al., 2012; Ito et al., 2013).

### **4. The Tohoku-oki earthquake**

The M9.0 Tohoku-oki earthquake occurred on March 11, 2011. Most of the geophysical observations indicate that a plate boundary region close to the Japan trench slipped more than 50 m (e.g., Lay et al., 2011a; Fujiwara et al., 2011; Iinuma et al., 2012; Satake et al., 2013), while high-frequency seismic waves were mainly radiated from a deeper region (e.g., Kurahashi and Irikura, 2011; Koper et al., 2011).

The reasons why such large slip occurred are still under debate but many researchers have tried to explain them using

several models based on such as dynamic overshoot (Ide, et al., 2011), a shallow strong patch (Kato and Yoshida, 2011), slip behavior change in conditionally stable regions (e.g., Hori and Miyazaki, 2011), thermal pressurization (e.g., Mitsui and Yagi, 2013), and a critical taper theory (e.g., McKenzie and Jackson, 2012).

### **5. Seismic activities after the Tohoku-oki earthquake**

Tohoku is located in a E-W compressional stress regime. However, E-W tensional normal-fault type aftershocks were dominant in the source region of the Tohoku-oki earthquake (e.g., Aasno et al., 2011).

Such change in the predominant focal mechanisms indicates that the strength of the plate boundary was as low as around 20 MPa and the Tohoku-oki earthquake released almost all of the accumulated elastic strain on the boundary (Hasegawa et al., 2011; Yagi and Fukahata, 2011).

Even in the land area, the Tohoku-oki earthquake triggered 'aftershock' activity dynamically (Miyazawa, 2011) and statically (Yoshida et al., 2012). These results indicate that many faults in the crust are under critical-state and they can generate earthquakes even when weak stress change as small as less than 1 MPa is applied.

It is known that normal-fault type events tend to be activated in outer-rise or outer trench-slope regions after large interplate earthquakes (Lay et al., 1989), and the outer-rise 1933 earthquake occurred 37 years after the 1896 tsunami earthquake off Sanriku. Therefore, we should provide against the future outer trench-slope huge earthquakes (Lay et al., 2011b).

### **References**

Asano, Y., T. Saito, Y. Ito, K. Shiomi, H. Hirose, T. Matsumoto, S. Aoi, S. Hori, and S.

- Sekiguchi (2011) Spatial distribution and focal mechanisms of aftershocks of the 2011 off the Pacific coast of Tohoku Earthquake, *Earth Planets Space*, 63, 669-673, doi:10.5047/eps.2011.06.016.
- Bilek, S. L. (2010) The role of subduction erosion on seismicity, *Geology*, 38, 479-480, doi:10.1130/focus052010.1.
- Fujiwara, T., S. Kodaira, T. No, Y. Kaiho, N. Takahashi, Y. Kaneda (2011) The 2011 Tohoku-oki earthquake: Displacement reaching the trench axis, *Science*, 334, 1240, doi:10.1126/science.1211554.
- Hasegawa, A., K. Yoshida, and T. Okada (2011) Nearly complete stress drop in the 2011 Mw9.0 off the Pacific coast of Tohoku Earthquake, *Earth Planets Space*, 63, 703-707, doi:10.5047/eps.2011.06.007.
- Hashimoto, M. (1990) Horizontal strain rates in the Japanese Islands during interseismic period deduced from Geodetic Surveys (Part I): Honshu, Shikoku and Kyushu, *Zisin*, 43, 13-26.
- Hori, T., and S. Miyazaki (2011) A possible mechanism of M9 earthquake generation cycles in the area of repeating M7~8 earthquakes surrounded by aseismic sliding, *Earth Planets Space*, 63, 773-777, doi:10.5047/eps.2011.06.022.
- Ide, S., A. Baltay, and G.C. Beroza (2011) Shallow dynamic overshoot and energetic deep rupture in the 2011 Mw9.0 Tohoku-Oki earthquake, *Science*, 332, 1426-1429, doi:10.1126/science.1207020.
- Igarashi, T., T. Matsuzawa, and A. Hasegawa (2003) Repeating earthquakes and interplate aseismic slip in the northeastern Japan subduction zone, *J. Geophys. Res.*, 108, doi:10.1029/2002JB001920.
- Iinuma, T., R. hino, M. Kido, D. Inazu, Y. Osada, Y. Ito, M. Ohzono, H. Tsushima, S. Suzuki, H. Fujimoto, and S. Miura (2012) Coseismic slip distribution of the 2011 off the Pacific Coast of Tohoku Earthquake (M9.0) refined by means of seafloor geodetic data, *J. Geophys. Res.*, 117, B07409, doi:10.1029/2012JB009186.
- Ito, Y., R. Hino, M. Kido, H. Fujimoto, Y. Osada, D. Inazu, Y. Ohta, T. Iinuma, M. Ohzono, S. Miura, M. Mishina, K. Suzuki, T. Tsuji, J. Ashi (2013) Episodic slow slip events in the Japan subduction zone before the 2011 Tohoku-Oki earthquake, *Tectonophys.*, 600, 14-26, doi:10.1016/j.tecto.2012.08.022,
- Kato, A., K. Obara, T. Igarashi, H. Tsuruoka, S. Nakagawa, and N. Hirata (2012) Propagation of slow slip leading up to the 2011 Mw9.0 Tohoku-Oki earthquake, *Science*, 335, 705-708, doi:10.1126/science.1215141.
- Kato, N., and S. Yoshida (2011) A shallow strong patch model for the 2011 great Tohoku-oki earthquake: A numerical simulation, *Geophys. Res. Lett.*, 38, L00G04, doi:10.1029/2011GL048565.
- Koper, K. D., A. R. Hutko, T. Lay, C. J. Ammon, and H. Kanamori (2011) Frequency-dependent rupture process of the 2011 Mw9.0 Tohoku Earthquake: Comparison of short-period P wave backprojection images and broadband seismic rupture models, *Earth Planets Space*, 63, 599-602, doi:10.5047/eps.2011.05.026.
- Kurahashi, S., and K. Irikura (2011) Source model for generating strong ground motions during the 2011 off the Pacific coast of Tohoku Earthquake, *Earth Planets Space*, 63, 571-576, doi:10.5047/eps.2011.06.044.
- Lay, T., L. Astiz, H. Kanamori, and D. H. Christensen (1989) Temporal variation of large intraplate earthquakes in coupled subduction zones, *Phys. Earth Planet. Inter.*, 54, 258-312.
- Lay, T., C. J. Ammon, H. Kanamori, L. Xue, and M. J. Kim (2011a) Possible large near-trench slip during the 2011 Mw9.0 off the Pacific coast of Tohoku Earthquake, *Earth Planets Space*, 63, 687-692, doi:10.5047/eps.2011.05.033.

- Lay, T., C. J. Ammon, H. Kanamori, M. J. Kim, and L. Xue (2011b) Outer trench-slope faulting and the 2011 Mw9.0 off the Pacific coast of Tohoku Earthquake, *Earth Planets Space*, 63, 713-718, doi:10.5047/eps.2011.05.006.
- McKenzie, D., and J. Jackson (2012) Tsunami earthquake generation by the release of gravitational potential energy, *Earth Planet. Sci. Lett.*, 345-348, 1-8, doi:10.1016/j.epsl.2012.06.036.
- Mitsui, Y., and Y. Yagi (2013) An interpretation of tsunami earthquake based on a simple dynamic model: Failure of shallow megathrust earthquake, *Geophys. Res. Lett.*, 40, 1523-1527, doi:10.1002/grl.50266.
- Miyazawa, M. (2011) Propagation of an earthquake triggering front from the 2011 Tohoku-Oki earthquake, *Geophys. Res. Lett.*, 38, L23307, doi:10.1029/2011GL049795.
- Nishimura, T. (2012) Crustal deformation of northeastern Japan based on geodetic data for recent 120 years, *J. Geol. Soc. Japan*, 118, 278-293, doi:10.5047/eps.2011.06.053.
- Ohta, Y., R. Hino, D. Inazu, M. Ohzono, Y. Ito, M. Mishina, T. Iinuma, J. Nakajima, Y. Osada, and H. Fujimoto, K. Tachibana, T. Demachi, S. Miura (2012) Geodetic constraints on afterslip characteristics following the March 9, 2011, Sanriku-oki earthquake, Japan, *Geophys. Res. Lett.*, 39, L16304, doi:10.1029/2012GL052430.
- Ruff, L., and H. Kanamori (1980) Seismicity and the subduction process, *Phys. Earth Planet. Inter.* 23, 240-252.
- Sagiya, T., S. Miyazaki and T. Tada (2000) Continuous GPS array and present-day crustal deformation of Japan, *Pure Appl. Geophys.*, 157, 2303-2322.
- Satake, K., Y. Fujii, T. Harada, and Y. Namegaya (2013) Time and space distribution of the 2011 Tohoku earthquake as inferred from tsunami waveform data, *Bull. Seismol. Soc. Am.*, 103, 1473-1492, doi:10.1785/0120120122.
- Stein, S., and E. A. Okal (2007) Ultralong period seismic study of the December 2004 Indian Ocean earthquake and implications for regional tectonics and the subduction process, *Bull. Seismol. Soc. Am.*, 97, S279-S295, doi:10.1785/0120050617.
- Suito, H., T. Nishimura, M. Tobita, T. Imakiire, and S. Ozawa (2011) Interplate fault slip along the Japan Trench before the occurrence of the 2011 off the Pacific coast of Tohoku Earthquake as inferred from GPS data, *Earth Planets Space*, 63, 615-619, doi:10.5047/eps.2011.06.053.
- Suwa Y., S. Miura, A. Hasegawa, T. Sato and K. Tachibana (2006) Interplate coupling beneath NE Japan inferred from three-dimensional displacement field, *J. Geophys. Res.*, 111, doi:10.1029/2004JB003203.
- Uchida, N., and T. Matsuzawa (2011) Coupling coefficient, hierarchical structure, and earthquake cycle for the source area of the 2011 off the Pacific coast of Tohoku earthquake inferred from small repeating earthquake data, *Earth Planets Space*, 63, 675-679, doi:10.5047/eps.2011.07.006.
- Uchida, N., and T. Matsuzawa (2013) Pre- and postseismic slow slip surrounding the 2011 Tohoku-oki earthquake rupture, *Earth Planet. Sci. Lett.*, 374, 81-91, doi:10.1016/j.epsl.2013.05.021.
- Yagi, Y., and Y. Fukahata (2011) Rupture process of the 2011 Tohoku-oki earthquake and absolute elastic strain release, *Geophys. Res. Lett.*, 38, L19307, doi:10.1029/2011GL048701.
- Yoshida, K., A. Hasegawa, T. Okada, T. Iinuma, Y. Ito, and Y. Asano (2012) Stress before and after the 2011 great Tohoku-oki earthquake and induced earthquakes in inland areas of eastern Japan, *Geophys. Res. Lett.*, 39, L03302, doi:10.1029/2011GL04972

# Tsunami generation mechanism due to the 2011 Tohoku-oki earthquake and a new method for the real-time tsunami inundation prediction

Yuichiro Tanioka<sup>a</sup> and Aditya Gusman<sup>a</sup>

<sup>a</sup>Institute of Seismology and Volcanology, Hokkaido University, 10N8W Kita-ku, Sapporo, Hokkaido 060-0810, Japan, tanioka@mail.sci.hokudai.ac.jp

## 1. Introduction

The 2011 Tohoku earthquake occurred within the Japan Trench subduction zone where the Pacific plate subducts beneath the Okhotsk plate. A large tsunami was generated by the 2011 Tohoku megathrust earthquake and devastated the coastal area along the north east coast of Honshu. The National Police Agency of Japan has confirmed casualties of about 16,000 deaths, 4,000 people missing. The tsunami was observed by tide gauges, pressure gauges, GPS buoys, and Deep-ocean Assessment and Reporting of Tsunamis (DART) buoys that are located offshore and across the Pacific Ocean (Fig.1).

A dense Global Positioning System (GPS) network of the Earth Observation Network (GEONET) on main islands of Japan that is maintained by Geospatial Information Authority of Japan (GSI) detected coseismic and postseismic displacements due to the 2011 earthquake [Ozawa *et al.*, 2011]. Crustal movement monitoring at underwater reference stations off the east coast of Tohoku reveals that coseismic displacement there due to the earthquake are large up to 24 m of horizontal motion [Sato *et al.*, 2011].

In this presentation, first, source processes of the Tohoku-oki earthquake and tsunami generation mechanism are discussed. Second, a new method for future real-time tsunami inundation prediction is developed from a lesson of 2011 Tohoku tsunami.

## 2. Tsunami generation mechanism

Joint inversion is performed using tsunami waveforms observed at triangles shown in Fig. 1, GPS data and seafloor deformation data discussed in the previous session to study the source model of the 2011 tsunami. The result indicates that slip distribution has a major slip region with the maximum slip amount of 44 m (Fig.2a). The earthquake ruptured the plate interface from the hypocenter all the way to the trench with large slip amounts up to 41 m on the shallowest subfaults. The total seismic moment calculated from estimated slip distribution is  $5.5 \times 10^{22}$  N m (Mw 9.1) which is similar to that estimated by GCMT ( $5.3 \times 10^{22}$  N m).

Tanioka and Seno [2001] suggested that the additional uplift along the unconsolidated

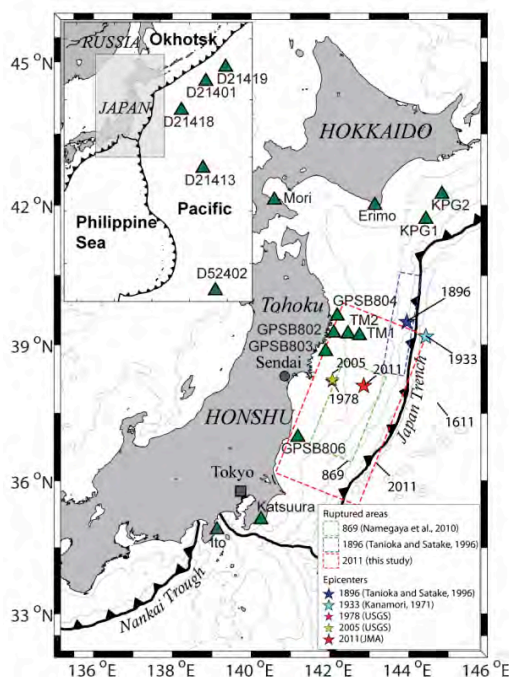


**Fig. 1.** Map of sea level observation stations (green triangles). Stars represent epicenters and rectangles represent rupture areas (after Gusman *et al.*, 2012).

sedimentary wedge near the Japan trench generated the additional tsunami for the 1896 Sanriku tsunami earthquake. We need to test that the observed tsunami waveforms can be explained by the additional uplift near the trench. The result indicates that not only coseismic vertical deformation, but also additional uplift near the

trench as suggested for the 1896 Sanriku tsunami earthquake [Tanioka and Seno, 2001] contribute to generate the large tsunami near the source of the 2011 Tohoku earthquake. In this case, the total seismic moment calculated from estimated slip distribution (Fig.2b) is reduced to  $5.1 \times 10^{22}$  N m (Mw 9.1).

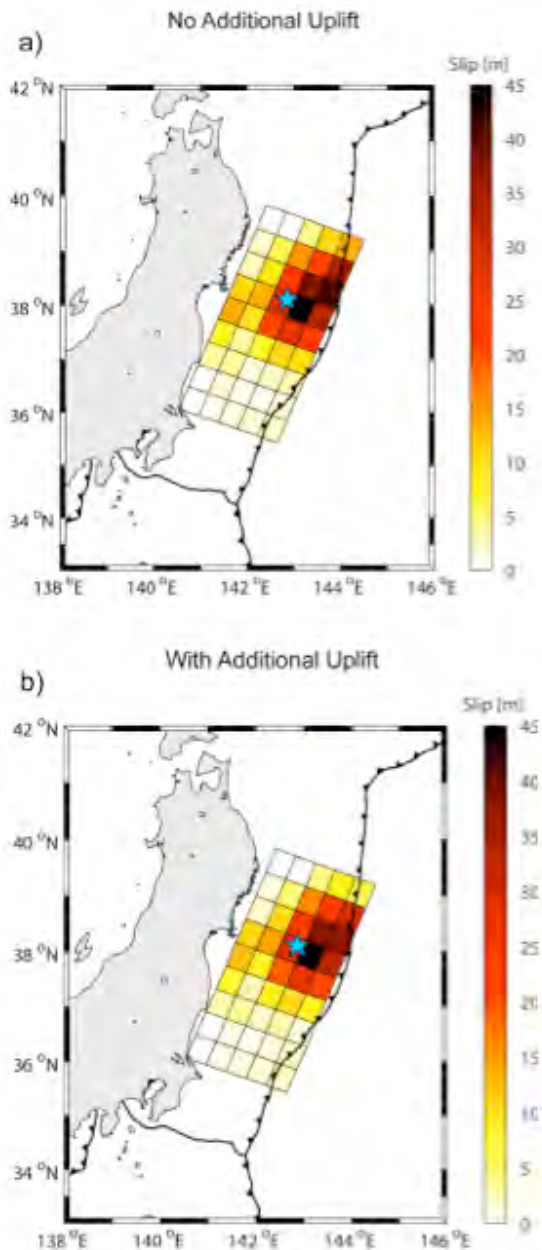


**Fig. 2.** a) Slip distribution of the 2011 Tohoku –oki earthquake estimated from tsunami waveforms and crustal deformation data and b) slip distribution estimated with both faulting and additional uplift (after Gusman et al., 2012).

### 3. A new method for tsunami inundation prediction

On 11 March 2011, only 3 min after the origin time of the 2011 Tohoku earthquake (14:46 JST), the Japan Meteorological Agency (JMA) warned that tsunami larger than 3 m would hit the east coast of the Tohoku area. The actual tsunami that struck the coastal area was more than 10 m and reached 40 m in some places [Mori et al. 2012]. The JMA used strong motion data to get the  $M_{jma} = 7.9$  that was then used to generate the first tsunami warning of the 2011 Tohoku earthquake. After an offshore tsunami data was analyzed by the JMA about 25 min later, the tsunami warning was updated in which the estimated coastal tsunami heights were larger than 10 m. After 54 min from the earthquake's origin time, a magnitude Mw 8.8 was obtained for the earthquake.

Lessons from those experiences, large-scale maps of the predicted tsunami inundation area and heights might have been able to better illustrate the dangers that threatened them and convinced them to evacuate immediately before the tsunami arrived. We developed a new method for real-time tsunami inundation.

To produce the map of predicted tsunami inundation, accurate moment magnitude estimation is required. The W phase, that arrives before S phase, can be used for rapid and robust determination of great earthquake source parameters with sufficient accuracy [Kanamori and Rivera 2008]. We estimated three centroid moment tensor solutions for the 2011 Tohoku earthquake, two of which are estimated using 5 min and 10 min of W phase data recorded at the Japan F-net stations, another one is a final W phase centroid moment tensor solution estimated

using the global data. A scaling relation ( $M_w = 4/3 \log A + 3.03$ ) by Hanks and Bakun [2002] is used to calculate the rupture area from the moment magnitude. Using a relationship between the length and width of the rupture area ( $L=2W$ ), we obtained earthquake fault parameters for tsunami inundation modeling (Fig.3).

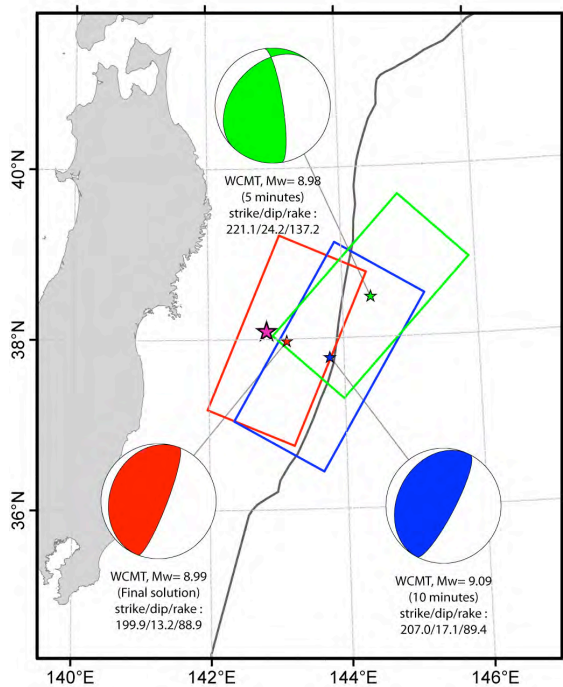


**Fig. 3.** The W phase centroid moment tensor solutions and the fault planes for the 2011 Tohoku earthquake. Black star represents the epicenter of the 2011 Tohoku earthquake, white stars represent the centroid locations for the 5, 10 min, and final W phase centroid moment tensor solutions, and rectangles are fault planes for the solutions. Rectangles on the coast represent the tsunami inundation simulation sites. (after Gusman and Tanioka, 2013)

Tsunami inundation area and heights are simulated in the Sendai Plain, Minamisanriku, Rikuzentakata, and Taro using the three estimated fault models for the 2011 Tohoku earthquake. Even the simulated tsunami heights and inundations from the W phase solution that used only 5 min data are considerably similar to the observations (Fig.4.). The results of inundation model in Sendai, Minamisanriku, and

Taro are improved when using 10 min of W phase data (Fig.4.). These show that the W phase solutions are reliable to be used for tsunami inundation modeling. Furthermore, the technique that combines W phase inversion and tsunami inundation modeling can produce results with sufficient accuracy for tsunami early warning purposes.

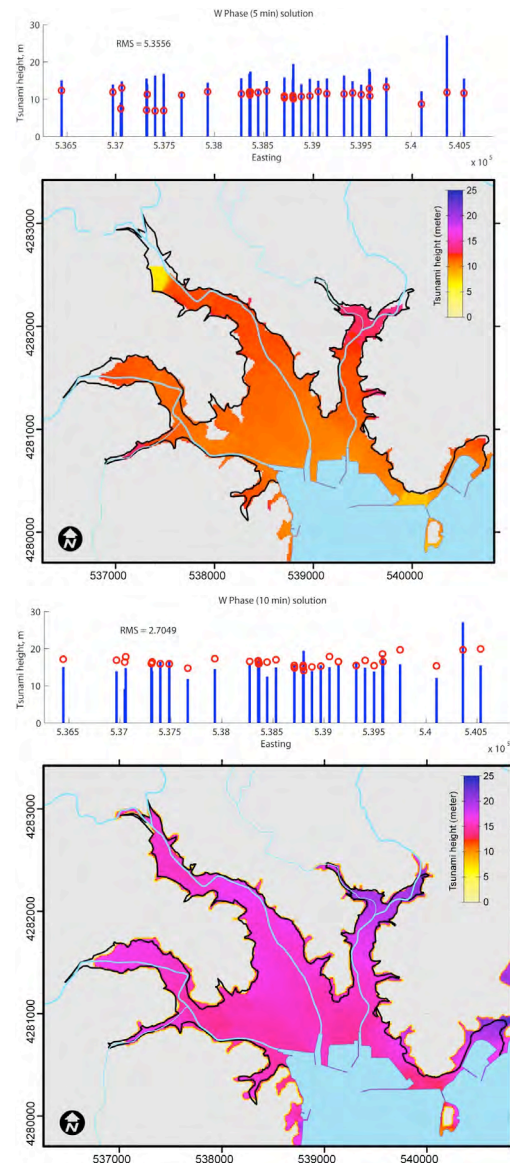


**Fig. 4.** Comparison between observed and simulated tsunami heights and inundation area in Minamisanriku. The simulated tsunami inundation areas from the 5 min W phase solution (upper), and 10 min W phase solution (lower), black lines represent the observed limit of tsunami inundation. Blue bars and red points represent the observed and simulated tsunami height, respectively.

However, the computation time for tsunami

inundation is still much longer than the available time for a tsunami forecast, we do not have a time to compute the tsunami inundation area after a large earthquake occurs. In this study, we develop a real-time tsunami inundation forecast method using a database where many tsunami inundation areas previously computed using various fault models are saved.

From that fault models estimated using 5min or 10 min of W phase data, a tsunami is computed using the linear long-wave equations. That tsunami simulation takes only 1-3 minutes using a typical PC, so it can be used for a tsunami forecast. Using that result, we develop a method to choose the best tsunami inundation area from the database.

In a database, tsunami inundation areas computed numerically using various fault models and tsunami waveforms at several locations near the inundation area at the ocean depth of about 50 m. The locations are chosen that tsunami propagation with a linear long-wave approximation is good enough for the first wave of tsunami. Those computed tsunami waveforms are used to compare the tsunami waveforms computed from the fault model of an actual earthquake using the linear long-wave equations we describe above. Therefore, the best tsunami inundation area will be chosen by comparison of tsunami waveforms in the database with the tsunami waveforms computed from the fault model of the earthquake.

This method is tested for the 2011 Tohoku-oki earthquake at Sendai Plain, Minamisanriku, Rikuzentakata in Tohoku-area. The tsunami inundation areas in those areas from various fault models are numerically computed and saved into a database. We found that the method worked well enough to forecast the tsunami inundation area at Sendai Plain, Minamisanriku, Rikuzentakata in Tohoku-area. This new real-time tsunami inundation forecast method is available for any region. We hope that the method saves lives from tsunami disasters in future.

## References

- Gusman, A.R., and Y. Tanioka, (2013), W phase inversion and tsunami inundation modeling for tsunami early warning: case study for the 2011 Tohoku event, *Pure Appl. Geophys.*, doi:10.1007/s00024-013-0680-z
- Gusman, A.R., Y. Tanioka, S. Sakai, and H. Tsushima, (2012). Source model of the great 2011 Tohoku earthquake estimated from tsunami waveforms and crustal deformation data, *Earth Planet. Sci. Lett.*, 341–344, 234–242, doi:10.1016/j.epsl.2012.06.006.
- Hanks, T.C., and H.W. Bakun, (2002). A bilinear source-scaling model for M-log A observations of continental earthquakes, *Bull. Seism. Soc. Am.*, 92 (5), 1841–1846.
- Kanamori, H., and L. Rivera, (2008). Source inversion of W phase: speeding up seismic tsunami warning, *Geophys. J. Int.*, 175, 222–238, doi:10.1111/j.1365-246X.2008.03887.x.
- Ozawa, S., T. Nshimura, H. Suito, T. Kobayashi, M. Tobita, and T. Imakiire, (2011), Coseismic and postseismic slip of the 2011 magnitude-9 Tohoku-oki earthquake, *Nature* 475, 373-376, <http://dx.doi.org/10.1038/nature10227>.
- Sato, M., T. Ishikawa, N. Ujihara, S. Yoshida, M. Fujita, M. Mochizuki, and A. Asada, (2011), Displacement above the hypocenter of the 2011 Tohoku earthquake, *Science*, 1-2, <http://dx.doi.org/10.1126/science.1207401>.
- Tanioka, Y., and T. Seno, (2001), Sediment effect on tsunami generation of the 1896 Sanriku tsunami earthquake, *Geophys. Res. Lett.*, 28, 3389-3392.

# Subduction Zone Tectonics: Subduction Accretion Versus Erosion and the Implications for Disastrous Earthquakes

Mark Cloos

*Department of Geological Sciences, University of Texas at Austin, Austin, Texas USA 78712, cloos@jsg.utexas.edu*

Uyeda and Kanamori (1979) were the first to recognize that there is a wide range in the fraction of plate convergence that occurs as thrust-type seismicity at subduction zones. They characterized the end-member behaviors as Mariana-type where only a small fraction of the convergence is evident from seismogenic movements and Chilean-type where a large fraction is accommodated by slip during large earthquakes ( $M > 7.5$ ). The compilation of global seismicity by Pacheco et al. (1993) supported this generalization. While it is clear that the historical record is inadequate to fully evaluate the seismicity of subduction zones, the global compilation for 1900 to 2007 by Heuret et al. (2011) reconfirms there has been an enormous variation in the fraction of plate convergence along different margins that was accommodated by seismogenic movements. Seismic coupling can be defined as the fraction of subduction that occurs as seismic slip events. Of the 49,700 km of subduction zone segments as divided by Heuret et al., about 27,900 km have less than 15% of their century+ convergence occur as seismogenic slip, while only about 11,300 km have more than 50% of their convergence occur as seismogenic slip. Moreover, the smallest seismic coupling is still along the 2100 km long Marianas segment, where only about 2% of the plate convergence occurred as seismogenic slip. Another 16,000 km of subduction zone segments had 10% or less of the last 107 years of convergence occur as seismogenic slip. The largest seismic

coupling is still along the 1100 km long southern Chile segment, the site of the largest recorded seismogenic movement ( $M 9.5$ ) in 1960. Along this segment, the equivalent of  $\sim 260$  years of plate convergence was accommodated during the 107 year period. The only other margins with more than a century+ of convergence occurring as seismogenic slip are the 1700 km long Andaman ( $M 9$ , 2004), the 950 km long Kamchatka ( $M 9$ , 1952), 840 km long eastern Alaska (with the  $M 9.2$ , 1964, event accounting for most of the equivalent of  $\sim 190$  years of plate convergence), and now, of course, the 1000 km long Northeast Japan margin. Clearly, multicentury/millennial scale  $M 9$  events dominate and their historical absence is not a basis for evaluating seismic potential. Nonetheless, the very low fraction of seismogenic plate convergence along the 3500 km long Izu-Bonin-Mariana subduction zone still appears to strongly suggest that there is a large spectrum in subduction zone seismicity.

Many studies attribute large subduction zone earthquakes to high friction or increased effective stress along a fault, commonly referred to as "the decollement." Decollement faults, tens of km long have been imaged in seismic reflection profiles along Southwest Japan (Nankai) and Lesser Antilles subduction zones. The decollements are within the layer of subducting sediment above the top of the descending ocean crust. Accounting for the origin of large earthquakes in

layered porous sediments zone is problematic as M7.5 to 9+ events require mechanical interactions across which large amounts of elastic strain energy can accumulate over timescales of centuries. It is now known that many margins are non-accretionary and large volumes of sediment subduct to mantle depths as evident from the small size of accretionary prisms and their scarcity of oceanic pelagics (Scholl et al., 1980). The discovery of ultrahigh-pressure blueschist facies metamorphics and the presence of Be-10 in many volcanic arc magmas during the 1980s directly confirm sedimentary materials reach 100 km depths. Cross-sectional mass balance observations and patterns of forearc subsidence indicate substantial mechanical abrasion and removal of the leading edge of the overriding plate during the Cenozoic along the margins of Mariana, Guatemala, Peru and Northeast Japan (von Huene and Scholl, 1991). It now appears that subduction erosion is of comparable global importance as subduction accretion.

The subduction channel model accounts for the spectrum of long-term convergent margin behavior (Shreve and Cloos, 1986; Cloos and Shreve, 1988a,b). The basic postulate is that the plate interface is best approximated as a viscous shear zone. Incoming sediment (oceanic pelagics overlain by recently deposited trench deposits) is carried into the shear zone with a local channel capacity determined by the speed of convergence, the pressure gradient along the roof, the bulk viscosity and density of the subducting sediment layer. Where sediment supply (base of trench slope thickness times subduction velocity) exceeds capacity at the inlet, material is offscraped. Where incoming sediment supply is less than inlet capacity, the entire pile enters the channel and experiences bulk shear strain that

increases with depth. Subducted material at the top of the channel can be underplated while the basal layers are transported to the depths of arc magmagenesis. Where the incoming sediment supply is much less than channel capacity, shear stresses along the base of the overriding block can be high enough that the bottom of the overriding plate is abraded by subduction erosion. Channel capacity can abruptly decrease where there is a sharp increase in the pressure gradient along the top of the shear zone. Where this occurs, subducted sediment can upwell and flow back towards the inlet, becoming highly deformed tectonic *mélange* as it turns. A key realization is that decollements imaged or detected in seismic reflection profiles are just the lowermost velocity discontinuity in a downward propagating zone of shear.

Reconciling the viscous behavior inferred along the plate interface zone in the subduction channel model with the global variations in subduction zone seismicity is a matter of geodynamic importance. Subduction speed is a first order parameter that is not accounted for in Coulomb wedge mechanical models. Some of the variation in subduction zone seismicity can be explained as due to temperature conditions at depth. Thermal modeling indicates that where subduction is slow (<2 cm/yr) or the incoming plate is very young (<5 Ma), 300°C temperatures are present at depths as shallow as 20 km. Consequently, intracrystalline creep dominates in the shear zone and interplate earthquakes are limited. Where subduction is fast (> 4 cm/yr), the forearc region cools and interplate earthquakes occur as deep as 60 km. Thermal modeling and many petrological observations indicate temperature/depth trajectories near the plate interface can become as cold as 6°C/km.

Overall, shear stresses should be

lower where the shear zone is thicker. The association of infrequent major (M7.5+) earthquakes with thicker layers of subducting sediment is especially problematic if the build up of large elastic strains is attributed to friction along a planer decollement within compacting and metamorphosing sediments. Similarly, the subduction channel concept postulates that the shear from convergence becomes distributed in the subducting layer of fluid-rich (10-20 volume % pore water), highly overpressured ( $P_{\text{fluid}} \sim P_{\text{lithostatic}}$ ) sediment. Such materials have limited ability to accumulate elastic strain energy. Major earthquakes require strong mechanical interactions between the converging plates. Volcanic seamounts welded to the top of descending plates are common and must become mechanical irregularities in subduction channels (Cloos, 1992). They can become major seismogenic asperities where they abut crystalline materials forming the base of the overriding plate.

The dichotomy of subduction zone seismicity recognized by Uyeda and Kanamori is explainable (Cloos and Shreve, 1996). Mariana-type margins are sites of subduction erosion because sediment supply is less than channel capacity, the shear zone is thin and shear stresses are high near the inlet. Where subduction erosion abrades the hanging wall block, subduction channels thicken downdip. Subducting seamounts will become truncated at low confining pressures near the inlet of tectonically erosive margins and their impingement may enhance the abrasion of material from the hanging wall. Where this occurs, interplate seismicity is limited because these mechanical irregularities are truncated at low pressures and temperatures, becoming shorter than the downdip thickness of the shear zone. In striking contrast, Chilean-type margins are

accretionary because sediment supply is greater than channel capacity. Where accretion occurs by underplating, subduction channels thin downdip. Incoming seamounts at accretionary margins can subduct largely intact until they become jammed against the roof of the subduction channel, commonly at depths of 20 to 30 km. The transition from aseismic subduction beneath weak accretionary prism materials to movements beneath higher density and strong crystalline material (the "backstop") is commonly demarked by the presence of seismic fronts.

Disasters arise from ground shaking and tsunami waves. Ground shaking is determined by earthquake size and local ground conditions. Most subduction zone earthquakes smaller than M8 do not generate significant tsunamis. However, Kanamori (1972) recognized that some moderate size events generate anomalously large tsunamis. He also deduced that "tsunami earthquakes" are products of slow ruptures. It is now evident that tsunami activity can be greatly amplified because trench walls slopes are steep and shaking can trigger enormous downslope gravitational movements (Kawamura et al., 2012). The triggered seaward movements can be so large in area and volume that they can generate tsunami waves that greatly exceed those generated by the surface displacements driven by the release of elastic strain energy.

## References

- Cloos, M., 1992, Thrust-type subduction-zone earthquakes and seamount asperities: A physical model for seismic rupture: *Geology*, v. 20, p. 601-604.
- Cloos, M., and Shreve, R. L., 1988a, Subduction-channel model of prism accretion, melange formation, sediment subduction, and subduction erosion at

- convergent plate margins: 1. Background and description: *Pure and Applied Geophysics*, v. 128, p. 455-500.
- Cloos, M., and Shreve, R. L., 1988b, Subduction-channel model of prism accretion, melange formation, sediment subduction, and subduction erosion at convergent plate margins: 2. Implications and discussion: *Pure and Applied Geophysics*, v. 128, p. 501-545.
- Cloos, M., and Shreve, R. L., 1996, Shear zone thickness and the seismicity of Chilean- and Mariana-type subduction zones: *Geology*, v. 24, p. 107-110.
- Heuret, A., Lallemand, S., Funicello, F., Piromallo, C., and Faccenna, C., 2011, Physical characteristics of subduction interface type seismogenic zones revisited: *Geochemistry, Geophysics, Geosystems*, v. 12, Q01004, doi:10.1029/2010GC003230, 26 pp.
- Kanamori, H., 1972, Mechanism of tsunami earthquakes: *Physics of Earth and Planetary Interiors*, v. 6, p. 346-359.
- Kawamura, K., Sasaki, T., Kanamatsu, T., Sakaguchi, A., and Ogawa, Y., 2012, Large submarine landslides in the Japan Trench: A new scenario for additional tsunami generation: *Geophysical Research Letters*, v. 39, L05308, doi:10.1029/2011GL050661, 5 pp.
- Pacheco, J. F., Sykes, L. R., and Scholz, C. H., 1993, Nature of seismic coupling along simple plate boundaries of the subduction type: *Journal of Geophysical Research*, v. 98, p. 14,113-14,159.
- Scholl, D. W., von Huene, R., Vallier, T. L., and Howell, D. G., 1980, Sedimentary masses and concepts about tectonic processes at underthrust ocean margins: *Geology*, v. 8, p. 564-568.
- Shreve, R. L., and Cloos, M., 1986, Dynamics of sediment subduction, melange formation, and prism accretion: *Journal of Geophysical Research*, v. 91, p. 10,229-10,245.
- Uyeda, S., and Kanamori, H., 1979, Back-arc opening and the mode of subduction: *Journal of Geophysical Research*, v. 84, p. 1049-1061.
- von Huene, R., and Scholl, D. W., 1991, Observations at convergent margins concerning sediment subduction, subduction erosion, and the growth of continental crust: *Reviews of Geophysics*, v. 29, p. 279-316.

# Crustal deformation of northeastern Japan clarified by geodetic observation over the past century

Takuya NISHIMURA<sup>a</sup>

<sup>a</sup>Disaster Prevention Research Institute, Kyoto University, Gokasho, Uji 611-0011, Japan, nishimura.takuya.4s@kyoto-u.ac.jp

## 1. Crustal deformation of the Tohoku-oki earthquake observed by GNSS

The 2011  $M_w$  9.0 Tohoku-oki earthquake is the first earthquake which pre-, co-, and post-seismic deformation is clarified by a dense GNSS (Global Navigation Satellite System; an high-precision space geodetic technique including GPS) network. A nationwide GNSS network GEONET operated by the Geospatial Information Authority of Japan detected eastward coseismic displacements and subsidence along the Pacific coast of the Tohoku region (Fig. 1b). The GEONET Oshika (960550) station closest to the epicenter moved 5.3 m in ESE and subsided as much as 1.2 m coseismically. GNSS data also clarified that significant displacement occurred not only in the Japanese Islands (Nishimura et al., 2011) but also throughout East Asia, extending more than 3,000 km away from the epicenter (e.g., Pollitz

et al. 2011). On the seafloor just above the source region, much larger coseismic displacements up to 60 m were detected by GPS/Acoustic technique (e.g., Sato et al., 2011).

Before the 2011 Tohoku-oki earthquake, GNSS showed compressional deformation of northeastern Japan parallel to the Pacific plate subduction along the Japan Trench (Fig. 1a). The observed deformation was interpreted as a result of interplate locking on the plate interface. The E-W compression had been observed since the start of GPS observation in 1994 but was gradually decelerated before 2011 (e.g., Nishimura, 2012). This tendency is evident in time-series of stations B, C, and D in Fig. 2. Interplate coupling estimates suggest that deceleration was caused by weakening of the coupling offshore of Fukushima and Ibaraki prefectures. This implies that the plate interface in part of the source region to the Tohoku-Oki

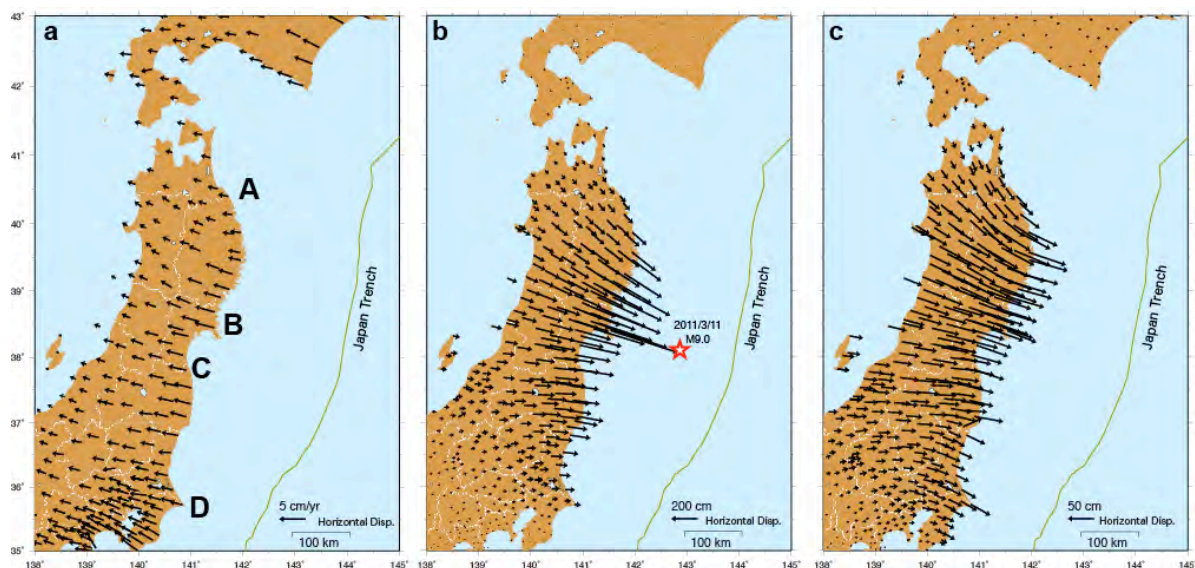


**Fig. 1.** Horizontal deformation of northeastern Japan at GEONET GNSS stations. (a) Preseismic velocity during 1997-2000. A-D denotes GNSS stations whose time-series are plotted in Fig. 2. (b) Coseismic displacement of the  $M_w$  9.0 2011 Tohoku-oki earthquake. (c) Postseismic displacement for a year following the Tohoku-oki mainshock.

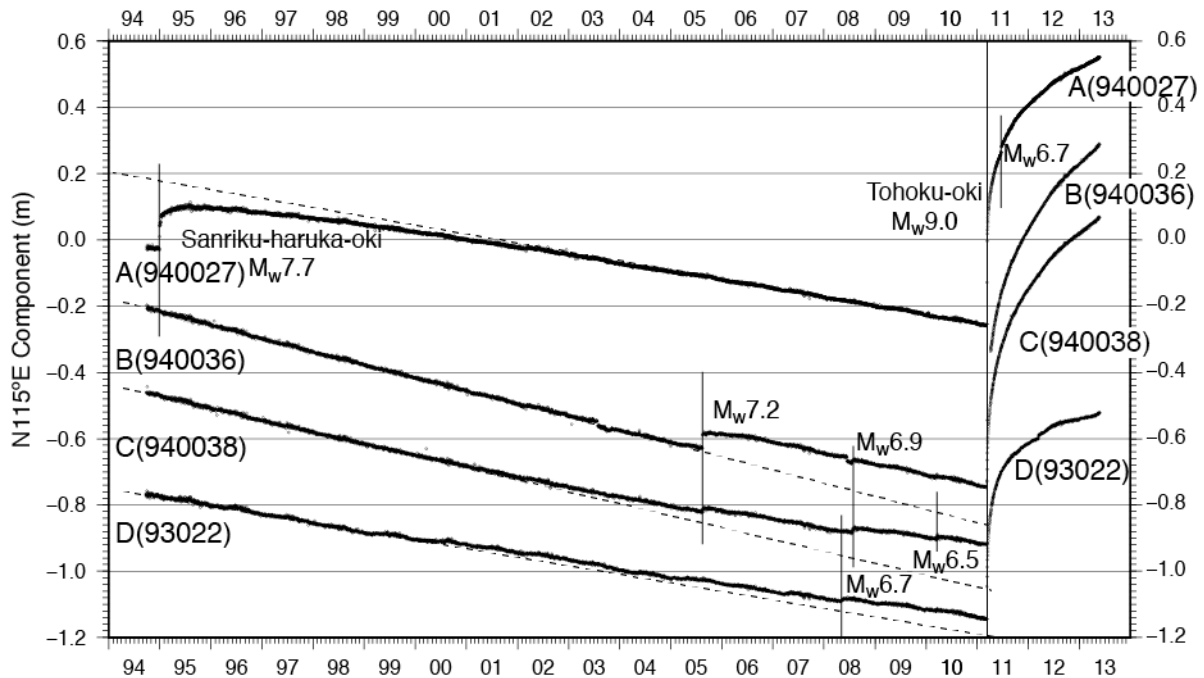


**Fig. 2.** Time-series of the selected GEONET GNSS stations along the Pacific coast of northeastern Japan. N115°E component is roughly parallel to a relative plate motion along the Japan Trench. Location of the GNSS station is plotted in Fig. 1a. A reference station is 940076 (Susa) in Yamaguchi Prefecture, western Japan. Coseismic offsets of the Tohoku-oki earthquake are not to scale.

earthquake was unlocked, contributing to the seismic rupture.

## 2. Crustal deformation for the past 120 years observed by geodetic surveys.

Terrestrial geodetic data has been accumulated to clarify the nature and temporal variation of crustal deformation in northeastern Japan for the 120-year period preceding the 2011  $M_w$  9.0 Tohoku-Oki earthquake. The Japanese government started modern geodetic survey including triangulation, trilateration, leveling, tide-gauge in 1880's. Based on triangulation and trilateration data, horizontal, regional strain is characterized by north–south extension for ~90 years. Large compressional strain in an east–west direction was observed only in the deformation zone in the central mountain range of northeastern Japan and along the eastern margin of the Japan Sea. Based on leveling data, vertical deformation is the result of subsidence up to 50 cm along the Pacific coast (Fig. 3a). The subsidence rate was roughly constant for 120 years, except for the Pacific side of the Fukushima prefecture where uplift

was observed for ~20 years beginning from 1939. Tide-gauge data on the Pacific coast shows sea-level rise, which is consistent with the rapid land subsidence observed by leveling.

In a geological time-scale, it is well-known that the Pacific coast of northeastern Japan was not subsided at a rate for the recent century. A part of the coast has marine terraces suggesting long-term uplift. Therefore, there was a discrepancy between geodetically-observed and geologically-observed deformations (e.g., Ikeda et al., 2012). There was a hypothesis that a giant earthquake would uplift the Pacific coast to resolve the discrepancy. However, the 2011 Tohoku-oki earthquake caused large-scale subsidence (Fig. 3b).

## 3. Ongoing postseismic deformation

Horizontal postseismic displacements are directed to the east similar to the coseismic one (Figs. 1b and 1c). However, significant postseismic deformation occurs over a larger area extending to the north and south from the coseismic one. A spatial pattern of vertical postseismic deformation is much different from

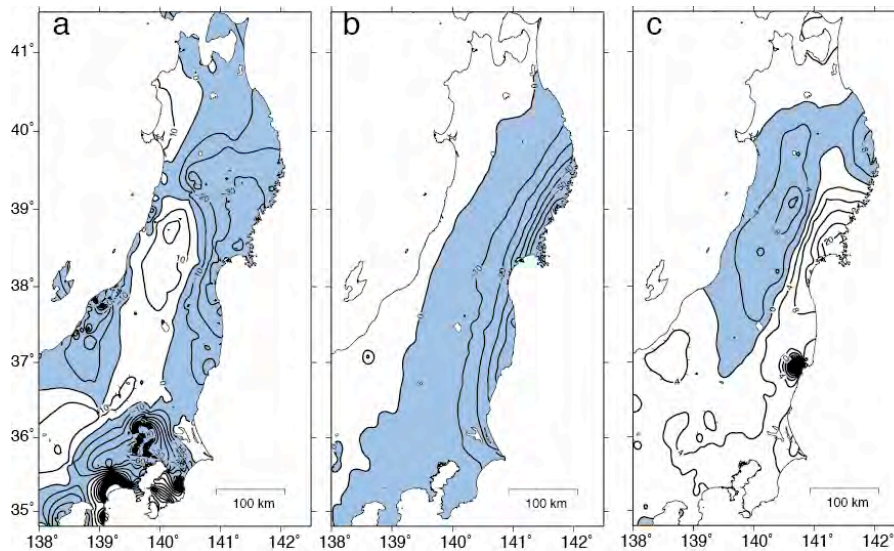


**Fig. 3.** Vertical deformation of northeastern Japan. A blue area is a subsided region. (a) Preseismic deformation measured by leveling for a century before the 2011 Tohoku-oki earthquake. (b) Coseismic deformation observed by GNSS. (c) Postseismic deformation measured by GNSS

that of coseismic one. The most part of coseismic subsided areas along the Pacific coast is uplifting after the mainshock (Figs. 3b and 3c). Uplift up to ~20 cm was observed for two years after the mainshock. On the other hand, the spatial distribution of the postseismic vertical deformation is quite similar to that of the preseismic deformation in a region between 36°N and 38°N, though a sign of up and down is opposite, suggesting the mechanism of the ongoing postseismic deformation is related with that of the preseismic deformation

Horizontal postseismic deformation decays with time and is at a rate of 1 cm per month now (Fig. 2). However, decay in vertical deformation seems to be slower than that in horizontal deformation. Fitting of an exponential decay curve to vertical daily displacement suggests that a time constant is 3-5 years and that the final uplift will be approximately a half of the coseismic subsidence. If the decay continues exponentially, another event needs to resolve the discrepancy of deformation between geodetic and geological time-scales. If the uplift rate is kept at that in the last year, the coseismic subsidence will be recovered in the next decade. Post-seismic deformation is the key to resolving the discrepancy

## References

- Ikeda, Y., S. Okada, and M. Tajikara (2012) Long-term strain buildup in the Northeast Japan arc-trench system and its implications for gigantic strain-release events, *J. Geol. Soc. Jpn.*, 118, 294-312 (in Japanese with English abstract).
- Nishimura, T. (2012) Crustal deformation of northeastern Japan based on geodetic data for recent 120 years, *J. Geol. Soc. Jpn.*, 118, 278-293 (in Japanese with English abstract).
- Nishimura, T., Munekane H., Yurai H. (2011) The 2011 off the Pacific coast of Tohoku Earthquake and its aftershocks observed by GEONET. *Earth Planets Space* 63: 631-636.
- Pollitz, F.F., Bürgmann R., Banerjee P. (2011). Geodetic slip model of the 2011 M9.0 Tohoku earthquake. *Geophys. Res. Lett.* 38: L00G08
- Sato M, Ishikawa T, Ujihara N, Yoshida S, Fujita M, Mochizuki M, and Asada A. 2011a. Displacement Above the Hypocenter of the 2011 Tohoku-Oki Earthquake, *Science* 332: 1395

# Strain buildup and release in the Northeast Japan orogen over geologic and geodetic time scales with implications for gigantic subduction earthquakes

Yasutaka Ikeda<sup>a</sup>

<sup>a</sup>Department of Earth and Planetary Science, University of Tokyo, Hongo 7-3-1, Bunkyo-ku, Tokyo 113-0033, Japan, ikeda@eps.s.u-tokyo.ac.jp

## 1. Introduction

Crustal strain is build up in and around a subduction zone in association with interseismic coupling on the plate interface. The elastic component of crustal strain is released during episodic decoupling events on the plate boundary; the remainder is accommodated as

permanent (= inelastic) deformation mainly within the subduction-related orogenic zone. Coseismic deformation is basically elastic, although damped by asthenospheric viscosity and thereby followed by postseismic deformation. Recent GPS observations have made it possible to detect crustal strain precisely and extensively, but are not sufficient in time to cover a whole cycle of strain buildup and release in subduction-related orogens. Furthermore, virtually no geophysical method exists to discriminate between elastic and inelastic components in geodetic signals. We propose here that geological methods and data should be used to evaluate inelastic strain buildup quantitatively, thereby to evaluate present-day elastic strain buildup, which may eventually result in gigantic earthquakes.

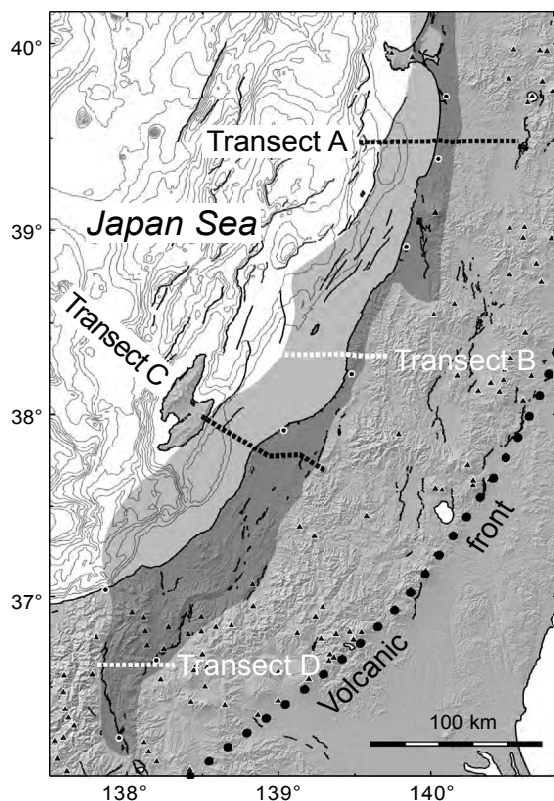


**Fig. 1.** Map of the backarc side of the Northeast Japan arc, showing distribution of faults and major tectonic elements (simplifying from Okada and Ikeda, 2012). Shaded area is the Uetsu-Northern Fossa Magna Basin, which was formed as a rift basin in Early-Middle Miocene time and has subsequently reactivated as a locus of contractive deformation since Early Pliocene time. Geologic cross sections along transects A and C are shown in Figure 2.

## 2. Discrepancy between geologic and geodetic strain observations

There has been a discrepancy between long-term (geologic) and short-term (geodetic) strain observations in both horizontal and vertical directions over the Northeast Japan (NEJ) arc. Geodetic observations in the past ~100 years have revealed strain accumulation across the NEJ arc at a rate as high as  $10^{-7}$  strain/yr, whereas geologically observed strain rates are one order of magnitude slower (Fig. 2). A similar discrepancy exists also in vertical movements; tide gauge records along the Pacific coast have indicated subsidence at a rate as high as ~10 mm/yr during the last ~80 years (Fig. 3), whereas late Quaternary marine terraces indicate long-term uplift at 0.1-0.4 mm/yr. The ongoing rapid coastal subsidence is due to dragging by

the subducting Pacific plate beneath the NEJ arc. Thus, most of the strain accumulated in the last 100 years at abnormally high rates is elastic, and is to be released by slip on the coupled plate interface. Only a fraction (~10%) of geodetically-observed crustal shortening is accommodated within the NEJ arc as long-term (inelastic) deformation.

### 3. Elastic strain buildup resulting in giant decoupling event

Fairly large (Mw 7-8) subduction earthquakes occurred in the past ~100 years on the Kuril-Japan subduction zone, but they had nothing to do with strain release or coastal uplift. The 2011 Tohoku earthquake of Mw 9.0, whose rupture surface encompassed those of previously occurred Mw 7-8 subduction earthquakes, is

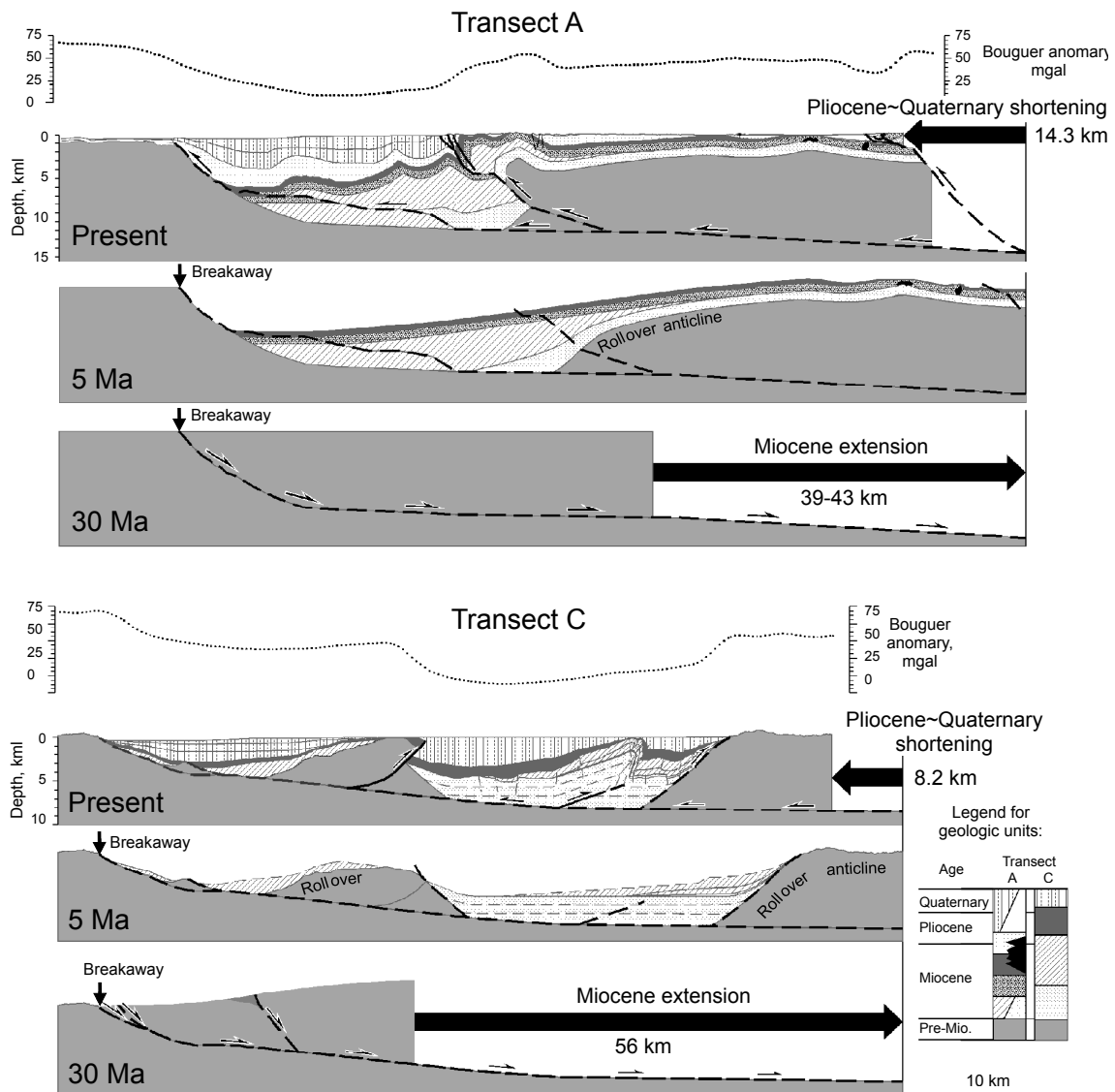


**Fig. 2.** Present-day and restored geologic cross-sections along two transects across the Uetsu–Northern Fossa Magna Basin on the back-arc side of Northeast Japan (simplified from Okada and Ikeda, 2012). See Fig. 1 for location. Each set of four figures shows, from the top to the bottom, Bouguer gravity anomaly, present-day geologic section, restored geologic section before the Pliocene positive tectonic inversion, and restored geologic section before Miocene extension. Note that contractive deformation across NEJ arc is concentrated within the Uetsu-Fossa Magna Basin, across which rates of contraction are calculated at 2-4 mm/yr during the last 3.5-5 Myr, much less than GPS-derived contraction rates.

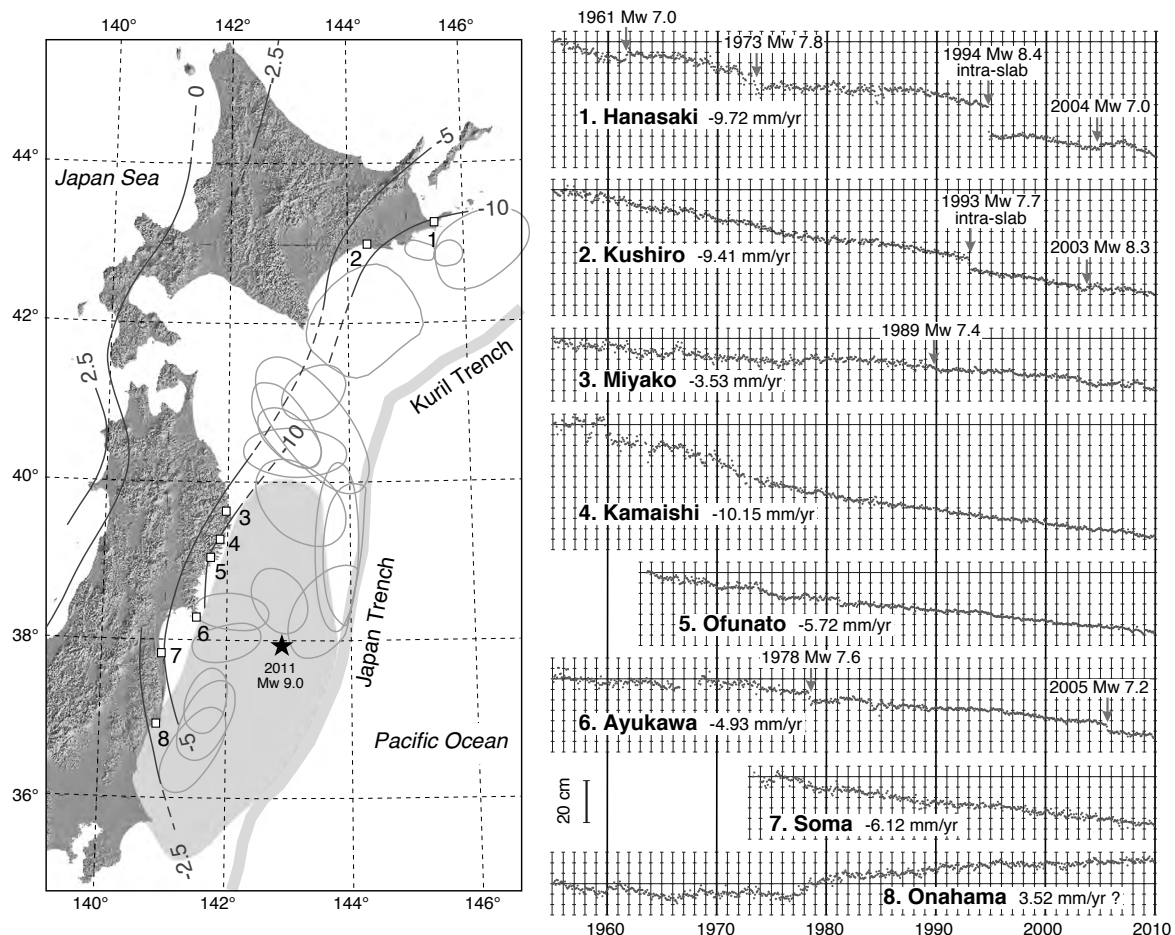


**Fig. 3.** [Left] Map showing recent vertical crustal movements and source areas of large subduction earthquakes (Ikeda and Okada, 2011; Ikea et al., 2012). Contour lines indicate rates of uplift (in mm/yr) revealed by tide gauge observations during the period 1955-1981 (Kato, 1983). Open ovals indicate source areas of subduction earthquakes of  $M_w \geq 7.0$  since 1896. The epicenter and source area of the 2011 Tohoku earthquake of  $M_w 9.0$  are indicated by an asterisk and a shaded oval, respectively. Open squares indicate tide-gauge stations; station numbers correspond to those in the right figure. [Right] Selected tide-gauge records along the Pacific coast (Geographical Information Authority of Japan, 2010). See the left figure for the location of each station. Arrows indicate large earthquakes ( $M_w \geq 7.0$ ) that occurred near each station. Note progressive subsidence of the Pacific coast at rates as high as 5-10 mm/yr, except for the Onahama station, which has likely been affected by coal mining.

likely to be such a decoupling event that effectively releases the elastic strain due to plate coupling. Pattern of interseismic subsidence indicates that, at 50~100 km depths down-dip of the 2011 rupture, there still exists a coupled part of plate interface, on which a large amount of aseismic after slip may occur in the coming decades.

#### 4. Global comparison

A global survey suggests that gigantic ( $M_w \geq 9.0$ ) subduction earthquakes are classified into two types: the NEJ type and the Chilean type. The Chilean type strain buildup/release process is simple and straightforward in the sense that seismogenic zone (down to a 40-50 km depth) plays everything. The source areas of the 1960 Chile, 1964 Alaska, and 1700 Cascadia

earthquakes lack evidence for interseismic deep

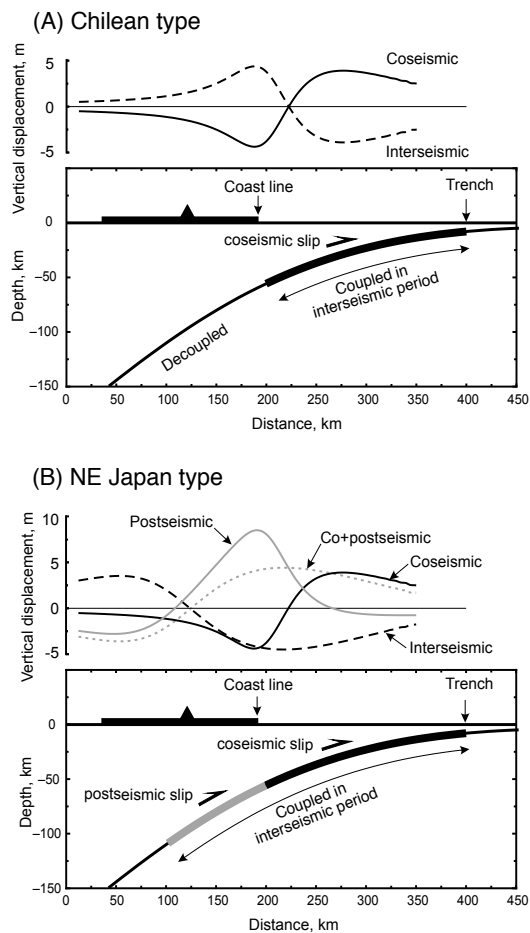


**Fig. 4.** Two types of strain buildup and release at subduction zones that produce gigantic ( $\geq 9.0$ ) subduction earthquakes (Ikeda, 2012; Ikeda et al., 2012). The geometry of plate interface and amounts of surface deformation could be arbitrary but are represented in this figure by those of the 2011 Tohoku earthquake. (A) Chilean type strain buildup/release process. The source areas of the 1960 Chile, 1964 Alaska, and 1700 Cascadia earthquakes lack evidence for interseismic deep coupling. Paleoseismological evidence indicates interseismic uplift around the down-dip edge of coseismic rupture, where coseismic subsidence is observed. This implies that the deeper plate interface is basically decoupled in interseismic periods, although subtle postseismic slip could exist on a transition zone down-dip of the coseismic rupture. (B) Northeast Japan type strain buildup/release process. The Northeast Japan subduction zone is, on the other hand, likely to be unique in that interseismic coupling occurs to a depth as deep as  $\sim 100$  km, and that seismic decoupling occurs only on the shallower plate interface (0–50 km depths) while the deeper interface (50–100 km depths) decouples aseismically following the earthquake.

coupling. Paleoseismological evidence indicates interseismic uplift around the down-dip edge of coseismic rupture, where coseismic subsidence is observed. This implies that the deeper plate interface is basically decoupled in interseismic periods, although subtle postseismic slip could exist on a transition zone down-dip of the coseismic rupture. In contrast, the NEJ type strain buildup/release process seems to be exceptional in that interseismic coupling occurs to a depth as deep as  $\sim 100$  km. Its decoupling process is two-fold: seismic decoupling occurs only on the shallower plate interface while the deeper interface (50–100 km depths) decouples aseismically following the earthquake. A possible cause for such deep coupling would be thermal; the oceanic lithosphere of the western Pacific is very old and therefore cold, and has subducted beneath the NEJ-Kuril arc.

## References\*

- Ikeda, Y. (2011) Long-term strain buildup in the Northeast Japan arc-trench system and its implications for the gigantic subduction earthquake of March 11, 2011, Proceedings of the International Symposium on Engineering Lessons Learned from the 2011 Great East Japan Earthquake, March 1-4, 2012, Tokyo, Japan, pp. 238-253.
- Ikeda, Y., Okada, S., and Tajikara, M. (2012) “Long-term strain buildup in the Northeast Japan arc-trench system and its implications for gigantic strain-release events,” *J. Geol. Soc. Japan* 118, 294-312. (in Japanese with English Abstract)
- Okada, S., and Ikeda, Y. (2012) Quantifying crustal extension and shortening in the back-arc region of Northeast Japan, *J. Geophys. Res.*, 117, B01404, doi:10.1029/2011JB008355.

\*Only selected references are listed here. For a complete set of references, see Ikeda et al. (2012).

# The 2011 Tohoku-oki tsunami and paleotsunami deposits at the Pacific coast of Tohoku

Kazuhisa Goto<sup>a</sup>

<sup>a</sup>*International Research Institute of Disaster Science, Tohoku University, Aoba 6-6-40-102, Aramaki, Aoba-ku, Sendai 980-8579, Japan, goto@irides.tohoku.ac.jp*

## 1. Introduction

Major objectives of tsunami geology are understanding histories and sizes of the paleotsunamis (e.g., Goff et al., 2012). Studies of recent examples are very useful to interpret the paleotsunamis and their deposits. This is because the tsunami flow characteristics of the recent events, which are usually unavailable for paleotsunami events, are well known. In this aspect, many post-tsunami geological surveys were conducted and our understanding regarding to the tsunami deposits has been significantly improved during the last ~10 years (e.g., Goff et al., 2012).

The 2011 Tohoku-oki tsunami was an important turning point to obtain vast data of both tsunami and tsunami deposits. Extensive post-tsunami surveys were conducted after the event and more than 5,000 data of the flow depths or run-up heights were collected by the effort of joint survey group (Mori et al., 2012). More than 1000 geological data of the 2011 Tohoku-oki tsunami were collected by many researchers (see summary by Goto et al., 2012).

In this presentation, I review our understanding of the tsunami histories along the Pacific coast of Tohoku that was obtained prior to the 2011 event mainly based on Goto et al. (2012) and introduce ongoing researches in this particular region to better understand the paleotsunami histories based on the lessons learned from the 2011 event.

## 2. Historical and geological evidence of tsunami at the Pacific coast of Tohoku

As Goto et al. (2012) summarized, 22

tsunamis excluding the 2011 Tohoku-oki event have been recorded since the 9th Century on the Pacific coast of Tohoku. Among them, fatalities exceeded 1,000 people in four of these events; the AD869 Jogan, AD1611 Keicho, AD1896 Meiji and the AD1933 Showa tsunamis (Shuto et al., 2007). However, except for the recent AD1896 and AD1933 events, historical descriptions are insufficient to estimate the tsunami source models. Therefore, geological studies before the 2011 event were mainly targeted to understand the inundation area and recurrence interval of these historical events as well as the prehistoric ones (e.g., Sawai et al., 2006). A recurrence interval for large-scale tsunamis on the Sendai Plain has been estimated at around 600-1300 years (e.g., Minoura and Nakaya, 1991). The AD869 Jogan event that was occurred approx. 1100 years ago is now assumed as possible predecessor of the 2011 Tohoku-oki event. In this sense, the 2011 Tohoku-oki tsunami was the first example of a large, low-frequency event occurring where historical and pre-historical tsunamis were already known to have occurred through historical and geological evidence (Goto et al., 2012).

## 3. Ongoing researches

The geological study of the paleotsunami after the 2011 event is mainly focused on re-evaluation of the magnitude of the AD869 Jogan earthquake and tsunami since it is critically important for the future understanding of tsunami risk along the Pacific coast of Tohoku (Goto et al., 2012). As seen in Figure 1,

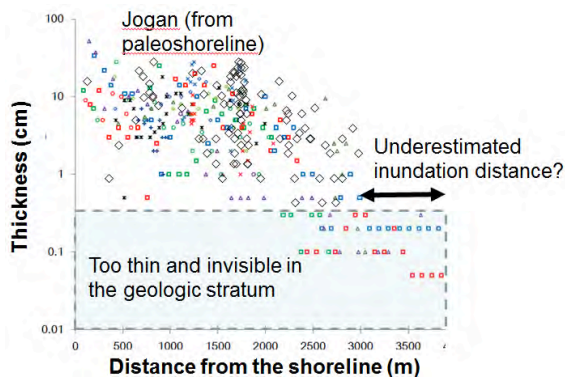


**Fig. 1.** Thickness distributions of the 2011 Tohoku-oki tsunami (Goto et al., 2011; Abe et al., 2012) and AD869 Jogan (Sugawara et al., 2012) deposits.

thickness distributions of the 2011 and the Jogan tsunami deposits against the distance from the shoreline (and paleo-shoreline at Jogan age) is remarkably similar (Goto et al., 2011; Abe et al., 2012; Sugawara et al., 2012). Beyond approx. 3 km from the shoreline, sand layer of <1 mm was deposited below the thick mud deposits in case of the 2011 tsunami deposits. Thin sand deposits, typically thinner than 0.5 cm, is very difficult to identify in the geologic record and such thin layer may not be recognizable (or not preserved). Moreover, mud deposit formed by the Jogan event has not been reported so far. Therefore, there is a potential that we might have underestimated the inundation distance of Jogan tsunami (Goto et al., 2011; Namegaya et al., 2013).

Namegaya et al. (2013) reported that  $M_w > 8.6$  is required as the moment magnitude of Jogan earthquake if we assume 1.2 m flow depth at the maximum extent of sand of Jogan deposit following the knowledge obtained from the 2011 event. This result may suggest that accurate estimation of the inundation distance plus flow depth is very important to better estimate the fault model.

In the mud deposits, geochemical signatures are observed (Goto et al., 2011; Chagué-Goff et al., 2012). Recognition of such muddy tsunami deposits from the geological record is a challenge issue but will be critically important for

future tsunami risk assessment (Chagué-Goff et al., 2012). Another important aspect in the re-evaluation of the magnitude of AD869 Jogan earthquake and tsunami is whether deposits can be identified further north (Goto et al., 2012) and such researches are now ongoing (e.g., Iijima et al., 2013; Tanigawa et al., 2013).

## References

- Abe, T., Goto, K., Sugawara, D. (2012) Relationship between the maximum extent of tsunami sand and the inundation limit of the 2011 Tohoku-oki tsunami on the Sendai Plain, Japan. *Sedimentary Geology*, 282, p. 142–150.
- Chagué-Goff, C., Andrew, A., Szczuciński, W., Goff, J., Nishimura, Y. (2012) Geochemical signatures up to the maximum inundation of the 2011 Tohoku-oki tsunami - Implications for the 869 AD Jogan and other palaeotsunamis. *Sedimentary Geology*, 282, p. 65–77.
- Goff, J., Chagué-Goff, C., Nichol, S.L., Jaffe, B., Dominey-Howes, D. (2012) Progress in palaeotsunami research. *Sedimentary Geology* 243-244, p. 70–88.
- Goto, K., Chagué-Goff, C., Fujino, S., Goff, J., Jaffe, B., Nishimura, Y., Richmond, B., Sugawara, D., Szczuciński, W., Tappin, D. R., Witter, R., Yulianto, E. (2011) New insights of tsunami hazard from the 2011 Tohoku-oki event. *Marine Geology* 290, p. 46–50.
- Goto, K., Chagué-Goff, C., Goff, J., Jaffe, B. (2012) The future of tsunami research following the 2011 Tohoku-oki event. *Sedimentary Geology*, 282, p. 1–13.
- Iijima, Y., Sugawara, D., Goto, K., Chagué-Goff, C., Hayase, R., Hashimoto, K., Kon, S., Nakamura, N., Goff, J., Possible paleo-tsunami deposits at Rikuzentakata City, Japan. IGU 2013 Kyoto Regional

Conference.

- Minoura, K., Nakaya, S. (1991) Traces of tsunami preserved in inter-tidal lacustrine and marsh deposits: some examples from northeast Japan. *Journal of Geology* 99, p. 265–287.
- Mori, N., Takahashi, T., and the 2011 Tohoku earthquake tsunami joint survey group (2012) Nationwide post event survey and analysis of the 2011 Tohoku Earthquake Tsunami: *Coastal Engineering Journal*, 54, 27 p.
- Namegaya, Y., Satake, K. (2013) Estimation and sensitivity of fault parameters from distribution of tsunami deposit. Japan Geoscience Union Meeting, MIS25-09.
- Sawai, Y., Shishikura, M., Okamura, Y., Aung, Than Tin, Matsu'ura, T., Takada, K., Fujii, Y., Satake, K. (2006) History of tsunami inundations in Sendai Plain, detected from coastal geology. Abstract of Japan Geoscience Union Meeting 2006. Japan Geoscience Union, Tokyo, S208-009.
- Shuto, N., Koshimura, S., Satake, K., Imamura, F., Matsutomi, H. (2007) An encyclopedia of tsunami. Asakura Publishing Co. Ltd., 368p.
- Sugawara, D., Goto, K., Imamura, F., Matsumoto, H., Minoura, K. (2012) Assessing the magnitude of the 869 Jogan tsunami using sedimentary deposits: Prediction and consequence of the 2011 Tohoku-oki tsunami. *Sedimentary Geology*, 282, p. 14–26.
- Tanigawa, K., Sawai, Y., Shishikura, M., Fujiwara, O., Namegaya, Y. (2013) Geological study on tsunami deposits in the Pacific coast of Aomori, northern Japan. Japan Geoscience Union Meeting, MIS25-12.

# Sediment transport by the 2011 Tohoku-oki tsunami at Sendai Plain: implications from numerical simulation

Daisuke Sugawara<sup>a</sup>, Tomoyuki Takahashi<sup>b</sup>, Fumihiko Imamura<sup>c</sup>

<sup>a</sup>International Research Institute of Disaster Science, Tohoku University, 6-6-11-1106 Aoba, Aramaki, Aoba-ku, Sendai, Miyagi 980-8579, Japan, sugawara@irides.tohoku.ac.jp

<sup>b</sup>Kansai University, 7-1, Hakubai-cho, Takatsuki, Osaka 569-1098, Japan, tomot@kansai-u.ac.jp

<sup>c</sup>International Research Institute of Disaster Science, Tohoku University, 6-6-11-1106 Aoba, Aramaki, Aoba-ku, Sendai, Miyagi 980-8579, Japan, imamura@irides.tohoku.ac.jp

## 1. Introduction

The 2011 Tohoku-oki tsunami struck Sendai Plain, northeast Japan, with up to 10-m-high waves and caused massive damages to the coastal areas. Post-tsunami field surveys revealed that the tsunami left sandy deposits onshore of the plain with few tens of centimeters to millimeters in thickness, which extended up to 2.5-3.0 km from the coastline (e.g., Abe et al.,

2012); meanwhile the tsunami inundated the plain up to 4-5 km from the coastline. The sandy tsunami deposits reached only ~60% of the inundation distance. Micropaleontological analysis of diatom assemblages showed notable lack of marine species in the tsunami deposits (Szczuciński et al., 2012). Thus, most of the tsunami deposit is considered to have been originated mainly from the nearshore zone and beach, rather than the offshore sea bottom.

It is still not clear why small amount of marine species were included in the tsunami deposit, and why such a considerable gap between the ultimate reach of the deposit and inundation was observed in the plain. In this study, a numerical modeling of the tsunami inundation coupled with sediment transport was performed to give answers to these questions.

## 2. Method

In this study, propagation and inundation of the tsunami was calculated using a tsunami hydrodynamic model (TUNAMI-N2; Goto et al., 1997) that is founded on the nonlinear shallow-water theory. The sediment transport model (Takahashi et al., 2000) was used to compute erosion, deposition and resulting morphological change due to the tsunami.

The datasets obtained before and after the 2011 Tohoku-oki tsunami are valuable for execution and validation of the modeling research on tsunami sediment transport. The tsunami source model by Sugino et al. (2013), which well reproduces the observed waveform at GPS buoys and coastal wave gauges, was used for the initial waveform of the tsunami (fig.

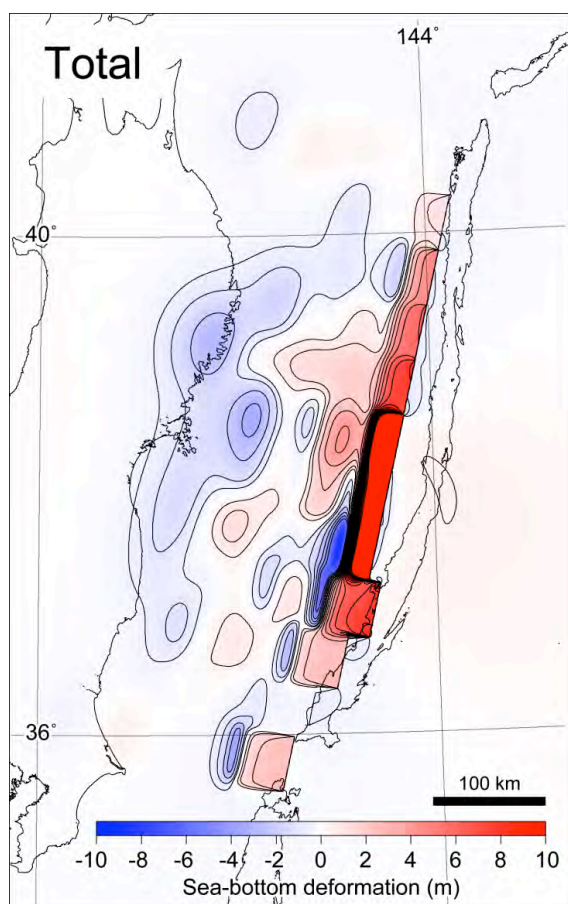


**Fig. 1.** Ultimate crustal deformation calculated by the fault model of the Tohoku-oki earthquake proposed by Sugino et al. (2013).

1). The waveform is calibrated to fit the simulation with available field data on inundation area and onshore tsunami heights. Generation, propagation, inundation and sediment transport of the tsunami were computed using a nesting grid system. A high-resolution digital elevation model and a land use map of Sendai Plain, with a spatial resolution of 5 m, was used to reproduce the effects from microtopography including engineering structures to the sediment transport, as well as initial distribution of sediment source.

### 3. Results and discussion

The simulation showed that erosion of the sea bottom was quite minor (Fig. 2). Small amounts of sea-bottom sediments were suspended during the passing of the largest first wave, although the flow speed exceeded 3 m/s in the offshore.

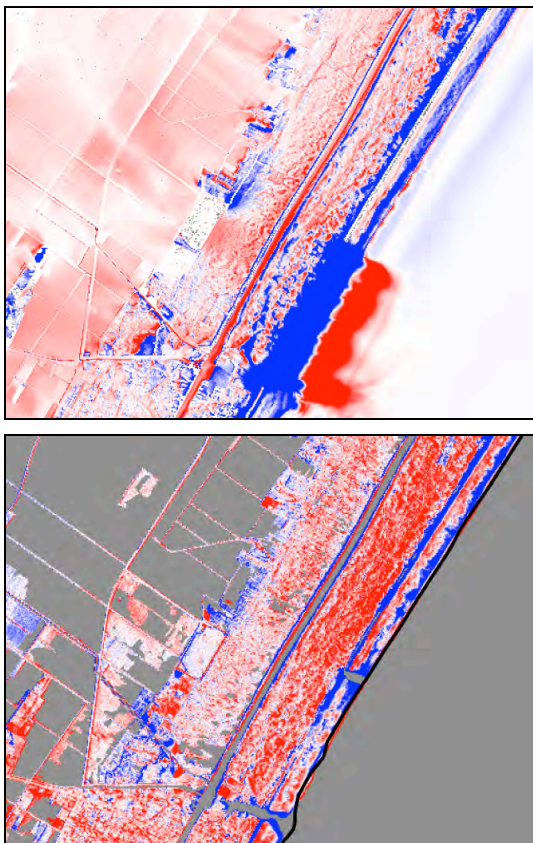


**Fig. 2.** Comparison of simulated and observed morphological change due to the tsunami. Top: simulation, bottom: estimation from pre- and post-tsunami digital elevation models.

In addition, most of the suspended sediment did not advect shoreward, because of the delay of the increase in the volume of suspended sediment in the offshore. This may explain the notable lack of marine diatoms in the tsunami deposit.

The simulated tsunami inundation reached 4 km from the present coastline, which is fairly consistent with the observation. Meanwhile the simulated deposition of the sand was terminated at ~2.5 km from the coastline, showing a good agreement with the field data. The comparison of the simulation with available pre- and post-tsunami topography data demonstrated a general agreement in the patterns of tsunami erosion and deposition (fig. 2). The results showed that overall thickness distribution of the simulated deposit is consistent with the observed deposit thickness, in particular shore-normal distribution pattern and local variability of the deposit (fig. 3). Visualization of the process of sediment transport showed considerable change in the amount of suspended sediment across the engineering structures, such as the coastal dikes and paved roadways. Deceleration and acceleration of the flow and the change in the flow depth took place across the elevated features. More sediment was deposited at the seaward face of the dikes, and less amount of sand was deposited in the lee of them. Thus, effects from microtopography cannot be neglected to interpret the difference between tsunami inundation and deposition.

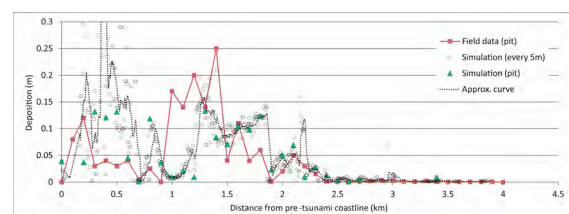


**Fig. 3.** Comparison of the simulated and observed thickness of tsunami deposits in Sendai Plain.

#### 4. Conclusion

Although the numerical modeling of tsunami sediment transport requires further improvement and validation, the simulation is useful to understand the regional characteristics of tsunami erosion and deposition, as well as to interpret the formation process of tsunami deposits.

#### Reference

- Abe, T., Goto, K., Sugawara, D., 2012. Relationship between the maximum extent of tsunami sand and the inundation limit of the 2011 Tohoku-oki tsunami on the Sendai Plain, *Sedimentary Geology* 282, 142-150.
- Goto, C., Ogawa, Y., Shuto, N., Imamura, F., 1997. IUGG/IOC Time Project, Numerical method of tsunami simulation with the Leap-Frog scheme. *IOC Manuals and Guides*, UNESCO, Paris, 130 p.
- Sugino, H., Wu, C., Korenaga, M., Nemoto, M., Iwabuchi, Y., Ebisawa, K., 2013. Analysis and verification of the 2011 Tohoku Earthquake Tsunami at Nuclear Power Plant Sites. *The Journal of Japan Association for Earthquake Engineering* 13, 2-21.
- Szczuciński, W., Kokociński, M., Rzeszewski, M., Chagué-Goff, C., Cachão, M., Goto, K., Sugawara, D., 2012. Sediment sources and sedimentation processes of 2011 Tohoku-oki tsunami deposits on the Sendai Plain, Japan – Insights from diatoms, nonnoliths and grain size distribution. *Sedimentary Geology* 282, 40-56.
- Takahashi, T., Shuto, N., Imamura, F., Asai, D., 2000. Modeling sediment transport due to tsunamis with exchange rate between bed load layer and suspended load layer. *Proc. Int. Conf. Coast. Eng.* 2000, 1508-1519.

# Tsunamis and tsunami deposits: Looking beyond the sand

James Goff<sup>a</sup>

<sup>a</sup> *School of Biological, Earth and Environmental Sciences, University of New South Wales, Sydney, NSW 2052, Australia, j.goff@unsw.edu.au*

## 1. Introduction

In the wake of a decade of large and unexpected tsunamis such as the 2004 Indian Ocean, 2009 South Pacific and 2011 Tohoku-oki events researchers, coastal managers, local and national governments and many others are all faced with the challenging task of trying to get a better understanding of the tsunami “problem”. Ultimately, any actions taken to address the risk, educate people, mitigate the effects and so on hinge upon our understanding of the hazard – how big, how often and where from?

Our ability to understand the tsunami hazard for any area is initially governed by the historical record of past events. Indeed, in many cases this forms the only basis for many probabilistic tsunami hazard assessments. Unfortunately, for many parts of the world, historical records are short - a little more than 200 years for Australia and less than that for New Zealand. Even in countries such as Japan where the historical record extends back well over a millennia, the evidence for earlier events becomes sparse and less reliable than their recent counterparts. In the absence of any other alternatives, researchers must fall back on other lines of evidence. The most popular form is that of the sediments that tsunamis leave behind and many geological studies have been the focus of attempts to better understand our tsunami past. Sadly, the recent decade of large and unexpected tsunamis has thrown into light some of the shortcomings of such work, but these events have also served as a catalyst for the development of innovative techniques and thinking in tsunami research.

## 2. Palaeotsunamis

In many parts of the world, palaeotsunamis are recognised as having been notably larger than anything reported in historical time, while in other regions they are at least of similar size to historically documented events (e.g. Cisternas et al., 2005). In all cases however, palaeotsunamis provide a window into the past, allowing us to better understand the magnitude and frequency of past events along a stretch of coastline, often adding several millennia to a short historical record. What is surprising however is that little use is made of these data for probabilistic and other types of tsunami hazard assessments (e.g. Power et al., 2012; Goff et al., 2011).

For a variety of reasons we continue to be surprised by the size of recent tsunamigenic earthquakes and, by association, the size of the resulting tsunamis and yet there in several cases palaeotsunami data already existed to inform those studying the hazard (Satake and Atwater, 2007; Goto et al., 2011). Much of the failure to incorporate palaeotsunami data into hazard assessments is not because of the absence of material but rather a longstanding reluctance to accept or use such forms of non-instrumental or historical information in scenario modelling (e.g. Power et al., 2012). In essence, evidence for palaeotsunamis based upon recognised multi-proxy techniques is considered to contain unquantified uncertainties that are too difficult to incorporate into models. It is only when inundation scenarios considered relatively “extreme” (when extrapolated from historical data) are modelled that surprise is expressed about how closely they match palaeo-tsunami

information. The implication here is that palaeotsunami data are now acceptable because they can be modelled as opposed to the physical evidence for these past events being used to guide the modelling in the first place. This is unfortunate since in the absence of the incorporation of palaeotsunami data, tsunami hazard assessments will likely continue to under-estimate the magnitude, frequency and sources of events (e.g. Goff et al., 2011).

Goff et al., (2012) produced a summary of the most recent “toolbox” of proxies used by tsunami and palaeotsunami researchers. It contained 30 different proxies, a significant advance on the 14 proposed in 2001 (Goff et al., 2001). This toolkit contains more than just geological proxies, but it also indicates that geologically, it is important to try and study the entire tsunami deposit, not just the coarse sediment fraction (the “tsunami sand”) but the finer sediments, organics, microfossils, and more importantly perhaps, the geochemistry. In this regards, there has been a significant sea change in the study of tsunami deposits over the past couple of years as new analytical equipment has become available allowing geochemical analyses to be carried out not only non-invasively but also at a sub-millimetre resolution. What used to be considered a somewhat expensive and tangential proxy analysis is now becoming significantly more relevant and capable of producing pertinent, fine resolution data far cheaper than its now somewhat time-consuming and invasive counterparts such as microfossil analysis. For example, in the absence of sediments and microfossil assemblages, the geochemical signature of the Tohoku-oki tsunami could be identified up to the maximum point of inundation – not surprisingly, such findings have wide-ranging implications for future tsunami research (Chagué-Goff et al., 2012; Goto et al., 2012).

The study of palaeotsunamis extends well beyond that of just the potential deposits themselves and recognises that in seismically

active regions such as Japan, giant earthquakes act as regionally significant drivers of both immediate and delayed environmental responses (Goff and McFadgen, 2002). On a region-wide basis, Goff and McFadgen (2002) linked post-seismic changes in a “Seismic Staircase” model in which factors such as tsunamis, landslides, increased fluvial sediment transport, coastal beach ridge formation and settlement abandonment combine to create a sequence of human and geomorphological responses to a large earthquake (Fig. 1). As a part of the sediment transfer model, large pulses of fine material created by co-seismic landsliding are moved to the coast by rivers and then by longshore drift to leave a clear signature in the landscape in the form of a new, prograding sand beach ridge. These can often form up to several decades after the earthquake driving event

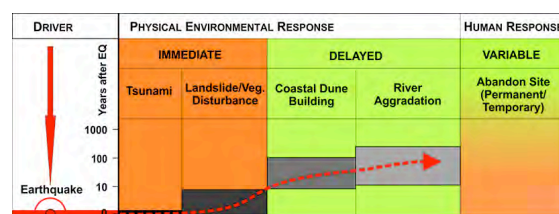


**Fig. 1.** Summary of the Seismic Staircase model (after Goff and McFadgen, 2002). Red dashed arrow follows the grey ‘steps’ of immediate and delayed responses of the physical environment. Human responses are both immediate and delayed.

(Wells and Goff, 2006; Fig. 1). The effects of a single large earthquake are often responsible for the ‘Seismic Driving’ of environmental after-effects well beyond a single catchment, causing near-contemporaneous beach ridge formation over 100’s km of coastline (Wells and Goff, 2007). Equally, it has been reported that multiple large earthquakes over hundreds of years were responsible for a coastal plain comprising numerous sand beach ridges (Wells and Goff, 2007).

### 3. Beach ridges in Japan

The beach ridges of northern Honshu, and in

particular those of the Sendai Plain on Japan's east coast, are located within a highly seismically active region. The question therefore arises as to whether or not these distinct geomorphological features are indicators of local or regional palaeoseismicity (and, by association, palaeotsunamis). Upon closer investigation there is a compelling link between the dates of past tsunamis and the ages of these beach ridges. Indeed, the sandy beach ridge system of the Sendai Plain can be used as an example of the seismic driving of coastal geomorphological change. However, this suite of processes extends well beyond the immediate environs of the coastal plain to include region-wide tsunami inundation, strong ground motion, vertical tectonic movement, landsliding, river sediment transport and beach ridge formation.

A comparison between several beach ridge systems throughout northern Honshu (e.g. Aomori, Akita) indicates that there is a widespread synchronicity to their formation that can also be explained by seismic driving. As an indirect proxy for palaeotsunamis, the beach ridge systems of northern Honshu may well represent a geomorphological record of past subduction earthquakes allowing us to extend our understanding of past events many thousands of years back in time. While more work needs to be done, the potential exists to gauge a better grasp of the region-wide or even nationwide magnitude and frequency of past earthquakes and tsunamis based partly upon the spatial and temporal extent of beach ridges.

#### **4. Into the future**

To reiterate the point, we continue to be surprised by the size of recent tsunamigenic earthquakes and, by association, the size of the resulting palaeotsunamis. As tsunami researchers it is imperative that we explore as many avenues as possible to try and understand that magnitude and frequency of these events. There are numerous proxy data available for us to use and while, as geologists, many of us may

be uncomfortable trying to make sense or even use the outputs of other disciplines (or even our own) they can serve to significantly enrich our knowledge base. While this abstract has focussed solely on earthquake-related scenarios, it is an interesting point to note is that by their very nature, the study of tsunamis extends well beyond earthquake sources. The development of proxy techniques and our understanding of the wider human and environmental signals of palaeotsunamis places tsunami research outside of the realm of mere seismology and as such it should be recognised that there is more to tsunamis than just earthquakes. Not only that, but recent developments have seen a reversal in the focus of tsunami research. As opposed to searching for the depositional evidence of a known tsunamigenic earthquake, we are now starting to use tsunami deposits to determine the magnitude and source of previously unknown palaeoseismic events (e.g. Goff et al., 2011). Therefore, not only must we strive to improve our understanding of the magnitude of past tsunamis, but we must also give a thought to their sources. In areas adjacent to subduction zones the need may be less immediate, but for more distant locations (e.g. Hawaii) it will be vital to know which source areas are of most concern. That cannot be achieved through seismic driving models but it can be through the proxy toolbox that continues to expand as we learn more about tsunamis.

#### **References**

- Chagué-Goff, C., Andrew, A., Szczuciński, W., Goff, J., Nishimura, Y., 2012. Geochemical signatures up to the maximum inundation of the 2011 Tohoku-oki tsunami – implications for the 869 AD Jogan and other palaeotsunamis. *Sedimentary Geology*, 282, 65-77.
- Cisternas, M., Atwater, B.F., Torrejón, F., Sawai, Y., Machuca, G., Lagos, M., Eipert, A., Youlton, C., Salgado, I., Kamataki, T., Shishikura, M., Rajendran, C.P., Malik, J.K., Rizal, Y., Husni, M., 2005.

- Predecessors to the giant 1960 Chile earthquake. *Nature*, 437, 404-407.
- Goff, J. and McFadgen, B.G. 2002. Seismic driving of nationwide changes in geomorphology and prehistoric settlement – a 15<sup>th</sup> Century New Zealand example. *Quaternary Science Reviews*, 21, 2313-2320.
- Goff, J., Chagué-Goff, C. and Nichol, S. 2001. Palaeotsunami deposits: A New Zealand perspective. *Sedimentary Geology*, 143, 1-6.
- Goff, J., Chagué-Goff, C., Dominey-Howes, D., McAdoo, B., Cronin, S., Bonté-Graptin, M., Nichol, S., Horrocks, M., Cisternas, M., Lamarche, G., Pelletier, B., Jaffe, B. and Dudley, W. 2011. Palaeotsunamis in the Pacific. *Earth-Science Reviews*, 107, 141-146.
- Goff, J., Chagué-Goff, C., Nichol, S.L., Jaffe, B. and Dominey-Howes, D. 2012. Progress in palaeotsunami research. *Sedimentary Geology* 243-244, 70-88.
- Goto, K., Chagué-Goff, C., Fujino, S., Goff, J., Jaffe, B., Nishimura, Y., Richmond, B., Suguwara, D., Szczuciński, W., Tappin, D.R., Witter, R. and Yulianto, E. 2011. New insights into tsunami risk from the 2011 Tohoku-oki event. *Marine Geology*, 290, 46-50.
- Goto, K., Chagué-Goff, C., Goff, J. and Jaffe, B. 2012. The future of tsunami research following the 2011 Tohoku-oki event. *Sedimentary Geology*, 282, 1-13.
- Power, W., Wallace, L., Wang, X., Reyners, M., 2012. Tsunami hazard posed to New Zealand by the Kermadec and southern New Hebrides subduction margins: An assessment based on plate boundary kinematics, interseismic coupling, and historical seismicity. *Pure and Applied Geophysics* 169, 1-36.
- Satake, K., Atwater, B.F., 2007. Long-term perspectives on giant earthquakes and tsunamis at subduction zones. *Annual Review of Earth and Planetary Science* 35, 349-374.
- Wells, A., Goff, J., 2006. Coastal dune ridge systems as chronological markers of paleoseismic activity – a 650 year record from southwest New Zealand. *The Holocene* 16, 543-550.
- Wells, A., Goff, J., 2007. Coastal dunes in Westland, New Zealand, provide a record of paleoseismic activity on the Alpine fault. *Geology* 35, 731-734.

# Did earthquake science reduce casualties of the Mw 9.0 Tohoku-oki earthquake?

Masataka Ando<sup>a</sup>

<sup>a</sup>Center for Integrated Research and Education of Natural Hazards, Shizuoka University, 856 Oya, Suruga, Shizuoka, Japan, ando@ipc.shizuoka.ac.jp

Three large tsunamis have struck in the 115 years preceding the tsunami of the 11 March 2011 Tohoku-oki earthquake (Mw9.0) in Tohoku. These past tsunamis remained in the collective memory of communities, and numerous measures against future tsunami damage, such as breakwaters and tsunami evacuation drills, had been implemented. Despite these preparedness efforts, approximately 18,500 deaths and cases of missing persons occurred in the 2011 tsunami. The death rate with the age 65 and above was particularly high, four times higher than that with other age groups.

One hundred fifty survivors were interviewed to study the causes of deaths from the associated tsunami in bay and foreland areas of Tohoku (Ando et al., 2011 & 2013). The first official tsunami warning underestimated the height of tsunami and 40% of the interviewees did not obtain this warning due to immediate blackouts and a lack of communication after the earthquake. Some people chose to remain in dangerous locations based on the underestimated warning and their experiences with previous smaller tsunamis and/or due to misunderstanding the mitigating effects of nearby breakwaters in blocking incoming tsunamis. Some delayed their evacuation to perform family safety checks, and in many situations, the people affected misunderstood the risks involved in tsunamis.

Based on the above interviews and observations, several issues influenced the local residents' decision *not to evacuate immediately*. Most interviewees imagined that the incoming

tsunami would not reach their location. The major reasons were that the previous tsunamis were low compared with most communities, and

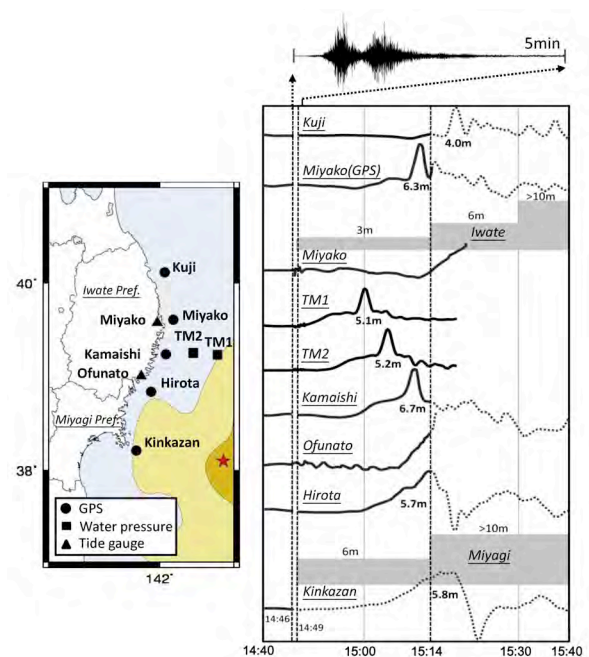


**Fig. 1.** Tsunami waveforms recorded at ocean-bottom pressure gauges (TM1 and TM2), five GPS buoy wave meters and two tidal gauge stations. The solid lines show the time ranges during which the data were monitored in real time, and the dashed lines show those for which data were stored at onshore stations and recovered later due to the blackout. At the top, the vertical strong-motion record from station HTKD of the National Institute of Disaster Mitigation and Science (NIED) is shown. HTKD was located near the tide gauge station “Ofunato (solid triangle). 5 min after the origin time of the 2011 Tohoku-oki earthquake. The gray boxes show the forecasted tsunami heights for Iwate (upper) and Miyagi (lower) prefectures, issued by the first warning at 14:49, the second at 15:14 and the third at 15:30. The major tsunami waves struck the interviewed towns at approximately 15:20-15:30. The 5-m and 30-m fault slip contours for the Tohoku-oki earthquake are also shown (Lee et al., 2011). The epicenter of the main shock is indicated by the star. (after Ando et al., 2013)

the emergency evacuation sites were not necessarily high. Throughout our survey, it was observed that recent earth science or technology did not help in reducing the death rate. Instead, the incorrect earthquake forecast may have increased the death rate to some extent. Earthquake science underestimated the earthquake size and tsunami heights, warning systems failed, and breakwaters produced a false sense of security. The advanced technology did not work properly, especially at the time of this severe disaster.

Regarding the tsunami early warning system, the data from real-time pressure gauges installed 46 and 76 km off the coast were not used in real time, although the data were transmitted continuously in real time to the Japan Meteorological Agency (JMA) and the University of Tokyo. As shown in Fig. 1, the TM1 water pressure gauge, located in the area of major coseismic crustal deformation, had detected a tsunami with a height of 2 m at 9 min and of 5.2 m at 14 min after the start of fault rupturing. These parts of the wave arrived at the coast approximately 25 and 20 min later, respectively, and its height was amplified 6 times at the coastal areas, according to an empirical rule of tsunami height estimated by the JMA's manual. The wave was recorded at TM2 5 min after it was recorded at TM1. Ten minutes later, the offshore Kamaishi GPS wave meter recorded the same tsunami wave (Fig. 1). If the data recorded at the pressure gauges had been used in real time for tsunami warning, more lives would have been saved, although many communication systems had already been damaged by that time.

The main motivation that caused the interviewees to evacuate was the unusual shaking (1/3) or the confirmation (or milling) of family or neighbors (1/3). Although 1/3 of the interviewees heard the tsunami warning through local loud-speakers, either directly or indirectly, only 1/4 of them responded to this warning. The

confirmation or milling of others is what led them to evacuate. This is a well-known and effective way of evacuating people in many cases. It should not be focused too much on the tsunami early warning system for the evacuation of local residents.

We recognized throughout the survey that most people did not understand how a tsunami is created under the sea. Therefore, the relation between earthquakes and tsunamis is not clearly linked. Nevertheless, even if these problems occur in future earthquakes, better knowledge regarding earthquakes and tsunami hazards could save more lives. People must take immediate action and identify locations that are higher than the designated evacuation sites, while encouraging others to evacuate and not spending time searching for others, even if warning systems or other technology cannot function at all. To avoid similar high tsunami death rates in the future, residents, including young children, should learn a simple mechanism of the generation of a tsunami in elementary school, especially as children have fresh minds. Although it requires time, this education is essential to ensure proper action during a tsunami in any location.

## References

- Ando, M., M. Ishida, Y. Hayashi and C. Mizuki, Interviews with survivors of Tohoku Earthquake provide insights into *fatality* rate, *EOS Forum, Am. Geophys. Union*, **92**, 411-412, 2011.
- Ando, M., M. Ishida, Y. Hayashi, C. Mizuki and Y. Tu, Interviewing insights regarding the fatalities inflicted by the 2011 Great East Japan Earthquake, *Natural Hazards of Earth Science System*, **13**, 1-15, doi:10.5194/nhess-13-1-2013, 2013.
- Lee, S.-J., Huang, B.-S., Ando, M., Chiu, H.-C. and Wang, J.-H.: Evidence of large scale repeating slip during the 2011 Tohoku- Oki earthquake, *Geophys. Res. Lett.*, **38**, L19306, doi:10.1029/ 2011GL049580, 2011.

# Implications of the 2011 Tohoku Earthquake for other subduction zones

Phil R. Cummins<sup>a</sup>

<sup>a</sup>*Research School of Earth Sciences, Australian National University, Canberra, ACT 0200, Australia, phil.cummins@ga.gov.au*

## 1. Introduction

The earthquake and tsunami that struck northeastern Japan in March 2011 was a terrible human tragedy that should serve as a wake-up call to earth scientists and disaster managers everywhere. It was a megathrust earthquake, involving rupture of the subduction zone plate boundary between the North American and subducting Pacific Plates. These earthquakes can be truly massive - nine out of the ten largest earthquakes ever recorded were megathrust earthquakes. Do we know how big such earthquakes can be, and where the biggest earthquakes can occur? The answers to these questions have important implications for countries that face a subduction zone, such as Indonesia, New Zealand, and many south Pacific Island countries.

Hazard assessments, for both earthquake and tsunamis, generally take into account some combination of prior earthquake or tsunami history, and geophysical considerations that may affect maximum magnitude and recurrence interval (e.g., 'segment' boundaries, depth to seismogenic zone, etc.). However, the recent earthquakes and tsunamis that struck both northern Sumatra in 2004 and northeast Japan in 2011, both accompanied by horrific economic and human losses, had no clear historical precedents, and geophysical considerations (at least non-retrospective ones) had suggested such massive earthquakes were unlikely.

An alternative approach would eschew the use of either historical events or geophysical considerations, and simply consider the most dangerous megathrust earthquake ever to have occurred worldwide as being the maximum

credible event for any subduction zone.

This approach is taken here, and we consider the possibility that an event like the 2011 Tohoku event might occur on either the Java or Tonga Trenches, two subduction zones that have previously been thought unlikely to experience massive megathrust earthquakes. Rather than attempting to model the earthquake dynamics in any detail, we consider a simple translation of the ground motion and seafloor deformation produced by this earthquake to the two scenario areas, and consider the implications for earthquake shaking and tsunami generation.

We argue that the 2011 Tohoku earthquake is indeed the most dangerous, for two reasons: (1) very large slip occurred over an area that was relatively compact compared to most megathrust earthquake, resulting in high stress drop and unusually strong ground motion, and (2) the area of anomalously high slip occurred near the trench axis, resulting in unusually efficient tsunami generation.

## 2. The Java Trench Scenario

Like the northeast Japan subduction zone prior to the 2011 earthquake, the subduction zone south of Java has no historical experience of an earthquake larger than roughly magnitude 8. The two subduction zones are similar in other respects, so we have to question whether a large event similar to the 2011 Tohoku earthquake could indeed occur off Java. In particular I will focus on the scenario in which an earthquake similar to the 2011 Tohoku earthquake occurs off West Java.

One feature of the 2011 Tohoku earthquake that may not be widely appreciated is that it

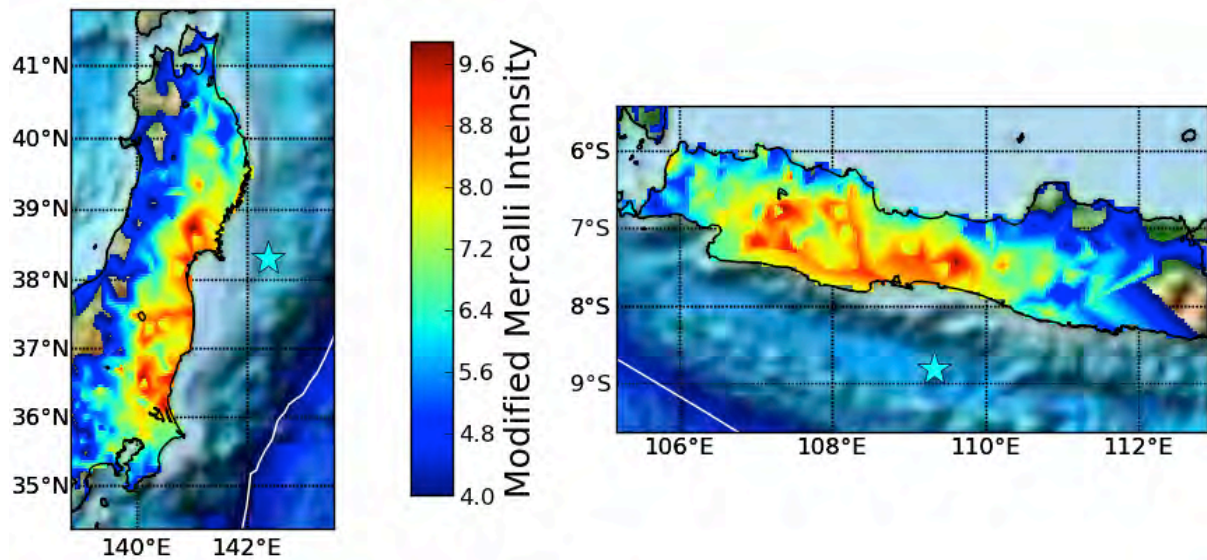


**Fig. 1.** Earthquake ground motion, expressed in Modified Mercalli Intensity, generated by the 2011 Tohoku earthquake (left), and translated from northeastern Japan to western Java (right).

struck a region of Japan with relatively low population density – Tohoku has less than 150 people per km<sup>2</sup>. West Java, by contrast, is one of the most densely populated regions of Indonesia, with almost 1,400 people per km<sup>2</sup>. Were such an event to occur off West Java, a much larger number of people would be exposed to strong ground shaking, and many of them live in buildings far less resilient than those in Japan. The tsunami generated by such an earthquake would similarly impact a much more densely populated coastline along the southern coast of west Java.

### 3. The Tonga Trench Scenario

It has long been argued that, with the combination of very fast convergence and few if any historical megathrust earthquakes, subduction at the Tonga Trench is largely aseismic. While this logic may seem unassailable, recent events such as the 2011 Japan earthquake bring into question our ability to characterize earthquake activity in any subduction zone. I will review recent evidence for locking of the Tonga megathrust, and show that if giant megathrust earthquakes can occur on the Tonga, they would pose a very serious tsunami threat to Tongatapu.

For this scenario, an earthquake causing seafloor uplift similar to that of the 2011 Tohoku earthquake was considered to occur along the Tonga Trench just opposite Tongatapu. Numerical modeling of the resulting tsunami shows that such an event could cause substantial tsunami inundation in Nuku'alofa, having a typical depth of several metres.

### 3. Conclusion

The scenarios considered here are extreme events, result in impacts far exceeding historical precedents for either Java or Tongatapu, and present enormous challenges for disaster management. The question is, should these really be considered the maximum credible events? Unless we can unequivocally state that such events can't occur on these subduction zones – unless we have certain knowledge that it is physically impossible for such events to occur – then we argue that such large events must be considered on any subduction zone, at least at a low level of probability.

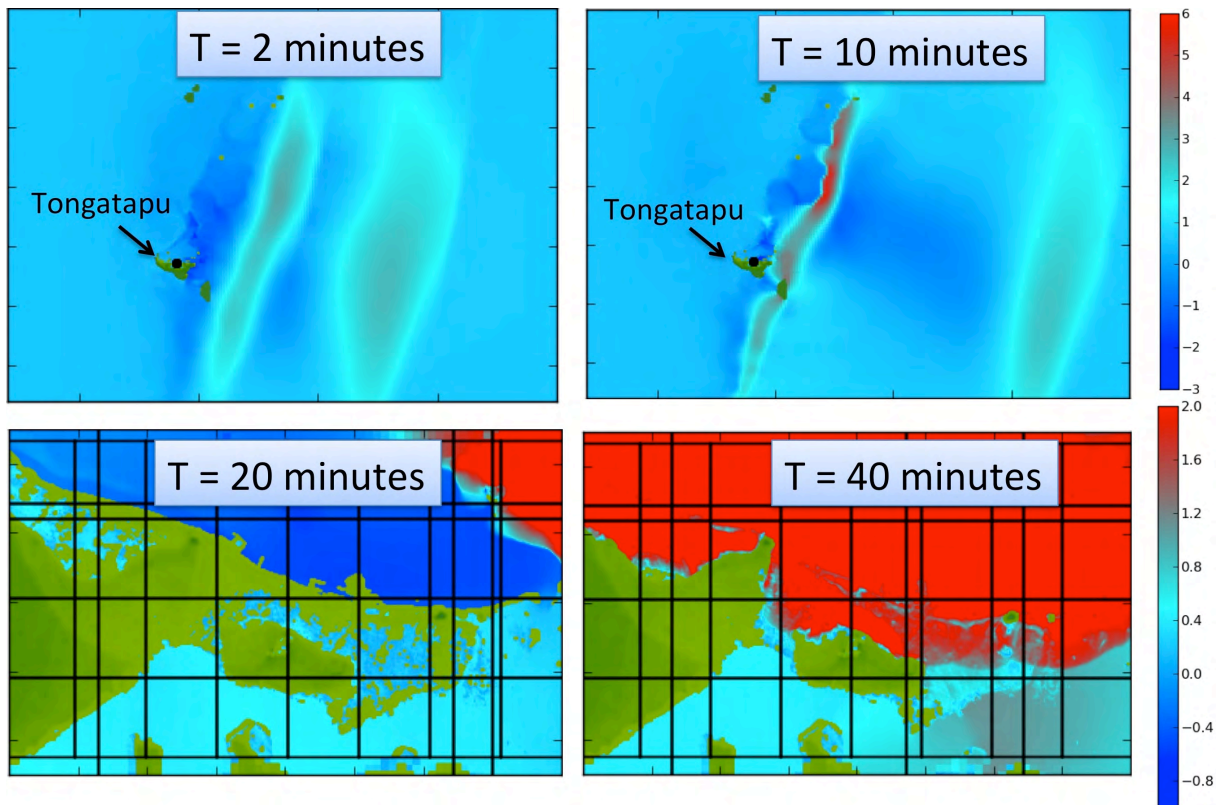


**Fig. 2.** Numerically modelled tsunami generated by an earthquake similar to the 2011 Tohoku earthquake occurring in the Tonga Trench. Upper panels show tsunami shoaling along the reef platform extending north and south of Tongatapu at 2 (left) and 10 (right) min after the earthquake. Lower panels show inundation in Nuku'alofa, 20 (left) and 40 (right) min after the earthquake.

# Who's Next? History of Tsunami Disasters in Indonesia

Ron Harris<sup>a</sup>, John Major<sup>a</sup> and Zac Yung-Chun Liu<sup>a</sup>

<sup>a</sup>*Department of Geological Sciences, Brigham Young University, Provo, Utah, USA*

## 1. Introduction

Two very important lessons were learned about tsunami disaster mitigation from the 2004 Sumatra and 2011 Honshu mega-thrust earthquakes and tsunami. First, that implementation of disaster mitigation strategies save hundreds of thousands lives. Even though the population density of the coasts of Sumatra and Honshu are the same, 10 times more fatalities happened in Indonesia where disaster mitigation strategies are not implemented. Second, we ignore pre-instrumental historical accounts and paleotsunami deposits, the geology of earthquakes and tsunami, to our peril.

## 2. Historical earthquakes and tsunami in Indonesia

Dutch colonists recorded several geophysical events throughout the Indonesian region starting in 1538, which are mostly documented in Arthur Wichmann's *Die Erdbeben Des Indischen Archipels* [The Earthquakes of the Indian Archipelago] (1918). We have translated the two volumes of this catalog into English and are parameterizing some of the better-documented events.

Emerging from our historical research are the sites of previously unknown mega-thrust earthquakes and tsunami (Liu and Harris, 2013). These long forgotten events caused severe devastation in the past and are likely to reoccur in the near future. When they reoccur ten times more Indonesians will be in harms way due to rapid population growth and urbanization in high-risk areas.

Recurrence of earthquakes and tsunami is evident throughout the 400 years covered by the historical records, particularly in Sumatra. One example of the earthquake forecasting power of historical records is the use of the Wichmann catalog to constrain mega-thrust earthquake source parameters and recurrence along the Sumatran subduction zone (Newcomb and McCann, 1987; Harris et al., 1997). The 2005 northern Sumatra earthquake near Nias Island

ruptured nearly the same area as reconstructed from accounts of the 1861 event.

Strain rates in eastern Indonesia are twice those in Sumatra and the historical records indicate that tsunami are much more frequent. Between 1538 and 1900 there were 32 regional earthquakes and 30 tsunami in eastern Indonesia. The largest and best documented are the events of 1629, 1674, 1852 and 1899 in the Banda Sea region, 1770, 1859 and 1889 in the Molucca Sea region, 1820 in Makassar, 1857 in Timor, 1815 in Bali, and 1699, 1771, 1780, 1815, 1848, 1852 and 1896 in Java (Figs. 1 and 2). All of these events caused damage over a broad region notwithstanding high seismic attenuation rates, and are associated with years of temporal and spatial clustering of earthquakes.

A.



B.



Fig. 1. Damaging historical and recent earthquakes in eastern Indonesia (A) and Java and Bali (B).

Several tsunami are also documented with run-up heights > 15 meters and one, which was likely assisted by a landslide, was locally as high as 80 meters. Earthquakes associated with most tsunami were felt over a region as large as the 2011 Tohoku Earthquake in Japan and were followed by decades of aftershocks.

Unfortunately, the rapid increase in population in Indonesia over the past century was also a time of relative seismic quiescence, which ended in 2004. Since the 2004 event Indonesia has had 6 earthquakes > Mw 8.0 and 8 tsunami. The number of fatalities from these and other events continues to rise to nearly 300,000.

Although the majority of these fatalities were from the 2004 tsunami historical records indicate that the coastline of Sumatra has been inundated by at least 19 other tsunami since the 17<sup>th</sup> century, including the one caused by the eruption of Krakatau. All of these previous events, which mostly happened before 1900 when the population of Indonesia was 5 times less than it is today, account for less than 60,000 fatalities. In other words, the increasing number of fatalities correlates with the increasing number of people, not the number of hazards.

Eastern Indonesia has not experienced a major shallow earthquake for the past 160 years. Because of this some characterize the region as unlikely to produce mega-thrust earthquakes (Heuret et al., 2012). However, historical records indicate otherwise. Based on amounts of strain accumulation, the most vulnerable areas are the Molucca and Banda Sea regions. The Java Trench area also poses a significant threat as well as poorly studied active faults in the Sulawesi region.

One of the largest and well-documented events in the Wichmann catalog is the great earthquake and tsunami affecting the Banda Islands on August 1, 1629 (Fig. 2). It caused severe damage from a 15-m tsunami that arrived at the Banda Islands about a half hour after violent shaking stopped. The earthquake was also recorded 230 km away in Ambon, but no tsunami is mentioned. This event was followed by at least 9 years of uncommonly frequent seismic activity in the region that tapered off with time like an aftershock sequence.

The combination of these observations indicates that the earthquake was most likely a mega-thrust event. We use an inverse modeling approach to numerically reconstruct the tsunami,

which constrains the likely location and magnitude of the 1629 earthquake. We apply various wave amplification factors (1.5–4) derived from simulations of recent, well-constrained tsunami to bracket the upper and lower limits of earthquake moment magnitudes for the event.

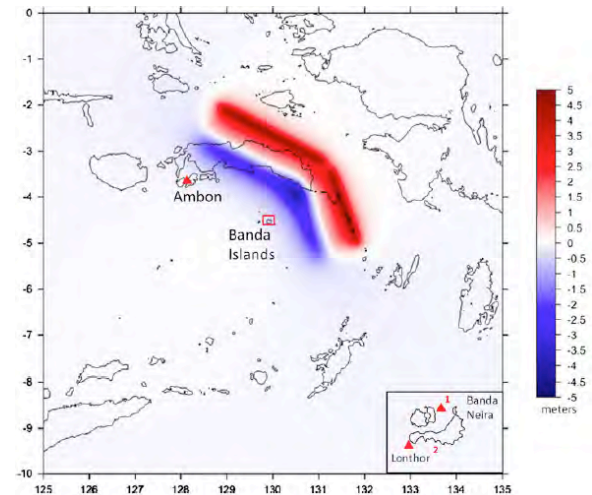


**Fig. 2.** Model of possible vertical component of surface deformation from the Seam forearc associated with the 1629 mega-thrust earthquake and tsunami. Tsunami heights in the Banda Islands reached >15 meters, with no tsunami recorded in Ambon.

The closest major earthquake sources to the Banda Islands are the Tanimbar and Seram Troughs of the Banda Arc subduction zone. Other source regions are too far away for such a short arrival time of the tsunami after shaking. Moment magnitudes of 9.8–9.2 on the Tanimbar Trough are required by the models to produce a 15-m tsunami in the Banda Islands. Whereas Mw 8.8–8.2 is required on the Seram Trough. The arrival times of these waves are 58 min for Tanimbar Trough and 30 min for Seram Trough. The model also predicts 5-m run-up for Ambon from a Tanimbar Trough source, which is inconsistent with the historical records. Ambon is mostly shielded from a wave generated by a Seram Trough source. Based on the modeling we conclude that the most likely source of the 1629 mega-thrust earthquake is the Seram Trough (Fig. 3).

Enough strain has already accumulated along the Seram Trough since the 1629 event to produce another mega-thrust earthquake.

Many more and larger coastal communities are in harms way of tsunami than ever before in Indonesia. The ‘Last Mile’ concept is

fundamentally flawed due to the lack of infrastructure to warn those nearest the coast. We recommend a three pillar approach that includes 1) hazard maps that integrate geological data and historical accounts, 2) tsunami disaster education that includes local

communities constructing inundation maps and posting warning signs, and 3) implementing protective measures and warning systems using existing cultural practices and technologies.

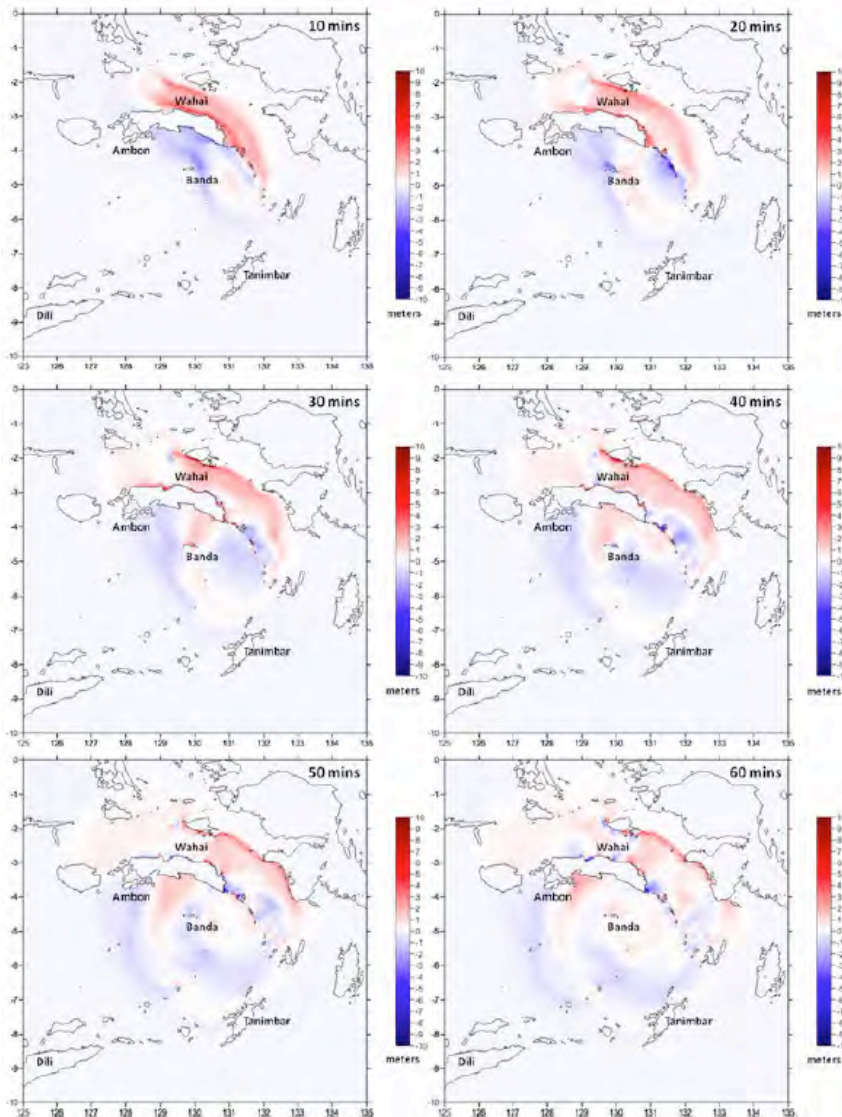


**Fig. 3.** Snapshots of the first 60 minutes of tsunami propagation for the 1629 Seram Trough earthquake. The tsunami arrives in the Banda Islands within 30 minutes of strong shaking and reaches > 15 meters as indicated in historical accounts.

## References

- Harris, R.A., Donaldson, K. and Prasetyadi, C. (1997) Geophysical disaster mitigation in Indonesia using GIS, *Buletin Teknologi Mineral* 5, p. 2–10
- Liu, Y.C. and Harris, R.A. (2013) Discovery of possible mega-thrust earthquake along the Seram Trough from numerical modeling of the 1629 tsunami in the eastern Indonesian Region, *Natural Hazards*, 10.1007/s11069-013-0597-y
- Newcomb, K.R. and McCann, W.R. (1987) Seismic history and seismotectonics of the Sunda arc. *J Geophys Res.*, 92(B1): p. 421–439.
- Wichmann, A. (1918) Die Erdbeben des Indischen Archipels Bis Zum Johpe 1857, (in Dutch), Koninkl. Nederlandse Akad. Wetensch. Verh. 2nd Sect. 20, 193 p.

# Globalization of Natural Disasters, and Geopolitics

Yildirim Dilek<sup>a</sup>

<sup>a</sup>*Department of Geology & Environmental Earth Science, Miami University, 116 Shideler Hall, Oxford, OH 45056, USA, dileky@miamioh.edu*

Naturally caused and human-induced environmental changes produce significant effects on political, social and economic systems at a global scale, potentially altering global economy, human security and geopolitical stability. Yet, most geopolitical analyses omit such environmental changes and natural disasters in extrapolating future political and economic circumstances. A scientific approach to the history and the distribution of past civilizations clearly shows that their rise and demise were greatly influenced by geological processes and catastrophic events that took place in various time scales. The Indian Ocean tsunami of December 2004, the Katrina hurricane and flood (USA) of August 2005, the Icelandic Eyjafjallajökull volcanic eruption of April 2010, and the Tohoku (Japan) earthquake and tsunami of March 2011 are some of the most salient, modern examples of major natural disasters that have had adverse implications on global economy and on the regional/national security of the countries involved.

Regardless of the basic premises of the leading geopolitical scenarios about the future

territorial configuration of power, the ramifications of large-scale natural events involving climate change, earthquakes, tsunamis, volcanic eruptions, floods and landslides are bound to be enormous and highly devastating for the sustainable development of the global economy and peace. The major geopolitical impacts of these events include: the collapse of agricultural productivity, the lack of fresh water, the disruption of electronic communication and industrial output, the destruction of coastal zones, and the unexpected shifts in shipping routes. These developments can easily lead to the creation of destabilizing problems and global conflicts as the nations and societies lose their resource base. In this talk, I discuss the importance of various geological processes and associated natural disasters for the present and future geopolitical balance in the world, and emphasize the necessity of international attention and preparedness for such environmental changes of global scales in order to maintain the world peace, security and prosperity.

## Quiescence in aftershock activity of the 2008 Iwate-Miyagi inland earthquake caused by the 2011 Tohoku-oki earthquake

Yuhei Suzuki<sup>a</sup> and Shinji Toda<sup>b</sup>

<sup>a</sup>Research Center for Prediction of Earthquakes and Volcanic Eruptions, Graduate school of Science, Tohoku University, Sendai, Japan, y-suzuki@s.tohoku.ac.jp

<sup>b</sup>International Research Institute of Disaster Science, Tohoku University, Sendai, Japan.

### 1. Static stress change and seismicity

Seismicity rate increase after a large earthquake is observed not only along the source fault but also nearby the source, called “off-fault aftershock.” One of the hypothetical mechanisms of such aftershock occurrence is the static Coulomb stress transfer (CFF) from the source to nearby faults. In contrast to the stress triggering, any region in which seismicity rate is reduced or suppressed by decrease of CFF is called “stress shadow”.

While numerous papers of stress triggering have been published since 1990s (e.g. King et al., 1994), only a few studies have evidently shown static stress shadow. The reason fewer reports exist is its limited conditions to detect stress shadow. To prove statistical significance, the following conditions should be satisfied: (i) high seismicity rate before a disturbance, (ii) long elapsed time since the disturbance to earn sufficient number of aftershocks, (iii) decrease CFF on most of the pre-existing faults in the area. A preceding aftershock activity before the disturbance is often used to satisfy the condition (i) (e.g. Toda and Stein, 2003).

We here focus on seismicity after the 2011 Tohoku-oki earthquake (Mw 9.0) in the aftershock areas of the 2008 Iwate-Miyagi inland earthquake (Mw 6.6), the 2003 North-Miyagi earthquake (Mw 6.0) and the 2010 Fukushima earthquake (Mw 5.5), all of which are mostly supposed to satisfy all the conditions.

### 2. Method and data

Due to an inherent temporal decay of aftershocks, one always sees seismicity rate decrease in a comparison between the early and later aftershock sequences. To calibrate such potential bias, we employ the Epidemic-Type Aftershock Sequence (ETAS) model (Ogata, 1988) which simulates the temporal decay and effect of secondary aftershocks. Here, we use the Japan Meteorological Agency (JMA) earthquake catalog from 2000 to June 2013 (depth  $\leq 25$ km). We then examine any deviation of observed rate from theoretical seismicity predicted by the ETAS model after the 2011 Tohoku-oki earthquake.

To detect seismicity rate change between before and after a stress perturbation, one must estimate the minimum magnitude of completeness ( $M_c$ ) throughout the testing period. Based on a report of JMA (2012) and our own magnitude-frequency plots, we assume  $M_c=3.0$  in the Iwate-Miyagi inland earthquake and the North-Miyagi earthquake, and  $M_c=2.0$  in the Fukushima earthquake regions. To define their aftershock zones rigorously, we calculate seismicity rate before ( $R_b$ ) and after ( $R_a$ ) their own mainshock and then assume the area of  $R_a/R_b \geq 1.5$  as an “aftershock zone”. We estimate the ETAS parameters during the period from their own mainshock to the Tohoku-oki earthquake by maximum likelihood method. We then retrospectively predict the seismicity after the Tohoku-oki earthquake. If observed post-Tohoku-oki seismicity rate is significantly lower than the predicted one, we regard it as relative quiescence.

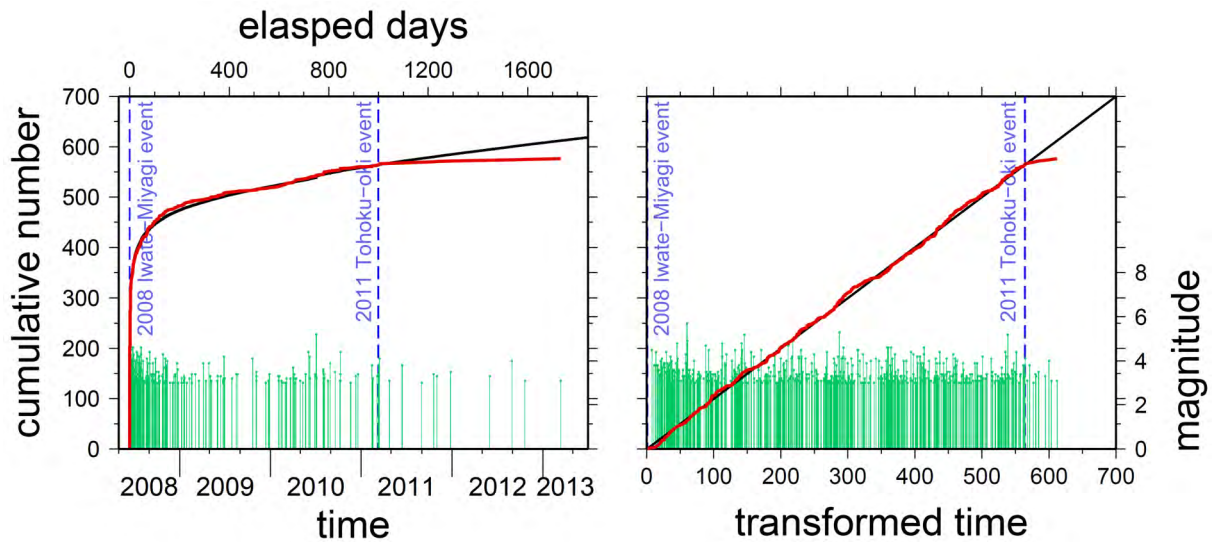


**Fig. 1.** (Left) Cumulative number of earthquakes as a function of time in the 2008 Iwate-Miyagi inland earthquake aftershock zone. Green stem plots are corresponding timing and magnitude of earthquakes. Red and black curves indicate observed cumulative curve and theoretical ETAS model respectively. The time on blue dashed lines is the 2008 Iwate-Miyagi inland earthquake or the 2011 Tohoku-oki earthquake. (Right) Residual analysis using transformed time that theoretical curve becomes linear with slope=1. Symbols are the same as the left figure.

### 3. Result

The ETAS model can accurately reproduce seismicity in the 2008 Iwate-Miyagi inland earthquake aftershock zone before the 2011 Tohoku-oki earthquake (Fig 1.). However, observed cumulative number deviates below the theoretical curve after the 2011 Tohoku-oki earthquake. It indicates that the productivity of aftershocks has been significantly lowered than the ETAS estimate since the 2011 Tohoku-oki earthquake. In the 2010 Fukushima earthquake aftershock zone, the seismic activity has also decreased since the 2011 Tohoku-oki earthquake. We interpret that these two areas are stress shadows because the majority of the nodal planes of pre-Tohoku-oki focal mechanisms as a proxy of regional faults brought further from failure by the 2011 Tohoku-oki earthquake (Toda et al., 2011).

In contrast, we cannot find any relative quiescence of aftershocks in the 2003 North-Miyagi aftershock zone, even though significant decrease of CFF is calculated.

### 4. Discussion and conclusion

We cannot detect relative quiescence in aftershock activity of the 2003 North-Miyagi

earthquake. The reasons are as follows: the seismicity had already sufficiently decayed to its background rate before the 2011 Tohoku-oki earthquake and/or the observation period after the 2011 Tohoku-oki earthquake is not long enough to compensate for the low seismicity rate (unsatisfied condition (i) or (ii)). We thus expect to detect moderate quiescence if we wait longer and further collect the data. Such long post-disturbance period instead may not allow us to separate the effect of the 2011 Tohoku-oki earthquake from other disturbances.

To summarize, stress shadows that are found in aftershock zones of the 2008 Iwate-Miyagi inland earthquake and the 2010 Fukushima earthquake are evident that seismicity has inhibited by the static Coulomb stress decrease due to the 2011 Tohoku-oki earthquake.

### References

- Japan Meteorological Agency (2012), The criterion of hypocenter determination process and the earthquake detection level after the 2011 off the Pacific coast of Tohoku Earthquake, *report of CCEP*, 87, 1-3.
- King, G. C. P., R. S. Stein, and J. Lin (1994), Static stress changes and the triggering of earthquakes, *Bull. Seis. Soc. Am.*, 84,

935-953.

- Ogata, Y. (1988), Statistical models for earthquake occurrences and residual analysis for point processes, *J. Am. Stat. Assoc.*, 83, 9-27, doi:10.2307/2288914.
- Toda, S. & R. Stein (2003), Toggling of seismicity by the 1997 Kagoshima earthquake couplet: A demonstration of time-dependent stress transfer, *J. Geophys. Res.*, 108(B12), 2567, doi:10.1029/2003JB002527.
- Toda, S., R. S. Stein, and J. Lin (2011) Widespread seismicity excitation throughout central Japan following the 2011 M=9.0 Tohoku earthquake and its interpretation by Coulomb stress transfer, *Geophys. Res. Lett.*, 38, doi:10.1029/2011GL047834.

## Characteristic thickness distribution of the 2011 Tohoku-oki tsunami deposits in a narrow valley at the southern end of Sendai Plain

Tomoya Abe<sup>a</sup>, Kazuhisa Goto<sup>b</sup>, Daisuke Sugawara<sup>c</sup>

<sup>a</sup>*Department of Geography, Nagoya University, D2-1(510), Furo-cho, Chikusa-ku, Nagoya 464-8601, Japan, [abe.tomoya@a.mbox.nagoya-u.ac.jp](mailto:abe.tomoya@a.mbox.nagoya-u.ac.jp)*

<sup>b</sup>*International Research Institute of Disaster Science, Tohoku University, Aoba 6-6-40-102, Aramaki, Aoba-ku, Sendai 980-8579, Japan [goto@irides.tohoku.ac.jp](mailto:goto@irides.tohoku.ac.jp)*

<sup>c</sup>*International Research Institute of Disaster Science, Tohoku University, Aoba 6-6-11-1106, Aramaki, Aoba-ku, Sendai 980-8579, Japan [sugawara@irides.tohoku.ac.jp](mailto:sugawara@irides.tohoku.ac.jp)*

### 1. Introduction

Case studies of recent tsunami impacts have proven to be extremely useful in understanding the geological processes involved in inundation and return flow, and refining the criteria to identify paleo-tsunami deposits in the geological record (Richmond et al. 2012). Many studies were conducted after recent tsunamis including 2004 Indian Ocean tsunami and the 2011 Tohoku-oki tsunami. Previous researches on tsunami deposits have typically conducted along shore-normal transects, that was set perpendicular to the shoreline. However, tsunami flow and sedimentary processes can be complex due to local topography and subsurface. Investigation on spatial characteristics of tsunami deposits may derive an improved understanding on the hydrodynamic and sedimentological features of the tsunami. The main objective of present study is to a) examine the influences of the local topography on tsunami deposit thickness and b) provide the new insights into the sedimentary process in a valley that occurs during large tsunami using geomorphological methods such as analyses of digital elevation model and aerial photographs, and sedimentological methods such as high resolution geological survey and analyses of grain size distributions and diatom assemblages.

### 2. Methods

We investigated tsunami deposits at 170 sites at 10-100 m spacing in a 2.2-km-wide narrow drowned valley and analyzed thickness, grain size and sedimentary structure of the tsunami deposits in order to clarify spatial characteristics and to estimate the volume of the sediments deposited. Grain size analyses using setting tube were performed to identify the source of the tsunami sand. The post-tsunami digital elevation model was compared with the distribution of the deposit. Satellite imageries and aerial photographs were analyzed to estimate the topographic change and area of erosion. We measured the flow height at the shrine located at center of the valley using DGPS survey equipment (Promark 100, Ashtech) and hand-held laser rangefinders. The flow heights and run-up heights measured by The 2011 Tohoku Earthquake Tsunami Joint Survey Group (TETJSG) were used for supplemental data. Diatom assemblages included in the muddy tsunami deposits were analyzed to estimate the source of the mud. Volumes of the sand and mud deposited by the tsunami were calculated from average thickness multiplied by depositional area by each area in Figure 2 (Area1: 351,200 m<sup>2</sup>, Area 2: 35,500 m<sup>2</sup>, Area3: 288,600 m<sup>2</sup>, and the pond: 20,500 m<sup>2</sup>) and added all volumes.

### 3. Study area

The Sendai Plain extends from Sendai-Shiogama Port in the north to Yamamoto Coast in the south. The narrow valley with 2.2 km width is located at the southern end of Sendai Plain (Fig. 1) and is surrounded by the elevated terraces. The natural geomorphology is characterized by beach and 2-3 m high sand dune. The 6.2 m high (elevation above Tokyo Peil, T.P.) seawall was constructed along back beach. Forests of black pine trees were planted on the sand dune. Wetland behind dune was used for agricultural rice fields. A small pond, Suijin-numa, with 0.2 km width is located at 0.7-0.9 km from the coastline. Most trees were knocked down landward as the results of the tsunami inflow.

### 4. Results

In this valley, tsunami inundated up to 2.2 km inland. Average flow height of the total measure points in this valley (11 points) was 9.7 m above mean sea level. According to eyewitness and video footage recorded by local people, at least three waves inundated over the 2-3 m high sand dune. The average tsunami directions of up flow, estimated from orientation of the knocked-down trees suggest that main direction of tsunami inflow was westward. On the other hand, return flow was complex on the basis of distribution of debris and shape of erosional features formed by backwash.

The tsunami eroded the foreshore, backshore landward side of seawall, and sanddune and formed up to 100 m wide scarp depressions.

The 2011 tsunami deposit in this area mainly is composed of layers of fine to medium sand and an overlying clay to silt layer. The sand layer ranged in a thickness up to 40 cm and generally thinned landward (Fig. 2A). The thickness of the mud layer was ranged from 0 to 39 cm and rapidly increased in the pond and on land behind the pond (Fig. 2B). Sharp contacts between pre-tsunami soil and the overlying tsunami deposit were typically recognized. Normal grading, rip-up clasts, parallel

lamination, multiple sand layers, were observed 25%, 14%, 16%, 31% out of the total sites, where the sand deposited. Multiple layers of sand were frequently observed in the deposits from the seaward area, while the deposit was mostly composed of single layer in the landward area. Sand thickness decreases with increasing elevation in the landward area (Area 3) (Fig. 3). On the other hand, such relationship was not observed in the seaward area (Area 1). Grain size distributions were similar between the tsunami sand and beach sand. Freshwater species dominated the diatom assemblages of the muddy tsunami deposit (GPS21, GPS185) as well as the pond-bottom sediment (GPS7).

The average sand and mud thicknesses of each area is calculated as 13.1 cm, 0.7 cm (Area1: 53 sites), 8.1 cm, 1.2 cm (Area 2: 14 sites), 6.9 cm, 2.4 cm (Area 3: 86 sites) and 8.4 cm, 15.5 cm (The pond: 14 sites). Thus, the volumes of the sand and mud were estimated at 46,000 m<sup>3</sup>, 2,500 m<sup>3</sup> in Area 1, 2,900 m<sup>3</sup>, 400 m<sup>3</sup> in Area 2, 19,900 m<sup>3</sup>, 6,900 m<sup>3</sup> in Area 3, and 1,700 m<sup>3</sup>, 3,200 m<sup>3</sup> in the pond. As a consequence, total volumes of the sand and mud deposited by the tsunami were estimated at 70,500 m<sup>3</sup> and 13,000 m<sup>3</sup>, respectively. Besides, erosion areas and depth of beach and sand dune were estimated 109,400 m<sup>2</sup> and more than 1-2 m, and the areas of the pond and rice paddy were estimated 2,500 m<sup>2</sup> and 494,200 m<sup>2</sup> at a maximum.

### 5. Discussions

The marine sediments offshore of the study area are mainly composed of coarse sand (Saito, 1989). Grain-size analysis showed that the tsunami sand in the valley comprised of fine to medium sand (median: 1.2-2.5 phi) and the beach sand composed of fine to medium sand (median: 1.7 phi). Therefore, it is highly likely that the sandy tsunami deposits were mostly sourced from the beach and sand dune. Evidence of severe erosion of the beach and sand dune supports the interpretation. The results of diatom analysis showed that the muddy tsunami

deposits were mostly originated from the land or the pond sediments. The erosion volumes at the beach and sand dune for sandy deposits and at the rice paddy field and the pond for muddy deposits were enough to explain the volumes of the sand and mud deposited by the tsunami. In middle of Sendai Plain, previous studies (Richmond et al., 2012; Szczuciński et al., 2012) pointed out that the tsunami deposits are primarily derived from the beach, sand dune, and agricultural soil sources, with minor contribution of marine sediments, as showed by detailed mineralogical, sedimentological and diatom data. Our results are consistent with previous results.

The tsunami sand thins landward in whole of the valley. Differences in the sand thickness distribution were observed between the seaward area (Area 1) and landward area (Area 3). According to the eyewitness account and video footages, at least three tsunami run-up waves crossed over the 2-3 m high sand dune. These waves might have formed the multiple sand layers over the inundation area. However, the multiple sand layers were observed only in the seaward area (Area 1, Fig. 4); meanwhile single unit of the sand was mostly found from the landward area (Area 3). Additionally, the sand thicknesses of the landward area showed negative correlation with the elevation. On the other hand, the thicknesses of the seaward area had no correlation with the elevation and fairly fluctuated associated with the number of the sand unit. Umitsu et al. (2007) in coastal plains in Thailand and Indonesia suggested the direction of run-up flow was almost perpendicular to the coastline, whereas backwash flow directions were controlled by local topography. Thus, these spatial fluctuations of the sand thickness in seaward area might be caused by the differences in influences on tsunami sedimentation process associated with the arrangement in space of micro landform. Overall, these differences among two areas suggest the change of tsunami hydrodynamics and sedimentary process at the

valley outlet 0.7 km from the shoreline.

Our survey revealed that the influence of local topography on tsunami deposit thickness and total balance of sedimentation and erosion volumes with higher-accuracy. Additionally, we clarified the characteristic sedimentation process in a narrow valley.

## References

- Richmond, B. Szczuciński, W., Chagué-Goff, C., Goto, K., Sugawara, D., Tappin, D.R., Jaffe, B.E., Fujino, S., Nishimura, Y., Goff, J. (2012) Erosion, deposition and landscape change on the Sendai coastal plain, Japan, resulting from the March 11, 2011 Tohoku-oki tsunami, *Sedimentary Geology*, 282, 27-39. 90–109.
- Saito, Y. (1989) Modern storm deposits in the inner shelf and their recurrence intervals, Sendai Bay, Northeast Japan, In: Taira, A. Masuda, F. (Eds.), *Sedimentary Facies in the Active Plate Margin*, Terrapub, Tokyo, 331-344.
- Szczuciński, W., Kokociński, M., Rzeszewski, M., Chagué-Goff, C., Cachão, M., Goto, K., Sugawara, D. (2012) Sediment sources and sedimentation processes of 2011 Tohoku-oki tsunami deposits on the Sendai Plain, Japan - insights from diatoms, nannoliths and grain size distribution, *Sedimentary Geology*, 282, 40–56.
- Umitsu, M., Tanavud, C., Patanakanog, B. (2007) Effects of landforms on tsunami flow in the plains of Banda Aceh, Indonesia, and Nam Khem, Thailand, *Marine Geology*, 242, 141–153.

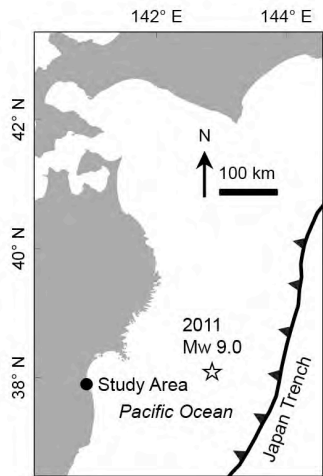


**Fig. 1.** Location of Study area

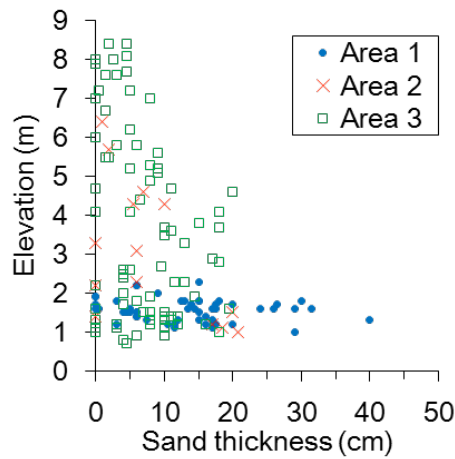


**Fig. 3.** Relationship between sand thickness (cm) and elevation (m)

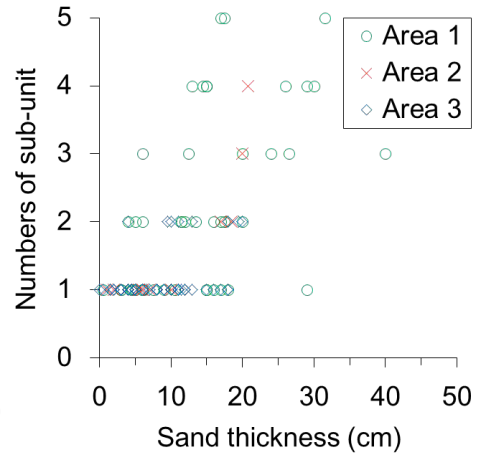


**Fig. 4.** Relationship between sand thickness (cm) and number of sub-unit

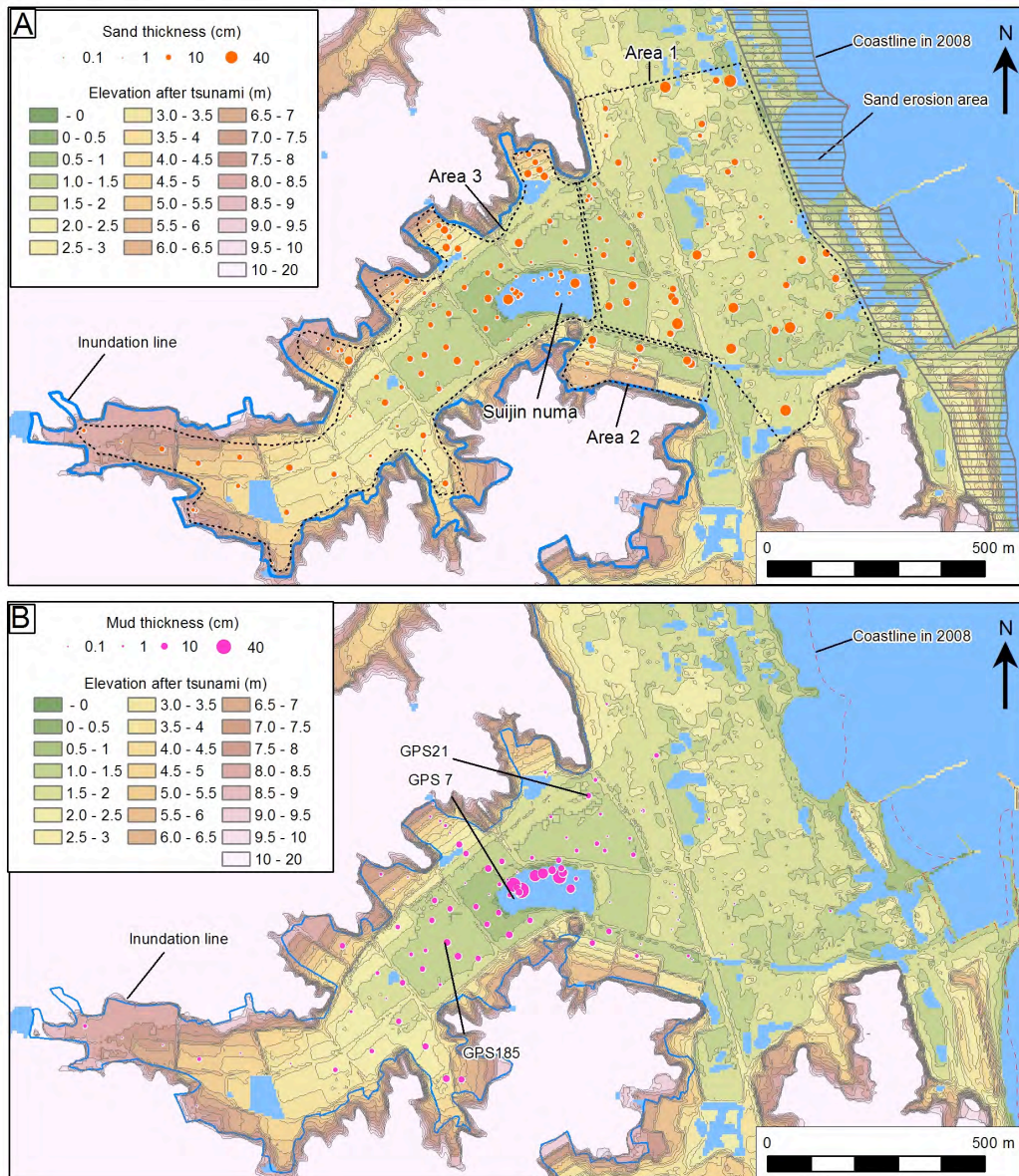


**Fig. 2.** A map showing the spatial distribution of sediment thickness of the sand (A) and the mud (B). Coastline data in 2008 and digital elevation model in 2011 are provided by GSI

# Tsunami deposits distribution in Sendai Plain evaluated by Sediment transport model

Kohei Hashimoto<sup>a</sup>, Kazuhisa Goto<sup>b</sup>, Daisuke Sugawara<sup>c</sup>, Fumihiko Imamura<sup>d</sup>

<sup>a</sup>School of Engineering, Tohoku University, Aoba 6-6-11-1106, Aramaki, Aoba-ku, Sendai 980-8579, Japan, [k\\_hashimoto@tsunami2.civil.tohoku.ac.jp](mailto:k_hashimoto@tsunami2.civil.tohoku.ac.jp)

<sup>b</sup>International Research Institute of Disaster Science, Tohoku University, Aoba 6-6-40-102, Aramaki, Aoba-ku, Sendai 980-8579, Japan

<sup>c</sup>International Research Institute of Disaster Science, Tohoku University, Aoba 6-6-11-1106, Aramaki, Aoba-ku, Sendai 980-8579, Japan

<sup>d</sup>International Research Institute of Disaster Science, Tohoku University, Aoba 6-6-11-1106, Aramaki, Aoba-ku, Sendai 980-8579, Japan

## 1. Introduction

Tsunamis can generate a large shear force on the ocean floor and move a large amount of sediments to land and form tsunami deposits. Because tsunami deposits cause secondary damages to coastal topography agricultural field, houses, and port function. Evaluation of tsunami-induced sediment transport is very important for engineering point of view (Shuto, 1989). Validity of numerical model of tsunami sediment transport has been less investigated in real scale. This is probably because (1) there were few tsunami events that struck the area where pre-tsunami topography is available and (2) the quantity and quality of the data on spatial distribution of tsunami deposits are not enough to verify the accuracy of the sediment transport model on land.

To validate the sediment transport model in the real scale, it is necessary to collect field data as many as possible. The purpose of this study is to validate the sediment transport model proposed by Takahashi et al. (1999), based on the field data on the 2011 Tohoku-oki tsunami deposits at Sendai Plain.

## 2. Regional setting and methods

### 2.1. Field observation and interpolation

We conducted field survey in the south of Abukuma River at the central Sendai Plain, during July to October, 2012 (Fig. 1). In order to investigate the spatial distribution of tsunami

deposits, we excavated survey pits about 500 m grid interval to cover the inundated area. Note that the surface of the tsunami deposits were affected more or less by post-tsunami wind action, rainfall and vegetation that have occurred during the period after the Tohoku-oki tsunami. Therefore, the reliability of the collected data were evaluated whether the sandy tsunami deposits were covered (and well

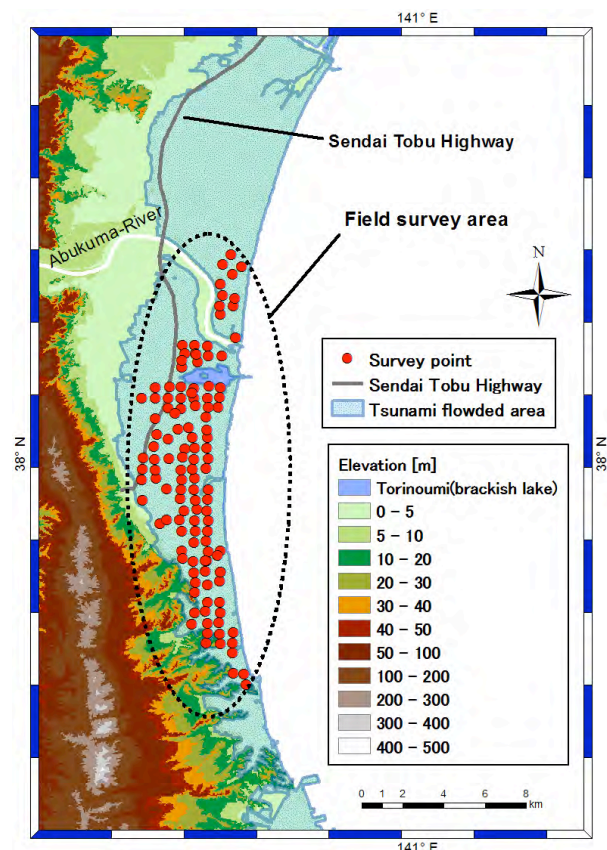


**Fig. 1.** Survey points of the tsunami deposits. Base map is the pre-tsunami 10 m DEM data provided by GSI. The inundation area is provided by JSG.

preserved) by the mud layer on its top. We identified the location of each pit and measured the thickness

of sandy deposits. In order to clarify the macroscopic distribution of the deposits, the survey sites were set on grid lines arranged by every 500 m spacing, which cover most of the tsunami inundation area.

The data was interpolated into a gridded data with 50 m spacing, using the Kriging technique. The grid size of 50 m is identical to the finest grid used in the numerical simulation of tsunami inundation. Therefore, the interpolated data on the sand thickness and calculated deposit thickness by sediment transport model can be directly compared.

## 2.2 Tsunami numerical simulation

The bathymetry data used for the tsunami simulation were provided by Central Disaster Prevention Council. This data was published prior to the 2011 Tohoku-oki earthquake, thus the coseismic crustal subsidence caused by the 2011 Tohoku-oki event is not included. We used a nesting grid system, which cover the offshore areas by coarser grids ( $dx = 1350$  m,  $450$  m and  $150$  m) to calculate the tsunami propagation. The finest grid ( $dx = 50$  m) includes the study area. The governing equations for the tsunami hydrodynamics are derived from non-linear long wave theory with equation of continuity (Eq.1), and equations of motion in the X- and Y-axis direction (Eq.2 and 3):

$$\frac{\partial \eta}{\partial t} + \frac{\partial M}{\partial x} + \frac{\partial N}{\partial y} = 0 \dots (1)$$

$$\frac{\partial M}{\partial t} + \frac{\partial}{\partial x} \left( \frac{M^2}{D} \right) + \frac{\partial}{\partial y} \left( \frac{MN}{D} \right) + gD \frac{\partial \eta}{\partial x} + \frac{gn^2}{D^{7/3}} M \sqrt{M^2 + N^2} = 0 \dots (2)$$

$$\frac{\partial N}{\partial t} + \frac{\partial}{\partial y} \left( \frac{N^2}{D} \right) + \frac{\partial}{\partial x} \left( \frac{NM}{D} \right) + gD \frac{\partial \eta}{\partial y} + \frac{gn^2}{D^{7/3}} N \sqrt{M^2 + N^2} = 0 \dots (3)$$

Where  $\eta$  is the water level,  $M$  and  $N$  are the x and y components of the water flux,  $D$  is the total depth,  $g$  is the gravitational acceleration,  $t$  is the time,  $n$  is the Manning's roughness coefficient. We solve these equations by Staggered Leap-Frog finite difference method.

The initial tsunami waveform was computed using the focal parameters determined by Imamura et al. (2012) (Tohoku University Model, version 1.2).

## 2.3 Sediment transport model

We used a sediment transport model, which has been developed by Takahashi et al. (1999). The sediment transport model assumes two distinguished layers, namely, bed and suspended layers. The numerical model can treat exchanges of sand between these layers. These layers are set virtually due to difference of sand moving form (rolling, sliding and saltation), hence there is no clear boundary like this in actual sediment transport phenomenon.

The numerical model of sediment transport consists of two governing equations, which describe the advection of suspended sediment (Eq.4) and conti suspended layer (Eq.5):

$$\frac{\partial Z_B}{\partial t} + \frac{1}{1-\lambda} \left( \frac{\partial q_B}{\partial x} + w_{ex} \right) = 0 \dots (4)$$

$$\frac{\partial \overline{C_s M}}{\partial x} - w_{ex} + \frac{\partial \overline{C_s h_s}}{\partial t} = 0 \dots (5)$$

$$q_B = 21 \sqrt{sgd^3} \tau_*^{\frac{2}{3}} \dots (6)$$

where  $C_s$  is depth-averaged concentration of suspended load,  $w_{ex}$  is exchange rate between the bed and suspended layer,  $h_s$  is the flow depth,  $Z_B$  is the bed level from the reference plane,  $\lambda$  is the porosity of the sand grains,  $q_B$  is the transport rate of bed load,  $s$  is the specific gravity of sand grain,  $d$  is the diameter of sand particle,  $\tau$  is the Shields parameter. In this study, a grain size of  $267 \mu m$  (medium-grained sand) was used for the calculation.

## 3. Results

### 3.1 Field survey

Fig.2 shows the relationship between the thickness of the sandy deposit and the distance from the coastline. The thickness of the sand deposit tends to decrease with increasing distance from the shoreline, and the deposits distribution limit is not consistent with the

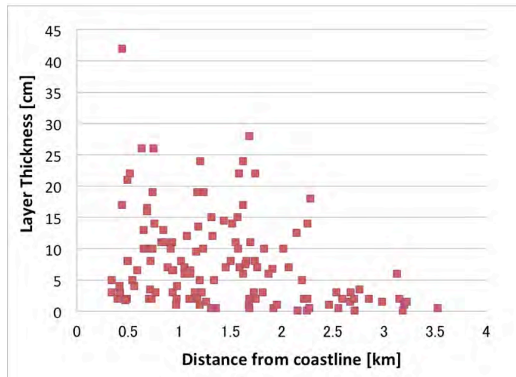


**Fig. 2.** Relationship between the thickness of the sand deposits and the distance from coastline

inundation limit in case of our survey area (Fig.1).

### 3.2 Numerical results

The numerical result of the sediment transport is shown in Fig.3. The deposition is significant near the coastal area. Erosion was evident on the beach, meanwhile deposition occurred at the inland areas from the beach to the limit of inundation.

### 3.3 Comparison of the interpolated thickness with the calculated thickness

We compared the calculated thickness with the interpolated thickness (Fig.4). The calculation result shows massive deposition up to about 2.0 km from the coastline. The calculated values in this section considerably overestimated the interpolated data of the measured deposit thickness. On the other hand, it can be seen that the difference between calculated and interpolated values were smaller at further inland areas.

In order to investigate the difference between the calculated and interpolated values at same point, we calculated the standard deviation of these differences (Fig.5). The result shows that the calculated values are well consistent with the observed value at distances farther than 1.5 km from the coastline, whereas a significant variation was calculated at the seaward areas.

### 4. Discussion

As shown in Fig. 4, a large difference

between calculated and interpolated thicknesses was observed at distances of 0-2.0 km from the shoreline, while the differences have decreased further inland. This feature can be clearly shown when we plot the standard deviation against the distance from the shoreline (Fig. 5).

This can be explained by complex topography near the coast, which did not reproduced in the digital elevation model used here. In this study, we used 50 m grid topography data as minimum size for calculation. The precision and resolution of the topography data near the coast is too rough to reproduce complex process of tsunami inundation and sediment transport. As a

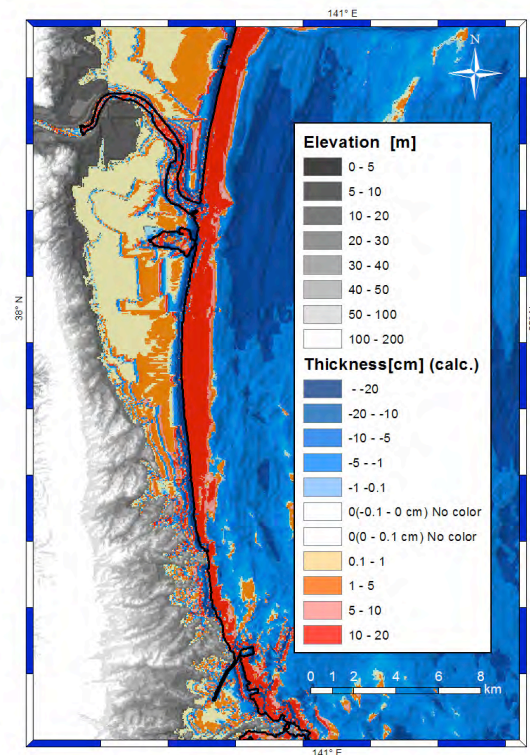


**Fig. 3.** The sediment distribution by sediment transport model (50 m mesh)

result, the calculated thickness near the coastal areas showed considerable variation from the measured data, whereas the variation is small in the inland areas in which the land is mainly composed of flat paddy field.

### 5. Conclusion

In this study, a numerical modeling of sediment transport by the 2011 Tohoku-oki tsunami was carried out. General distribution

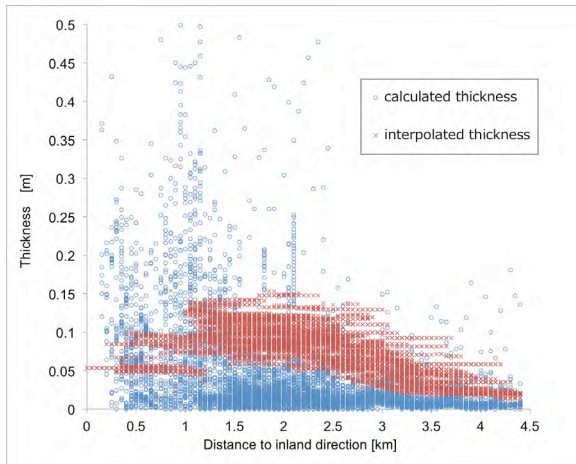


**Fig 4.** Comparison of the calculated thickness and interpolated thickness in the study area (deposition only)

pattern of the simulated deposit and reproducibility of the modeling were investigated.

We used a topography data with a spatial resolution of 50 m as minimum grid size of the nesting grid systems, to calculate the tsunami inundation and sediment transport. The grain size was set as constant ( $267\mu\text{m}$ ). The result of the numerical modeling showed that the difference (standard deviation) between interpolated thickness and calculated thickness becomes smaller in inland at distances of more than 1.5 km from the coastline.

The results suggested that use of topography data with a higher-resolution is required for further improvement of the modeling.

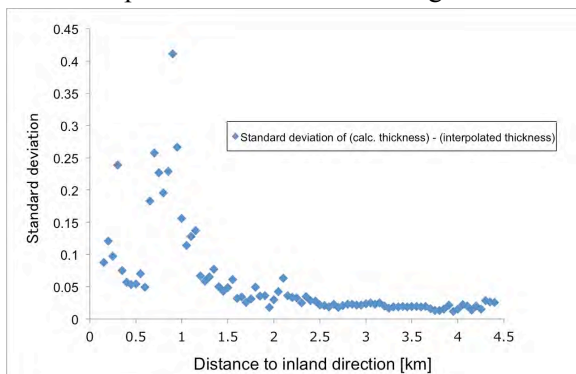


**Fig 5.** Standard deviation of the difference between the interpolation layer thickness and layer thickness calculation

## References

- Abe, T., Goto, K., Sugawara, D. (2013) Grain size and thickness of the tsunami deposits by the 2011 off the Pacific coast of Tohoku Earthquake in Sendai Plain (written in Japanese only) : Japan Geoscience Union Meeting, poster session, MIS25-P06.
- Imamura, F., Koshimura, S., Mabuchi, Y., Oie, T., Okada, K. (April 25, 2012) The 2011 East Japan off the Pacific Coast Earthquake and Tsunami. Tohoku University Source Model version 1.2. Sendai, Miyagi, Japan: Disaster Control Research Center
- Shuto, N. (1989) Transport of sand due to the tsunami event (written in Japanese only) : Tsunami Engineering Research report published by Tohoku University Tsunami Engineering Lab, vol.6, p.1-55
- Takahashi, T., Syuto, N., Imamura, F., Asai, D. (1999) Development of tsunami sediment moving model takes into the exchange amount of sand between suspended layer and bed load layer (written in Japanese only): Coastal Engineering Committee , vol.47, p.606-610
- Takahashi, T., Kurokawa, T., Fujita, M., Shimada, H. (2011) Hydraulic Experiment on Sediment Transport due to Tsunami with Various Sand Grain Size : Coastal Engineering Committee , vol.67, No.2, p.231-235

## Geochemical characteristics of paleotsunami deposits

Tetsuya Shinozaki<sup>a</sup>, Shigehiro Fujino<sup>b</sup>, Minoru Ikehara<sup>c</sup>

<sup>a</sup>Graduate School of Life and Environmental Sciences, University of Tsukuba, Tennodai 1-1-1, Tsukuba, Ibaraki 305-8572, Japan, shinozakit@geol.tsukuba.ac.jp

<sup>b</sup>Faculty of Life and Environmental Sciences, University of Tsukuba, Tennodai 1-1-1, Tsukuba, Ibaraki 305-8572, Japan

<sup>c</sup>Center for Advanced Marine Core Research, Kochi University, Monobe 200, Nankoku, Kochi, 783-8502, Japan

### 1. Introduction

Understanding paleotsunami event is required for comprehension of modern tsunami and prediction of future tsunami. Tsunami deposits, which are translated by the tsunami, especially sand deposits, are generally used for identification of paleotsunamis. However, because sand deposit does not always form up to inundation limit according to some recent researches (e.g. Abe et al., 2012), paleotsunami inundation area estimated from sand deposits has possibilities of underestimation. Meanwhile, sea-derived elements, such as Cl, Na and Mg, were detected within seawater inundation area (e.g. Minoura et al., 1994; Chagué-Goff et al., 2012). This means that using geochemical approach may enable us to identify an evidence of seawater inundation. However, only few studies have made an attempt to apply geochemical technique for paleotsunami research. Applying geochemical analysis for tsunami research leads to better understanding of prehistoric tsunami events.

In this study, we analyzed paleotsunami deposits by using biomarkers, such as *n*-alkane and alkenone, elemental analysis, stable carbon and nitrogen isotope ratio, and C/N ratio in order to understand geochemical characteristics of tsunami deposits. Because geochemical characteristics are different between terrestrial and marine derived organic/inorganic materials, it may be possible to identify sand deposits as tsunami evidence. In addition to these analysis, water content, loss on ignition, total nitrogen,

total carbon and total organic carbon were also analyzed to obtain fundamental data about the sediment.

### 2. Materials and methods

Study site is the Sendai coastal plain, Northeast Japan (Fig. 1), where a 1.0 m long sediment core was obtained c. 1.5 km inland from the shoreline. This area has often been inundated by large tsunami, such as the 869 Jogan tsunami, the 1611 Keicho tsunami and the 2011 Tohoku-oki tsunami. The reasons selecting this area are as follows: (1) Some sand layers transported by paleotsunami are confirmed (e.g. Sawai et al., 2012). (2) Numerous researches concerned with paleotsunamis are made around the Sendai coastal plain (e.g. Minoura et al., 2001).

Collected sediment core is dominated by mud that rests on sand, and contains two sand layers and one tephra layer. The 1 cm thick sandy deposit is existed at 24–25 cm depth just below the tephra layer at 16–24 cm depth, and it was

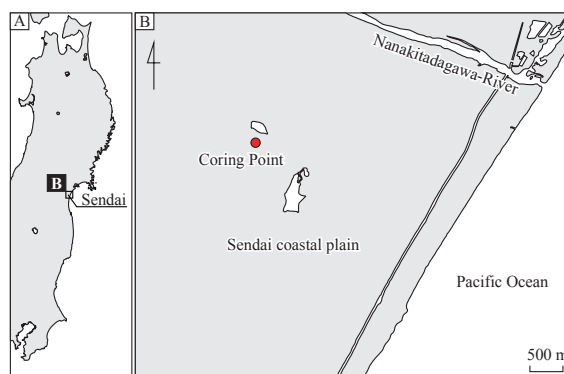


**Fig. 1.** Location of the study area. The red circle indicates the coring point

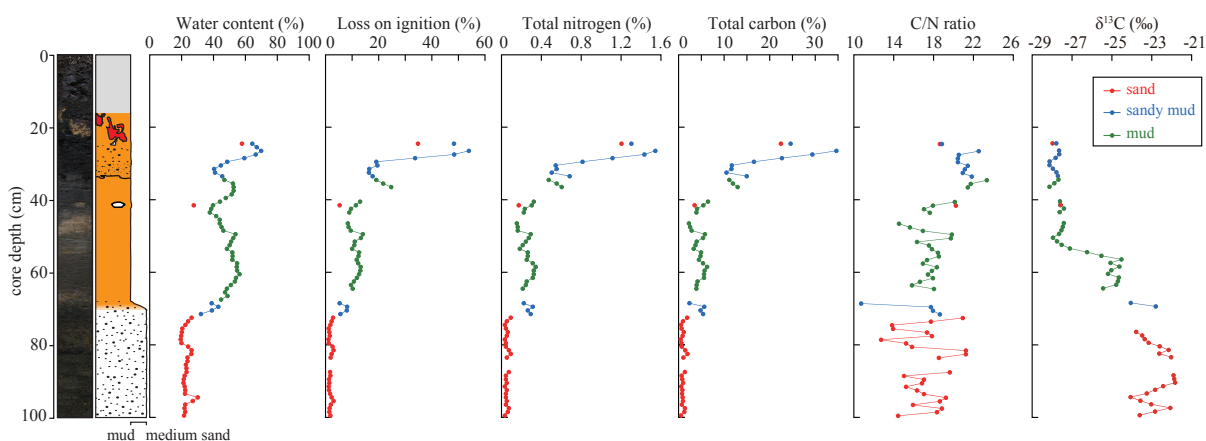


**Fig. 2.** Core lithology, and depth profile of water content (%), loss on ignition (%), total nitrogen (TN; %) total carbon (TC; %), C/N ratio and  $\delta^{13}\text{C}$  (‰)

probably formed by the 869 Jogan tsunami from some previous studies (e.g. Minoura et al., 2001). Sandy mud deposits were at 25–35 cm depth. Mud deposit was at 34–68 cm depth, and the 3 cm thick sand deposit was at 40–43 cm depth. The basal sand layer is at 68–100 cm depth. Samples are sliced in 1 cm interval except for the tephra layer.

### 3. Results and discussion

Temporal variation of water content (%), loss on ignition (LOI; %), total nitrogen (TN; %), total carbon (TC; %), C/N ratio and  $\delta^{13}\text{C}$  (‰) are shown in Fig. 2. The variability pattern among water content, LOI, TN and TC were significantly resemble. Sand deposits at 24–25 cm depth and 40–43 cm depth shows relatively low values compared to the sandy mud deposits at 24–25 cm depth and the mud deposits at 40–43 cm depth, respectively.

C/N ratio range from 10 to 22. Especially the sand layer at 68–100 cm depth shows large variability.  $\delta^{13}\text{C}$  shows high value (-24.1 to -21.8‰) in the basal sand deposits, incidentally the value rapidly shift at c. 55 cm depth. C/N ratio and  $\delta^{13}\text{C}$  values of mud and sandy mud deposits were within the range of reported terrestrial C3 plant and freshwater dissolved organic matter (DOC) (Lamb et al., 2006). On the other hand, these values of sand deposits were almost within the range of reported terrestrial C3 plant and seawater DOC. It is highly possible that sand deposits are oceanic

origin, although sand deposits at 24–25 cm depth and 40–43 cm depth are within the range of freshwater DOC and almost same value with the same layers.

Major elements, such as Na, Ca, Mg, Fe, Ti, Si, K, P and Mn, were determined by the X-ray fluorescence (XRF). Geochemical normalization is required to reduce the effect of grain size and to correct mineralogical variation. Fe or Al is generally used for normalization. The values of  $\text{Na}_2\text{O}/\text{Al}_2\text{O}_3$  and  $\text{CaO}/\text{Al}_2\text{O}_3$  are relatively high in sand deposits, while  $\text{MgO}/\text{Al}_2\text{O}_3$  of sand deposits shows almost same or little lower relative to mud and sandy mud deposits.

$\text{C}_{23}\text{--}\text{C}_{33}$  odd *n*-alkane, which mainly originate from terrestrial plants, were detected, however, ocean-derived *n*-alkane, such as  $\text{C}_{15}\text{--}\text{C}_{19}$  odd *n*-alkane, were not detected in the two sand layers (Fig. 3). In addition, alkenone originated from coccolith was also not detected in the sand layers. If sand deposits were transported from ocean by tsunami, ocean-derived biomarker is expected to be detected, however, the results were contrary to our intention. Although this result may mean that these sand deposits were not transported by tsunami, it is quite likely that ocean-derived biomarker was not detected due to supplied amount from ocean was extremely small relative to soil organic matter. We will continue discussing about fatty acid and sterol as well as *n*-alkane and alkenone.

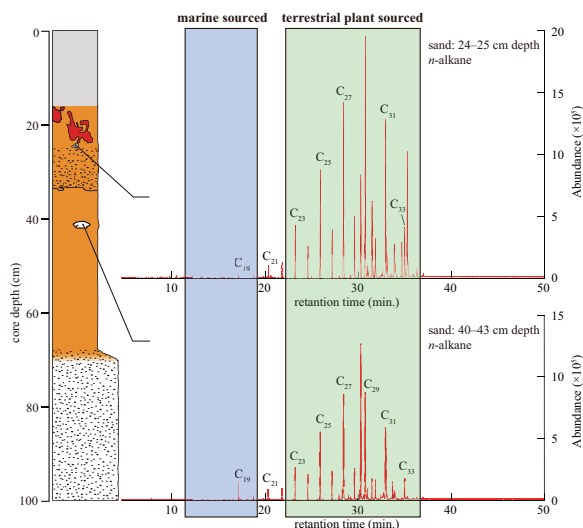


**Fig. 3.** Distribution of *n*-alkanes in the sample of sand deposits

#### 4. Summary

The geochemical characteristics of sand deposits, which is highly possible to be formed by paleotsunamis were investigated at c. 1.5 km inland from the shoreline on the Sendai coastal plain.  $\delta^{13}\text{C}$  showed distinct difference among sand, mud and sandy mud deposits. It is possible that sand deposits are derived from ocean according to the relationship between  $\delta^{13}\text{C}$  and C/N ratio. However, *n*-alkane and alkenone biomarkers did not indicate the evidence of marine origin. This may result from much smaller amount of sea material than soil organic matter in the sand layers.

#### References

Abe, T., Goto, K., Sugawara, D. (2012)

Relationship between the maximum extent of tsunami sand and the inundation limit of the 2011 Tohoku-oki tsunami on the Sendai Plain, Japan, *Sedimentary Geology*, 282, p.142-150.

Chagué-Goff, C., Andrew, A., Szczucinski, W., Goff, J., Nishimura, Y. (2012) Geochemical signatures up to the maximum inundation of the 2011 Tohoku-oki tsunami –Implications for the 869 AD Jogan and other palaeotsunamis, *Sedimentary Geology*, 282, p.65-77.

Lamb, A.L., Wilson, G.P., Leng, M.J. (2006) A review of coastal palaeoclimate and relative sea-level reconstructions using  $\delta^{13}\text{C}$  and C/N ratios in organic material, *Earth-Science Reviews*, 75, p.29-57.

Minoura, K., Imamura, F., Sugawara, D., Kono, Y., Iwashita, T. (2001) The 869 Jōgan tsunami deposit and recurrence interval of large-scale tsunami on the Pacific coast of northeast Japan, *Journal of Natural Disaster Science*, 23, p.83-88.

Minoura, K., Nakaya, S., Uchida, M. (1994) Tsunami deposits in a lacustrine sequence of the Sanriku coast, northeast Japan, *Sedimentary Geology*, 89, p.25-31.

Sawai, Y., Namegaya, Y., Okamura, Y., Satake, K., Shishikura, M. (2012) Challenges of anticipating the 2011 Tohoku earthquake and tsunami using coastal geology, *Geophysical Research Letters*, 39, L21309.

## Distribution and age of a possible paleotsunami deposit in a coastal lowland, southeastern Kyushu

Masaki Yamada<sup>a</sup>, Shigehiro Fujino<sup>b</sup>, Takashi Chiba<sup>b</sup>, Kazuhisa Goto<sup>c</sup>, James Goff<sup>d</sup>

<sup>a</sup>Graduate School of Life and Environmental Sciences, University of Tsukuba, Tennodai 1-1-1, Tsukuba, Ibaraki 305-8572, Japan, [yamada@geol.tsukuba.ac.jp](mailto:yamada@geol.tsukuba.ac.jp)

<sup>b</sup>Faculty of Life and Environmental Sciences, University of Tsukuba, Tennodai 1-1-1, Tsukuba, Ibaraki 305-8572, Japan

<sup>c</sup>International Research Institute of Disaster Science, Tohoku University, Aoba 6-6-40-102, Aramaki, Aoba-ku, Sendai 980-8579, Japan

<sup>d</sup>School of Biological, Earth and Environmental Sciences, University of New South Wales, Sydney 2052, Australia

### 1. Introduction

According to the Central Disaster Prevention Council (CDPC) (2012), the apparent rupture area for the largest possible earthquake that may occur along the Nankai Trough extends as far as southeastern Kyushu (Fig. 1). However, it is not known whether such an event and its associated tsunami have actually occurred along the Nankai Trough in the past. This is largely because there are few historical documents concerning tsunamis in Kyushu. The oldest historical tsunami recorded in the region is the AD 1596 Keicho-Bungo earthquake tsunami (Hatori, 1985) and while many paleotsunami studies have been conducted throughout Japan, there have been

few in eastern Kyushu.

The fault rupture area of the AD 1707 Hoen earthquake is thought to have extended to the west of the Cape Ashizuri (Fig. 1; Furumura et al., 2011). While the AD 1707 Hoen tsunami was 3.0–4.5 m high on the northeast coast of Kyushu, it was thought to have been comparatively small in the southeast (Hatori, 1985). However, if the rupture area of an earthquake extended southwards down east coast of Kyushu as proposed by CDPC (2012), the resultant tsunami may strike much of the southeastern coast of Kyushu.

Paleotsunami deposits contain useful information for disaster prevention such as the areal extent of the inundation area and the recurrence intervals such events. In eastern Kyushu, sandy paleotsunami deposits were reported in Ryujin Lake, Oita Prefecture (e.g., Okamura and Matsuoka, 2012), but there have been no detailed studies carried out further south in Miyazaki Prefecture (Goto et al., 2012). Therefore, the main purpose of this study is to unravel the tsunami history of southeastern Kyushu over thousands of years.

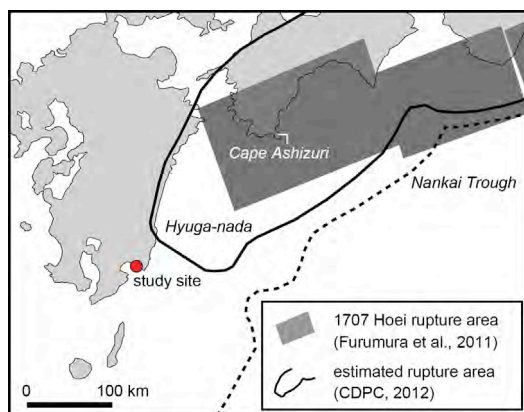


**Fig. 1.** Map showing the AD 1707 Hoen rupture area (Furumura et al., 2011) and the estimated rupture area (CDPC, 2012).

### 2. Study site and method

The study site is on the coastal lowland of Kushima City, Miyazaki Prefecture (Figs. 1 and

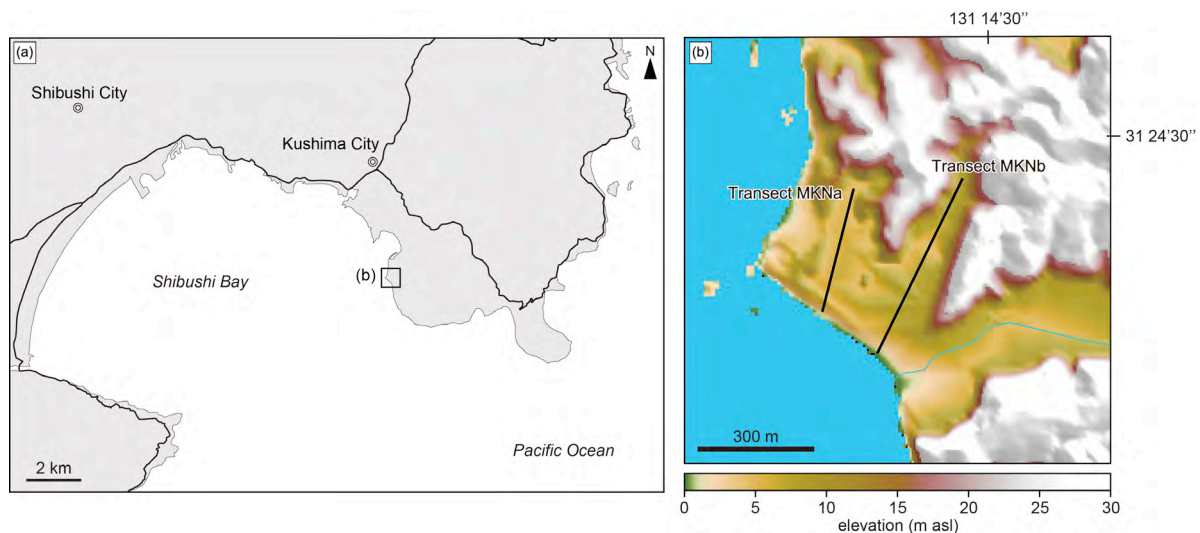


**Fig. 2.** (a) Location map of the study site in eastern Kyushu. (b) Elevation of the study site and location of the two transects (digital elevation model is based on data from the Geospatial Information Authority of Japan).

2a). The approx. 550 m wide lowland facing Shibushi Bay is drained by a small river and surrounded by 10–30 m high hills. It is mainly occupied by paddy fields (Fig. 2b).

We conducted hand coring at 19 study points along two (300 and 450 m) shore-perpendicular transects (Transect MKNa and MKNb) (Fig. 2b). A hand-held GPS was used to record the position of each study point and a ProMark 100 for topographic measurements. Samples were prepared for radiocarbon dating and diatom analysis. A microscope was used to identify plants, seeds and insect remains for radiocarbon dating. The radiocarbon analysis was carried out by accelerator mass spectrometry (AMS) at Beta Analytic Radiocarbon Laboratory. Subsamples for diatom analysis were taken at 27 points from 3.0–5.0 m depth in core MKNa-06 (Fig. 3). At least 300 diatoms were counted in each sample.

### 3. Results

In this abstract, we provide specific data only on the cores from transect MKNa because data for transect MKNb are currently undergoing analysis.

#### Sedimentary characteristics

The 3.0–5.0 m sedimentary successions from the study sites were composed of numerous

units ranging from a basal fine to medium dark-gray sand with some granules, green-brown organic-rich mud, through black-brown organic-rich and blue-gray mud to the upper agricultural soil (Fig. 3). One or two sand layers were evident in the organic-rich mud in all cores along transect MKNa. In addition, a tephra layer was present at around 2.0–3.5 m depth in all cores. These sand and tephra layers were bounded by sharp contacts with organic-rich muds. The color of the organic-rich mud varied markedly above and below the sand layers (Fig. 3).

#### Diatom analysis

Below 4.5 m in core MKNa-06, the diatom assemblages were mainly composed of marine taxa (Fig. 4). They accounted for up to 80.2% of the total at 450–451 cm depth. Above 4.5 m on the other hand, brackish and fresh water diatoms were common, and marine diatoms gradually decreased in number (Fig. 4). They constituted about 10.2%, 6.7% and 1.5% of total at 440–441 cm, 420–421 cm and 401–402 cm, respectively. While the percentage of marine diatoms was only about 1% between 3.7–4.0 m depth, marine diatoms accounted for 3–8% of the total at 363–365 cm and 368–369 cm in and below the sand layer (Figs. 3 and 4).

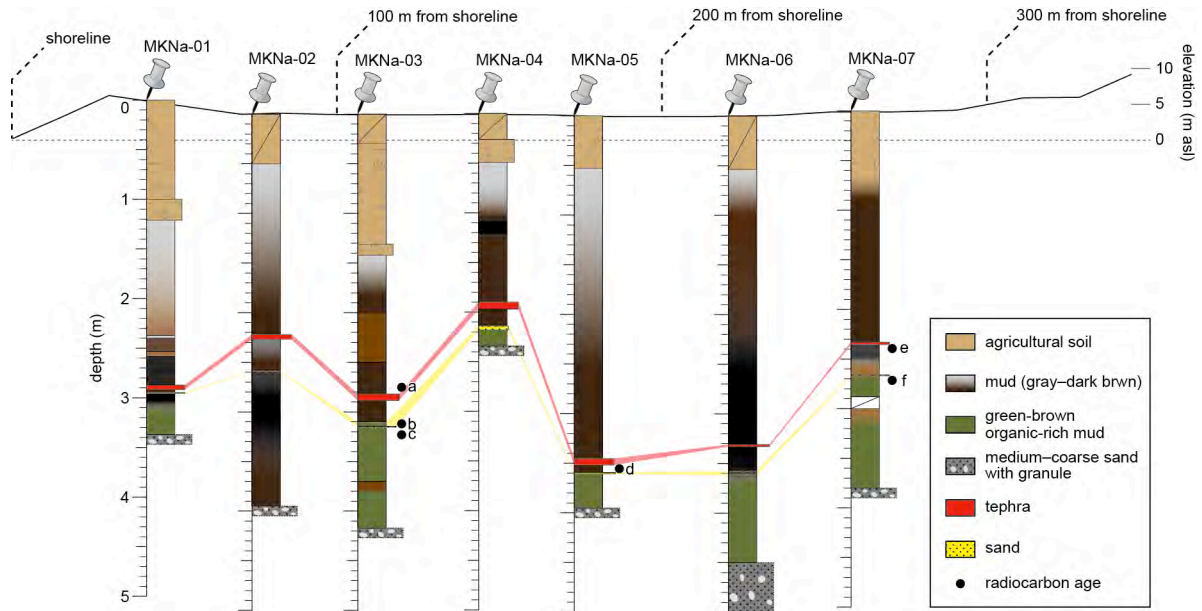


Fig. 3. Cross-sections of sedimentary columns and positional relation of sand and tephra sheets.

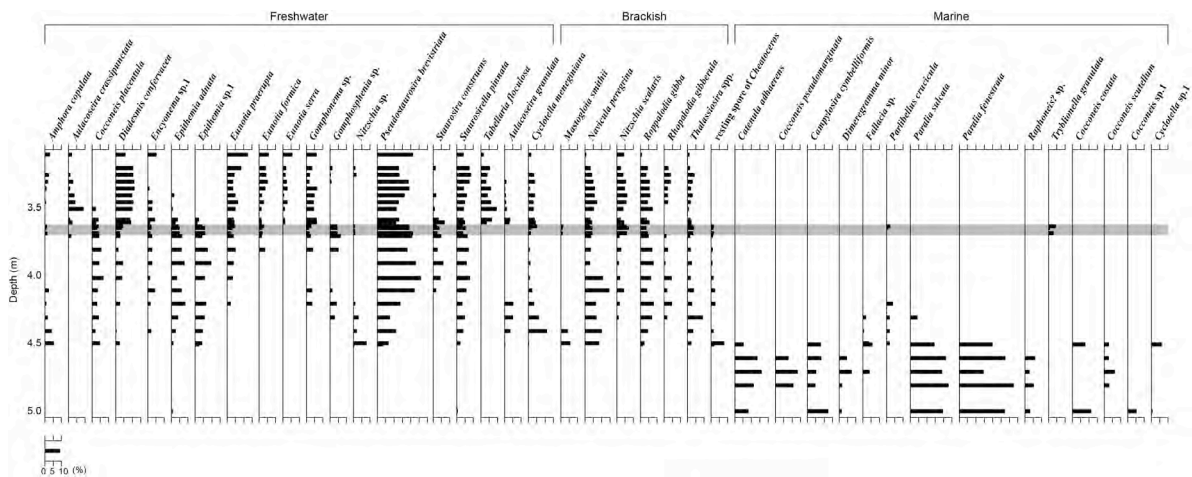


Fig. 4. Abundance of diatom assemblages in core MKNa-06.

### Radiocarbon ages

Radiocarbon ages were determined around the tephra and sand layers (Fig. 3 and Table 1). With one exception the organic-rich mud layers bracketing the tephra and sand units were deposited around 4500–4800 years ago (Table 1). Although we have not determined the age of tephra yet, it is known that the eruption of Kirishima Miike (Kr-M) occurred about 4600 years ago (Kino and Ota, 1977).

### 4. Discussion

It seems likely that the sand layers observed at around 2.0–3.5 m depth were formed by an unusual inundation event because the boundary between sand layer and organic-rich mud was extremely clear. The lateral consistency of the sand sheet (40–260 m from the shoreline) indicates that it was likely formed by extensive wave inundation of the lowland. The extent of inundation makes it more likely to have been the result of tsunami inundation, not storm. Furthermore, since the river is small, it seems unlikely to have flooded the entire lowland with sandy material. The interpretation is supported

**Table 1.** Radiocarbon ages of plants, seeds and insect remains.

Sample no.	Core	Depth (cm)	Position	Age ( $^{14}\text{C}$ yr BP)	Age (cal yr BP)	Lab no. (Beta-)
a	MKNa-03	287–290	Above tephra	4230±30	4848–4817	341396
b	MKNa-03	326–330	Between sand layers	3040±30	3269–3215	341397
c	MKNa-03	332–336	Below sand	4170±30	4761–4693	341398
d	MKNa-05	352–355	Below tephra	4070±30	4583–4518	341399
e	MKNa-07	210–214	Below tephra	4130±30	4651–4579	341400
f	MKNa-07	238–242	Below sand	4050±30	4569–4514	341401

by the presence of marine diatoms that indicate that the sand was sourced from the seafloor or beach (Fig. 4). Based on these findings and the radiocarbon ages, it is highly probable that this sand sheet was formed by a paleotsunami that inundated the area about 4500–4800 years ago.

## 5. Conclusion and future plan

We have reported on a sand sheet that was probably laid down by a paleotsunami around 4500–4800 years ago. Further work will involve additional radiocarbon dating and tephra identification in order to provide a more precise age for the sand sheet. In addition, we will attempt to reconstruct the nature of the tsunamigenic crustal movement associated with this event using differences in the diatom assemblages identified in sediments immediately above and below the sand layer.

## References

- Central Disaster Prevention Council (2012) [http://www.bousai.go.jp/jishin/nankai/taisaku/pdf/1\\_1.pdf](http://www.bousai.go.jp/jishin/nankai/taisaku/pdf/1_1.pdf).
- Furumura, T., Imai, K. and Maeda, T. (2011) A revised tsunami source model for the 1707 Hiei earthquake and simulation of tsunami inundation of Ryujin Lake, Kyushu, Japan. *Journal of Geophysical Research*, 116, B02308.
- Goto, K., Nishimura, Y., Sugawara, D. and Fujino, S. (2012) The Japanese tsunami deposit researches (in Japanese with English abstract). *Journal of Geological Society of Japan*, 118, 431–436.

Hatori, T. (1985) Field investigation of historical tsunamis along the East Coast of Kyushu, West Japan (in Japanese with English abstract). *Bulletin of the Earthquake Research Institute, University of Tokyo*, 60, 439–459.

Kino, Y. and Ota, R. (1977) Miyakonojo chiiki no chishitsu (in Japanese). *Chiiki chishitsu kenkyu hokoku*, 45p.

Okamura, M. and Matsuoka, H. (2012) Nankai Earthquake recurrences from tsunami sediment (in Japanese). *Kagaku*, 82, 182–191.

## Estimation of the sizes of paleotsunamis using tsunami boulders at Ishigaki Island, Japan

Akifumi Hisamatsu<sup>a</sup>, Kazuhisa Goto<sup>b</sup>, Fumihiko Imamura<sup>b</sup>

<sup>a</sup> Department of Civil and Environmental Engineering, Graduate School of Engineering, Tohoku University, 6-6-11-1106 Aoba, Sendai, Miyagi 980-8579, Japan, Hisamatsu@tsunami2.civil.tohoku.ac.jp

<sup>b</sup> International Research Institute of Disaster Science, Tohoku University

### 1. Introduction

Coralline boulders that were transported by past tsunamis were deposited at Sakishima Islands, the southern Ryukyu Islands, Japan (Fig. 1). Makino (1968) is suggesting that boulders' transportation would be described in historical documents related to the AD1771 Yaeyama earthquake tsunami (so-called Meiwa tsunami). Kawana and Nakata (1994), Goto *et al.* (2010), and Araoka *et al.* (2013) measured numerous radiocarbon dating of boulders and clarified that tsunami recurrence interval around Sakishima Islands is 150-400 years.

However, each size of tsunamis prior to the 1771 Meiwa tsunami has been less discussed. In this study, we calculated the transportation of a boulder at the southeastern coast of Ishigaki Island and estimated the size of tsunamis prior to the 1771 event.

### 2. Previous studies for the Meiwa tsunami and tsunami boulders

Several source models of the Meiwa tsunami were proposed in order to explain the maximum run-up heights of up to 30 m (Goto *et al.*, 2010). Imamura *et al.* (2001) proposed  $M_w=7.8$  earthquake plus submarine landslide model. Nakamura (2009) proposed  $M_w=8.0$  tsunami earthquake along the Ryukyu trench (Fig. 2). Recently, Miyazawa *et al.* (2012) compared accuracy of several source models and proposed  $M_w=8.2$  earthquake plus landslide model (Fig. 2) better explains the tsunami traces although they also acknowledged that the other models have potential to be improved by future works.

There are numerous boulders formed by the paleotsunamis including those deposited by the

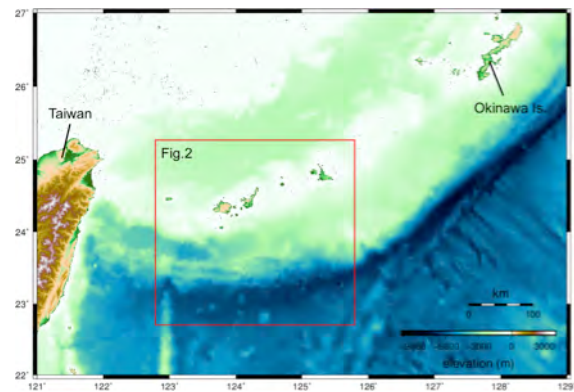


**Fig. 1.** Southern Ryukyu Islands (Sakishima Islands) between Okinawa Island and Taiwan.

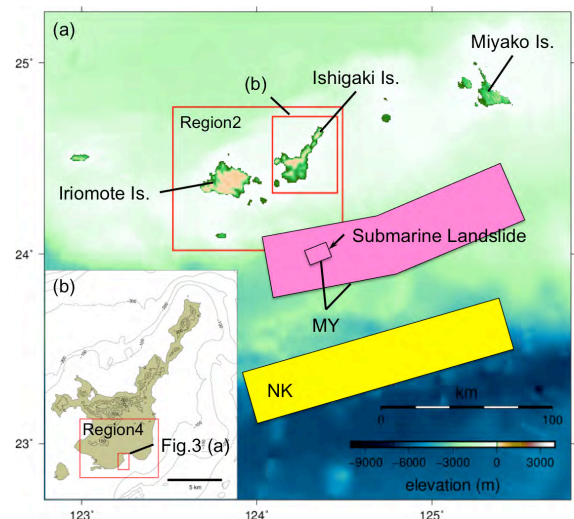


**Fig. 2.** (a) Region 1 of the numerical regions and tsunami source model of the Meiwa tsunami proposed by Nakamura (2009, NK) and Miyazawa *et al.* (2012, MY). (b) Ishigaki Island.

1771 Meiwa tsunami (Goto *et al.*, 2010). A boulder that we studied here, so-called *tsunami ufu-ishi*, is weighed an estimated over 500 t. The radiocarbon dating result showed 1980 $\pm$ 80 yrBP (Kawana and Nakata, 1994). Kawana and

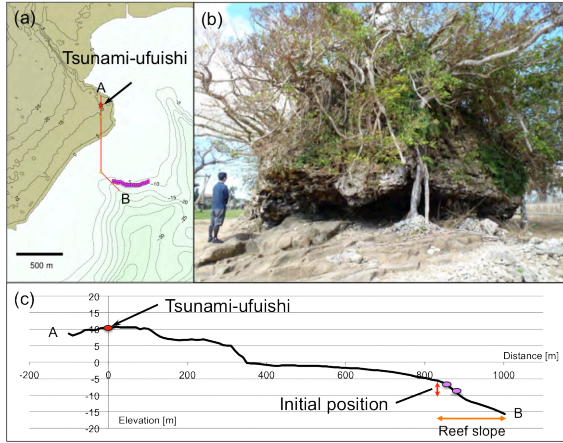


**Fig. 3.** (a) Location of *tsunami ufu-ishi* at Ishigaki Island and its presumed initial position in the numerical calculation (purple points). (b) *Tsunami ufu-ishi*. (c) Cross-section around *tsunami ufu-ishi* (A-B in (a)).

Nakata (1994) also suggested that its initial position was reef slope (Fig. 3 (c)), shallower than 10 m based on the coral assemblages on the boulder. Therefore, it can be considered that the *tsunami ufu-ishi* was cast ashore from the reef slope around 2000 years ago. However, it should be noted that the boulder was not necessarily reached its present position by a single tsunami at 2000 years ago. In fact, Sato *et al.* (2012) suggested that this boulder was rotated twice by two tsunami events according to the paleomagnetic analysis.

### 3. Numerical calculation

Based on the tsunami and boulder transport models, we numerically tested the size and number of tsunami(s) that can deposit *tsunami ufu-ishi* at its present position. For tsunami propagation in the deep-sea area (Region 1, 10 sec grid), we used a linear equation in spherical earth with allowance made for the Coriolis force. We used a nonlinear equation (shallow water equation) in Region 2 (100 m grid), Region 3 (50 m grid) and Region 4 (10 m grid) in a Cartesian coordinate system made for bottom friction. For analyses of boulder transport by tsunami, we used a BTT model developed by Imamura *et al.* (2008).

We set 40 boulders at 20 m interval in an area from 6 to 10 m water depth (Fig. 3 (a), (c))

**Table.1.** Dislocation parameters of tsunami source models of landslide in case of MY and fault in case of NK. Inundations are those at *tsunami ufu-ishi*'s present position.

Model	MY		NK		Inundation
	LS	label	F	label	
Dis-Location [m]	35	MY1	16	NK1	1 m
	60	MY2	19	NK2	2 m
	90	MY3	22	NK3	3 m
	120	MY4	24	NK4	4 m
	150	MY5	25	NK5	5 m
	180	MY6	27	NK6	6 m
	240	MY7	29	NK7	7 m
	300	MY8	31	NK8	8 m

because assumed original location of this boulder has some uncertainties. The fault model of the 1771 Meiwa tsunami is the basis of this analysis: whether it has enough force to deposit this boulder at its present position. However, the tsunami(s) that moved the *tsunami ufu-ishi* do not necessarily the same size to the 1771 Meiwa tsunami. Therefore, in case of model proposed by Miyazawa *et al.* (2012), we changed dislocation of the landslide while dislocation of the fault was changed in case of the model proposed by Nakamura (2009) (Table. 1). Because of the assumption of various dislocations, flow depth at the present position of *tsunami ufu-ishi* varies ranging from 1 to 8 m at about 1 m interval (Table.1).

Finally, we estimated the adequate tsunami source model(s), which transport the *tsunami ufu-ishi* from the initial position to the present position (within 100 m) at one or two tsunami events.

### 4. Result

As a result of numerical calculation, we found that MY7 (Fig. 4 (a)), MY8, NK7, and NK8 are appropriate models to explain the transportation of this boulder near the present position by a single event. In fact, boulders could not reach its present position by a single tsunami if we adopt the other models. On the other hand, MY4 (Fig. 4 (b)), MY5, MY6 and

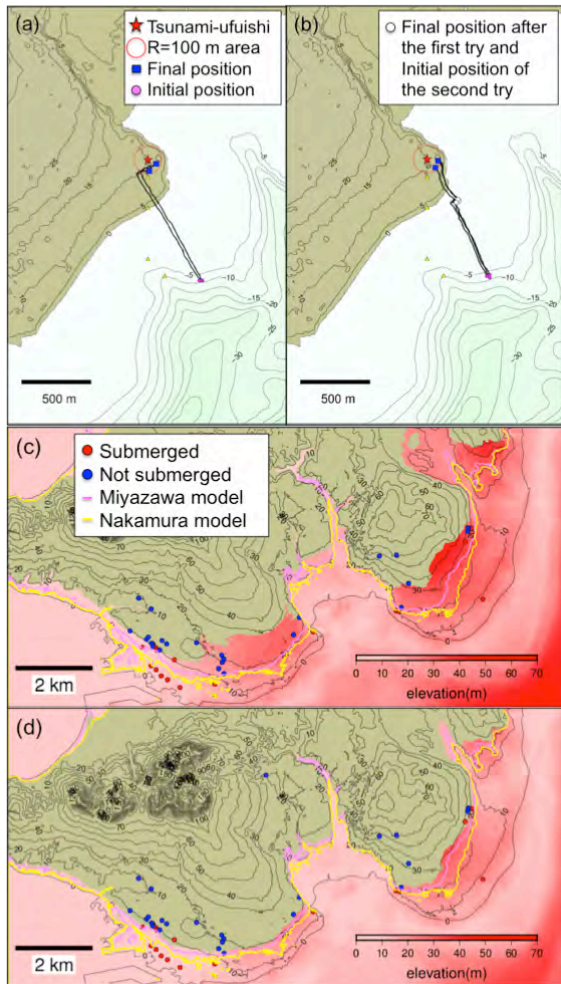


**Fig. 4.** Results of the numerical calculation. Boulder transport by (a) MY7 and (b) MY4. Inundation area of (c) MY7 and (d) MY4 with maximum run-up line of Miyazawa and Nakamura model and submerged and not submerged points of Meiwa tsunami.

NK6 models are appropriate if we assume two tsunamis that transport the boulder to its position. Tsunamis with <3 m flow depth at the present position of the boulder was not able to deposit it even if we assume multiple tsunami events.

## 5. Discussion

The tsunami that transported *tsunami ufu-ishi* at one time is remarkably larger than the size of the Meiwa tsunami. Although we cannot fully exclude the possibility at this moment, it is unlikely that such an extremely large tsunami was occurred because their dislocation parameters are far beyond the ordinary ones. In contrast, if we assume that a boulder was

transported by two tsunami events whose sizes are similar to that of the Meiwa event, the boulder can reach its present position. Therefore, it is more reasonable to conclude that the boulder was moved and reached its present position after 2000 years ago by twice in the past as suggested by Sato *et al.* (2012).

## 6. Conclusion

Our preliminary modeling results suggest that the *tsunami ufu-ishi* boulder was moved twice by the similar size to the 1771 Meiwa tsunami to reach its present position. This indicates that multiple large tsunamis with similar size to that of the Meiwa event were occurred at least twice prior to the 1771.

## References

- Araoka, D., Yokoyama, Y., Suzuki, A., Goto, K., Miyagi, K., Miyazawa, K., Matsuzaki, H., Kawahata, H. (2013) Tsunami recurrence revealed by *Porites* coral boulders in the southern Ryukyu Islands, Japan, *Geology*, 41, p.919-922.
- Goto, K., Kawana, T., Imamura, F. (2010) Historical and geological evidence of boulders deposited by tsunamis, southern Ryukyu Islands, Japan, *Earth-Science Reviews*, 102, p.77-99.
- Imamura, F., Yoshida, I. and Moore, A. (2001) Numerical study of the 1771 Meiwa tsunami at Ishigaki Island, Okinawa and the movement of the tsunami stones, *Proceedings of Coastal Engineering, Japan Society of Civil Engineers*, 48, p.346-350.
- Imamura, F., Goto, K., Ohkubo, S. (2008) A numerical model for the transport of a boulder by tsunami, *Journal of Geophysical Research*, 113, C01008.
- Kawana, T., Nakata, K. (1994) Timing of Late Holocene tsunamis originated around the southern Ryukyu Islands, Japan, deduced from coralline tsunami deposits, *Journal of Geography, Japan*, 103, p.352-376 (in Japanese with English abstract).

- Makino, K. (1968) The Meiwa Tsunami at Yaeyama, published by author, Ishigaki, 462 p. (in Japanese).
- Miyazawa, K., Goto, K., Imamura, F. (2012) Re-evaluation of the 1771 Meiwa Tsunami source model, southern Ryukyu Islands, Japan. In: Yamada, Y.; Kawamura, K.; Ikehara, K.; Ogawa, Y.; Urgeles, R.; Mosher, D.; Chaytor, J.; Strasser, M. (Eds.), *Advances in Natural and Technological Hazards Research, Submarine Mass Movements and Their Consequences*, Springer, 31, p.497-506.
- Nakamura, M. (2009) Fault model of the 1771 Yaeyama earthquake along the Ryukyu Trench estimated from the devastating tsunami, *Geophysical Research Letters* 36, L19307.
- Nandasena, N.A.K., Paris, R. and Tanaka, N. (2011) Reassessment of hydrodynamic equations: Minimum flow velocity to initiate boulder transport by high energy events (storms, tsunamis), *Marine Geology*, 281, p.70-84.
- Noji, M., F. Imamura, and N. Shuto (1993) Numerical simulation of movement of large rocks transported by tsunamis, *Proceedings of IUGG/IOC International Tsunami Symposium*, p.189-197.
- Nott, J. (2003) Waves, coastal boulders and the importance of the pre-transport setting, *Earth and Planetary Science Letters*, 210, p.269-276.
- Sato, T., Nakamura, N., Minoura, K., Nagahama, Y. (2012) Sedimentation record according to the paleomagnetism of tsunami boulders at Ishigaki Island, Japan Geoscience Union Meeting 2012.

## The combination of anisotropy of anhysteretic remanent magnetization (AARM) and grain size data provide information about the hydrodynamic conditions of the tsunami deposits

Shusaku Kon<sup>a</sup>, Norihiro Nakamura<sup>a,b</sup>, Daisuke Sugawara<sup>b</sup>, Kazuhisa Goto<sup>b</sup>, Yasutaka Iijima<sup>a</sup>

<sup>a</sup> Department of Earth Science, Tohoku University, Sendai, JAPAN, b2sm6014@s.tohoku.ac.jp

<sup>b</sup> International Research Institute of Disaster Science, Tohoku University, Sendai, JAPAN

### 1. Introduction

Some of the proxies used to identify paleotsunami deposits have been reviewed in the light of new findings following the 2004 Indian Ocean Tsunami, the 2009 South Pacific Tsunami, and 2011 Tohoku-oki Tsunami, and a revised toolkit was provided. Chagué-Goff et al. (2011) reviewed that the proxies for modern and paleotsunami deposits, and a summary of most of the commonly used proxies as well as more detailed information on less frequently used diagnostic criteria for sandy sediment. Both tsunamis and severe storms cause a coastal flooding with high overland flow, resulting in the similar physical attributes of the deposition. Therefore, it is important to distinguish between them without some *a priori* evidence (e.g., Dawson and Shi 2000). The discriminations of tsunami deposits with storm ones are related to differences in the hydrodynamics and sediment-sorting processes during sediment transportation.

According to Morton et al. (2007), tsunami deposition results from a few high-velocity, long-period waves that emplace sediment from the shoreface, beach, and landward erosion zone. Moreover, tsunami can have flow depths greater than 10 m, transport sediment primarily in suspension, and distribute the load over a broad region where sediment falls out of suspension when flow decelerates. In contrast, severe storm inundation generally is gradual and prolonged, consisting of many waves that erode beaches and dunes with no significant overland return flow until after the main flooding. Severe storm flow depths are commonly < 3 m, sediment is

transported primarily as bed load by traction, and the load is deposited within a zone relatively close to the beach. Thus, sandy tsunami deposits should provide valuable information on tsunami inundation as well as hydrodynamics. However, if the deposit does not show any sedimentary structures such as cross laminations, it is difficult to infer the flow direction, which is important to interpret the behavior of the tsunami, such as inflow and outflow as well as repetition of waves.

Anisotropy of magnetic susceptibility (AMS) appears to be a promising tool to study flow directions during tsunami inundation. It might allow us to reconstruct transport directions because it provides a cryptic alignment of ferromagnetic and paramagnetic minerals, such as coarse-grained magnetite or silicate minerals (e.g. biotite and amphibole). These minerals behave differently in different hydrodynamic conditions: for example, platy biotite and parallelepiped amphibole may deposit in a cryptic micro-ripple. This therefore suggests that the usefulness of bulk AMS together with limited optical observations in the study of flow fabric in tsunami deposits. Although AMS provides a cryptic grain alignment of ferromagnetic and paramagnetic minerals, the oxidation and alteration of these minerals by an underground water circulation during their deposition weaken the intensity of magnetic susceptibility, causing a large error of AMS's inclination and declination.

The anisotropy of anhysteretic remanent magnetization (AARM) on the other hand isolates only the fine-grained magnetite

subfabric of needle-shaped inclusions exsolved in silicate minerals. Moreover, grain size analysis and interpretation of various grain size parameters provide valuable information for both the description of the sediment and hydrodynamic interpretation of the tsunami deposits. Thus, the combination of AMS, AARM, and grain size data, can provide information about the hydrodynamic conditions prevailing during the emplacement of tsunami sequences.

## **2. Fabrics of tsunami deposits using AARM and its interpretation**

The fore-arc region of northeast Japan is an area of extensive seismic activity and tsunami generation. On July 13, 869 a tsunami triggered by a large-scale earthquake invaded its coastal zones, causing extensive deposition of well-sorted fine sand over the coastal plains of Sendai. According to Minoura et al. (2001), the first tsunami wave triggered by an earthquake of magnitude 8.3 would have spread 4 km inland from the coast. Samples from tsunami deposits, believed to have been laid down by the Jogan event, were collected from a section on the Sendai Plain, east Japan. The transport direction in these deposits could not be determined by AMS analysis due to large declination and inclination errors. The AARM technique was thus applied to determine the cryptic subfabric of magnetite exsolutions along cleavages in biotite and amphibole. Our scanning electron microscopy (SEM) observations confirmed that the maximum AARM orientation is parallel to the needle-shaped magnetite microexsolutions in biotite and amphibole by alteration. We therefore infer that the large error of AMS is caused by the alteration of these paramagnetic minerals, and AARM provides a cryptic alignment of fine-grained magnetite microexsolutions, mimicking the orientation for a long axis of these silicate minerals.

## **3. Attempt of the distinction between**

### **tsunami and other flooded deposits**

In order to apply our AARM method to diagnostic criteria or proxies of historical and paleotsunamis, we also collected 44 samples from alternating layers of possible tsunami deposits and non-tsunami deposits at the ruin of the Yayoi period in the township of Yamamoto, northeast Japan (Now this ruin has been backfilled). We observed and sampled at the outcrop (fig. 1) which located vertical coastline. The bottom layer, consists of organic mud, includes some Yayoi potteries (about 2000 years ago). The middle layer, consist of fine sand, was observed much of mud intraclasts, in which may be originated in a tsunami deposit. And the top is coarse sand layer, including about 1 cm white-color clasts without any mud inclusions. This layer does not show any sediment-sorting texture, suggesting the non-tsunami deposit, but there is no way to confirm. Therefore, the AARM may be confirmed if the orientation of the deposited each layer is different. Moreover, it is important to conduct the grain size analysis because each layer has different grain size, and the grains alignment related to hydrodynamic conditions. Several approaches have been reported to the grain size analysis of tsunami deposits. Where the coarser grains do not exceed 1 mm, laser diffraction particle size measurements are suitable for clay to sand-sized sediment. Statistical parameters (e.g. mean grain size) are normally calculated according to the computation method of moments of Seward-Thompson and Hails (1973). According to Chagué-Goff et al. (2011), this method is particularly well adapted for obtaining grain size statistical parameters, because the whole frequency distribution is used in the computation, instead of a few selected percentiles. These parameters appear to be the most useful to the study of tsunami and other flooded deposits.

Moreover, the middle layer becomes smaller in grain diameters gradually, and it was not observed in the point where the proceeded

about 16 meters from the first sampling. These proxies will provide valuable information on tsunami inundation as well as hydrodynamics, such as flow speed.

We will report the combination examination of AARM measurements and grain size determination in this conference in order to avail of the diagnostic criteria.

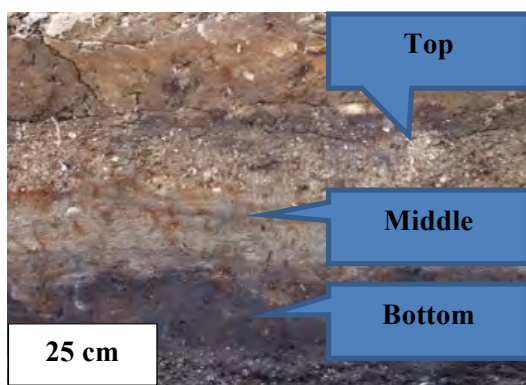


**Fig. 1.** Three successive layers at the ruin of the Yayoi period

## References

- Chagué-Goff, C., Schneider, J.-L., Goff, J. R., Dominey-Howes, D., Strotz, L., (2011) Expanding the proxy toolkit to help identify past events – Lessons from the 2004 Indian Ocean Tsunami and 2009 South Pacific Tsunami, *Earth-Science Reviews* 107, pp.107-122.
- Dawson, A. G. and Shi, S. (2000) Tsunami deposits, *Pure and Applied Geophysics* 157, pp. 875-897.
- Minoura, K., Imamura, F., Sugawara, D., Kono, Y., Iwashita, T (2001) The 869 Jogan tsunami deposit and recurrence interval of large-scale tsunami on the Pacific coast of northeast Japan, *Journal of Natural Disaster Science* 23, pp. 83-88.
- Morton, R. A., Gelfenbaum, G., Jaffe, B. E., (2007) Physical criteria for distinguishing sandy tsunami and storm deposits using modern examples, *Sedimentary Geology* 200, pp.184-207.
- Wassmer, P., Schneider, J.-L., Fofrège, A.-V., Lavigne, F., Paris, R., Gomez, C.,

(2011) Use of anisotropy of magnetic susceptibility (AMS) in the study of tsunami deposits: Application to the 2004 deposits on the eastern coast of Banda Aceh, North Sumatra, Indonesia, *Marine Geology* 275, pp. 255-272.

# Deep structure of the seismic dangers regions in the Sea of Okhotsk

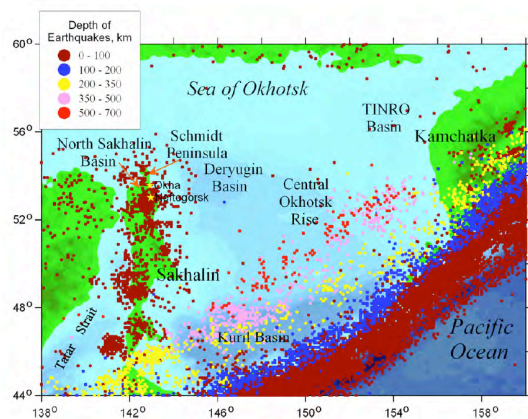
Alexander Rodnikov<sup>a</sup>

<sup>a</sup>Geophysical Center of the Russian Academy of Sciences, Moscow, Russia, rodnikov@wdbc.ru

## 1. Introduction

During the past few years the numerous natural hazards have essentially changed approaches to studying seismic, volcanic and other natural dangers. As a result of this the new strategy and tactics for research of modern geological processes are required. The most dangerous zones all over the world are transition zones between continents and oceans. They are characterized by the tremendous seismic activity, volcanic eruption, tsunami and other catastrophic events. More than thirds of population of globe live in seismically dangerous zones of the Earth. Therefore the study of a deep structure and geodynamic conditions of such regions is necessary to minimize the population loss in case of natural hazards.

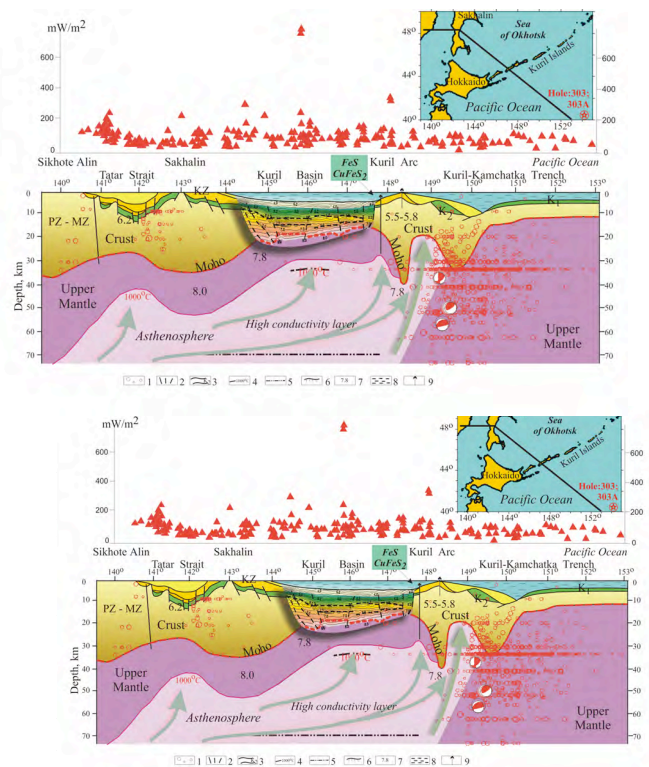
of 700 km. In the west, the Okhotsk Sea plate is bounded by deep faults extending along Sakhalin. There the earthquakes for the major part are localized in the crust. In Kuril Island arc the majority of earthquakes are confined to depth up to 100 – 150 km and seismic activity maximum is at depths of approximately 30 – 40 km. At depths greater than 100 – 150 km seismic activity abruptly decreases and a sharp fracture of focal surface is noted at depths of 200 – 300 km. Sakhalin seismicity is associated with sub-meridian deep faults bounding the Okhotsk Sea plate from Eurasian plate (Rodnikov et al., 2008). Earthquakes distribution along the geotraverse is shown in Fig. 2.



subduction zone.

**Fig. 1.** Spatial distribution of earthquakes in the Okhotsk Sea region illustrating location of shallow and deep hypocenters. Hypocenters are shown on the bathymetry chart. Hypocenter depths are scaled by color

The highest seismic activity is noted along the Kuril island arc. There the Pacific plate was subducted under the continent, forming a seismofocal zone, which is traced to the depth



### 3. Geotraverse of the Okhotsk Sea Region

Deep basins of the Sea of Okhotsk are located over asthenospheric diapirs containing hot mantle fluids. The Tatar rift basin locates in the western part of the geotraverse. Its basement incorporates a thin continental crust (up to 25 km) with the velocity of seismic waves ranging from 5.8 to 7.2 km/s. The asthenospheric layer is up to the level of 50 km. This region is characterized by a high heat flow of 123–132 mW/m<sup>2</sup>. The temperature in the upper zone of the asthenospheric diapir is about 1200°C. In the Tatar rift basin where oil-gas manifestations were found out, three stages of magmatic activity stand out. This clearly demonstrates various depths of magma generation areas. The Eocene-Oligocene basalts (55-24 million years) of initial riftogenesis are assigned to them. The low – middle Miocene stage (23-15 million years) is represented by tholeiites, associated with a stage of the maximum stretching. The formation of hydrocarbon deposits in the sedimentary basin is dated to this time. The magmatic activity comes to the end with the middle Miocene - Pliocene basalts (Filatova, Rodnikov, 2006). The Kuril basin is bounded by deep fault zones. This area incorporates the asthenospheric diapir (up to 20 km high) accompanied by high heat flow of 346–354 mW/m<sup>2</sup>. A high seismic velocity (8 km/s) in the overlying lithospheric mantle drops to anomalously low values (7.0–7.5 km/s) at the asthenospheric roofs with the temperature increasing to 1200°C. In the south-western part of the basin the Moho surface is located at a depth of 11–13 km, the continental crust is absent and the marine marginal crust of the Miocene age is only 7–10 km. In the Kuril basin a magma eruption occurred in the low-middle Miocene (14-11 million years), middle-upper Miocene (9-7 million years) and Pliocene (1.07 and

0.84 million years) times. Basalt eruptions are associated with stages of the extension of the continental crust caused by introduction of the asthenospheric diapir. Over the asthenospheric diapir at tops of submarine volcanoes the sulfide mineralization is revealed (Rodnikov et al., 2008).

### 4. Geodynamic model of the deep structure of the Neftegorsk earthquake region

As an example, we consider deep structure and geodynamic conditions formed in northern Sakhalin after the large Neftegorsk earthquake in 1995 (fig.3). On the basis of complex interpretation of the geological and geophysical data the geodynamic model of deep structure of this area has been constructed (fig.4).

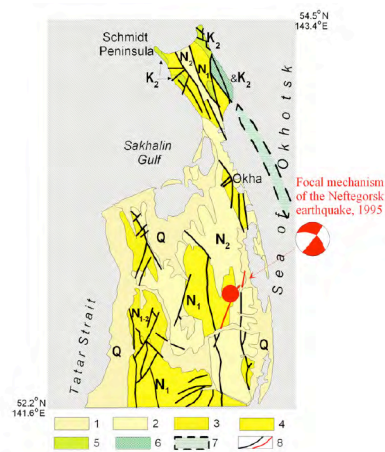


**Fig. 3.** Geological map of North Sakhalin: 1—Quaternary (sand, clay); 2—Pliocene (sedimentary rocks); 3—Neogene (sedimentary rocks); 4—Miocene (sedimentary rocks); 5—Upper Cretaceous (sandstone, claystone); 6—ophiolite complex of the Schmidt Peninsula; 7—ophiolite complex along the eastern coast of Sakhalin Island; 8—faults.

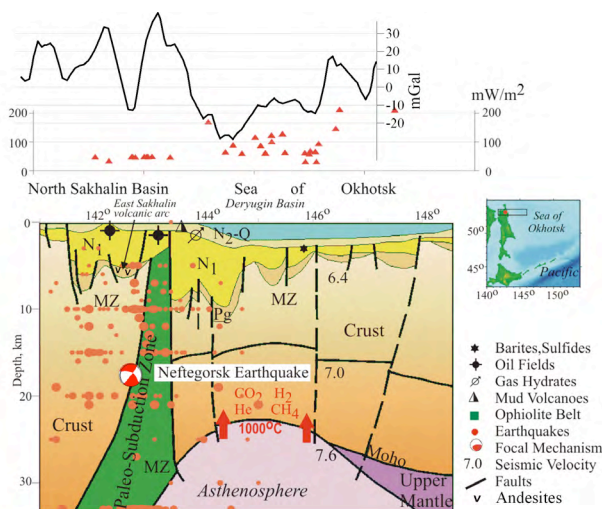


**Fig.4.** Geodynamic model of the deep structure of the Neftegorsk earthquake region with the area scheme (see upper right). The Deryugin Basin was formed on the side of an ancient deep trench after the subduction of the Okhotsk Sea Plate under Sakhalin which had been completed in the Neogene. The basin is located above a hot plume in the mantle that is an asthenosphere diapir of partial melting revealed at a depth of 25 km. The ophiolite belt of ultramafic magmatic rocks is an ancient (Late Cretaceous to Paleogene) paleo-subduction zone separating the Deryugin Basin from the North Sakhalin Basin. The North Sakhalin Basin was formed on the side of the Late Cretaceous–Paleocene back-arc basin.

Sakhalin Island was initially a part of the east coast of the Eurasian Continent. In the Late Cretaceous the Okhotsk Plate was being subducted under Sakhalin. In the Early Miocene the lithospheric plate movements have led to formation of the Tatar Strait rift. In the Late Miocene the subduction of the Okhotsk Plate has come to the end, but tectonic activity proceeded and the frequent earthquakes testified to the continuity of these processes beneath. Sakhalin belongs to the zone with jar intensity of earthquakes up to 9-10 MSK. Most earthquake hypocenters are concentrated in the crust. The Neftegorsk earthquake has occurred with magnitude  $M_s=7.2$  on May 27, 1995 in the North Sakhalin caused victims and destructions. The hypocentre of Neftegorsk earthquake was determined at depth of 18 km (fig.4). The ophiolite complex combined by the ultrabasic

rocks, fixes position of ancient subduction zone acting in Upper Cretaceous- Paleogene. As a result of movement along ancient subduction zone, considerable displacements in the crust along numerous faults and deformation of the earth surface go on. On a surface the subduction zone manifests itself as deep faults running along Sakhalin. The focus of the Neftegorsk earthquake was directly formed by burst of activity of this ancient subduction zone. The position of ancient subduction zone under Sakhalin is a cause of strong earthquakes here. Therefore this region is one of seismic dangerous in Russia (Rodnikov et al.,2010).

## 5. Conclusion

Constructed on the basis of complex interpretation of the geologic-geophysical data the geodynamic models of active continental margins give the chance: (a) to study a deep structure of the Earth under seismic dangerous zones, volcanic areas, mineralization regions and sedimentary basins; (b) to investigate a role of the deep processes in mantle which have an influence on formation of crust units; (c) to present dynamics of development of continental margins; (d) to spend correlation between the geological features, tectonomagmatic, hydrothermal activity and the processes in the upper mantle; (e) to plot detailed maps with allocation of zones of increased risk to prevent active building or other economic activities in such dangerous regions (Rodnikov et al.,2013). **The risk will always be, but it should be estimated and minimized.**

## Acknowledgement

We would like to thank the Russian Foundation for Basic Research for financial support of our research work (Project No: 12-05-00029-a).

## References

- Rodnikov A.G., Sergeyeva N.A., Zabarinskaya. L.P., Filatova N.I., Piip

V.B., Rashidov V.A. (2008). The deep structure of active continental margins of the Far East (Russia) // Russian Journal of Earth Sciences, 10 (4): 1-24.

Rodnikov A.G., Sergeyeva N.A. and Zabarinskaya L.P.(2010) Application of the interdisciplinary database for the construction of the geodynamic models of deep structure of the natural disaster regions (Neftegorsk earthquake, Sakhalin Island). Russian Journal of Earth Sciences. Vol 11, No. 3.

Rodnikov A.G., Sergeyeva N.A., Zabarinskaya L.P.(2013) Ancient subduction zone in the Sakhalin Island // Tectonophysics (in press).

## Repeating earthquake activity along the Izu-Bonin trench

<sup>a</sup>Kota Hibino, <sup>a</sup>Naoki Uchida, <sup>b</sup>Takeshi Matsushima, <sup>a</sup>Toru Matsuzawa

<sup>a</sup>Graduate School of Science Tohoku University; <sup>b</sup>Faculty of Sciences, Kyushu University  
hibino@aob.gp.tohoku.ac.jp

### 1. Introduction

The Mw9.0 Tohoku-oki mega-thrust earthquake on 11 March 2011 caused tremendous damage to eastern Japan. This earthquake is characterized by large slip near the trench and consequent huge tsunami. Before this event, most of the seismologists did not consider that the plate boundary near the trench was locked. Therefore the near-trench large-slip and giant tsunami were beyond their expectations.

We found that few repeating earthquakes (REs) are located in the main slip area for the Tohoku-oki earthquake and slip rate estimated from REs was low (i.e., interplate coupling was high) surrounding the area. This indicates that the locations of asperities can be estimated from RE data to some extent. This research aims to estimate distribution of REs and interplate coupling to help assess the locations of rupture zones of future large earthquakes, especially along the Izu-Bonin trench.

### 2. Data and Method

To find REs, we use the High Sensitivity Seismograph Network (Hi-net) and Japan Meteorological Agency (JMA) permanent seismograph stations from 8 May 2003 to 31 December 2012 and calculate coherences of 40 s waveforms from 2 s before the theoretical P-wave arrival times between all the events located within 100 km. We mainly follow the method of Uchida et al. (2010) where an earthquake pair with coherence of larger than 0.95 at multiple stations is considered to belong to a repeating earthquake group. However, S/N ratios of the waveform data are not so good

because the study region is far from most of the stations. Therefore, we adopt a coherence threshold of 0.8 and even if S/N ratios of the waveform are good at only one station, earthquake pairs that satisfy the threshold in multiple components are considered as candidates of REs in this study.

### 3. Result

Figure 1 shows the distribution of the RE candidates (color circles) estimated in this study. In spite of the non-strict threshold, we find much fewer REs than in NE Japan. Because all REs to the south of 32°N occurred with short recurrence times, these can be burst-type REs or neighboring earthquakes after the Mw7.4 22 December 2010 normal fault event (Figure 2). On the other hand, the groups with magnitudes 2.5-3.9 to the north of 32°N show continuous slip from the recurrence times of around 4 years. The slip rate estimated from the scaling relationship proposed by Nadeau and Johnson (1998) was comparable with background interplate velocity (5-6cm/yr), suggesting weak coupling near the REs. Our result suggests that REs are relatively rare along the Izu-Bonin trench despite the presence of many earthquakes.

### 4. Conclusions

We search for repeating earthquakes along the Izu-Bonin trench using Hi-net and JMA data. Our preliminary results show that the repeating earthquake activity is lower than that east-off Tohoku. This suggests difference in interplate slip mode between these subduction zones.

## Acknowledgement

We used waveforms from Hi-net and JMA stations. We thank all the staff for maintaining long-term valuable data.

## Reference

Uchida, N., T. Matsuzawa, J. Nakajima, and A. Hasegawa (2010), Subduction of a wedge-shaped Philippine Sea plate beneath Kanto, central Japan, estimated from converted waves and small repeating earthquakes, *J. Geophys. Res.*, *115* (B07309), doi: 10.1029/2009JB006962.

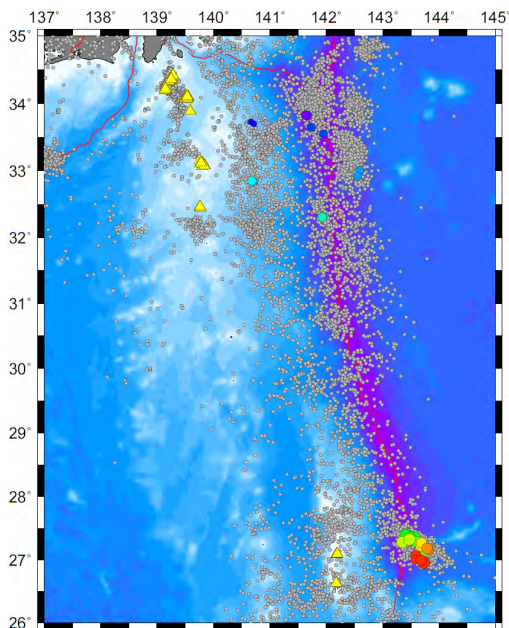


**Fig. 1.** Distribution of repeating earthquakes (colored circles: same color represents same group), background seismicity (gray circles) and stations used in this study (yellow triangles)

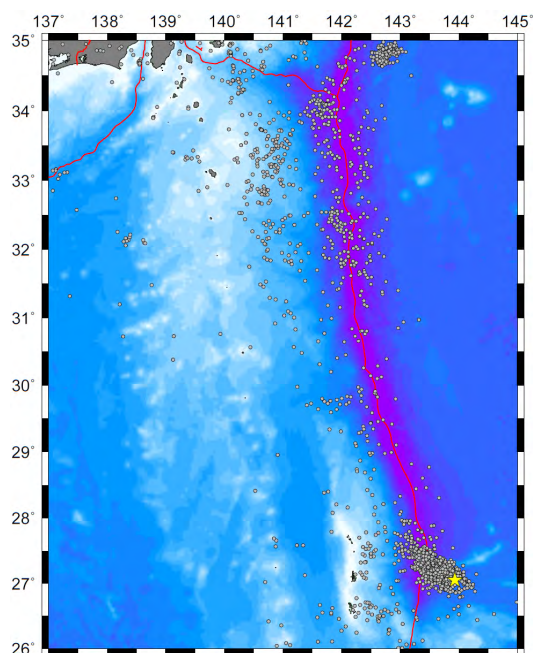
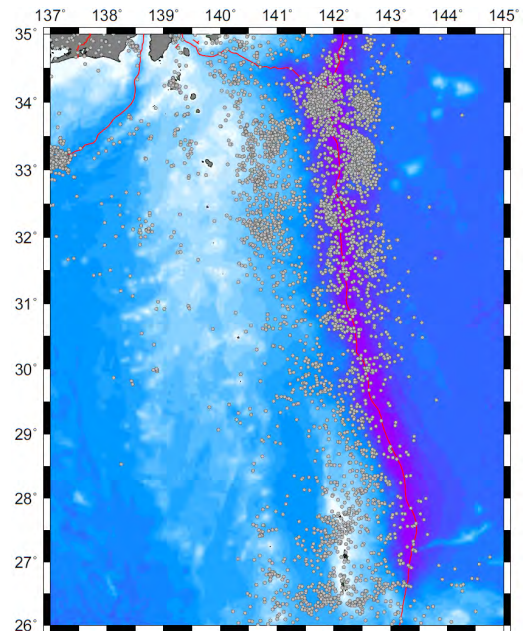


**Fig. 2.** Comparison between background seismicity before (above) and after (below) the Mw7.4 22/12/2010 event (yellow star)

## Japan trench and Nankai trough: New scope of the two contrasting features of subduction zones and geo-hazardous aspect

Yujiro Ogawa<sup>a</sup>, Kiichiro Kawamura<sup>b</sup>, Tomoyuki Sasaki<sup>c</sup>

<sup>a</sup> *Professor Emeritus of The University of Tsukuba, Japan: (Home) 1-1-2-C-740 Yokodai, Tsukubamirai 300-2358, Japan, fyogawa45@yahoo.co.jp*

<sup>b</sup> *Graduate School of Science and Engineering, Yamaguchi University, 1677-1 Yoshida, Yamaguchi 753-8511, Japan, kiichiro@yamaguchi-u.ac.jp*

<sup>c</sup> *Ocean Engineering & Development Co. Ltd., Tokyo, Japan, t\_sasaki@oed.co.jp*

### 1. Subduction zone geohazards

Important aspects are that we must be aware of any possible geo-hazards in subduction zones where not only tectonically active motions but also gravitational effects that might further affects the potential risk for the generation of large tsunamis work. The three trench areas exemplified here are the well-studied deep-seas by integrated studies including submersible dives (Ogawa et al., 2011 (eds.)). The Japan trench and Nankai trough (J & N in Fig. 1) have been thought to be the best examples of

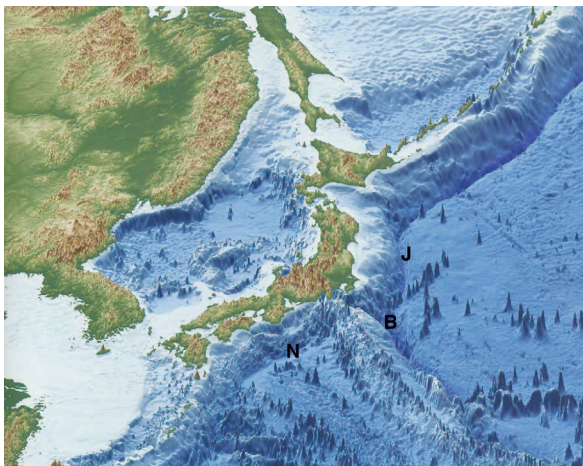


**Fig. 1.** Japan and surroundings topographic map adopted from JAMSTEC leaflet. J, N and B are Japan trench, Nankai trough and Boso triple junction.

subduction erosion type and an accretionary prism type trenches, respectively (von Huene et al., 2004; Taira and Ogawa, 1991). More importantly, they have been thought to be type examples of the Mariana type and Chilean type

margins (without and with a large earthquake), respectively. However, the 2011 Tohoku-oki Earthquake ( $M_w$  9.0) along the Japan trench clearly shows that the previous classification was not for such simple two cases but a new scope is needed for general understanding.

### 2. Japan trench

The Tohoku-oki Earthquake recovered a back slip of 25 m at the hypocentral area (25 km depth) and much longer slip (50 m) at the trench slope toe after 500 to 1000 years absence of the same scale subduction earthquake (Yagi and Fukahata, 2011 and many others). A small, but typical, frontal prism of stacked thrusts was known at the very toe on the trench (Kodaira et al., 2012; Nakamura et al., 2013; Strasser et al., 2013). Although Maeda et al. (2011) have shown that the second peak of the tsunami gauges is due to this trench thrusting 10 min. after the broad peak of the first tsunami pressure, only Kawamura et al. (2012) insisted the strong plausibility of the normal-fault related gravitational slides on the lower slope (particularly in the northern part) are for this tsunami peak by great slip including 10 m uplift. Such large listric normal faults (Tsuru et al., 2002) and resulting submarine sliding during the earthquake occurred as trench slope stretching including accretionary prism-like slide bodies to the graben of the Pacific plate on the trench floor (Fig. 2) (Kawamura et al., 2012; Strasser et al., 2013). Armoured mud balls of Miocene diatomaceous, calcite-cemented mudstone

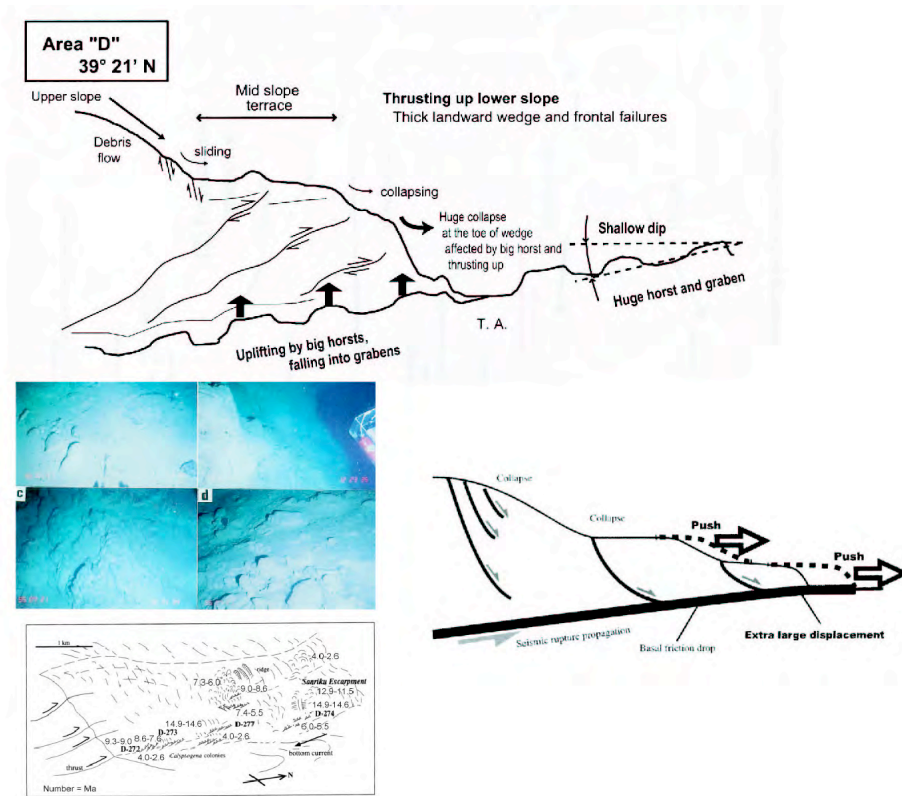


**Fig. 2.** Topographic and structural section of the northern part of the Japan trench (top) (Sasaki, 2004), interpretation for the tsunami generation by large sliding (lower right) (Kawamura et al., 2012), and trench lower slope Miocene rocks (lower left) (Ogawa, 2011).

breccia surrounded by Pliocene mudstone are largely exposed in the erosional trench slope as showing gravitational flow and recycling of the previously accreted materials (Fig. 2) (Ogawa, 2011). The mechanism of this exhumation is considered chiefly by surface gravitational collapse by frontal wasting as graben fill for tectonic (subduction) erosion (von Huene and Lallemand, 1990; Ogawa, 2011). However, more important is such gravitational sliding occurred during earthquake and thrusting (Fig. 2).

### 3. Nankai trough

On the other hand, the Nankai trough is not in all places the Chilean type with active present frontal prism formation but in some areas are without prisms but with abundant submarine sliding by gravitational collapsing showing unstable slope failure (Kawamura et al., 2010). In the Nankai trough's two submarine canyons which expose the total accretionary prism, the

frontal part on the splay fault is composed mostly of Quaternary slumped beds, under which the present prism being as young as only 3 Ma. In particular, in the east of the trough where the present and paleo-Zenisu ridges are being subducted, the previously accreted trench sediments are largely collapsed gravitationally, exposing complicated folds and faults structures on the canyon walls with 3 Ma phyllitic rocks

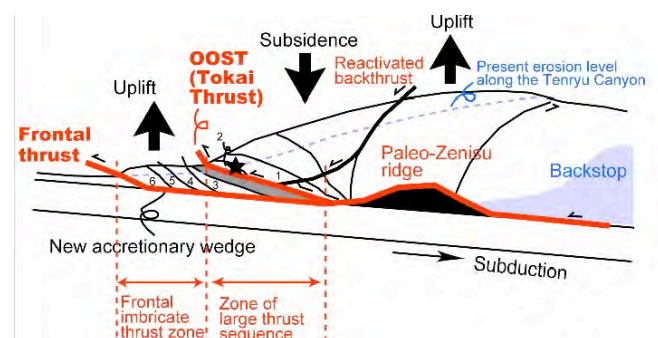


**Fig. 3.** Collapsed accretionary prism in the eastern Nankai trough accretionary prism due to Paleo-Zenisu ridge subduction (adopted from Kawamura et al., 2011)

exhumed from the depths (Star in Fig. 3) (Kawamura et al., 2009; 2011).

#### 4. Boso triple junction area

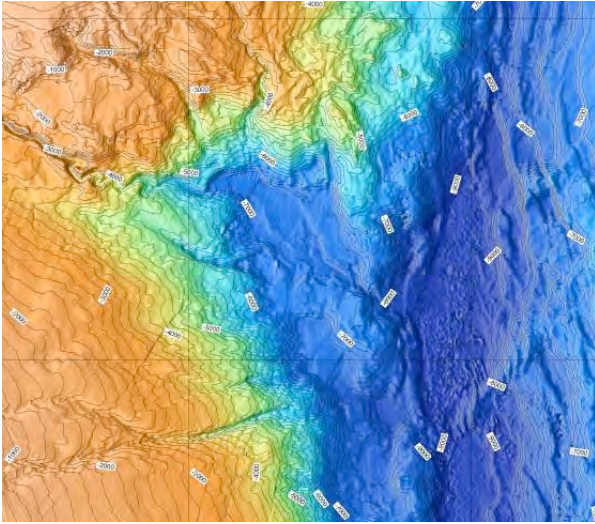


**Fig. 4.** Boso trench triple junction area based on SEABEAM swath mapping by courtesy of Masao Nakanishi after JAMSTEC data. The map is ca 200 km wide. See also profiles of Fig. 5.

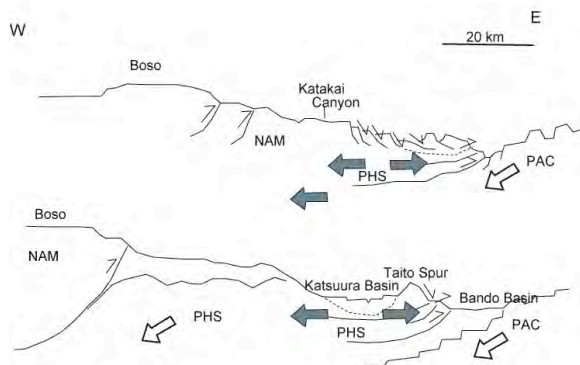


**Fig. 5.** Tectonic interpretation after seismic profiles by Iwabuchi et al. (1990) and our bathymetric chart, suggesting the W-E horizontal stretching in the toe area on the trench triple junction area (Adopted and interpreted after Ogawa and Yanagisawa, 2011).

Additionally, in the Boso triple junction area, where three plates are merging with all subduction boundaries south of Tokyo (B in Fig. 1, Fig. 4), horizontal stretching is dominant in the trench lowermost part, showing a large scale submarine gravitational bodies collapsing to the deepest 7400 m triple junction trench floor (Fig. 4). In this case, too, the lowermost part on the triple junction is of gravitationally very unstable

to collapse the Miocene to Recent prisms to the very toe of the slope to fill the trench (triple junction) floor, probably due to the instability in between the three plate subduction interaction (Ogawa et al., 2008; Ogawa and Yanagisawa, 2011).

#### 5. Large earthquakes, tsunamis and related tectonics in the three trench areas

These three lines of recent researches indicated that the Japan trench, Nankai trough, and Boso triple junction areas must be defined as repeated development of prism formation and collapsing, in the latter case with large-scale gravity sliding of the toe area to the trench floor. The Miocene prism formation might be caused by trench outward proceed with massive sand supply to the trench, and the Quaternary collapse might be caused by volcanic ridge subduction in the Nankai, by large-scale thrusting which triggers a trench toe collapse. In the Japan trench case the large-scale gravitational collapse might be related to the horst-and-graben structure in the subducting plate to cause slope instability as well as trench-toe prism formation, probably during large earthquakes with tsunamis. Boso triple junction case is the same, resulting in both gravitational collapse with horizontal stretching and tsunami generation. Thus the trench wedge is controlled by the total balance in island forearc, topographic and stress regime conditions, and this concept is in accordance with the wedge stability discussion in thrust belts. In all cases gravitational collapse are dominant. In each case, large tsunamis mostly associated with large earthquakes have been known historically since the beginning of the history of Japan from 7<sup>th</sup> century, most particularly in these four hundred years. We need to correlate each case to each phenomenon for the future potentially anticipated hazards to avoid any risks.

## References

- Iwabuchi, Y., Asada, A. and Kato, Y. (1990) Multichannel seismic profiling of the Boso triple junction. *Journal Japan Society of Marine Survey and Technology*, 2, 29–38.
- Kawamura, K., Kanamatsu, T. et al. (2010) Redistribution of Sediments by Submarine Landslides on the Eastern Nankai accretionary Prism. In: D.C. Mosher et al. (eds.), *Submarine mass movements and their consequences*, 313, (*Advances in natural and technological hazards research*, Vol. 28), Springer, 313-322.
- Kawamura, K., Ogawa, Y. et al. (2009) Structural architecture and active deformation of the Nankai Accretionary Prism, Japan: submersible survey results from the Tenryu Submarine Canyon. *GSAB*, 121, 1629-1646; doi: 10.1130/B26219.1.
- Kawamura, K., Ogawa, Y. et al. (2011) Rapid exhumation of subducted sediments due to seamount subduction and out-of-sequence thrust with gravitational collapse in an active eastern Nankai accretionary prism. In: Ogawa, Y., Anma, R. and Dilek, Y. (eds.) *Accretionary prisms and convergent margin tectonics in the Northwest Pacific Basin (Modern approaches in solid earth sciences Vol. 8)*, Springer, (Hereafter refer to Springer Book), 215-227.
- Kawamura, K., Sasaki, T., Kanamatsu, T., Sakaguchi, A. and Ogawa, Y. (2012) Large submarine landslides in the Japan Trench: A new scenario for additional tsunami generation, *GRL*, 39, doi:10.1029/2011GL050661
- Kodaira, S., No, T. et al. (2012) Coseismic fault rupture at the trench axis during the 2011 Tohoku-oki earthquake: *Nature Geoscience*, 5, 646–650, doi:10.1038/ngeo1547.
- Maeda, T., T. Furumura, S. Sakai, and M. Shinohara (2011) Significant tsunami observed at the ocean-bottom pressure gauges at 2011 off the Pacific coast of Tohoku earthquake, *Earth Planets Space*, 63, 803–808, doi:10.5047/eps.2011.06.005.
- Nakamura, Y., Kodaira, S., Miura, S., Regalla, C. and Takahashi, N. (2013) High-resolution seismic imaging in the Japan Trench axis area off Miyagi, northeastern Japan, *GRL*, 40, 1713–1718, doi: 10.1002/grl.50364
- Ogawa, Y. (2011) Erosional subduction zone in the northern Japan trench: Review of submersible dive reports. In: Springer Book, 39-52.
- Ogawa, Y., Anma, R. and Dilek, Y. (eds.) (2011) *Accretionary prisms and convergent margin tectonics in the northwest Pacific basin*, in the series: *Modern approaches in solid earth sciences*, Vol. 8. Springer, 277pp.
- Ogawa, Y., Takami, Y. and Takazawa, S. (2008) Oblique subduction in island arc collision setting: *GSASpecial Paper*, 436, 155-170.
- Ogawa, Y., and Yanagisawa, Y. (2011) Boso TTT-type triple junction: Miocene to Quaternary accretionary prisms and presned-day gravitational collapse. In: Springer Book, 53-73.
- Sasaki, T. (2004) *Subduction tectonics of the northern Japan trench based on the regional seabeam mapping*. PhD Theses, University of Tokyo, 159 pp
- Strasser, M., Kölling, M. et al. (2013) A slump in the trench: Tracking the impact of the 2011 Tohoku-Oki earthquake, *Geology*, 41, 935–938. doi:10.1130/G34477.1
- Taira, A. and Ogawa, Y. (1991) Cretaceous to Holocene forearc evolution in Japan and its implication to crustal dynamics. *Episodes* 14, 205–212
- Tsuru, T., Park, J.-O. et al. (2002) Along-arc structural variation of the plate boundary at the Japan Trench margin: Implication of interplate coupling. *JGR*, 107, B12, 2357, doi:10.1029/2001JB001664.
- von Huene, R. and S. Lallemand (1990) Tectonic erosion along the Japan and Peru convergent margins, *GSAB*, 102, 704–720.
- von Huene, R., Ranero, C.R. and Vannucchi, P. (2004) Generic model of subduction erosion: *Geology*, 32, 913–916, doi:10.1130/G20563.1.
- Yagi, Y. and Fukahata, Y. (2011) Rupture process of the 2011 Tohoku-oki earthquake and absolute elastic strain release. *GRL*, 38, doi: 10.1029/ 2011GL048701.

## Sanriku-oki large slump deposits and feasibility studies for future scientific drilling accounting for submarine landslide mechanism

Sumito Morita<sup>a</sup>, Shusaku Goto<sup>a</sup>, Yuichiro Miyata<sup>b</sup>, Yuki Nakamura<sup>c</sup>, Yu Kitahara<sup>d</sup> and Yasuhiro Yamada<sup>e</sup>

<sup>a</sup>*Institute for Geo-Resources and Environment, Geological Survey of Japan, AIST, 1-1-1 Higashi, Tsukuba, Ibaraki 305-8567, Japan, morita-s@aist.go.jp*

<sup>b</sup>*Graduate school of Science and Engineering, Yamaguchi University, 1677-1, Yoshida, Yamaguchi 753-8511, Japan*

<sup>c</sup>*Atmosphere and Ocean Research Institute, The University of Tokyo, 5-1-5 Kashiwanoha, Kashiwa, Chiba 277-8564, Japan*

<sup>d</sup>*Center for Advanced Marine Core Research, Kochi University, B200, Monobe, Nankoku, Kochi 783-8502, Japan*

<sup>e</sup>*Department of Earth Resources Engineering, Kyoto University, Nishikyo-ku, Kyoto 615-8540, Japan*

### 1. Slump deposits in northern Sanriku-oki Basin

A high-resolution 3D seismic data analysis revealed that there are a great number of large slump deposits buried in the Pliocene and younger formations in the northern Sanrikuoki Basin off Shimokita Peninsula, NE Japan (Morita *et al.*, 2011a; 2011b). In the survey area, the sedimentary basin is composed of well stratified formations parallel to very flat present seafloor, which is a very gentle continental slope of less than one degree in gradient. The slumpings are also thought to have occurred in such almost horizontal slope. Accordingly, the slump deposits have several unique characteristics, such as layer-parallel slip avoiding fatal collapse (Fig. 1). The slump deposits basically indicate block-supported structure containing imbricated thrust sheets of slid ancient surface layers and little matrix of chaotic cover. Dewatering structure strongly dependent on the imbrication forms parallel dikes occurring from the base of the slid layers, i.e. from slip plane. The layers corresponding to the slip plane typically show low-amplitude reflection in the high-resolution seismic data and some of the layers seem to decrease thickness by the dewatering just in the base of the slump sheet (Morita *et al.*, 2011b).

Integrated Ocean Drilling Program (IODP) raised submarine landslide as one of science targets on the new science plan for 2013 and beyond (Integrated Ocean Drilling Program Management International, 2011). We recognize that the group of the large slump deposits in the northern Sanriku-oki basin is an appropriate target to determine submarine landslide mechanism. This idea is supported by the above-mentioned characteristics of the simple layer-parallel slip and ensuing regular re-depositional structure and the traceable slip planes. For that reason, we started various research activities to examine the feasibility of future scientific drilling.

### 2. Research activities for future scientific drilling

For better understanding geologic structure of the sedimentary basin and to extract suitable locations for drill sites, further detailed structural analysis is being performed using 2D and 3D seismic data in the survey area (Nakamura *et al.*, this symposium).

Typical seismic features of the slump deposits and surrounding formations, e.g. dimmed facies and enhanced reflections, imply that slumping in the survey area is related to natural gas in formation fluid. Physical status of

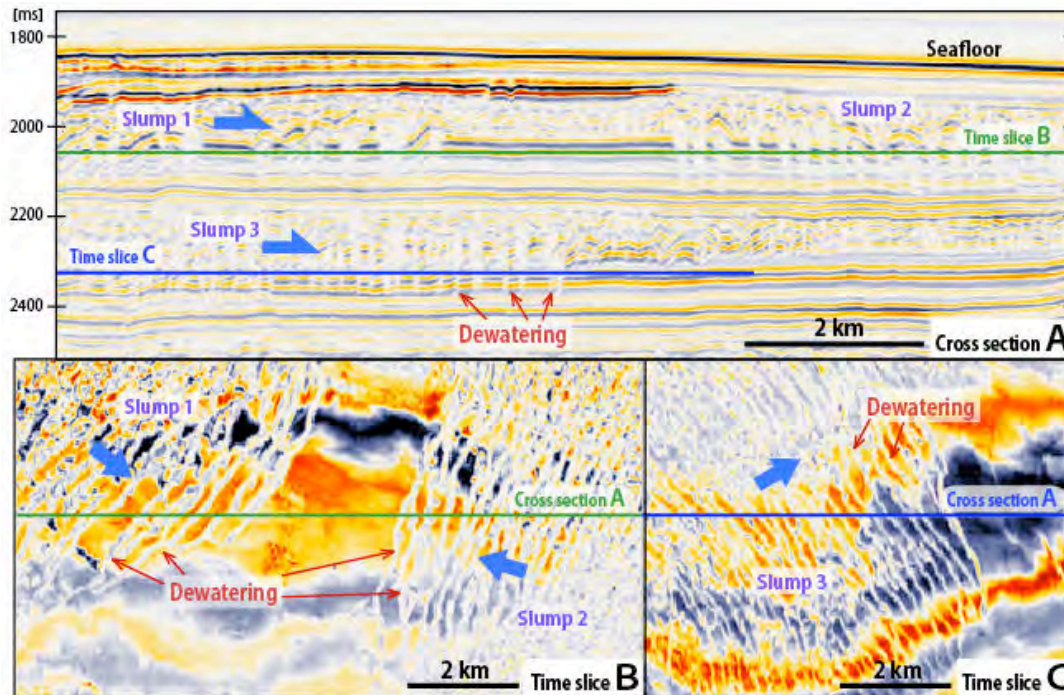


**Fig. 1.** Seismic images of submarine landslide (slump) deposits in northern Sanriku-oki Basin showing relation of slumps and dewatering structures in vertical cross section (A) and time slices (B and C). Modified from Morita and Nakajima (2012).

natural gas is strongly affected by temperature in natural circumstances so that detailed heat flow measurements were performed in the study area in July, 2013. A long-term water temperature monitoring system was precedently deployed on the seafloor in October, 2012. The collected water temperature variation is applied to precise correction of heat flow values.

Vitrinite reflectance analysis and Rock-Eval pyrolysis are being carried out using sediment samples recovered by IODP Expedition 337, which is conducted just in a part of the study area from July through September in 2012. Results of the analyses will be available to determine maturity of organic materials and to model thermal history in the basin.

### 3. Field excursion of slump deposits and dewatering structures

In September, 2012, we held a field excursion in Nichinan Group in Miyazaki Prefecture for the aim to observe typical geologic structures related to slumping and dewatering. The slumping and dewatering in the

outcrops are considered to have occurred in low-angle slope where flute cast remarkably develops. This was a good opportunity to share general ideas with respect to the Sanriku-oki slump deposits among the science community. At a science meeting combined to the excursion, we discussed feasibility of the future scientific drilling.

### Acknowledgements

The seismic analysis, the vitrinite reflectance analysis, the Rock-Eval pyrolysis, and the field excursion and science meeting in Miyazaki were supported by the foundation of “Feasibility studies for future IODP scientific drillings” by JAMSTEC CDEX in 2012-2013. A part of organic materials analyses are supported by the CDEX’s fund for IODP post-expedition researches. The detailed heat flow analysis was funded by 2012 GREEN Grant, AIST. This study uses the 3D seismic data from the METI seismic survey “Sanrikuoki 3D” in 2008.

## References

- Integrated Ocean Drilling Program Management International (2011) Illuminating Earth's Past, Present, and Future: Science Plan for 2013-2023, 84p.  
[http://www.iodp.org/doc\\_download/3160-highnsp](http://www.iodp.org/doc_download/3160-highnsp).
- Morita, S., and Nakajima, T. (2012) Fluid circulation from submarine landslides in a high methane flux sedimentary basin. Ten Big News Items 2011, Institute for Geo-Resources and Environment, AIST, p7.  
<http://unit.aist.go.jp/georesenv/english/result-e/ten-big-news/2011/2011-7-8.pdf>.
- Morita, S., Nakajima, T., and Hanamura, Y. (2011a) Submarine slump sediments and related dewatering structures: observations of 3D seismic data obtained for the continental slope off Shimokita Peninsula, NE Japan. *Journal of Geological Society of Japan*, 117, 95-98. (in Japanese)
- Morita, S., Nakajima, T., and Hanamura, Y. (2011b) Possible ground instability factor implied by slumping and dewatering structures in high-methane-flux continental slope. *Submarine Mass Movements and Their Consequences, Advances in Natural and Technological Hazards Research*, 31, 311-320.
- Nakamura, Y., Morita, S., and Ashi, J. (this symposium) Structural characteristics of large-scale submarine landslides on a very gentle continental slope from 3D seismic data off Shimokita Peninsula, Northeast Japan.

## Structural characteristics of large-scale submarine landslides on a very gentle continental slope from 3D seismic data off Shimokita Peninsula, Northeast Japan.

Yuki Nakamura<sup>a, b</sup>, Sumito Morita<sup>b</sup>, Juichiro Ashi<sup>a</sup>

<sup>a</sup>*Atmosphere and Ocean Research Institute, The University of Tokyo, 5-1-5 Kashiwanoha, Kashiwa, Chiba 277-8564, Japan, yukinaka@aori.u-tokyo.ac.jp*

<sup>b</sup>*Institute for Geo-Resources and Environment, Geological Survey of Japan, AIST, 1-1-1 Higashi, Tsukuba, Ibaraki 305-8567, Japan, morita-s@aist.go.jp*

### 1. Introduction

Submarine landslides have been observed even on very low-angle slope well below the angle of repose, and are often greater in size and in migration distance than landslides on land. It is known that submarine landslides sometimes cut submarine communication cables or pipelines, and generates tsunamis, however, surveys focusing on submarine landslides are still limited and the whole picture and their mechanism have not been understood very much. Hence, submarine landslide can be recognized as one of the most important geo-hazard issues. Integrated Ocean Drilling Program (IODP) also raised submarine landslide as one of the themes on geo-hazard category for the next phase from 2013 through 2023 (Integrated Ocean Drilling Program Management International, 2011).

### 2. Slump Deposits off Shimokita Peninsula

A number of large-scale submarine landslide (slump) deposits were identified in Pliocene and upper formations off Shimokita Peninsula by analyzing METI Fundamental seismic survey 2008, “Sanrikuoki 3D” (Morita et al., 2011a; 2011b). The slump deposits generally indicate layer-parallel slip on a very gentle and flat continental slope, and often exhibits imbrication structure formed by repeated thrusting of slide sedimentary sheets. The slump deposits have accompanying dewatering structure which occurs in the slip planes and cuts the imbrication vertically. The distribution of dewatering structure is strongly dependent on the

imbrication so that the structure is identified as parallel dikes on time-slice images. Our research aims to understand modes of submarine landslide occurrence that form in such low-angle continental slope.

### 3. Strategies in Structural Analysis

Using 3D seismic data in the survey area, we have investigated detailed distribution and geometry of the slump deposits with criteria determining slip plane, seabed before sliding, top of slump deposit (Fig. 1), and slip direction. Slip plane corresponds to the bottom of slid sedimentary layers and to a specific horizon of layer-parallel slip. Seabed before sliding is identified as a horizon overlaid by slump deposits at the distal portion of the slumping. The vertical domain between the layer corresponding to slip plane and the seabed before sliding indicates original thickness of slid sedimentary bed. Top of slump deposits is recognized at a boundary covered by normal stratified layers. Slip direction is determined by imbrication and related parallel dike structure which are both basically perpendicular to the slip direction.

### 3. Consequences and Considerations

Being based on the criteria, we identified slump-dominant horizons and structural characteristics of each slump deposits. The slump-dominant horizons are interbedded among normal formations in the Pliocene and Quaternary sequences, and indicate there were

some ages in which slumping repeatedly occurred. Each slump deposits is basically composed of the above-mentioned imbrication of thrust sheets and some chaotic cover sequence. The coherent portion composed of the imbricated thrust sheets are typically dominant in volume rather than the chaotic portion probably because the slumpings avoided fatal collapse of original sedimentary structure. Characteristics of the internal structure of the slump deposits are considered to be associated with the slumping system occurring on such very gentle and flat continental slope.

As mentioned before, parallel dikes of dewatering structure is dependent on the imbrication structure so that some parallel dikes show concentric distribution following shapes of slump deposits which form lingulate or fan-shaped spread feature.

For further determination of slumping system and deformation patterns, we are carrying on further analysis of the 3D seismic data in order to outline morphology, reveal precise internal structure, and estimate volume of the slump deposits. Since the slump-dominant horizons are keys to discuss periodicity of the slumping events, chronological analysis using

sedimentary cores by scientific drilling will be necessary for the future science.

## References

- Integrated Ocean Drilling Program Management International (2011) Illuminating Earth's Past, Present, and Future: Science Plan for 2013-2023, 84p.  
[http://www.iodp.org/doc\\_download/3160-highnsp](http://www.iodp.org/doc_download/3160-highnsp).
- Morita, S., Nakajima, T., and Hanamura, Y. (2011a) Submarine slump sediments and related dewatering structures: observations of 3D seismic data obtained for the continental slope off Shimokita Peninsula, NE Japan. *Journal of Geological Society of Japan*, 117, 95-98. (in Japanese)
- Morita, S., Nakajima, T., and Hanamura, Y. (2011b) Possible ground instability factor implied by slumping and dewatering structures in high-methane-flux continental slope. *Submarine Mass Movements and Their Consequences, Advances in Natural and Technological Hazards Research*, 31, 311-320.

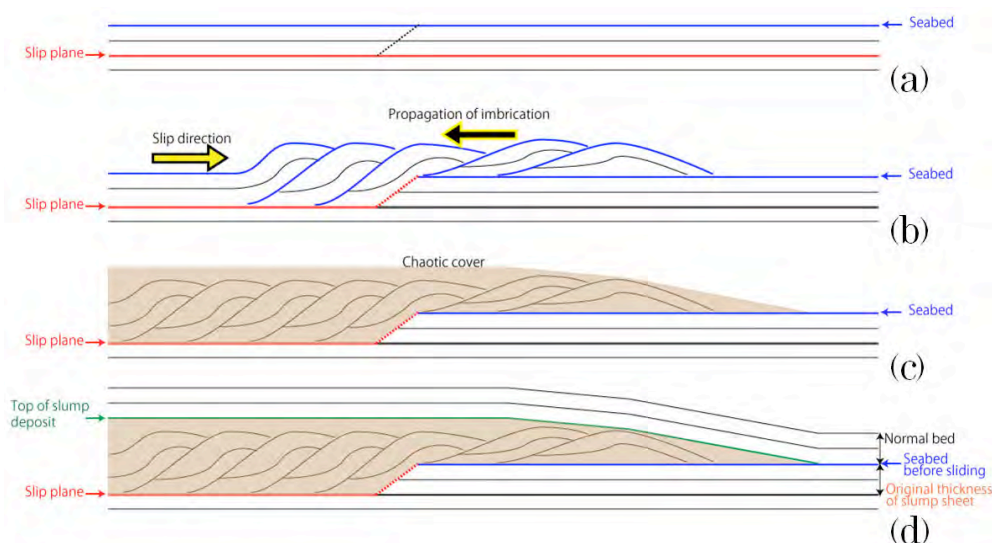


**Fig. 1.** Major formation pattern of slump deposits off Shimokita Peninsula.

- (a) Normal beds before slumping.
- (b) Syn-slumping deformation. Formation of imbrication structure and overlying seabed.
- (c) Syn-slumping deformation. Covering of chaotic sediments over the imbrication structure.
- (d) Covering by normal stratified formation.

## The estimation of the low-velocity subducting crust of the Pacific slab beneath Hokkaido, northern Japan

Takahiro Shiina<sup>a</sup>, Junichi Nakajima<sup>a</sup>, Genti Toyokuni<sup>a</sup>, and Toru Matsuzawa<sup>a</sup>

<sup>a</sup>*Research Center for Prediction of Earthquakes and Volcanic eruptions, Grad. Sch. of Science, Tohoku Univ., Sendai, Miyagi, Japan, shina@aob.gp.tohoku.ac.jp*

### 1. Introduction

Seismological studies have revealed the existence of a low-velocity layer which associated with the oceanic crust at the uppermost part of a subducting plate (e.g., Ferris et al., 2003). Released aqueous fluid from hydrous minerals which carried down with the subducting crust is considered to facilitate seismic activity in the subducting plate (e.g., Kirby et al., 1996). Therefore, distribution of fluids in the subducting crust is important to understand genesis of the intraslab earthquakes.

On the other hand, the seismic structure in the subducting plate is considered that closely linked to seismic wave propagation and seismic intensity pattern from deep-focus and intermediate-depth earthquakes. For example, these effects are shown as abnormal seismic intensity pattern of earthquakes in the Pacific slab beneath the Japan Sea, which larger seismic wave amplitude is observed at along the Pacific coast than other region (e.g., Ishikawa, 1993). Moreover, it is known that the low-velocity layer generates trapped and multi-reflected waves. These waves travel long distance by guided along the low-velocity layer (e.g., Martin et al., 2003). Therefore, it is considered that the low-velocity subducting crust contributes to travel of seismic strong motion from intraslab earthquakes. As the one the goal of this study, we try to reveal that relations between the seismic structure and wave propagation of intraslab earthquakes in the Pacific slab.

### 2. Observations and Method

Later phase, such as mode-converted waves and guided waves, are often observed from intraslab earthquakes (e.g., Hori et al., 1985). Some later phases are generated which associated with the top of the Pacific slab and the low-velocity subducting crust, and these later phases are much more sensitive to seismic velocity in the subducting crust because these later phases propagate along the crust (e.g., Matsuzawa et al., 1986). A P-to-S converted wave which conversion occurred at the top of the Pacific slab is one of the later phases (Matsuzawa et al., 1986), and Shiina et al. (2013) estimated the detailed P-wave velocity structure in the subducting crust of the slab beneath northeast Japan by using travel time of the PS-converted waves.

The PS-converted wave from intraslab earthquakes in the Pacific slab is also observed at Hokkaido, northern Japan. In addition, we found other later phase (X phase) that the arrival 2-3 sec after the P-wave arrival (Fig. 1). X phase has large amplitude in vertical components and is observed at the southern part of Hokkaido from earthquakes which are located near the upper surface of the Pacific slab.

In this study, in order to identified the origin of X phase, we simulated wave propagation of intraslab earthquakes by applied a 2-D finite difference modeling (e.g., Virieux, 1986). In addition, we picked travel times of PS-converted waves and X phases. Then, we investigated the velocity structure in the subducting crust of the Pacific slab beneath Hokkaido.

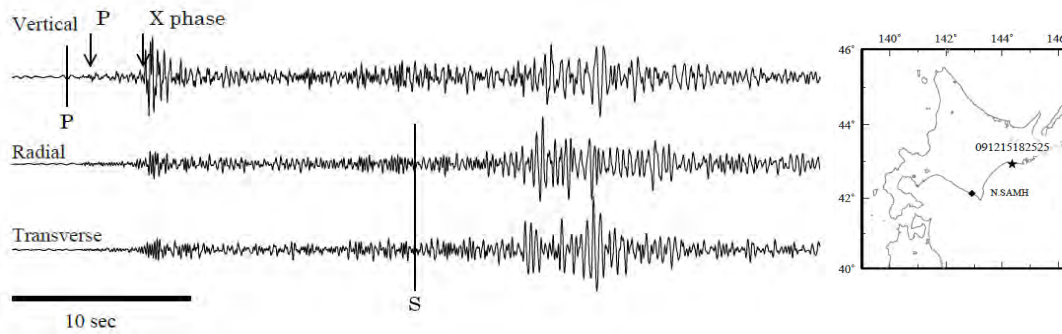


**Fig. 1** Example seismograms of X phase from intraslab earthquakes which occurred at upper part of the double-seismic zone. Hypocenter (★) and station (◆) are shown in the inset map. Arrows denote arrival times of P wave and X phase. Theoretical travel times of P and S waves are calculated using the JMA2001 1-D velocity model and plotted as vertical solid lines.

### 3. Result and Discussion

From result of the numerical modeling, we inferred X phase as a guided wave in the low-velocity subducting crust. Also, the observed travel times of PS-converted waves and guided waves are explained by assumed the P-wave velocities in the subducting crust of 10-15% lower than those of the surrounding mantle. This obtained P-wave velocity in the subducting crust consistent with a P-wave velocity estimated by Shiina et al. (2013) at Tohoku region, northeast Japan.

The observation of guided waves in the subducting crust indicates that the low-velocity subducting crust is in contact with the continental lower crust beneath the region where the guided wave is observed (e.g., Miyoshi et al., 2012). Therefore, our observations confirm the presence of continental crustal materials above the Pacific slab at depths of 60-80 km beneath the southern part of Hokkaido, as estimated in Kita et al. (2010).

### References

- Ferris, A., G. A. Abers, D. H. Christensen, and E. Veenstra (2003), High resolution image of the subducted Pacific (?) plate beneath central Alaska, 50-150 km depth, *Earth Planet. Sci. Lett.*, 214, 575–588.
- Hori, S., H. Inoue, Y. Fukao, and M. Ukawa (1985), Seismic detection of the untransformed “basaltic” oceanic crust subducting into the mantle, *Geophys. J. R. astr. Soc.*, 83, 169–197.
- Ishikawa, T. (1933), The abnormal distribution of seismic intensities, 2 (in Japanese), *Q. J. Seismol.*, 7, 37–70.
- Kirby, S., E. R. Engdahl, and R. Denlinger (1996), Intermediate-depth intraslab earthquakes and arc volcanism as physical expressions of crustal and uppermost mantle metamorphism in subducting slabs, *Geophysical Monograph*, 96, 195–214.
- Kita, S., Okada, T., Hasegawa, A., Nakajima, J. and Matsuzawa, T. (2010), Anomalous deepening of a seismic belt in the upper-plane of the double seismic zone in the Pacific slab beneath the Hokkaido corner: possible evidence for thermal shielding caused by subducted forearc crust materials, *Earth Planet. Sci. Lett.*, 290, 415–426.
- Martin, S., and A. Rietbrock (2006), Guided waves at subduction zones: Dependencies on slab geometry receiver locations and earthquake sources, *Geophys. J. Int.*, 167, 693–704.
- Matsuzawa, T., T. Kono, A. Hasegawa, and A. Takagi (1990), Subducting plate boundary beneath the northeastern Japan arc estimated from SP converted waves, *Tectonophysics*, 181, 123–133.
- Miyoshi, T., Saito, T., & Shiomi, K. (2012), Waveguide effects within the Philippine Sea slab beneath southwest Japan inferred from guided SP converted waves. *Geophys. J. Int.*, 189(2), 1075-1084.
- Shiina, T., J. Nakajima, and T. Matsuzawa (2013), Seismic evidence for high pore pressures in the oceanic crust: Implications for fluid-related embrittlement, *Geophys. Res. Lett.*, 40, 2006–2010.
- Virieux, J. (1986), P-SV-wave propagation in heterogeneous media: velocity stress finite difference method, *Geophysics*, 51, 889–901.

**A study of earthquake location by artificial explosive data**

Chien-Hsin Chang<sup>a</sup>, Peih-Lin Leu<sup>a</sup> and Tzay-Chyn Shin<sup>a</sup>

<sup>a</sup>Department of Seismological Center, Central Weather Bureau, No.64 Gongyuan Rd., Taipei 10048, Taiwan, gensin@scman.cwb.gov.tw

A good quality of earthquake location is very important factor to all of the earthquake studies. From February to March, 2008, ten explosions were taken by the Taiwan Integrated Geodynamics Research (TAIGER) project at north and south on land in Taiwan. The explosions signals were recorded by the Central Weather Bureau Seismic Network (CWBSN), the Broadband Array in Taiwan for Seismology (BATS) and the Seismic Network for TAIGER. It offers a good opportunity to study the location accuracy of the CWBSN. We relocated this event using the layered model that routinely used in the CWBSN and a recently 3-D model by Wu et al. (2007). Our results show that the event locations determined by layered and 3-D model were caused 4.0 and 2.0 km from the true location, respectively. Base on this result, we suggest that the CWBSN location may have about 4.0 km error in routinely operation. The location error may shorten to 2.0 km by using 3-D model. Those are good reference values for the Taiwan earthquake studies using the CWBSN catalog.

**References**

Wu, Y. M., C. H. Chang, L. Zhao, J. B. H. Shyu, Y. G. Chen, K. Sieh, and J. P. Avouac, (2007) Seismic tomography of Taiwan: Improved constraints from a dense network of strong motion stations, *J. Geophys. Res.*, 112, B08312.

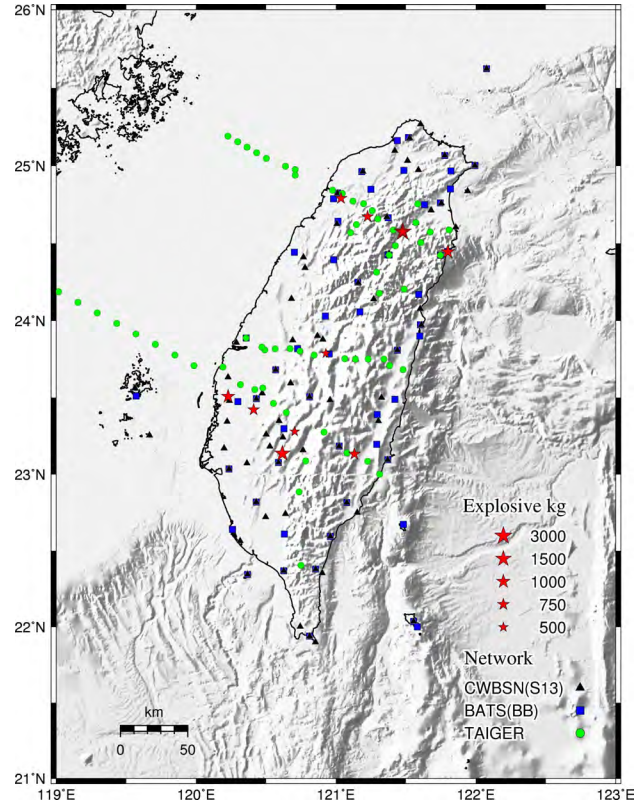


**Fig. 1.** The stations and explosions distributions used in this study.

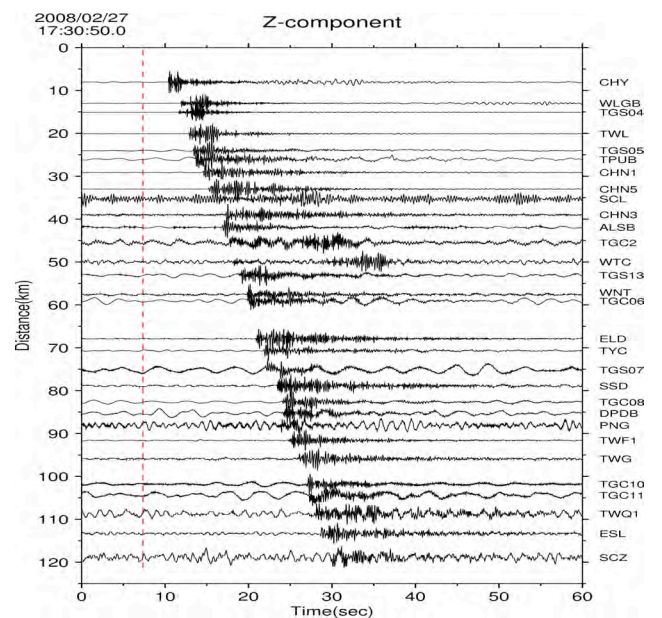


**Fig. 2.** An example of seismic wave that generated by explosions.

## **Cooperative hydrological and geochemical research for earthquake forecasting in Taiwan between Disas.Prev.Res.Center, NCKU, Taiwan and Geological Survey of Japan, AIST.**

Naoji Koizumi<sup>a</sup>, Norio Matsumoto<sup>a</sup>, Wen-Chi Lai<sup>b</sup>, Mamoru Nakamura<sup>c</sup>

<sup>a</sup>*AIST, Geological Survey of Japan, AFERC, 1-1-1 Higashi, Tsukuba, Ibaraki 305-8567, Japan, koizumi-n@aist.go.jp*

<sup>b</sup>*Disaster Prevention Research Center, National Cheng Kung University, Taiwan*

<sup>c</sup>*Faculty of Science, University of the Ryukyus*

### **1. Introduction**

The 1999 Chi-chi earthquake (Mw7.6), which occurred on September 21, 1999, caused severe damage in Taiwan. Then Taiwan started the project of earthquakes and active-fault research (PEAR) from 2001. As part of this project, Disaster Prevention Research Center (DPRC), National Cheng-Kung University (NCKU) started hydrological and geochemical research for earthquake forecasting in Taiwan with support of Water Resources Agency, Ministry of Economic, Taiwan.

Geological Survey of Japan (GSJ), AIST, made technical supports to DPRC before the above research started because GSJ has been continued hydrological and geochemical research for earthquake prediction since the late 1970's. Since 2002 GSJ has been carrying out the cooperative research entitled "Hydrological and geochemical research for earthquake prediction in Taiwan" with DPRC. We hold the workshop for promoting the research every year.

### **2. Results**

#### **2.1 First Stage (2001-2005)**

We prepared 16 observation wells for monitoring earthquake-related groundwater changes. We constructed 4 wells and chose 12 wells of the 500 wells of WRA which were originally made for managing groundwater resources. The system of monitoring the data of the 16 wells was designed in consideration of the system of GSJ. We also analyzed coseismic and postseismic groundwater level changes related to the 1999 Chi-chi earthquake.

In a typical fan area near the epicenter, the

groundwater levels coseismically rose. In the slope area near the earthquake fault, the groundwater levels coseismically dropped. We concluded that those changes were caused not by coseismic volumetric strain changes but by ground shaking (Koizumi et al., 2004, Lai et al, 2004).

#### **2.2 Second Stage (2006-2009)**

We analyzed the long-term groundwater level changes or recoveries after the 1999 Chi-chi earthquake. It took several years or longer to recover the groundwater level drops in the slope area. On the other hand, it took only 3 months or shorter to recover the groundwater level rises in the fan area. We also evaluated the data of the observation wells prepared in the first stage (Lai et al., 2010). The number of the observation wells decreased from 16 to 10 in the second stage.

#### **2.3 Third Stage (2010-2012)**

We analyzed precursory groundwater level changes at one of the observation wells in Hualien in the northeastern part of Taiwan and carried out the detailed analysis of coseismic groundwater level changes and seismic ground motion in the case of the 1999 Chi-chi earthquake.

Usually the groundwater level at the Hualien well, which is close to the seashore, shows clear tidal changes responding to the sea level near the well. But the response often changes several hours before the local earthquakes whose

magnitudes are around 4-5. There is a fault between the well and the seashore. The precursory hydrologic parameter change around the fault before the local earthquake is a possible reason of the precursory abnormal response.

The number of the observation wells decreased from 10 to 7 in the third period.

#### **2.4 Fourth Stage (2013-2016)**

The fourth stage has already started. As part of the Taiwan Geophysical Network for Seismology (TGNS) managed by the Central Weather Bureau (CWB), Taiwan, we continue groundwater observations at the 7 wells. The purpose of TGNS is an early warning of seismic disaster prevention in Taiwan including earthquake prediction. TGNS also has 150 GPS stations, 11 magnetism stations and 9 borehole strain stations. Through these integrated observations, we will try to promote our research.

### **3. Summary**

GSJ, AIST and DPRC, NCKU have been carrying out the cooperative research entitled "Hydrological and geochemical research for earthquake prediction in Taiwan" since 2001 (Officially 2002). We clarified the mechanism of groundwater changes and their recoveries related to the 1999 Chichi earthquake and prepared a groundwater observation network in Taiwan. Taiwan and Japan are under the same seismo-tectonics and have similar earthquake risks. So our cooperation will enable us to make rapid progress in the research. This cooperation will also give important information for evaluation of long-term groundwater changes in tectonically active areas like Japan and Taiwan.

### **References**

Koizumi, N, W.-C. Lai, Y. Kitagawa and N.Matsumoto (2004) Comments on " Coseismic hydrological changes associated with dislocation of the September 21, 1999 Chichi earthquake, Taiwan" by Min Lee, Tsung-Kwei Liu,

Kuo-Fong Ma and Yen-Ming Chang, *Geophys.Res.Lett.*, 31, L13603, doi:10.1029/2004GL019897.

Lai, W.-C., Koizumi, N, N.Matsumoto, Y. Kitagawa, C.-W. Lin, C.-L. Shieh and Y.-P. Lee (2004) The effect of the seismic ground motion and geological setting on the coseismic groundwater level changes caused by the 1999 Chi-Chi Earthquake, Taiwan, *Earth Planets Space*, 56, 873-880.

Lai, W.C., K.C. Hsu, C.L.Shieh, Y.P.Lee, K.C.Chung,N.Koizumi and N.Matsumoto (2010) Evaluation of the effects of ground shaking and static volumetric strain change on earthquake-related groundwater level changes in Taiwan, *Earth Planets Space* , 62, 391-400.

## Experimental analysis on Rowe's stress-dilatancy relation and frictional instability of fault gouges

Momoko Hirata<sup>a</sup>, Jun Muto<sup>a</sup>, Hiroyuki Nagahama<sup>a</sup>, Kenshiro Otsuki<sup>a</sup>

<sup>a</sup>Dept. Earth Science, Tohoku University, 6-3 Aoba, Aramaki-aza, Aoba, Sendai, Miyagi, 980-8578, Japan, HIRATA: m.ume1234@gmail.com

### 1. Introduction

The principle of minimum energy ratio was introduced by Rowe (1962) to obtain a stress-dilatancy relation for granular materials under axisymmetric stress condition. Rowe (1962) postulated that the ratio of energy dissipation in internal friction to energy supply in the direction of the major principal stress in a constant minimum value. The Rowe's theory can be applied not only to granular materials such as fault gouges but also to blocky materials such as rocks. Chappell (1979) proposed a relationship between the principle stresses in terms of the joint friction angle, whose magnitude is not only dependent on the smooth joint friction angle and roughness but also on the rotation of the blocks brought about by slip.

Detailed experimental measurements of frictional properties of gouges at pressures appropriate to seismogenic conditions are sparse (Marone, 1991). So, Rowe's theory has not been proved to be applicable in general, except in the dense state of particulate materials tested at low stress level (Ramamurthy, 2001). Hence, it has not been utilized much for fault mechanics until now. Moreover, some of the failure strength criteria, which are commonly adopted for soils and rocks, are often found not to hold for a wide range of confining pressures (Ramamurthy, 2001). However, the stress-dilatancy relation of fault gouge correlates with the onset of frictional instability. Therefore, dilatancy is related to earthquakes, so to clarify the stress-dilatancy relationship is very important from the point

of disaster prevention. Here, in order to test whether Rowe's hypothesis of constant energy ratio holds for frictional instability of simulated fault gouge, we conducted the friction experiments using the gouge in a gas-medium apparatus.

### 2. The friction experiments with a gas-medium apparatus

The friction experiments using simulated fault gouge were conducted in a gas-medium apparatus under the confining pressure ( $P_c$ ) of 140-180 MPa (Fig. 1). Strain rate was held constant at  $10^{-3}$  /s. Dry quartz powders (0.1 or 0.2 g) for gouge were sandwiched into two gabbroic forcing blocks (20 mm in diameter, 40 mm in length, and cut by a  $50^\circ$  to their cylindrical axis). To clarify mechanical behaviors of fault gouge, we held loads at different levels as shown in Fig. 2 (1st holding at axial stress of about 190 MPa, 2nd at 450 MPa, 3rd at 640 MPa, 4th at 800 MPa). Three strain gauges were glued onto a

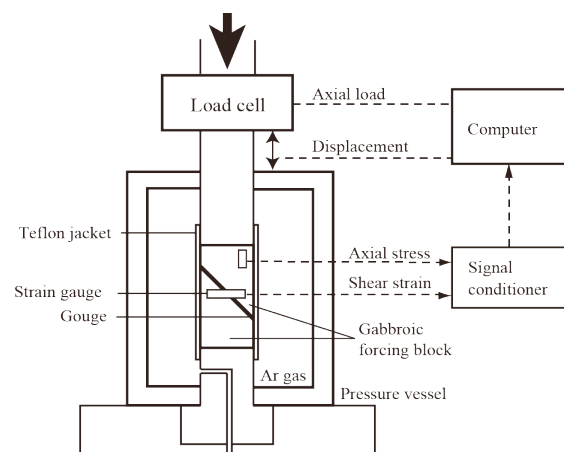


**Fig. 1** Schematic drawing of sample assembly and experimental setup.

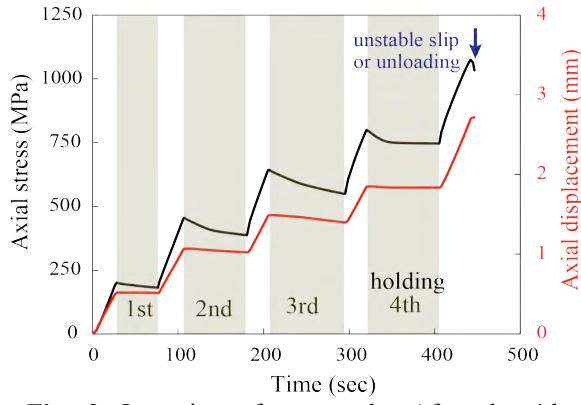


**Fig. 2** Operation of one cycle. After the 4th holding, the sample was loaded again until unstable slip happened or strain gauges could not measure strains. If the latter happened, we unloaded and replaced to new strain gauges. Arrow means the end of one cycle. The gray shaded areas indicate the time ranges of holdings.

gouge layer through the Teflon jacket. Sampling rate was 2 MHz. When strains exceeded the measurable ranges by gouges, we replaced them to new gauges. This succession of work, called cycle, was repeated until unstable slips happened.

### 3. Results

We conducted 12 friction experiments at different confining pressures  $P_c$  and different weights of gouges (Table1).

The representative stress-strain curves and the mechanical behaviors of gouges during holding stages are shown in Fig. 3. The positive value of strain means extension. Under lower stress, gouges behaved elastically. Under higher stress, they behaved plastically. After repeated cycles, unstable slip happened at higher stress.

During holding stages, we also obtained the ratio of energy rate of the major principal compressional stresses to minor compression stresses, or the ratio of input energy rate to

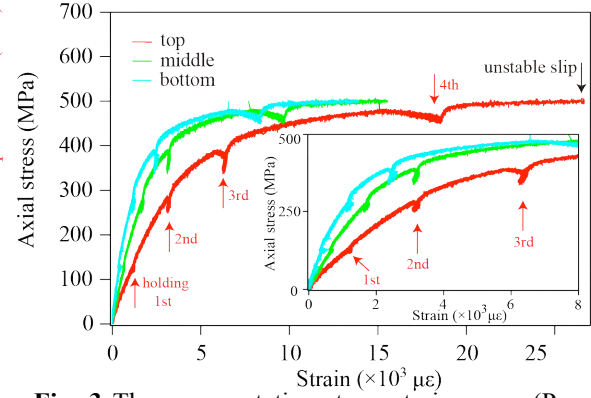


**Fig. 3** The representative stress-strain curve ( $P_c$ : 140 MPa, gouges: 0.1 g, cycle 4). Top, middle and bottom mean position of strain gauges. Black arrow indicates unstable slip.

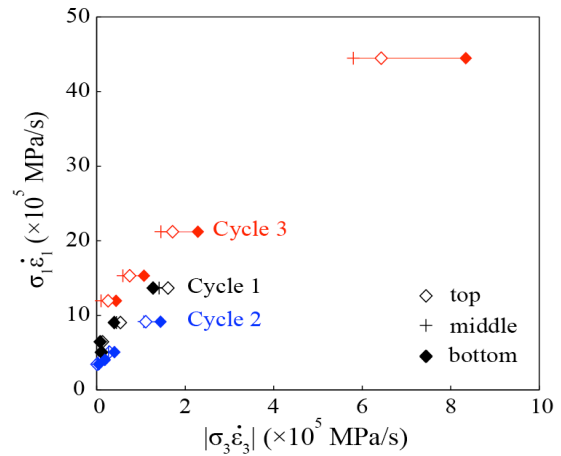


**Fig. 4** The ratio of energy rate of the major principal compression stresses to minor compression stresses under a confining pressure of 180 MPa and gouge of 0.2 g. Top, middle and bottom mean position of strain gauges.

output one. Under each confining pressure, the ratio of energy rates showed a constant value in lower energy rates. On the other hand, it deviated from the constant value in higher energy rates (Fig. 4). Therefore, the energy rates in both directions show a linear relation, which almost passed through the origin. This relation is expressed by

**Table1** Experimental parameters

$P_c$ (MPa)	Weight (g)	Cycle
140	0.1	4
160	0.1	3
180	0.1	2
180	0.2	3

$$\sigma_1 \dot{\epsilon}_1 = K \sigma_3 \dot{\epsilon}_3, \quad (1)$$

where  $K$  is the ratio of energy rates,  $\sigma_1$  and  $\sigma_3$  are the major and minor compression stresses, and  $\dot{\epsilon}_1$  and  $\dot{\epsilon}_3$  are strain rates of each

directions, respectively. Eq. (1) can be rewritten by

$$\frac{\sigma_1}{\sigma_3} = K \frac{\dot{\epsilon}_3}{\dot{\epsilon}_1} \quad (2)$$

#### 4. Discussions

In the triaxial compression state, the Rowe's theory has been written by,

$$\frac{\sigma_1}{\sigma_3} = \left(1 - \frac{\dot{\epsilon}_v}{\dot{\epsilon}_1}\right) \tan^2\left(\frac{\pi}{4} + \frac{\varphi}{2}\right), \quad (3)$$

where  $\dot{\epsilon}_v$  is the volumetric strain rate and  $\varphi$  is the internal friction angle (Niiseki, 2001). Eq. (3) indicates that the volumetric strain rate is related to the stress, so it is called the stress- dilatancy relation which can be derived from the critical state (Scheffeld and Wroth, 1968) or the variational principle of granular mechanics (Niiseki, 2001). Based on the relation:  $\dot{\epsilon}_v = \dot{\epsilon}_1 + \dot{\epsilon}_2 + \dot{\epsilon}_3 = \dot{\epsilon}_1 + 2\dot{\epsilon}_3$ , the stress ratio is rewritten as,

$$\frac{\sigma_1}{\sigma_3} = -\frac{2\dot{\epsilon}_3}{\dot{\epsilon}_1} \tan^2\left(\frac{\pi}{4} + \frac{\varphi}{2}\right) \quad (4)$$

So, using Eq. (2) and Eq. (4),  $K$  is given by

$$K = -2 \tan^2\left(\frac{\pi}{4} + \frac{\varphi}{2}\right) \quad (5)$$

Therefore,  $K$  is related to the internal friction angle  $\varphi$  of the fault gouges.

Riedel shear angles related to the internal friction angle decreases with shear strain in connection with microstructure development (Gu and Wong, 1994). From our experiments, it is cleared that the energy ratio in the lower energy is constant at which gouges behaved elastically, and the ratio varied at higher stress at which gouges behaved plastically (Figs. 3 and 4). This deviation from the constant energy ratio implies frictional instability and reflection of arrangements or fabrics of gouge particles.

Unconsolidated materials such as fault

gouges and soft sediments exist in shallower parts of active faults and accretionary wedges in subduction zones. From our experimental results, the fault gouges are proved to obey Rowe's theory of the constant energy ratio until frictional instability occurs. Moreover, it has been known that this Rowe's theory can be applied not only granular material but also a blocky material such as rocks (Chappell, 1979). This indicates that the Rowe's theory can be applied to seismogenesis in active faults and subduction zone plate boundary. Therefore, various natural geohazards related to frictional or mechanical instability of granular and blocky geomaterials, such as earthquakes and landslides, can be evaluated with Rowe's theory of constant energy ratio.

#### 5. Conclusion

We conducted friction experiments using simulated fault gouges. The Rowe's theory of the constant energy ratio is proved to hold for fault gouges in lower energy rates, but deviate from the constant in higher energy rates leading to unstable slip. The occurrence of natural disasters such as earthquakes and landslides in active faults and plate boundaries in subduction zones can be assessed by Rowe's theory of constant energy ratio.

#### References

- Chappell, B. A. (1979) Deformation response in discontinua, *Int. J. Rock Mech. Min. Sci. & Geomech. Abstr.*, **16**, 377-390.
- Gu, Y. and Wong, T-f. (1994) Development of shear localization in simulated quartz gouge: Effect of cumulative slip and gouge particle size, *PAGEOPH*, **143**, 387-423.
- Marone, C. (1991) A note on the stress-dilatancy for Simulated fault gouge, *PAGEOPH*, **137**, 409-419.
- Niiseki, S. (2001) Formulation of Rowe's stress-dilatancy equation based on

- plane of maximum mobilization, *Powders and Grains 2001 Proc. Fourth Int. Conf. Micromech. Granular Media*, Swets & Zeitlinger, Sendai, 213-216.
- Ramamurthy, T. (2001) Shear strength response of some geological materials in triaxial compression, *Int. J. Rock Mech. Min. Sci.*, **38**, 683-697.
- Rowe, P. W. (1962) The Stress-dilatancy relation for static equilibrium of an assembly of particles in contact, *Proc. R. Soc. London A*, **269**, 500-527.
- Scheffeld, A. and Wroth, P. (1968) *Critical State Soil Mechanics*, McGRAW-HILL, London, 310 pp.

## Self-affinities Analysis of Fault-related Folding

Kazuhei Kikuchi <sup>a\*</sup>, Kazutoshi Abiko<sup>b</sup>, Hiroyuki Nagahama<sup>a</sup>, Jun Muto<sup>a</sup>

<sup>a</sup> Department of Earth Science, Tohoku University, 6-3, Aramaki Aza Aoba, Aoba, Sendai, Miyagi 980-8578, Japan, \*E-mail: b2sm6010@s.tohoku.ac.jp

<sup>b</sup> Forestry and Fisheries Department, Yamagata Prefectural Government, 8-1, 2 Chome, Matunami, Yamagata, Yamagata, Japan

### 1. Introduction

The Mid Niigata Prefecture Earthquake in 2004 ( $M_w$  6.6), Niigata Prefecture, Japan killed about 40 people and injured about 3000, largely as the result of building collapse. More than 100,000 residents were forced to evacuate their homes (Sidle et al., 2005). Moreover, despite the moderate size of the earthquake, thousands of landslides caused damages to roads, farmland, or residential areas. This earthquake did not rupture the earth's surface and occurred along a fault hidden well under folded terrain. These earthquakes are called "surface-folding earthquake" or "fold earthquake" for short (Stein and Yeats, 1989).

The epicenter region of the Mid Niigata Prefecture Earthquake is located near the Niigata-Kobe Tectonic Zone recognized as a region of large strain rate along the Japan Sea coast and in the northern Chubu and Kinki districts, Japan (Sagiya et al., 2000). The main shock was followed by a large number of aftershocks with four being over  $M_6$  (Konagai et al., 2012). The focal mechanisms of these strong shocks determined by Hi-net and F-net (Honda et al., 2005) were reverse fault type concordant with the pre-existing fold axis (Konagai et al., 2012). The epicenters of the aftershocks were distributed along the NNE and SSW direction within a length of about 30 km (Honda et al., 2005). Okamura et al. (2007) pointed out that the earthquake happened by fault-related folding. Such earthquake take place on "blind" folded terrain is named "hidden earthquakes" (Stein and Yeats,

1989). The location and amount of slip for the hidden earthquakes cannot in fact be observed directly.

In general, many folds are apparently curved or jagged on a wide range of scales, so that their geometries appear to be similar when viewed at different magnifications. By Matsushita and Ouchi (1989a, 1989b)'s method, we also analyzed the self-affinities of folds in the North Honshu Arc, Japan (Kikuchi et al., 2013). Nagumo (1969a, b) pointed out that the  $b$ -value of Gutenberg–Richter's law is related to the sharpness of the plastic bending deformation of the medium. Under this Nagumo's assumption, Kikuchi et al. (2013) proposed a new relation between the  $b$ -value of Gutenberg–Richter's law and the self-affinities of folds related to earthquakes. Here we analyze the self-affinity for the folds existed near the epicenter of the Mid Niigata Prefecture Earthquake. Then, from the analyzed data of the folds, we estimate the  $b$ -value of the hidden earthquake under the fault-related folds.

### 2. Data of the transect profiles of folds

The Northeast Honshu Arc on the North American plate is pushed and deformed by the subducting Pacific Plate. Kikuchi et al. (2013) applied a method of self-affinity analyses to transect profiles of folds along measurement lines numbered from 1 to 9 in the inner belt of the Northeast Honshu Arc (Fig. 1).

Kikuchi et al. (2013) used the following method; first define the smallest fixed length scale as a unit length scale  $\alpha$  and measure

the curve length  $N\alpha$  by this scale between arbitrary points  $A$  and  $B$  on the curve. Then calculate the  $x$ - and  $y$ -variances,  $X^2$  and  $Y^2$  of all measured points between the two points  $A$  and  $B$ . The standard deviations of  $X$  and  $Y$  indicate the approximate width of that part of the curve. Let us then repeat this measurement procedure for many pairs of points on the curve and determine the distribution using log-log plots of  $X$  and  $Y$  vs.  $N$  whether they scale as

$$(1) \quad X \propto N^{\nu_x}, \quad Y \propto N^{\nu_y},$$

where  $\nu_x$  and  $\nu_y$  are different in general.

The profiles near the epicentral region of the Mid Niigata Prefecture Earthquake (Fold 8 in the transect line 8 and Fold 9 in the transect line 9) are shown in Fig. 2a and Fig. 3a. From these profiles,  $\log X$ - $\log N$  and  $\log Y$ - $\log N$  can be approximated by straight

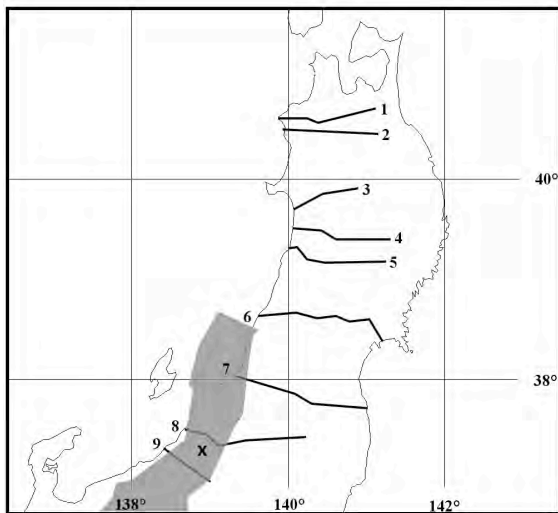


**Fig. 1.** Map of the Northeast Honshu Arc. Transect profiles are used for the analyses of self-affinity after Kitamura (1986).  $\times$  represents epicenter of the Mid Niigata Prefecture Earthquake in 2004 ( $M_w$  6.6,  $37.3^\circ$  N,  $138.8^\circ$  E). The Niigata-Kobe Tectonic Zone is denoted by a gray shaded area. Niigata-Kobe Tectonic Zone is recognized as a region of large strain rate along the Japan Sea coast and in the northern Chubu and Kinki districts, Japan (Sagiya et al., 2000).

lines (dotted lines) with different slopes ( $\nu_x \neq \nu_y$ ). This means that these profiles are differently scaled in a different direction indicating self-affine. The self-affine properties can be characterized by a Hurst exponent ( $H = \nu_y/\nu_x$ ; Mandelbrot, 1977, Feder, 1988, Peitgen and Saupe, 1988). From Fig. 2b,  $H = 0.84$  and  $H = 0.88$  from Fig. 3b.

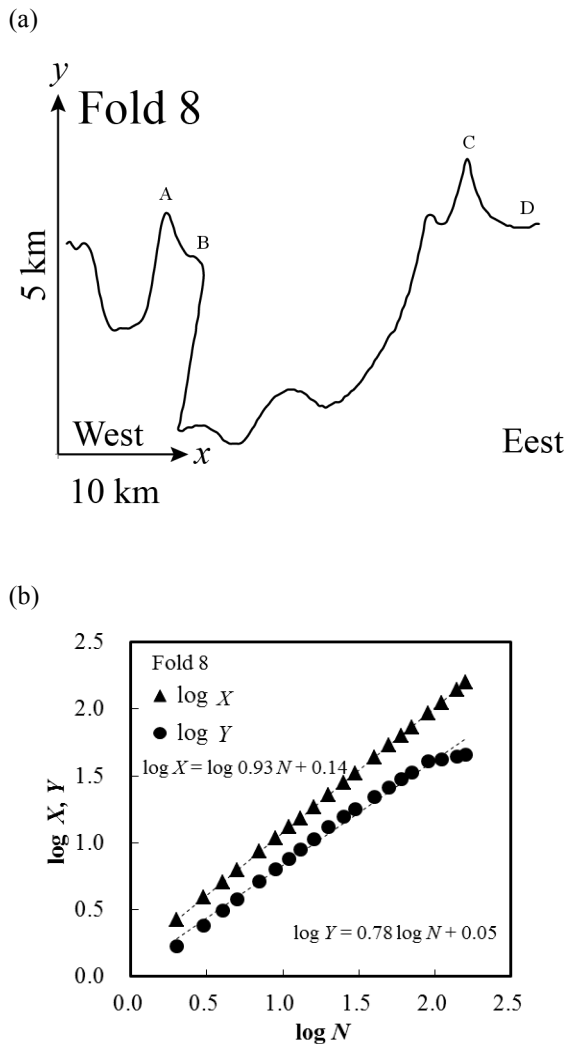
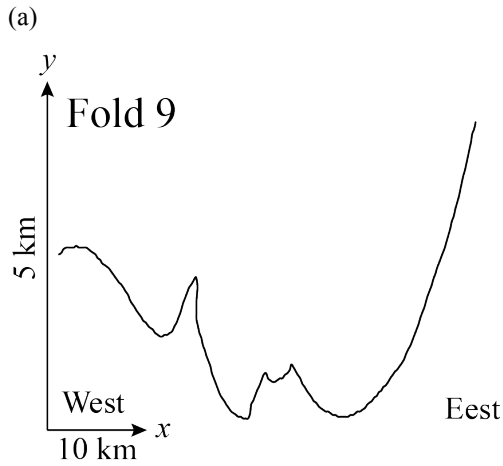


**Fig. 2.** Analysis of the self-affinity of Fold 8. (a) Transect profile of Fold 8. Oginajo anticline (A), Yakushitoge pass (B), Higasiyama anticline (C) and the vicinity of Muikamachi fault (D). Muikamachi fault is the source fault of the Mid Niigata Prefecture Earthquake. (b) Log-log plot of horizontal and vertical standard deviations ( $X$  and  $Y$ ) and curve length  $N$ . Pairs ( $\log X$ ,  $\log N$ ) and ( $\log Y$ ,  $\log N$ ) are linearly approximated by the method of least square fitting. The slopes represent  $\nu_x \approx 0.93$ ,  $\nu_y \approx 0.78$ , and  $H = 0.84$ .



$$2H = 5 - 4b. \quad (2)$$

The  $b$ -value in the Gutenberg-Richter's law is widely used as a measure of seismicity. Based on Eq. (2) and the Hurst exponent  $H$  of the fault-related folds, we can estimate  $b$ -values for the epicenter region of the Mid Niigata Prefecture Earthquake hidden below the fault-related fold. From the analyzed data  $H = 0.84$  of Fold 8 and  $H = 0.88$  of Fold 9,  $b$ -value can be estimated to be 0.83 and 0.81, respectively. These estimated  $b$ -values are concordant with seismologically obtained  $b$ -values of 0.80-0.87 in the aftershock sequence of the Mid Niigata Prefecture Earthquake (Enescu et al., 2007). Thus, for the mitigation of natural disasters, we can evaluate statistical properties of seismicity ( $b$ -value) of the hidden earthquakes by self-affinities of fault-related folds.

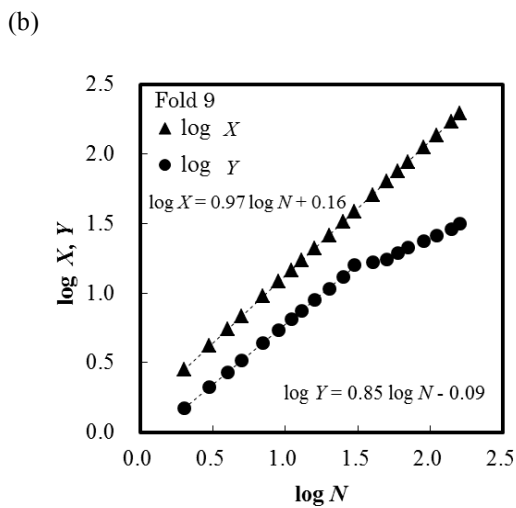


**Fig. 3.** Analysis of the self-affinity of Fold 9. (a) Transect profile of Fold 9. (b) Log-log plot of horizontal and vertical standard deviations ( $X$  and  $Y$ ) and curve length  $N$ . Pairs ( $\log X$ ,  $\log N$ ) and ( $\log Y$ ,  $\log N$ ) are linearly approximated by the method of least square fitting. The slopes represent  $\nu_x \approx 0.97$ ,  $\nu_y \approx 0.85$ , and  $H = 0.88$ .

### 3. Discussions

Nagumo (1969b) pointed out that the  $b$ -values of Gutenberg-Richter's law is the sharpness of the spectrum of the deformation in the focal region. Kikuchi et al. (2013) regarded the Hurst exponent of fold as the spectrum of the deformation of the crust. Then they derived a new relation between the  $b$ -value of Gutenberg-Richter's law and the Hurst exponent  $H$  for the crustal deformation expressed by,

### 4. Conclusion

In order to evaluate the seismic activity of hidden earthquakes below the fault-related folds, a new method to analyze self-affinities is introduced. We applied it to large scale fold geometries of the Tertiary around epicenter region of the Mid Niigata Prefecture earthquake. Based on this analysis, the geometry of the fold is self-affine and can be differently scaled in different directions. Based on the self-affinity of active folds, we can pre-estimate the  $b$ -values of the Gutenberg-Richter's law for hidden earthquakes under the fault-related folds. Therefore, this analysis method is useful to evaluate the risk of hidden earthquakes associated with fault-related folding.

### References

- Enescu, B., J. Mori, and M. Miyazawa, (2007) Quantifying early aftershock activity of the 2004 mid-Niigata Prefecture earthquake ( $M_w 6.6$ ): Journal of Geophysical Research, v. 112, B04310, DOI:

- 10.1029/2006JB004629.
- Feder, J. (1988) *Fractals*: Plenum Press, New York.
- Honda, R., S. Aoi, N. Morikawa, H. Sekiguchi, T. Kunugi, and H. Fujiwara, (2005) Ground motion and rupture process of the 2004 Mid Niigata Prefecture earthquake obtained from strong motion data of K-NET and KiK-net: *Earth, Planets and Space*, v. 57, pp. 527–532.
- Kieffer S. D., R. Jibson, E. M. Rathje, and K. Kelson, (2006) Landslides triggered by the 2004 Niigata Ken Chuetsu: Japan, Earthquake. *Earthquake Spectra*: v. 22, S1. pp. 47-73, DOI: 10.1193/1.2173021.
- Kikuchi, K., K. Abiko, H. Nagahama, H. Kitazato, and J. Muto, (2013) Self-affinities of landforms and folds in the Northeast Honshu Arc, Japan: *Acta Geophysica*, in press, DOI: 10.2478/s11600-013-0151-z.
- Kitamura, N. (ed.) (1986) *Cenozoic Arc Terrane of Northeast Honshu, Japan: Hobundo*, Sendai (in Japanese).
- Konagai, K., Z. A. Kazmi, and Y. Zhao, (2012) Extracting earthquake induced coherent soil mass movements: in S. D. Amico., ed, *earthquake Research and Analysis - New Frontiers in Seismology*, Tech, Shanghai, pp. 361-380.
- Mandelbrot, B.B. (1977) *Fractals: Form, Chance, and Dimension*: W.H. Freeman, San Francisco.
- Matsushita, M., and S. Ouchi, (1989a) On the self-affinity of various curves: *Physica D*, v. 38, 1-3, pp. 246-251, DOI: 10.1016/0167-2789(89)90201-7.
- Matsushita, M., and S. Ouchi, (1989b) On the self-affinity of various curves: *Journal of the Physical Society of Japan*. v. 58, 5, pp. 1489-1492, DOI: 10.1143/JPSJ.58.1489.
- Nagumo, S. (1969a) A derivation of Ishimoto-Iida's formula for the frequency distribution of earthquakes from a deformation~fracture relation, *Zisin (J. Seismol. Soc. Jpn.)*, v.22, 136-143 (in Japanese with English abstract).
- Nagumo, S. (1969b) Deformation~fracture relation in earthquake genesis and derivation of frequency distribution of earthquakes, *Bull. Earthq. Res. Inst., Univ. Tokyo*, v.47, 6, 1015-1027.
- Okamura, Y., T. Ishiyama, and Y. Yanagisawa, (2007) Fault-related folds above the source fault of the 2004 mid-Niigata Prefecture earthquake, in a fold-and-thrust belt caused by basin inversion along the eastern margin of the Japan Sea: *Journal of Geophysical Research*, v. 112, B03S08, DOI: 10.1029/2006JB004320, 2007
- Peitgen, H. O., and D. Saupe (eds.) (1988) *The Science of Fractal Images*, Springer, Berlin.
- Sagiya, T., S. Miyazaki, and T. Tada, (2000) Continuous GPS array and present-day crustal deformation of Japan: *Pure and Applied Geophysics*: v. 157, 11-12, pp. 2303–2322. DOI: 0033–4553/00/122303– 20 \$ 1.50+0.20/0.
- Sidele, C. R., T. Kamai, and A. C. Trandafir, (2005) Evaluating landslide damage during the 2004 Chuetsu Earthquake, Niigata Japan: *EOS*, v. 86, 13, pp. 133-140.
- Stein, R. and R. S. Yeats, (1989) Hidden earthquakes: *Scientific American*, v. 260, pp. 48-57.

## Application of GIS Technology in heavy metal source analysis of river water in mining area

Qingqing Lu<sup>a</sup>, N. Tsuchiya, T. Watanabe, R. Yamada and S. Yamasaki

<sup>a</sup>Graduate School of Environmental Studies, Tohoku University, Aramaki, Aoba, 6-6-20, Aoba-ku Sendai, 980-8579, JAPAN

*lulu@geo.kankyo.tohoku.ac.jp; tsuchiya@mail.kankyo.tohoku.ac.jp*

### 1. INTRODUCTION

Heavy metal concentrations in the river water increase environmental risks as a toxicity, particularly, copper, zinc and arsenic, which may be representative polluted elements in mine drainage<sup>[1-2]</sup>. They are introduced naturally through the weathering of land covers as well as a variety of human activities, including mining, smelting, and agricultural practices, have released countless tons of trace elements into the environment<sup>[3-4]</sup>. The topography characteristic guides the natural hydrographic features in terrestrial environment, thus affects flow direction and diffusion of aquatic pollutants. This study is aiming to monitor and control regional pollution source based on the topography characteristics by the application of GIS, to access the pollutant load contribution of tributaries from individual watershed and/or human drainages, which would clear out the pollution sources and is commonly required for environment impact assessment.

### 2. THERORETICAL CONSIDERATIONS AND METHODS

The gaining water of the tributary outlet to mainstream is fed by small, non-permanent streams and/or diffuses flows of groundwater, which completely located within the watershed. Consisting with other catchment-scale models, Fig.1 illustrates an individual watershed polygon that can be regarded to a conceptual model of a non-point contaminant source zone. The contaminant mass cannot be lost to other tributaries out of this polygon. That is, for an

individual non-point source, the contaminant outflow at the outlet to mainstream depends on and only depends on all the internal features of the sub-watershed polygon.



**Fig. 1.** Conceptual model of an individual non-point contaminant source zone

River network and related watershed information directly derived from DEM, is the basis of development and application of distributed hydrological models. The extraction of natural hydrographic net from DEM data is based on the principle that water always flows in the direction along the steepest slopes, to determine the flow direction of each elevation points in DEM. Then, the upper stream catchment of each elevation points can be calculated by the flow direction data. Afterward, the elevation points pertaining to hydrographic net can be determined by the Threshold Method according to the altitude data of upper stream catchment. Finally, based on the water flow

direction data, the entire hydrographic net would be extracted starting from the headstream. Besides, sub-watershed division is performed, the river networks and sub-watersheds were coded, and the topology of was constructed. Supported by ArcGIS, the method of hydrology modeling based on DEM (Digital Elevation Model) data was applied to generate basin network, to divide sub-watershed polygon and generate basin boundary automatically. The whole study area was divided to several sub-watershed polygons (Fig.2).

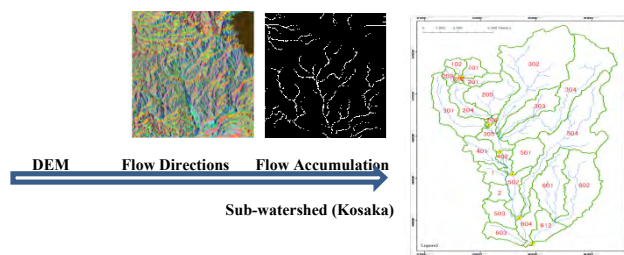


Fig. 2. Sub-watershed division

For each individual sub-watershed polygon, the heavy metal outflows are depended on the inside features of this polygon. To clear out the characteristics this non-point source, specific investigation should be carried out. Usually the investigation includes “water discharge measurement” and “Heavy metal concentration in each discharge (ICP-MS analysis)”. Corresponding to each sub-watershed polygon, these two indexes are necessary to clear out where and how much the heavy metals come from. If to know more about the characteristics of the pollution sources and the impact factors of the pollution sources, other information within each sub-watershed polygon are also needed, such as, current land use structure (land cover), Geological features, Human activities including industrial information, agriculture activities and others.

### 3. CASE STUDY

#### Site descriptions

A case is being carried out in the Hokuoku basin, one of the most popular mining areas in

Japan, located in Northeast Japan (Fig. 1). The Hokuoku region in Akita Prefecture is one of the most famous and important mining districts for Zn-Pb-Cu-Au-Ag massive sulphide deposits that formed on the seafloor. At present, wastewater from Furutobe mine, Ainai mine, and the Kosaka refinery is being poured into Kosaka River. The heavy metals in the mainstream are derived from both the anthropogenic origin and natural origin. It is possible to capture the effects of the geological features or the abandoned mines for each tributary watershed by the investigation carried out in this kind of area.

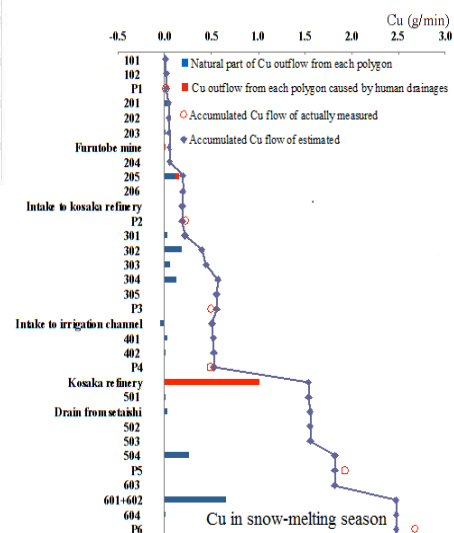


Fig. 3. Cu outflows into Kosaka mainstream

### Results

The 10 meter resolution DEM data was applied to in this case, and the whole study area was divided into several sub watershed polygons (Fig.2). Heavy metals, Cu, Zn, Pb, Cu, Al, and As were selected for source analysis because of their association with mining activities. The outflows of pollution sources are indicated in the form showing in Fig.3. In Fig.3, the blue bars stand for the non-point source part of heavy metal outflows. This part is derived from the natural dissolved out heavy metals from the land cover (soils and rocks) while the rainwater flow through and act with them within the watershed before reach the rivers. The red bars express the outflows caused by human

drainages (point sources). The blue bars changes a lot among different polygons and had different influence on the mainstream water quality. The red bars show that dominant human drainages significantly affect the river water quality in local. The blue line shows the accumulated heavy metal outflows of all the upstream drainages. The small red circles are the actually measured heavy metal outflows at the monitoring points. They can be used to check the accumulative effects of the upstream outflows.

With the objective to determine the influence of land use on heavy metal pollutions within Kosaka watershed, the correlation analysis of aquatic heavy metal pollution and land use was carried out by calculating the Pearson's correlation coefficient between the heavy metal concentration and land use percentage of each land use type within a sub-polygon. But the results showed that there are no obvious correlations between land use structure and pollutant outflows. Since the land use intensity is very low in the study area. The forest coverage percentage is over 70% for the whole study area.

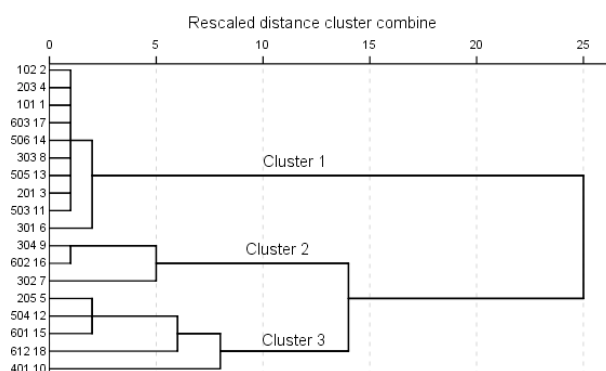


**Fig. 4.** Dendrogram showing hierarchical clustering of sampling sites according Ward's method with Euclidean distance

Cluster Analysis was applied to the tributary water quality data (heavy metal concentrations) for grouping the similar sampling sites. The cluster classifications varied with significance level because the sites in these cluster had similar characteristic features and natural

backgrounds that were affected by similar sources. The picture (Fig.4) shows the hierarchical clustering of the sub-watershed polygons were grouped into three significant clusters. The cluster 3 corresponds to sampling sites with the highest heavy metal concentrations. The abandoned mines can be found in these sub-watershed polygons. There is a strong correlation between heavy metal concentration and the proximity of sampling sites to the abandoned mines.

#### 4. CONCLUSIONS

It is possible to clear out the heavy metal load contribution of one individual watershed polygon or human drainages, which would clear out the source of the heavy metals and is commonly required for environment impact assessment. Through mass balance closure, it is possible to estimate the heavy metal flow in downstream river by the accumulation of all the upstream tributaries and human drainages. The mass flow contributions of unmonitored river branches or mine site drainages can be estimated in a similar way, by given that there are upstream and downstream monitoring data in the main river, relatively close to the confluence point.

The sub-watershed division based on DEM by GIS is helpful to monitor and control the pollutant sources in regional basin. This method can be regarded as a transition of macroscopic to microcosmic, contributing to separate, dwindle in bound, and then clarify the pollution sources. This method offers an effective way for the comprehensive understanding in the spatial characteristics of regional pollution, and the relation with the features in natural environment and human activities.

#### References

- LEI Xiaohui, TIAN Yu, JIANG Yunzhong etc. 2009. General Catchment Delineation Method and its Application into the Middle Route Project of China's

- South-to-north Water Diversion. The Hong Kong Institution of Engineers Transactions, Vol 17, No 2, pp1-7
- David R. Lenat.1994. Effects of land use on water quality and aquatic biota of three north Carolina piedmont streams.
- A.H.Charkhabi, 2008. Land use effects on heavy metal pollution of river sediments in Guilan, southwest of the Caspian sea.
- G. I. Littlewood, Estimating Contaminant Loads in Rivers, A Review. In: Report no 117, Institute of Hydrology, Oxfordshire, England, 1992.

## Inhomogeneity of fractal property in rock minerals using 3D X-ray CT measurement

Junko Yamaki<sup>a</sup>, Jun Muto<sup>a</sup>, Hiroyuki Nagahama<sup>a</sup>,  
Osamu Sasaki<sup>b</sup>, Harumasa Kano<sup>b</sup>,

<sup>a</sup>Department of Earth Science, Tohoku University, <sup>b</sup>Tohoku University Museum, 6-3 Aoba, Aramaki, Aoba-ku, Sendai, 980-8578, Japan, b2sm6034@s.tohoku.ac.jp

### 1. Introduction

The fracture geometry in rocks influences a mechanical behavior of rocks (Oncel *et al.*, 2001; Dieterich and Richards-Dinger, 2010). So, in order to prevent the natural hazard (e.g., rock burst), it is important to evaluate the complexity of fracture geometry of natural rocks.

After the birth of fractal geometry (Mandelbrot, 1967), the concept of the fractal geometry was introduced as the measurement the complexity of rock fracture systems (e.g., Korvin, 1992; Turcotte, 1997). Although actual fracture patterns in rocks spread inhomogeneously and anisotropically with self-similar in a certain finite range of scale (Kruhl, 2013), many studies had remained the fractal analysis in one-dimension or two-dimension. These measurements have not considered three-dimensional heterogeneity of fracture patterns. Therefore, we should analyze the fracture geometry spreading in the space and measure them with considering the heterogeneity and anisotropy of fracture geometry.

In this study, we pointed out the spatial characteristics and anisotropy of fracture geometry for experimentally fractured samples using 3D micro X-ray computed tomography (CT) techniques.

### 2. Method

The samples were initially homogeneous borosilicate glass and single crystals of quartz and calcite. They were shaped into cylinders of 12.7 mm length and 6.0 mm diameter for glass, and 7.5 mm length and 3.0 mm diameter for

single crystals of quartz and calcite. The c-axes of quartz and calcite were parallel to the direction of the long axis of the cylinders.

The fracture experiments were performed using a Griggs apparatus with a lead confining medium. The experiments were carried out at a confining pressure ( $P_c$ ) of 0~300 MPa with a nominal axial strain rate of  $5 \times 10^{-4}$  /s at room temperature. The axial loads were increased until the sample was fractured brittlely.

The obtained samples were scanned with 3D micro X-ray CT (ScanXmate-E090; manufactured by Comscantecno Co., Ltd.). The scanning conditions were at 5~10  $\mu\text{m}$  spatial resolution using a 111~121 kV and  $61 \sim 111 \times 10^{-6}$  A X-ray source.

The gained images were processed with ImageJ (<http://rsbweb.nih.gov/ij/>). After noise reduction processes were carried out, the images were transformed to the binary images. The space distributions of fracture pattern were expressed as a fractal dimension  $D_{BC}$  by using a Box-Counting method. This analysis was carried out on the images sliced along each coordinate axis; XY-planes (red in Fig. 1), YZ-planes (green in Fig. 1) and ZX-planes (blue in Fig. 1) from one side to the other side of the samples.

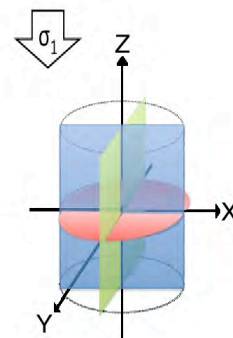


Fig. 1. Coordinate system

### 3. Results

#### 3.1. Distribution of $D_{BC}$ values

The values of  $D_{BC}$  at each analyzed location were showed in Fig. 2.

The sample of single crystals of quartz and calcite fractured under uniaxial compression (QTZ-0 and CAL-0) and the borosilicate glass sample fractured at  $P_c = 300$  MPa (GLS-300) were broken significantly toward the bottom of the sample. QTZ-0 and CAL-0 had many fractures perpendicular to the direction of maximum compressive stress ( $\sigma_1$ ). The oblique fault was made in the sample of single crystal of quartz fractured at  $P_c = 300$  MPa (QTZ-300).

$D_{BC}$  of XY-planes of these samples increased toward the highly fractured sides.  $D_{BC}$  of QTZ-0 increased gently from 1.5 to 1.8.  $D_{BC}$  of QTZ-300 showed from 1.4 to 1.7, a little bit

higher at the both sides.  $D_{BC}$  of GLS-300 increased from 1.1 to 1.7 and  $D_{BC}$  of CAL-0 increased drastically from 1.0 to 1.7. On the YZ-planes and ZX-planes,  $D_{BC}$  showed constant value (around 1.7 for QTZ-0 and 1.5 for GLS-300) or increased toward the center of the sample (QTZ-300 and CAL-0) (Table. 1).

#### 3.2. $D_{BC}$ depending on distance from highly fractured sides

$D_{BC}$  of XY-planes for QTZ-0, GLS-300 and CAL-0 increased toward the highly fractured bottom, while  $D_{BC}$  of that on QTZ-300, which fractured by the oblique fault, increased toward the both sides. The increasing trends of these  $D_{BC}$  are shown in Figure. 3.  $d$  is the distance from the top of samples. Udagawa (1999) shows that the fractal dimension of fractures increased

**Table 1.** Results of fracture experiments and fractal box counting

	QTZ-0	QTZ-300	GLS-300	CAL-0
sample	single crystal of quartz	single crystal of quartz	borosilicate glass	single crystal of calcite
$P_c$ (MPa)	0	300	300	0
peak strength (MPa)	4700	6200	3200	300
strain (%)	2.2	1.6	6.5	5.1
$D_{BC}$ XY-planes	1.5 to 1.8 (bottom)	1.4 to 1.7 (top&bottom)	1.1 to 1.7 (bottom)	1.0 to 1.7 (bottom)
$D_{BC}$ YZ, ZX-planes	$\sim 1.7$	1.4 to 1.6 (center)	$\sim 1.5$	1.2 to 1.7 (center)

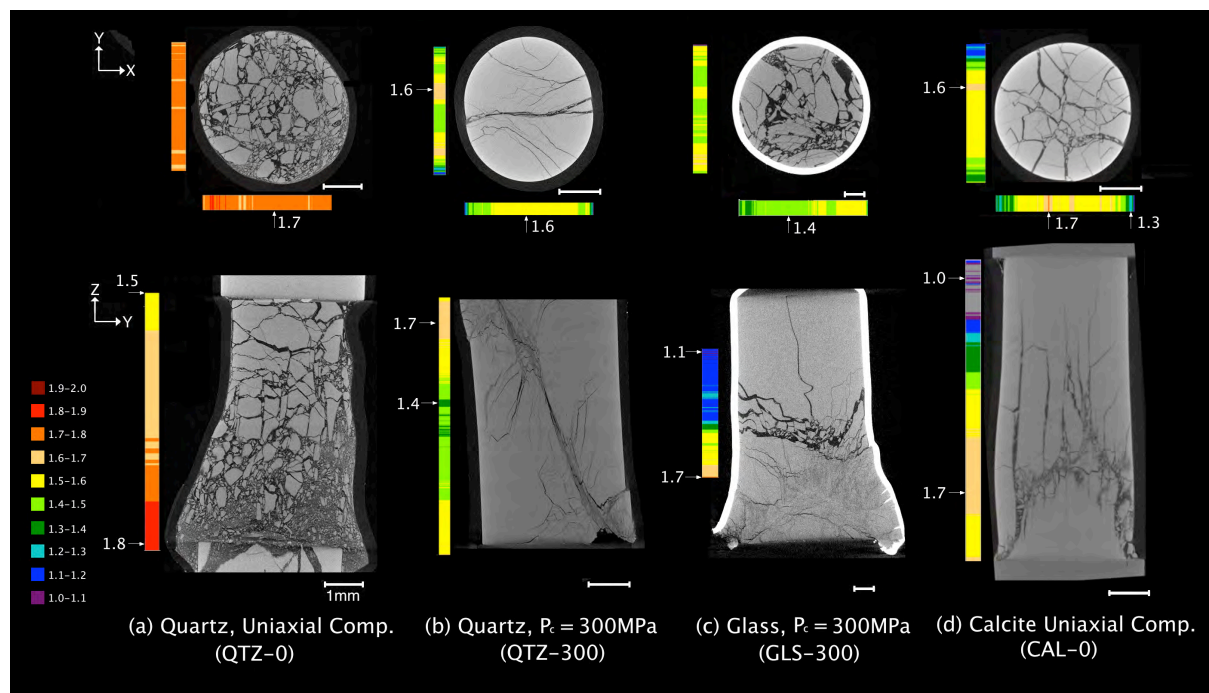


**Fig. 2.**  $D_{BC}$  of each sample

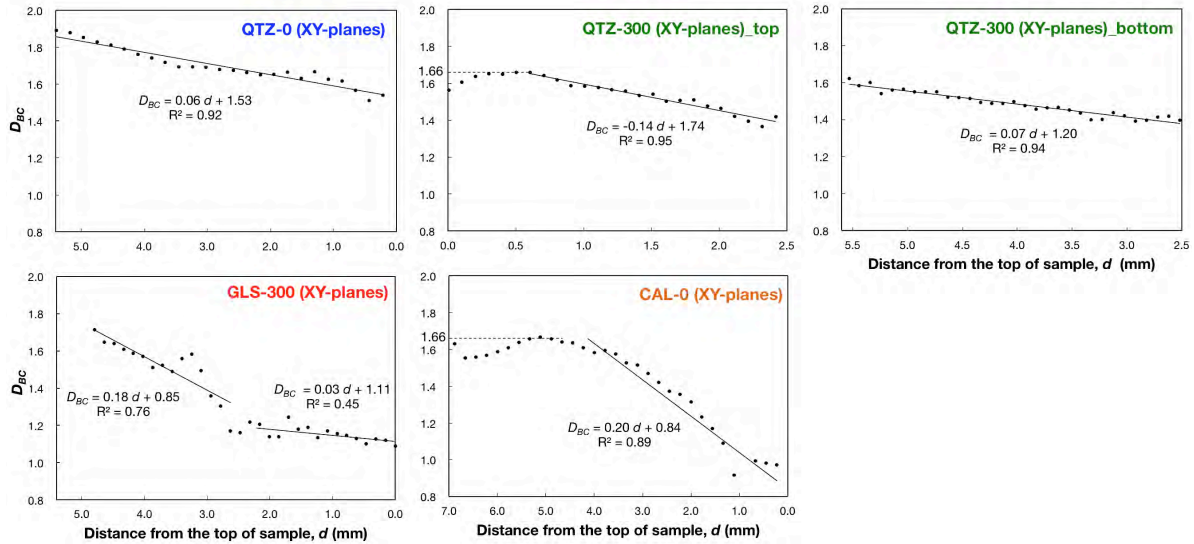


Fig. 3.  $D_{BC}$  and distance from the highly fractured sides

linearly toward to a fault. Our results were consistent with Udagawa (1999)'s results. The difference in reduction rate of  $D_{BC}$  might depend on the differences in  $P_C$  and rock minerals of samples. The  $D_{BC}$  of CAL-0 and the top of QTZ-300 reached the plateau around 1.66.

#### 4. Discussions

$D_{BC}$  values and distributions were different in analyzed location and direction even in the same sample. What does cause the inhomogeneous distributions of  $D_{BC}$ ?

The relationship between the fracture toughness  $K_C$  and fractal dimension  $D$  of the fracture surfaces for brittle fractures can be linear on semi-log plots (Mecholsky and Mackin, 1988; Nagahama, 1994). Moreover the fractal dimension of fracture surface roughness is known to be proportional to the energy per unit mass required for fracturing (Nagahama and Yoshii, 1993; Nagahama, 1994). Therefore, the differences in  $D_{BC}$  values in our results indicate heterogeneity in fracturing energy distribution even in highly homogeneous samples.

$D_{BC}$  of XY-planes increased toward the highly fractured sides. The  $D_{BC}$  behavior similar to near actual faults depends on the partitioning the fracture energy locally. The  $D_{BC}$  of CAL-0 and the top of QTZ-300 reached the plateau around 1.66. Because there is an upper limit to the  $D_{BC}$  of fracture geometry of rocks, of about

1.60 (Hirata, 1989; Sammis and Biegel, 1989), reaching the plateau was regarded as saturation with fracture energy.

For further discussion, we examined the relation between natural logarithm of real area distortion  $\varepsilon$  and  $D_{BC}$  of XY-planes (Fig. 4). The real area distortion  $\varepsilon$ , that can be a measure of fracture energy, were estimated by natural logarithm of  $A/A_0$ , where  $A$  is the area of XY-planes after deformation and  $A_0$  is the initial area of XY-planes.

The relationship between natural logarithm of real area distortion and  $D_{BC}$  can be expressed by

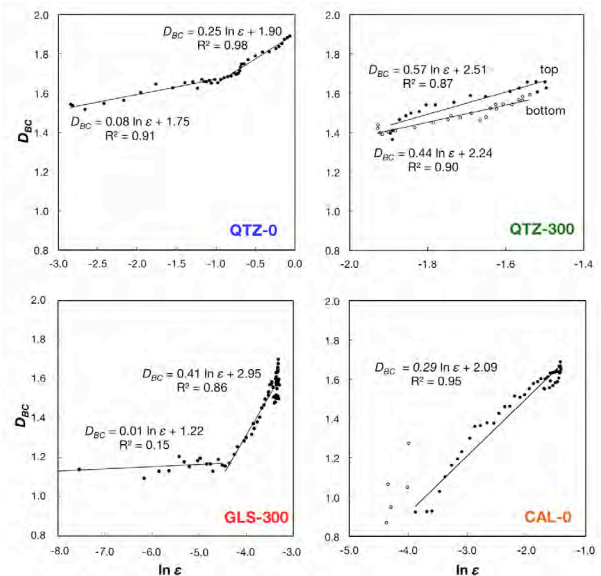


Fig. 4. Logarithm of area strain  $\varepsilon$  and  $D_{BC}$

$$D_{BC} = a \ln \varepsilon + b = a \ln_2 (A/A_0) + b, \quad (1)$$

where  $a$  and  $b$  are constants. The graph of QTZ-300 had two slopes depending on the location of images (the top or the bottom). The relation indicates that inhomogeneity of  $D_{BC}$  value is related to heterogeneity in fracturing energy distribution regardless of analyzed locations.

## 5. Conclusions

We analyzed the fractal characteristic of fracture geometry of experimentally fractured borosilicate glass and single crystals of quartz and calcite samples using 3D micro X-ray Computed Tomography (CT) techniques.

$D_{BC}$  values and their distributions were different in analyzed location and direction even in the same sample.  $D_{BC}$  of XY-planes increases toward the highly fractured side. It is consistent with the  $D_{BC}$  behavior observed near the actual fault.  $D_{BC}$  of YZ-planes and ZX-planes are the almost constant or increased toward the center of the sample. Therefore, we should consider the inhomogeneity and anisotropy of the fracture space distribution in case of comparison with the fractal dimensions of different analyzing directions or locations.

Moreover, the relationships between natural logarithm of real area distortion  $\varepsilon$  and  $D_{BC}$  in XY-planes showed the positive correlation.

## Acknowledgements

We thank K. Otsuki, J. Fukuda, and K. Kikuchi for their valuable and helpful comments. We are grateful to Y. Kinoshita for using the X-ray CT.

## References

Dieterich, J. H. and Richards-Dinger, B. R., 2010, Earthquake recurrence in simulated fault systems, *Pure and Applied Geophysics* 167, 1087-1104.

Hirata, T., 1989, Fractal dimension of fault systems in Japan: fractal structure in rock fracture geometry at various scales, *Pure and Applied Geophysics* 131, 157-170.

Korvin, G., 1992, Fractal Models in the Earth Sciences, *Elsevier, Asterdam*.

Kruhl, J. H., 2013, Fractal-geometry techniques in the quantification of complex rock structures: A special view on scaling regimes, inhomogeneity and anisotropy, *Journal of Structural Geology* 46, 2-21.

Mandelbrot, B. B., 1967, How long is the coast of Britain? Statistical self-similarity and fractional dimension, *Science, New Series* 156, no. 3775, 636-638.

Mecholsky, J. J. and Mackin, T. J., 1988, Fractal analysis of fracture in Ocala chert, *Journal of Materials Science letters* 7, 1145-1147.

Nagahama, H. and Yoshii, K., 1993, Fractal dimension and fracture of brittle rocks, *International Journal of Rock Mechanics and Mining Sciences & Geomechanics Abstracts* 30, 173-175.

Nagahama, H., 1994, A fractal criterion for ductile and brittle fracture, *Journal of Applied Physics* 75, 3220-3222

Oncel, A. O., Wilson, T. H. and Nishizawa, O., 2001, Size scaling relationships in the active fault networks of Japan and their correlation with Gutenberg-Richter  $b$  values, *Journal of Geophysical Research* 106, 21827-21841.

Sammis, C. G. and Biegel, R. L., 1989, Fractals, fault-gouge, and friction, *Pure and Applied Geophysics*, 131, 255-271.

Turcotte, D. L., 1997, Fractals and Chaos in Geology and Geophysics, *second ed. Cambridge University Press, Cambridge*.

Udagawa, Y., 1999, Application of fractal geometry in the field of tunnel construction Proceedings : Ninth International Congress on Rock Mechanics, International Society on Rock Mechanics, Pari, France, Balkema, 241-244.

## Seismic luminous phenomena and VHF electromagnetic emission originated from radon emanation

Asuka Seki<sup>a</sup>, Izumi Tohbo<sup>b</sup>, Yasutaka Omori<sup>c</sup>, Jun Muto<sup>a</sup>, Hiroyuki Nagahama<sup>a</sup>

<sup>a</sup>*Department of Earth Science, Graduate School of Science, Tohoku University, 6-3 Aoba, Aramaki, Aoba-ku, Sendai, Miyagi 980-8578, Japan, b2sm6019@s.tohoku.ac.jp*

<sup>b</sup>*Science and Safety Policy Research Division, Mitsubishi Research Institute, 2-10-3 Nagatacho, Chiyoda-ku, Tokyo 100-8141, Japan*

<sup>c</sup>*Research Center for Radiation Protection, National Institute of Radiological Sciences, 4-9-1 Anagawa, Inage-ku, Chiba 263-8555, Japan*

### 1. Introduction

Anomalous luminous phenomena and electromagnetic wave emission before or during earthquakes have been reported. These seismic anomalous phenomena may be helpful as a short-term predictive method of the earthquakes. Although many researchers have proposed and discussed various models for these phenomena, their mechanisms are still uncertain.

Recently, as a source of these phenomena, exhalation of radon from the ground surface with the earthquake attracts attention. Yasuoka and Shinogi (1997) reported an anomalous increase in atmospheric radon concentration before the 1995 Kobe earthquake. This anomaly was caused by change in concentration of radon exhaled from the ground surface before the earthquake. Radon in the uranium decay chains is noble gas produced by radioactive decay of radium ( $^{226}\text{Ra}$ ), distributes universally in the crust. This gas can leave the earth's crust and exhale into the atmosphere as an ideal gas. As a result of decay of radon, the short-lived daughter nuclides are generated:  $^{218}\text{Po}$ ,  $^{214}\text{Pb}$ ,  $^{214}\text{Bi}$  and  $^{214}\text{Po}$ . Radon and its daughters  $^{218}\text{Po}$  and  $^{214}\text{Po}$  are alpha emitters. These alpha particles ionize atmospheric molecules, and their ionization effect is major and more dominant than cosmic rays near the ground surface.

Here, we propose a new model for seismic luminous phenomena and electromagnetic wave emission by focusing on atmospheric  $^{222}\text{Rn}$  and  $^{218}\text{Po}$ ,  $^{214}\text{Po}$ . In this study, we employ ionization effect of alpha particles for nitrogen molecules

or polyatomic molecules in the atmosphere, and discuss VHF (very high frequency; 30-300MHz) electromagnetic wave emission at the 2005 off-Miyagi earthquake.

### 2. Model of luminous phenomena and VHF emission by using atmospheric radon and its daughters

Einstein (1916) proposed that atoms excited to higher energy levels can be de-excited by ejecting electrons or by emitting energy as discrete quanta called photons, which have characteristic wave lengths. We employ this mechanism to our model in the viewpoint of electromagnetic radiation in quantum theory.

#### 2-1 Luminous phenomena

A light emission phenomenon, called the "air luminescence", is caused by de-excitation of the ionized molecules of atmospheric nitrogen by electron impact ionization from alpha particles. The light emission comes mostly from the second positive system (SPS;  $C^3\Pi_u \rightarrow B^3\Pi_g$ ) of neutral nitrogen molecules (Fig. 1). There is also light emission with a low transition probability from a first negative system (FNS;  $B^2\Sigma_u^+ \rightarrow X^2\Sigma_g^+$ ) of nitrogen molecule ion (Fig. 1). In the field of radioisotope analysis, air luminescence generated in the gaseous space above a liquid scintillator in a counting vial, employing a liquid scintillation spectrometer, has been already proposed to measure  $^{222}\text{Rn}$  (e.g., Takiue and Ishikawa, 1979; Homma et al., 1987). Therefore, radon and its daughters can cause air

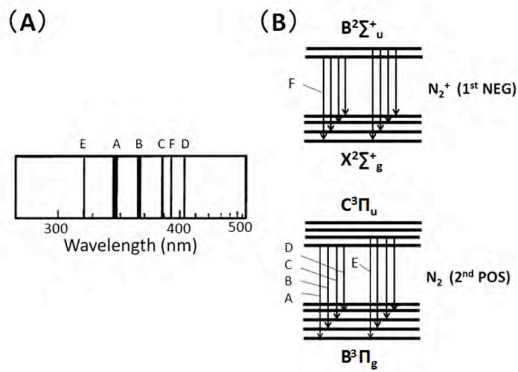


**Fig. 1** (A) The emission spectra for the N<sub>2</sub> SPS (A-E) and the N<sub>2</sub><sup>+</sup> FNS (F). (B) Simplified energy diagrams showing the N<sub>2</sub> SPS and the N<sub>2</sub><sup>+</sup> FNS. The figure is modified after Homma and Morita (2001).

luminescence theoretically and experimentally.

We propose the following model for the mechanism of luminous phenomena: 1. The concentration of atmospheric radon and its daughter nuclides increase anomalously before or during earthquakes, 2. Neutral nitrogen molecules and nitrogen molecule ions are excited by alpha particles emitted from the nuclides (<sup>222</sup>Rn, <sup>218</sup>Po and <sup>214</sup>Po), and air luminescence is generated by their de-excitation.

### 2-2 VHF electromagnetic emission

Boyarchuk et al. (2005) proposed a model that VHF wave emission is originated when excited state of neutral clusters changes. Radon gas forms positively and negatively charged heavy particles through air ionization. These ions react immediately with surrounding water vapor molecules and grow to hydrated ion complexes (NO<sub>2</sub><sup>-</sup>(H<sub>2</sub>O), H<sup>+</sup>(H<sub>2</sub>O)<sub>6</sub>, and others). As a result of the association of such hydrated ion complexes, a neutral cluster (e.g., NO<sub>3</sub><sup>-</sup>(H<sub>2</sub>O)<sub>n</sub>H<sub>3</sub>O<sup>+</sup>) is formed, which is dipole quasi-molecules consisting either of large hydrated cluster ions or dipole aerosols. Rotation-rotation transition in a neutral cluster causes VHF wave emission. They described theoretical relations among concentration of neutral cluster, radiation intensity and frequency of electromagnetic wave by rotation-rotation transitions, based on air ionization rate.

### 3. Discussions

3-1 Possibility of luminous phenomena originated radon and its daughters

Takaki and Ikeda (1998) proposed “a dark discharge model” for luminous phenomena, and estimated the luminous intensity and area. This model agrees with ours on that a light emission is produced by the ionization of atmospheric molecules. But they considered that atmospheric molecules were ionized by free electrons in atmosphere accelerated under the electric field produced by piezoelectric effects of quartz. In the case of the 1965 Matsushiro earthquake swarm, Hagiwara (1966) proposed that natural radiation intensity including <sup>222</sup>Rn was anomalously high in the epicentral regions. These regions roughly correspond to ones with many reports of luminous phenomena (e.g., Yasui, 1968). This result supports our model for the light emission mechanism due to radon and its daughters. Our model has an advantage in that it is not necessary to assume the electric field generation by the piezoelectric effect of the quartz.

Alpha particles emitted from <sup>222</sup>Rn, <sup>218</sup>Po and <sup>214</sup>Po have energy of about 5.49 MeV, 6.00 MeV and 7.69 MeV, respectively. On the other hand, an excitation energy of about 11.01 eV is at least required to excite N<sub>2</sub> from its ground state (X<sup>1</sup>Σ<sub>g</sub>) to the C<sup>3</sup>Π<sub>u</sub> state (Itikawa et al., 1986). An energy of 18.75 eV is required to cause to emit photons from B<sup>2</sup>Σ<sup>+</sup><sub>u</sub> state of N<sub>2</sub><sup>+</sup> (Itikawa et al., 1986). Therefore, alpha particles can excite N<sub>2</sub> and N<sub>2</sub><sup>+</sup>.

Moreover, wavelengths of lights by these transitions are within 220-390 nm (SPS band of N<sub>2</sub>) and 390-520 nm (FNS band of N<sub>2</sub><sup>+</sup>), respectively, including visible wavelengths (Lofthus and Krupenie, 1977) (Fig. 1). So air luminescence can be observed as seismic luminous phenomena (e.g., the 1965 Matsushiro earthquake swarm).

3-2 VHF wave emission before the 2005 off-Miyagi earthquake

We consider the relationship between VHF

wave emission and radon anomaly before the 2005 off-Miyagi earthquake ( $M_j7.2$ ,  $M_w7.1$ ) in Miyagi Prefecture, Japan, on August 16, 2005. The hypocenter is located at  $38.1^\circ\text{N}$  and  $142.4^\circ\text{E}$ , and the depth of 42 km. Electromagnetic wave anomalies in VHF band (49.5 MHz) was observed about 2-5 days before the earthquake by the observation system at monitoring stations in Dairokuten ( $38.24^\circ\text{N}$ ,  $141.27^\circ\text{E}$ ) (Yonaiguchi et al., 2007). Moreover, anomalous increase in atmospheric radon concentration was also observed in Kozumi ( $38.22^\circ\text{N}$ ,  $141.27^\circ\text{E}$ ) near the observatory of electromagnetic wave (Omori et al., 2009). Comparing VHF wave and radon concentration data, both of the anomaly dates are clearly conformed to each other. In the night time on 11 and 13 August, two anomalous phenomena of radon and VHF noise occur before the earthquake (Tohbo, 2010MS).

Due to variation of atmospheric radon concentration before the earthquake, we calculate the ionization rate of radon and its daughters  $3.9\text{-}5.5 \times 10^7$  ion-pairs/ $\text{m}^3/\text{s}$  (Hoppel et al., 1986), which is predicted to be more than twice of ordinary ionization rate of  $1.5\text{-}2.2 \times 10^7$  ion-pairs/ $\text{m}^3/\text{s}$  around the observatory, calculated from normal atmospheric radon concentrations of  $40\text{-}50$  Bq/ $\text{m}^3$  there (Omori et al., 2009). Therefore, the concentration of neutral cluster is estimated to be  $6\text{-}10 \times 10^5/\text{cm}^3$  at this ionization rate (Boyachuk et al., 2005). Based on the calculation method (Boyachuk et al., 2005), we can obtain the relationship between emission intensity and frequency of emitted electromagnetic wave due to radon emanation. Fig. 2 shows a relationship between the emission intensity and the frequency of rotation-rotation transition in a neutral cluster, when the concentration of neutral cluster is the range of  $6\text{-}10 \times 10^5/\text{cm}^3$ . In Fig. 2, solid lines indicate the region with the allowance of elastic collisions where electromagnetic wave emission is possible.

On the other hand, VLF emission is impossible in the region showed by dashed lines; electromagnetic wave emission due to

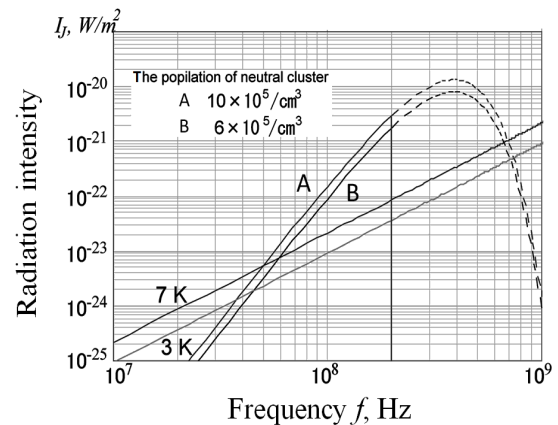


**Fig. 2** The relationship between radiation intensity and frequency of electromagnetic wave. 3K and 7K indicate the background radiations from cosmos at temperature 3K and 7K, respectively.

seismic radon emanation is possibly caused by the frequency belong 200 MHz before the 2005 off-Miyagi earthquake. Cosmic background radiation, electromagnetic wave emitted by cosmic rays, is observed as a noise constantly. Therefore, we take into account the cosmic background radiation at the cosmic temperature of 3-7K to examine the detectable range of the observation equipment of the electromagnetic wave, because the radiation frequency, of which intensity is less than that of cosmic background radiation, is lost among the background noise and could not be detected. The detectable frequency range is estimated to be 40-60 MHz, so electromagnetic wave anomalies in 49.5 MHz before the earthquake was not hidden by cosmic background radiation.

There are also other possible sources of electromagnetic wave anomalies, for example increase in ion and electron density in atmosphere and abnormal reflection of the existing electric wave due to hydration effect. However, taking into account the temperature, humidity and ion concentration when VHF wave anomalies were observed, these sources were unlikely to occur in this case. Therefore, the emission of VHF wave from seismic exhaled radon could be the source of VHF electromagnetic anomalies.

#### 4. Summary

Based on the ionization effect of alpha particles from radon and its daughter, we tried to reveal the mechanism of various seismic electromagnetic phenomena. A model of the “air luminescence” caused by de-excitation of nitrogen molecules and ions due to alpha particle from radon and its daughters was proposed to explain seismic luminous phenomena. On the other hand, we also discussed a possibility of electromagnetic wave emission from excitation of polyatomic molecules by alpha particles. VHF wave emission before the 2005 off-Miyagi earthquake could be caused by rotation-rotation transition of neutral clusters, induced by the ionization due to radon.

#### References

- Boyarchuk, K. A., Karelin, A. V., and Shirokov, R.V. (2005) Neutral cluster and its influence on electromagnetic effects in the atmosphere, *Izvestiya, Atmos. Oceanic Phys.*, 41, 487-497
- Einstein, A. (1916) Strahlungs-Emission und absorption nach der quantentheorie, *Vech. Deutsch. Phys. Ges.*, 18, 318-323 (in Germany)
- Hagiwara, Y. (1966) Natural radioactivity in the Matsushiro earthquake area, *Bull. Earthq. Res. Inst.*, 44, 1385-1395
- Homma, Y., Murase, Y. and Takiue, M. (1987) Determination of  $^{222}\text{Rn}$  by air luminescence method, *J. Radioanal. Nucl. Chem.*, 119, 458-465
- Homma, Y. and Morita, Y. (2001) Development of the radiochemical theme, *Jour. Pharm. Soc. Jpn.*, 121, 327-344
- Hoppel, W. A., Anderson, R. V., and Willett, J. C. (1986) Atmospheric electricity in the planetary boundary layer, in: *The Earth's Electrical Environment* (E. P. Krider and R. G. Roble, eds.), *Natl. Acad. Press, Washington, D. C.*, 149-165
- Itikawa, Y., Hayashi, M., Ichimura, A., Onda, K., Sakimoto, K., Takayanagi, K., Nakamura, M., Nishimura, H. and Takayanagi, T. (1986) Cross sections for collisions of electrons and photons with nitrogen molecules. *J. Phys. Chem. Ref. Data*, 15, 985-1010
- Loftus, A. and Krupenie, P. H. (1977) The spectrum of molecular nitrogen, *J. Phys. Chem. Ref. Data*, 6, 113-307
- Omori, Y., Tohbo, I., Nagahama, H., Ishikawa, Y., Takahashi, M., Sato, H., and Sekine, T. (2009) Variation of atmospheric radon concentration with bimodal seasonality, *Radiat. Meas.*, 44, 1049-1054
- Takaki, S and Ikeda, M. (1998) A dark discharge model of earthquake lightning, *Jpn. J. Appl. Phys.*, 37, 5016-5020
- Takiue, M. and Ishikawa, H. (1979)  $\alpha$ -ray measurement due to air luminescence employing a liquid scintillation spectrometer, *Nucl. Instrum. Methods*, 159, 139-143
- Tohbo, I. (2010MS) VHF electromagnetic anomaly and radon emanation before earthquakes, Master Thesis, Depart. Earth Science, Graduate School of Science, Tohoku Univ.
- Yasui, Y. (1968) A study on the luminous phenomena accompanied with earthquake (Part 1), *Mem. Kakioka Mag. Obs.* 13, 25-61
- Yasuoka, Y. and Shinogi, M. (1997) Anomaly in atmospheric radon concentration: a possible precursor of the 1995 Kobe, Japan, earthquake, *Health Phys.*, 72, 759-761
- Yonaiguchi, N., Ida, Y., Hayakawa, M. and Masuda, S. (2007) A comparison of different fractal analyses for VHF electromagnetic emissions and their self-organization for the off-sea Miyagi-prefecture earthquake, *Nat. Hazards Earth Syst. Sci.*, 7, 485-493

## Electromagnetic radiations from semiconductor minerals

Mitsuyuki Ozawa<sup>a</sup>, Jun Muto<sup>a</sup>, Hiroyuki Nagahama<sup>a</sup>, Toshiro Nagase<sup>b</sup>

<sup>a</sup>*Dept Earth Science, Tohoku University, 6-3 Aoba, Aramaki-aza, Aoba, Sendai, Miyagi, 980-8578, Japan.*

<sup>b</sup>*The Tohoku University Museum.*

OZAWA: b3sm6007@s.tohokut.ac.jp

### 1. Introduction

It has been reported that the anomalous electromagnetic radiations related to various geohazards such as earthquakes, volcanic eruptions, landslides were observed. Even before the tectonic activities, micro fracturing processes occur and elastic wave is generated in the crust. Therefore, anomalous electromagnetic radiations may be used to evaluate these geohazards. These electromagnetic radiations contain various range of frequency. Particularly, in complex deposits composed of semiconductor minerals, electromagnetic radiations in the radio frequency (30 kHz ~ 3 MHz) are induced by propagation of elastic waves [1].

There are a number of sources of the seismo-electromagnetic radiations such as electrokinetic effect and piezoelectricity. These two effects require, the presence of water flowing into rocks and piezoelectric minerals such as quartz in the rocks, respectively. These mechanisms can not explain the experimental result on electromagnetic radiation from non-piezoelectric and dry rocks.

Contact or separation electrification is also one of the possible sources of electromagnetic radiations [3, 4]. When two types of rocks make contact, electrons move between the surface of rocks until their fermi levels are coincident, producing the potential difference between the two rock. The contact potential is given by the difference of work functions of two types of rocks.

Semiconductor minerals such as pyrite and chalcopyrite are abundant in the orebody. Semiconductor minerals are divided into n- or p-type conductivity by its charge carrier. When

p-type and n-type are joined, the resulting junction (p-n junction) has the rectifying property. Many natural orebodies show this property [2]. Although semiconductor minerals may be involved in electromagnetic radiation, their effect is not fully understood.

In this research, we measured the electrical properties and work functions of semiconductor pyrite (FeS<sub>2</sub>). To understand the electromagnetic radiations related to geohazards, we discussed the possible mechanism of charge generation in rocks in terms of the contact or separation electrification and the effect of rectifying properties of semiconductor minerals.

### 2. Sample and methods

Due to the presence of impurities and lattice defects, composition of natural semiconductor minerals is heterogeneous in various scales [5]. Furthermore, the semiconductor properties are strongly dependent on the composition of the zone or region of the sample. Thus, clarifying the microscopic variation in chemical composition or defect species/concentration is required to understand the bulk semiconductor properties.

Samples of pyrite are from Waga-Sennin mine, Akita prefecture, Japan. A sample was cut with area cross section of 1.4 cm<sup>2</sup> and thickness of 0.38 mm<sup>2</sup>. We applied electroetching method and scanning electron microscope (SEM) analysis to obtain composition of the sample surface. In the electrolytic etching, we used the HCl as electrolyte and a carbon rod as the anode. Pyrite worked as cathode and it was reduce itself. Applied voltage is 3.0 V and the sample was

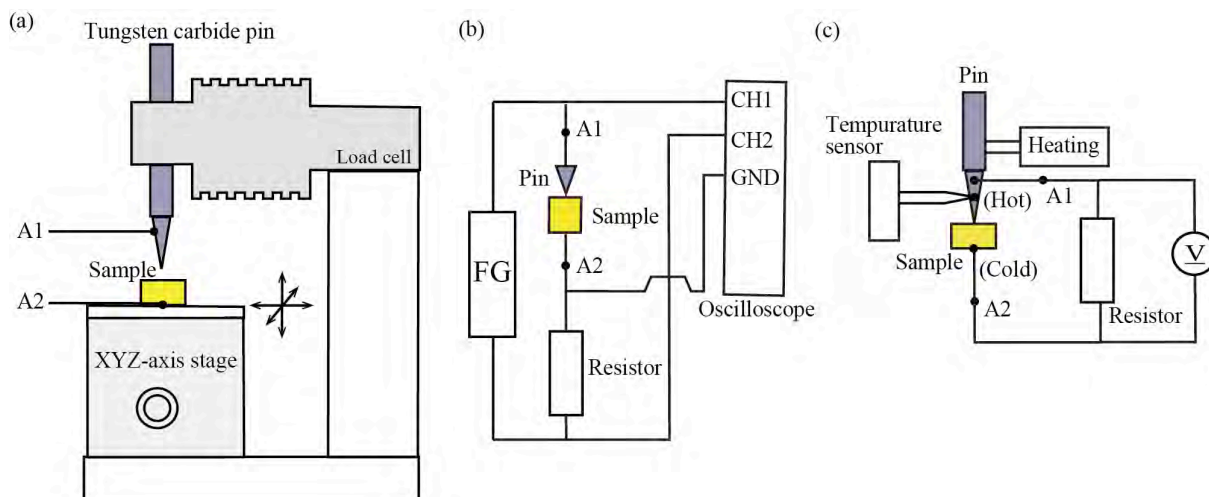


**Fig. 1.** Schematic drawing of the indentation-type probe method. (a) An indentation apparatus. (b) Diagram of circuit for measuring  $I$ - $V$  characteristics and (c) diagram of circuit for measuring thermoelectric motive force.

etched 20 minute. After the etching process, chemical composition were measured by SEM-EDS analysis. To measure the semiconductor properties of the each micro region of the sample surface, we used indentation-type probing method (Fig. 1a). The properties were measured by tungsten carbide probe along the profiles spaced at 0.1 - 0.5 mm. The normal force of 1.0 N was applied to the surface.

We constructed circuits for measuring current ( $I$ ) and voltage ( $V$ )  $I$ - $V$  characteristics (Fig. 1b), and thermoelectric motive force (Fig. 1c). In the circuit for measuring  $I$ - $V$  characteristics, 10 Vpp, 100 Hz- 1 GHz and AC bias, was applied by function generator. Voltage drops at the sample were measured directly by oscilloscope, and following current was evaluated from voltage drops at resistor. In Fig. 1c, probe tip was heated to 100 °C by a heating element. Thermopower is caused by diffusing the charge carrier. Therefore, the conduction type of semiconductor was determined by measuring thermopower, which is positive for p-type conductivity and negative for n-type conductivity.

### 3. Results

In the electrolytic etching (Fig. 2), the surface of the sample shows etching figures. Some of the etching figures are composed of zonal structures with widths of about 10-100  $\mu$ m.

According to the SEM-EDS analysis, Pb inclusions were observed to be precipitated parallel to crystallographic planes (Fig. 2). Indentation-type probing method clarified that electric properties of each area were changed according to etching figures. Thermoelectric motive force profile (Fig. 3b) indicates that the

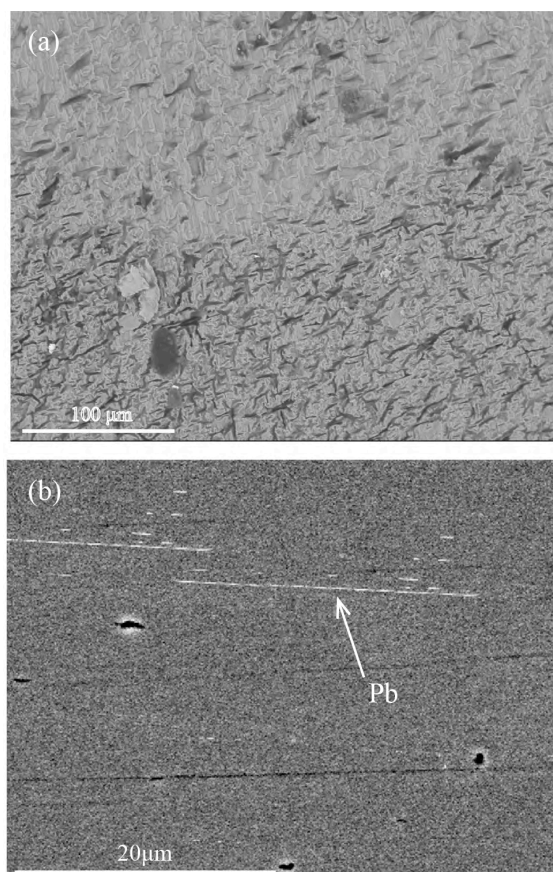


**Fig. 2.** SEM image of pyrite after electroetching. (a) scale bar : 100  $\mu$ m. (b) scale bar : 20 $\mu$ m.

regions of p-n type differences were also consistent well with etching figure patterns and there are a number of p-n junctions. Rectification ratio is defined as the ratio of the forward current to reverse current. The higher rectification ratio was measured at alternating area of the p-n junctions (Fig. 3c). P-type regions showed relatively a higher solubility and resistivity than n-type regions (see Figs. 2 and

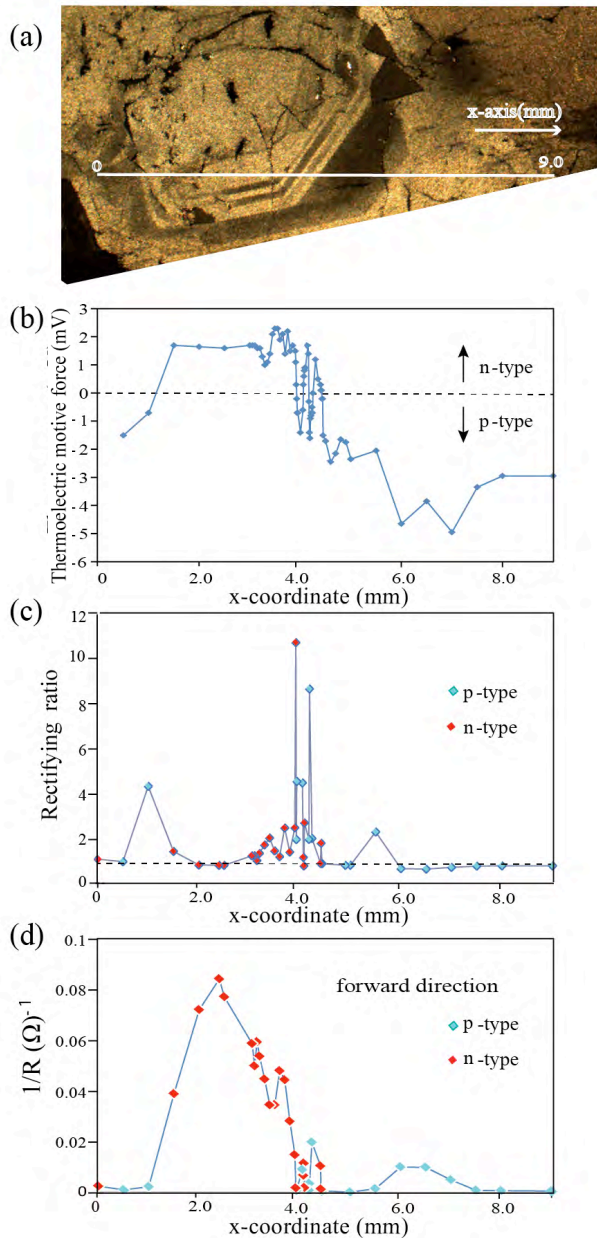


**Fig. 3.** Results of indentation-type probe method. (a) Reflectance photomicrograph of etched pyrite surface. White line indicates measurement profile. (b) Profile of thermoelectric motive force. (c) Profile of rectification ratio at 1.0 V. (d) Profile of the reciprocal of resistivity.

3d). Fig. 4 is  $I$ - $V$  characteristic at x-coordinate of 11.56 mm shows rectified property. The reverse and forward breakdown voltage was estimated to be 1.5 V and 0.3 V, respectively. Rectifying effect was observed up to an input frequency reaching 100 kHz. However its effect decreased over the 100 kHz and disappeared above 900 kHz.

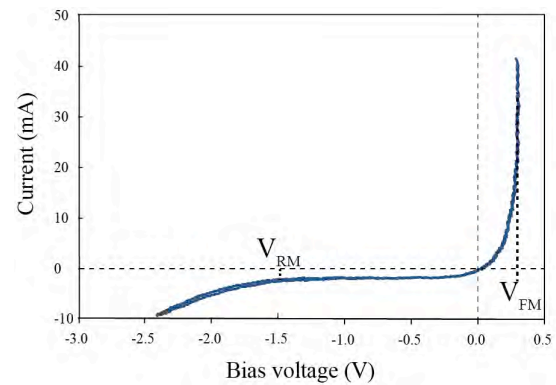


**Fig. 4.** Typical  $I$ - $V$  characteristic of p-n junction (x-coordinate of 3.5 mm in Fig. 3). The junction exhibited rectifying property. The forward breakdown voltage of  $V_{FM} = 0.3V$  and The reverse breakdown voltage of  $V_{RM} = -1.5 V$  are obtained.

#### 4. Discussions

The contact potential along the p-n junction is given by the forward breakdown voltage. When the p-n junction is split into two pieces, the reverse process for contact electrification occur. The electrons move back from the lower potential side (n-type) to the higher potential side (p-type) by tunnel effect. This effect works until separation distance  $d$  reaches  $d_0 = 1.0$  nm [6]. Separated surfaces can be regarded as capacitance plates. If we apply the measured forward breakdown voltage of 0.3 V to the contact potential, the surface bound charge density at  $d = d_0$  is estimated to be  $2.7 \times 10^{-4} C/m^2$ . Takeuchi and Nagahama [7] estimated the surface charge density of granite rocks plates  $5.0 \times 10^{-4} C/m^2$  by applying results of rock friction experiment. Our result is consistent with this value. Furthermore, its value is satisfied with Paschen's law (e.g.,  $5 \times 10^{-5} C/m^2$  for breakdown of air [8]). Therefore, it is expected that corona discharge of air occur by separating p-n junction of pyrite.

On the other hand, due to the rectifying effect, electron is accumulated at the p-n junction. Without separation, when the external voltage reaches a reverse breakdown voltage, avalanche-like redistribution of electric charge is occurs. The electric signals induced by elastic waves as the trigger and it also could be a source of electromagnetic radiation by semiconductor minerals.

During preparation stages of various geohazards, small amount of slip or separation in grain contacts in orebody causes charge separation and electric discharges there. Those signals would be a source of the electromagnetic anomaly associated with the catastrophic hazards. Therefore, further investigation of the electromagnetic radiation from semiconductor minerals is required to evaluate geohazards.

## 5. Conclusion

We measured semiconductor properties of pyrite and discuss the relation between semiconductor minerals and electromagnetic radiations. The mechanisms of electromagnetic radiations at p-n junction were discussed in terms of the contact or separating electrification and avalanche-like redistribution of electric charge. Both mechanisms were shown possible source mechanism for electromagnetic radiation induced by tectonic activities.

## References

- [1] Sobolev, G.A., Demin, V.M., Los', V.F., Maibuk, Z.-Yu. Ya., 1980, Mechanoelectrical emission by ore bodies, *Dokl. Akad. Nauk SSSR*, **252**, 1353-1355.
- [2] Demin, V. M., Z.-Yu. Ya. Maibuk., R. A. Lamentueva, 2004, Rectifying properties of complex ore, *Fizika Zemli* 40, 91–96; translated in *Izv. Phys. Sol. Earth.*, **40**, 262-266.
- [3] Muto, J., Nagahama, H., Miura, T., Arakawa, I., 2006, Frictional discharge plasma from natural semiconductor/insulator junctions : Origin of seismo-electromagnetic radiation, *Phys. Chem. Earth*, **31**, 346-351.
- [4] Muto, J., Nagahama, H., Miura, T., Arakawa, I., 2008, Frictional discharge plasma and seismo-electromagnetic phenomena, *Phys. Earth. Planet. Inter.*, **168**, 1-5.
- [5] Abraitis, P.K., Patrick, R.A.D., Vaughan, D.J., 2004, Variations in the compositional, textural and electrical properties of natural pyrite: a review, *Int. J. Miner. Process.*, **74**, 41– 59.
- [6] Harper, W.R., 1951, The Volta effect as a cause of static electrification, *Proc. R. Soc. Lond.*, **A205**, 83-103.
- [7] Takeuchi, A., Nagahama, H., 2002, Interpretation of charging on fracture or frictional slip surface of rocks. *Phys. Earth. Planet. Inter.*, **130**, 285-291.
- [8] Paschen, F., 1889. Über die zum Funkenübergang in Luft, Wasserstoff und Kohlensäure bei verschiedenen Drucken erforderliche Potentialdifferenz. *Ann. Phys. Chem.*, **37**, 69-96.

## Sinusoidal model for the annual variation of atmospheric radon concentration in Japan

Saki Nakamura<sup>a</sup>, Koseki Hayashi<sup>a</sup>, Yumi Yasuoka<sup>a</sup>, Hiroyuki Nagahama<sup>b</sup>, Jun Muto<sup>b</sup>, Yasutaka Omori<sup>c</sup>, Tetsuo Ishikawa<sup>d</sup>, Toshiyuki Suzuki<sup>d</sup>, Yoshimi Homma<sup>d</sup>, Hayato Ihara<sup>e</sup>, , Takahiro Mukai<sup>a</sup>

<sup>a</sup>Kobe Pharmaceutical University, 4-19-1 Motoyamakita-machi, Higashinada-ku, Kobe, Hyogo, 658-8558, Japan, yasuoka@kobepharm-u.ac.jp

<sup>b</sup>Tohoku University, 6-3 Aramaki Aza-Aoba, Aoba-ku, Sendai 980-8578, Japan

<sup>c</sup>National Institute of Radiological Sciences, 4-9-1 Anagawa, Inage-ku Chiba, Chiba, 263-8555, Japan

<sup>d</sup>Fukushima Medical University, 1 Hikarigaoka Fukushima Fukushima, 960-1295, Japan

<sup>e</sup>Wakayama Medical University, 811-1 Kimiidera, Wakayama, Wakayama, 641-8509, Japan

### 1. Introduction

The unusual change in the radon concentration in soil, groundwater, and atmosphere has been well reported as precursory phenomena before earthquakes. Hatanaka et al. (2013) reported that unusual variation of the atmospheric radon concentration observed before the 2011 Tohoku-Oki Earthquake in Japan. They analyzed the daily minimum value of the radon concentration measured with RI facilities of Fukushima Medical University (FMU). This unusual variation was obtained by comparing the normal variation from 2003 to 2007 with the precursory variation which was computed from the measured value at FMU. Hayashi et al. (2013) reported the annual variation of atmospheric radon concentration was estimated using a sinusoidal model. In this report, we investigated appropriateness by comparing with the normal variation at FMU and at other measurement points.

### 2. Method

Tajika et al. (2013) reported that the change in atmospheric radon concentration could be determined using data obtained by a gas-flow ionization chamber which has been used to monitor radioisotope (RI) leakage in exhaust air from the RI Institute, in the case of negligibly small RI leakage. The continuous and automatic measurements of atmospheric radon concentration have been made with the DGM-101 flow-type ionization chambers

(Hitachi-Aloka Medical, Tokyo, Japan) with an effective volume of 0.014 m<sup>3</sup> at the following three sites: Sapporo Medical University (SMU; N43.05°, E141.33°) in Hokkaido Prefecture, National Institutes of National Sciences, Okazaki Research Facilities, Center for Radioisotope Facilities (NINS; N34.94°, E137.17°) in Aichi Prefecture, and Wakayama Medical University (WMU; N34.18°, E135.18°) in Wakayama Prefecture. Also, Measurement data of FMU (N37.69°, E140.47°) reported by

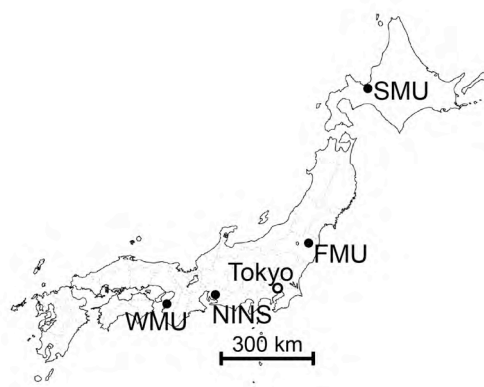


Fig. 1. Map of the sampling sites.

Hayashi et al. (2013) was compared with these data (Fig. 1).

Outdoor air was led into the RI institute. The height of the air supply ports were set more than 7 m above the ground, and the ventilation frequencies were more than 0.5 h<sup>-1</sup>. The exhaust air lines were passed through HEPA filters. The hourly measurement data were recorded by the

ionization chamber as ionization current. The ventilation systems were operated on a 24-hour basis in FMU and WMU and on more than 8-hour basis (9:00-17:00) in NINS and SMU. Generally, the daily minimum radon concentration is obtained in the afternoon (Sesana et al., 2003). Daily minimum data were collected during the operating time of the ventilation systems. The data on the 29th of February in leap-years were excluded in the data set. Missing data were linearly interpolated. We analyzed the daily minimum data for the normal periods in Table 1.

### 3. Data analysis

Using the analysis of the data in FMU proposed by Hayashi et al. (2013), we analyzed the data at three monitoring sites as follows.

#### 3.1 Long-term data

The daily minimum data (minimum data), varied seasonally with minimum levels recorded in summer and maximum levels recorded in winter. The minimum data also show a gradual decrease with time. We assumed that the observed linear decline in the data with time was a consequence of radioactive decay of the calibration source in the monitor.

The radon variation  $R_i$  during the normal period was calculated in the follow procedure. Measuring the ionization current (fA) with the ionization chamber, the daily minimum data were gathered. The smoothed minimum data were generated from the minimum data by the exponential smoothing method. The long-term trend was calculated on the smoothed minimum data basis. The residual minimum data were obtained by subtracting the long-term trend from the smoothed minimum data. To obtain  $R_i$ , the residual minimum data were converted from the ionization current to the radon concentration using the converting factor  $1.8 \text{ Bq m}^{-3} \text{ fA}^{-1}$  (Tajika et al., 2013).

#### 3.2 Seasonal variation

The annual component  $f(t)$  is given by

$$f(t) = a \sin\{2\pi(t + \varphi)/365\}, \quad (1)$$

where  $t$  (day) is the elapsed time from the start of the observation (1 January 2003 was set to be zero in Fig. 2),  $a$  is the amplitude, and  $\varphi$  is the phase shift.

The annual component of  $R_i$  was obtained in the follow procedure. First, the annual mean value of each day was calculated by the minimum data. For example, by taking the mean of the daily minimum value for 1 January for each year from 1 January 2003 to 1 January 2007, the mean value of the daily minimum value for 1 January was calculated. Second, the annual residual data were gotten by subtracting the long-term trend from the annual mean values of each day. Third, the annual residual data were smoothed using the exponential smoothing method. To obtain the annual radon variation  $S_i$ , the smoothed data were converted from the ionization current to the radon concentration. Finally, the annual component  $Sm_i$  was obtained by applying Eq. (1) to  $S_i$ .

In addition, Trenberth (1983) reported that two sinusoids (365-day period) depicted the response in the mean U.S. surface temperature and solar radiation. When temperature decreases, radon concentration tends to increase surface (inverse correlation). Because the atmospheric turbulence is strongly affected by the surface temperature variation. The phase shift of the sinusoidal model for the inverse correlation of solar radiation variation in the northern hemisphere is around 101 days (Autumnal Equinox Day). Trenberth (1983) also reported a phase lag of 27.5 days between those two waves. The phase shift of the sinusoidal model for the inverse correlation of U.S. surface temperatures was estimated to be 73.5 days. Therefore a linear regression is an approach to modeling the relationship between  $S_i$  and the normal air temperature variation  $T_i$  (instead of the surface temperature) in each place. The normal seasonal variations have been reported by the Japan Meteorological Agency (2013a; 2013b), using

the air temperatures derived based on air temperature adjusted to the 1981 – 2010 baseline. Another annual radon variation ( $Se_i$ ) was also estimated from the normal air temperature variation. Another annual component of  $Se_i$  ( $Sem_i$ ) was obtained by Eq. (1).

Finally, a strong correlation was determined between  $R_i$  and  $Sem_i$  (estimation from the normal air temperature variation) as well as between  $R_i$  and  $Sm_i$ . For example, Fig. 2 shows the results at FMU.

#### 4. Results

The results of our analysis clearly showed that the two annual components of daily minimum radon variations ( $S_i$  and  $Se_i$ ) fit the sinusoidal model. Table 1 shows the parameters in Eq. (1). The phase shifts of the sinusoidal model were obtained around 72 ~ 82 days. These results were estimated around the phase shift (73.5 days in U.S.) of the inverse correlation of surface temperature variation. Finally, the variation in  $Sm_i$  from  $R_i$  yielded high values of coefficient of determination ( $R^2$ ) (Table 1).

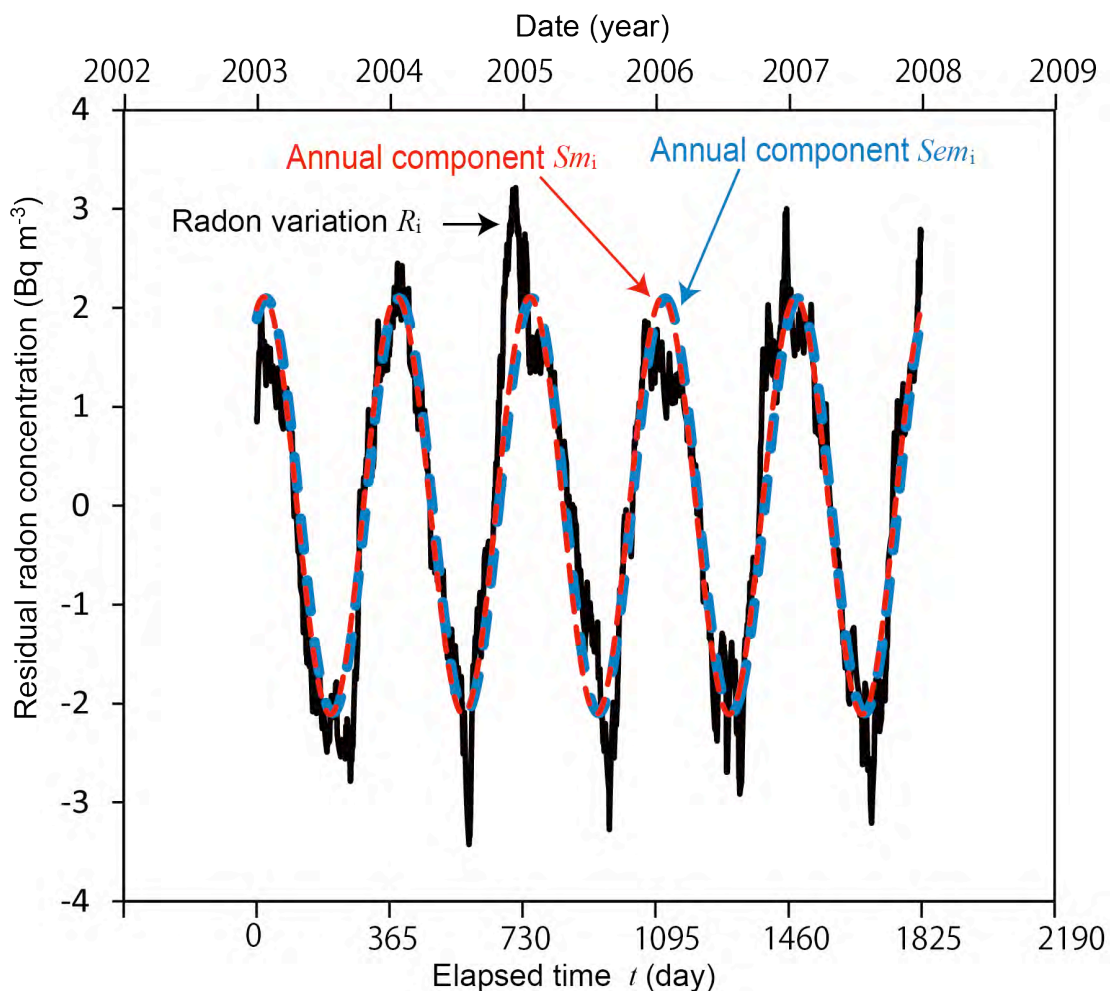


**Fig. 2.** Comparison of a long term variation between the radon variation and the annual components in FMU (Hayashi et al., 2013). The black line represents the radon variation  $R_i$ . The red dash line represents the annual component  $Sm_i$  which was decided on the basis  $S_i$ . The blue dash line represents the annual component  $Sem_i$ , which was determined on the basis of the radon variation estimated from the normal air temperature variation.

**Table 1.** Estimation of the annual components of atmospheric radon concentration at four sites using the sinusoid model (Eq. 1).

Sampling site	Normal periods	Annual component $S_{m_i}$			Annual component $S_{e_{m_i}}$		
		$a$	$\varphi$	$R^2$	$a$	$\varphi$	$R^2$
SMU <sup>*)</sup>	2005-2009	2.6	72 days	0.95	2.6	64 days	0.93
NINS	2003-2011	1.7	81 days	0.81	1.7	65 days	0.75
WMU	2000-2011	1.3	82 days	0.79	1.2	65 days	0.73
FMU	2003-2007	2.1	72 days	0.88	2.1	65 days	0.87

\*) SMU: the data reported by Hatanaka et al. (2013) were used.

## 5. Conclusion

We used the daily minimum data of atmospheric radon concentration in order to reduce the effect of topography. In all cases, the radon concentrations are mainly affected by atmospheric turbulence, and there is a strong negative correlation between the seasonal variation of radon concentration and the seasonal variation of the normal air temperature variation. We established annual component of the daily minimum radon concentration in the air by fitting it with the sinusoidal model using four place data. Moreover, we consider 70 ~ 85 days estimated around the phase shift (73.5 days in U.S.) of the sinusoidal model for the inverse correlation of surface temperature variation. By determining the amplitude with a sinusoidal model, the normal seasonal variation of the daily minimum radon concentration can be estimated.

## Acknowledgment

The authors thank the staff of NINS (National Institutes of Natural Sciences, Okazaki Research Facilities, Center for Radioisotope Facilities) for allowing them to analysis the data of RI monitor. This study is supported by Observation and Research Program for Prediction of Earthquakes and Volcanic Eruptions from the Ministry of Education, Culture, Sports, Science and Technology (MEXT).

## References

- Hatanaka, H. et al. (2013). In: Proceedings of the 14th Workshop on Environmental Radioactivity, Miura T, Kinoshita N (eds), High Energy Accelerated Research Organization (KEK), Tsukuba, in press.
- Hayashi, K. et al. (2013). J. Radioanal. Nucl. Chem., in submission.
- Japan Meteorological Agency, (2013a). Meteorological Information (in Japanese). Available at: <http://www.data.jma.go.jp/obd/stats/etrn/index.php>, access: 23 July 2013.
- Japan Meteorological Agency, (2013b). Annual Report on the Climate System 2012. Available at: [http://ds.data.jma.go.jp/tcc/tcc/products/clisys/arcs/arcs2012\\_chapter01.pdf](http://ds.data.jma.go.jp/tcc/tcc/products/clisys/arcs/arcs2012_chapter01.pdf), access: 19 August 2013.
- Sesana, L. et al. (2003). J. Environ. Radioact. 65, p.147-160.
- Tajika, Y. et al. (2013). J. Radioanal. Nucl. Chem. 295, p.1709-1714.
- Trenberth, K. E. (1983). Bull. Amer. Meteor. Soc. 64, p.1276-1282.

## Hazard mitigation of a caldera-forming eruption: From past experience in Indonesia to modern society

A. Takada<sup>a</sup>, R. Furukawa<sup>a</sup>, K. Toshida<sup>b</sup>, S. Andreastuti<sup>c</sup>, N. Kartadinata<sup>c</sup>

<sup>a</sup>Geological Survey of Japan, AIST, 1-1-1 Higashi, Tsukuba, 305-8567, Japan, a-takada@aist.go.jp

<sup>b</sup>Central Research Institute of Electric Power Industry,

<sup>c</sup>Center of Volcanology and Geological Hazard Mitigation

### 1. Introduction

A caldera-forming eruption, erupted volume~ 10-1000 km<sup>3</sup>, causes huge direct damages such as widespread pyroclastic flow, ash fall, and tsunami, and global impacts such as climate change. The recovering time is more than 10 years for climate, food, human health, and 100-1000 years for land use. Japanese have forgotten such a caldera-forming eruption, because the last one occurred 7,000 years ago. Indonesia was suffered twice for the last 200 years, and three times within 1,000 years (Fig.1). We must learn valuable experiences from Indonesia.

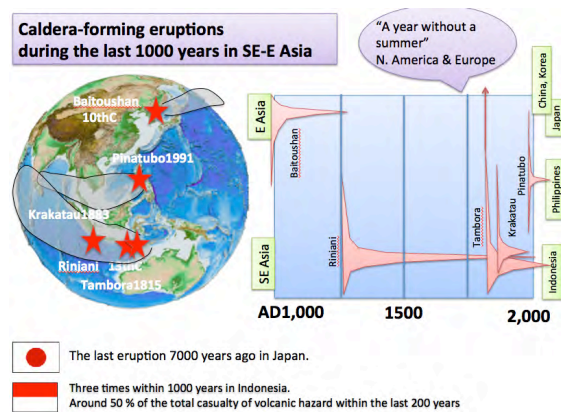


**Fig. 1.** Caldera-forming eruptions during the last 1000 years in E and SE Asia.

### 2. Evaluation of potentiality for a caldera-forming eruption

We proposed an evolutionary model to a caldera-forming eruption in Indonesia (Fig. 2). The long-term evolution into caldera-forming eruption in Indonesia was studied by Takada et al. (2000), Matsumoto and

Takada (2000) and Toshida et al. (2012). This study can identify volcanoes evolving into caldera formation from those without caldera formation. The volcanoes became quiet with a few explosive eruptions during the last 10,000-5,000 years before the first caldera formation (Takada et al, 2012; Takada et al., 2013). Some volcano caused caldera-formation multiply. Furukawa et al. (2012) studied multiple cycle of caldera formation in Bali. According to the model, the candidate evolving into a caldera-forming eruption is a dormant volcano after large stratocone building. We must, however, distinguish a target volcano accumulating magma from that terminating its activity. Moreover, some volcanoes are decreasing in potentiality of eruption by continuous degassing.

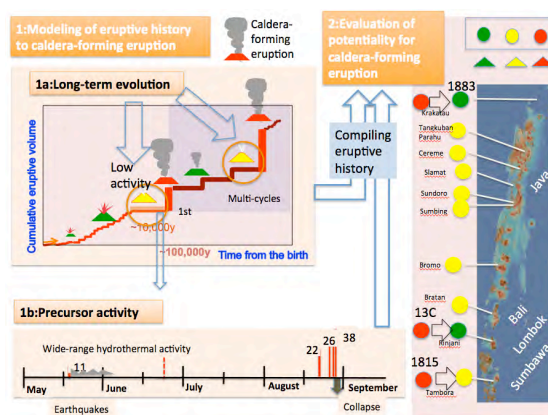


**Fig. 2.** Compiling eruptive history of long-term evolution (General case), and precursor activity (an example of Krakatau 1883), we have started to evaluate the potentiality of caldera-forming eruption.

### 3. Precursor events

During the last a few months, we may have

caught geologically the short-term process as the progressive activity to the climax eruption in cases of Tambora 1815 eruption and Krakatau 1883 eruption (Takada, 2010; Takada et al., 2012; Takada et al., 2013) (Fig. 2). If a volcano comes into the stage just before the climax at the present time, we can catch unusual geophysical signs from various monitoring system. However, the problem is to evaluate or predict when the volcano reaches a climax condition, and how much the volcano erupts. The evacuation plan depends on them.

#### 4. Linkage of disaster in the short-term (<10 years)

A caldera-forming eruption can cause wide range linkages of disasters (Fig. 3). During the last a few months, we may have caught geologically the short-term process as the progressive activity to the climax eruption as mentioned above. If a volcano comes into the stage just before the climax at the present time, we can catch unusual geophysical signs from various monitoring system. However, the problem is to evaluate or predict when the volcano reaches a climax condition, and how much the volcano erupts. The evacuation plan depends on them, for such as the secondary, and the thirdly ones as well as the direct damage. (1) The population on the earth increased abruptly. For example, the modern population in Sumbawa is 0.9 million, compared with 0.1 million when Tambora 1815 eruption. The other areas in Asian country are the same case as those above (Fig. 4). (2) Recently human being develops its society with high technology, compared with the age of the caldera-forming eruptions in the 19<sup>th</sup> century. The larger the eruptive volume becomes, the wider the linkage is spread to cause traffic damage, energy plant damage, and various shortage, such as food, water, medicine, which connect each other. For example, the damage of traffic system in an island country will close from outside rescue. Volcanic ash fall close airports. Tsunami cause various coastal damage including ports or

harbors. (3) Climate change will cause a possibility for plague (epidemic). Aftermath of Tambora 1815 eruption caused "The year without a summer" (Stommel and Stommel, 1983).

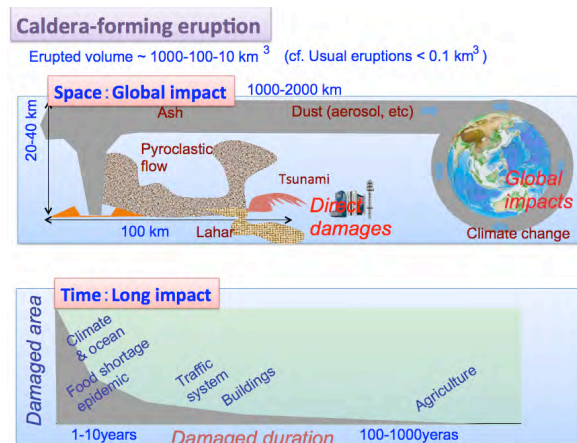


Fig. 3. Impact of caldera-forming eruption.

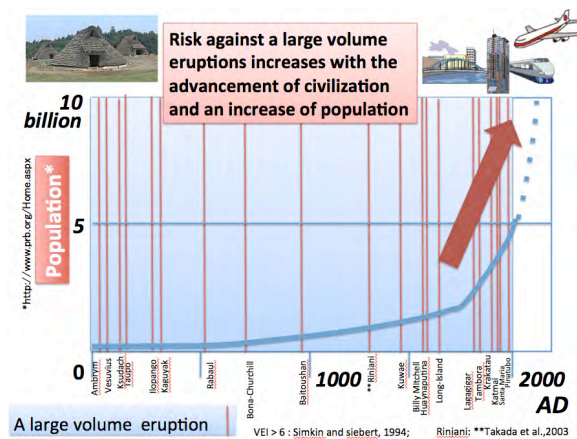


Fig. 4. Risk against a large volume eruptions increases with the advancement of civilization and an increase of population.

#### 5. Long-term damage (> 10 years)

The damage in the area near the volcano that caused a caldera-forming eruption continues long-time. Accumulation of volcanic ash will cause lahar, close drainage (sewer) in a city, and ash pollution. Thick pyroclastic flow deposits remain long time without erosion, and prevent from agriculture. For example, the case of Tambora 1815 eruption, 200 years ago, and that of Rinjani 13<sup>th</sup> Century, 700 years ago are presented.

## References

- Furukawa, R., Takada, A., Toshida, K., Andreastuti, S., Kadarsetia, E., Kartadinata, N., Heriwaseso, A., Pramboda, O., Wahyudi, Y., and Firmansyah, N. (2012) Explosive eruptions associated with Batur and Bratan calderas, Bali, Indonesia, *G-EVER1 Abstracts Volume, Open-File Report of GSJ*, **557**, 114-115.
- Matsumoto, A., and Takada, A. (2000) K-Ar age determination of lavas around Tmbora volcano, Indonesia, *Report of International Research and Development Cooperation ITIT Projects. Research on Volcanic Hazard Assessment in Asia. AIST, METI*, 83-87.
- Stommel, H, and Stommel, E.(1983) Volcano Weather. *Seven Seas Press, Newport RI*, 177p.
- Takada, A (2010) Caldera-forming eruptions and characteristics of caldera volcanoes in the Sunda Arc, Indonesia. *J. Geol. Soc. Jpn*, **110**, 473-483 (in Japanese with English abstract).
- Takada, A, Yamamoto, T,, Kartadinata, N., Budianto, A., Munandar, A., Matsumoto, A., Suto, S., and Venuti, M. C (2000) Eruptive history and magma plumbing system of Tambora volcano, Indonesia, *Report of International Research and Development Cooperation ITIT Projects. Research on Volcanic Hazard Assessment in Asia. AIST, METI*, 42-79.
- Takada, A., Furukawa, R., Toshida, K., Andreastuti, S., Karatadinata, N. (2012) Geological evaluation of frequency and process of caldera-forming eruption: a compiled study of Indonesian caldera volcanoes, G-EVER1 Abstracts Volume, *Open-File Report of GSJ*, **557**, 119-121.
- Takada, A., Furukawa, R., Toshida, K., and CVGHM (2013) Can we evaluate a potentiality of caldera-forming eruption?, *G-EVER1 International Symposium Abstracts Volume, Open-File Report of GSJ*, **576**, 44-46.
- Toshida, K., Takeuchi, S., Furukawa, R., Takada, A., Andreastuti, S., Kartadinata, N., Heriwaseso, A., Prambada, O., Mulyana, R., and Nururim, A. (2012) Long-term variation of pre-caldera volcanic activity in Bali and in Tengger caldera region, East Java, *G-EVER1 Abstracts*

*Volume, Open-File Report of GSJ*, **557**, 110-113.

## **Rainfall induced disasters in India with special reference to Uttarakhand calamity**

Ravi Kumar Umrao<sup>a</sup>, Rajesh Singh and T.N. Singh

<sup>a</sup>*Indian Institute of Technology, Bombay, Powai, Mumbai-400076, Maharashtra, India, ravi.umrao@gmail.com*

### **1. Natural disasters in Indian perspective**

In last one decade, India experienced natural disasters like earthquake, tsunami, flood, drought, extreme temperature (cold and heat waves), storm, heavy rainfall and landslides. With the advancements in technology, we have yet to build our capability to minimize the impact of these disasters and moreover its well-timed prediction is of utmost importance. It is not always easier to predict the uncertainties of nature but its impact can certainly be minimized by developing a culture of prevention and preparedness.

The heavy rainfall and cloud burst followed by floods are becoming most common calamities and are responsible for many disasters in recent few years in India. The hilly terrains of Himalaya are most pretentious regions of India facing natural disasters. Cloudburst and heavy rainfall cause flash floods and severe landslides in Himalayan regions every year as in Uttarkashi in August 2012, Rudraprayag, Uttarkashi, Chamoli, Pithoragarh districts of Uttarakhand state during June 2013. Kinnaur district in Himachal Pradesh during June 2013.

The heavy rainfall by erratic monsoon led to flood in major river basins like Brahmaputra, Ganga, Central India and Deccan rivers that worse affect Assam, Uttar Pradesh, Bihar, Haryana, West Bengal, Orissa, Andhra Pradesh, Kerala, Gujarat and Punjab. It is the most common disaster in India causes immense loss to the property and lives each year.

### **2. Recent landslide hazards in India**

Landslides are one of the natural hazards

that influence at least 15% of land area of India exceeding 0.49 million km<sup>2</sup> (Sharda, 2007). Diverse kind of landslides occurs frequently in geodynamically active domains in Himalaya, northeastern India, Western Ghats and Nilgiri hill ranges of south India. Landslides in Himalayan region occur due to neo-tectonic activities, seismic waves (earthquakes), heavy rainfalls and are increasing due to large scale anthropogenic activities with time. All these activities are increasing the vulnerability of slope mass to failure. The increasing population, over-exploitation of natural resources always make these area under menace. Highway and road networks are only mode of transportation, public networks and all kind of socio-economic activities in high hills of Himalaya but these unplanned road always threat to severe landslides during heavy rainfall events.

There are several cases of landslides and rockfall are being reported every year during monsoons. The Kinnaur district in Himachal Pradesh was the worst hit during June 2013 with nine persons dead in landslides that blocked important roads leaving thousands of tourists stranded. In August 2013, a cloudburst in Lahaul and Spiti district swept away more than hundred animals, five windmills and a vital bridge and also heavy rainfall lashed Kangra, Mandi, Sirmaur and parts of Shimla district, triggering landslides in interior parts and disrupting vehicular traffic. In Jammu and Kashmir's Kathua district, about 12 people were trapped in flash floods in August 2013.



**Fig. 1.** Massive rock fall on 25<sup>th</sup> July, 2013 along NH-222 in Malshej Ghat, Maharashtra crushed two people in a van.

Heavy rains on August 2012 led to flash floods and landslides in Uttarakashi, 31 people died and about twenty thousand pilgrims stranded due to wiped out roads which cut off 80 villages of Uttarkashi from rest of Uttarakhand. Cloudburst in Deval and Tharali area of Chamoli district, Uttarakhand on 15 August 2013 swept animals, buildings, bridge. Badrinath highway (NH-58) breached in Chamoli district.

The rock fall took place on 25 July 2013 in Malshej Ghat on NH-222 causing blockade of highway for one week and trapped one vegetable carrier van. Two men were discovered crushed to death due to tumbling of a giant boulder of more than two trucks size onto the highway. The landslide took place in the wee hours at late night in the Malshej Ghat stretch of NH-222, which is notorious for landslides during the rainy season (Fig.1).

Nine people were killed as a series of landslides triggered by heavy rainfall stuck the high range Idukki and neighboring districts of Kerala state on 5 August 2013. Few houses on the hills were swept away by flash floods and



**Fig. 2.** Landslide triggered after overnight rainfall blocked NH-40, Ri-Bhoi district, Meghalaya

heavy crop and property loss is reported.

There are several landslide events every year in north eastern states of India in Arunachal, Mizoram, Manipur and Nagaland. The remote places disconnect to the other parts of country during monsoon season. Major Landslide in Phesama in Kohima District, Nagaland, along NH-29 that connects to some villages of Southern Angami area and also to Manipur State is cut off from Kohima. Sikkim also experience severe landslides during monsoon. As per media reports of 23 September 2012, flash flood and landslides in remote areas of North Sikkim have claimed 27 lives. The landslide triggered by heavy downpour in Ri-Bhoi district, Meghalaya blocked NH-40 at several places in June 2012 (Fig. 2). Two members of a family were killed in Ri-Bhoi district of Meghalaya when their house was buried in a landslide on 26 July 2012.

#### **Uttarakhand calamity**

A major catastrophe struck on 16<sup>th</sup> and 17<sup>th</sup> June 2013 in Uttarakhand after prolonged heavy rainfall started on 15 June 2013 triggered possibly due to the fusion of westerlies with the monsoonal cloud system in parts of the State. As per IMD sources, the state had received more than 400% rainfall during this period. The worst affected Rudraprayag district received more than 580% rainfall during 13-19 June 2013 (Fig. 3). The pre and post disaster satellite images acquired from Cartosat clearly demarcate the devastation of Kedarnath town and breached Rudraprayag - Kedarnath Highway (Fig. 4 & 5; [www.nrsc.gov.in](http://www.nrsc.gov.in)).

On 16 June 2013 evening, the torrential rains resulted in excessive flow across all the channels causing excessive water and sediment accumulation in the major rivers. As a result, large volumes of water struck the Kedarnath town along with huge amount of loose debris material. The large amount of water washed off upper part of the city. Due to heavy downpour, the town of Rambara was completely washed away on 16 June evening. On 17 June 2013 morning, the breaching of moraine dammed

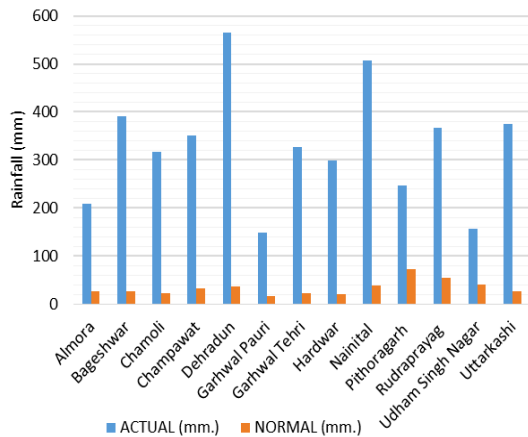


**Fig. 3.** Rainfall distribution in Uttarakhand state during 13-19 June, 2013 (<http://www.imd.gov.in>)

Chorabari Lake water caused another flash flood in the Kedarnath town. The huge water by flash flood in Mandakini River advancing with debris led to biggest ever destruction in Gaurikund, Sonprayag, Phata, Agastmuni etc. Thousands of pilgrims and locals at Kedarnath town were buried under debris or flowed away by flash flood of 17 June 2013. The exact number of casualty may never confirmed of this disaster. Moreover, landslide activity in hill slopes detached this part to the country and hence, hampered the rescue efforts that made it a major disaster. The rescue operations were operated only through helicopters by Indian Air Force,



**Fig. 4.** The satellite images of Cartosat acquired during 2011 showing pre flood scenarios of Kedarnath region ([www.nrsc.gov.in](http://www.nrsc.gov.in)).

ITBP and other agencies efforts will be always appreciated. At least one lakh people stranded in Kedarnath, Badrinath, Hemkund Sahib and enroute places were evacuated from different parts of the state. The major reason behind for huge death toll was due to lack of early warning by authorities. If alerted by authorities, people could have taken shelter in higher places that could have been saved thousands of lives.

Apart rainfall water, the huge quantity of water accumulated by rapid melting of snow due to rainwater in adjoining Chorabari Lake during the period. The large amount of water in millions of gallons accumulation in Chorabari Lake, also known as Gandhi Sarovar Lake, located about 2 km upstream of Kedarnath town cause breaching of the loose-moraine dam that washed Kedarnath town (Dobhal et al., 2013). Also, a landslide in upstream of Mandakini river may have blocked its course on 15 June and the accumulated water blocked behind might have spouted out on 17 June morning that washed off both the banks of the Mandakini river causing massive devastation to the Kedarnath town (Srinivasan, 2013).

Numerous landslides also took place after heavy rainfall and toe erosion of the slopes by the high velocity of voluminous river water

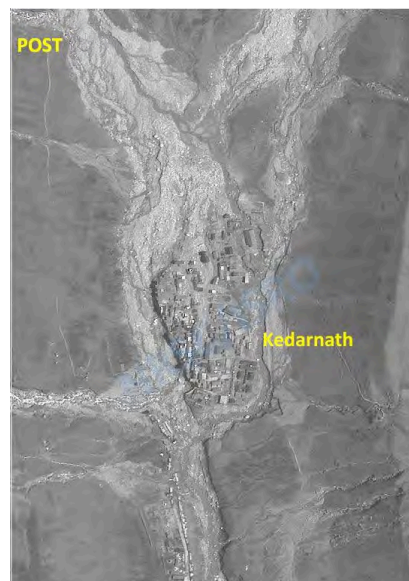


**Fig. 5.** The satellite images of Cartosat acquired on 20th June, 2013 showing post flood scenarios of Kedarnath region ([www.nrsc.gov.in](http://www.nrsc.gov.in)).

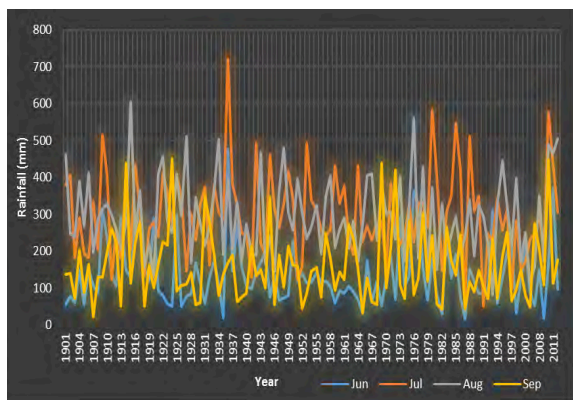


**Fig. 6.** Rainfall data of Rudraprayag district during monsoon season (June-September) since 1901 to 2012(except 2003-07) (<http://www.imd.gov.in>)

loaded with sediments, rock boulders, uprooted trees and other materials caused breaching of the roads at many places and washed away several bridges. The flooded Alaknanda river and its tributary Mandakini river started flowing along their old passages which now inhabited by human beings. The vicious river destroyed the buildings and other infrastructure that came in its course of flow.

The heavy rainfall in the parts of Uttarakhand especially in worst affected Rudraprayag district is not rare during July and August. The monsoon average rainfall statistics of Rudraprayag district between 1901 and 2012 (except 2003 to 2007) are 137 mm, 298 mm, 294 mm and 158 mm in months of June, July, August and September respectively (Fig. 6). These heavy rainfall incidents in Uttarakhand in past caused landslides and deaths. The present calamity due to pre-monsoon extreme rainfall in June covered all parts of Uttarakhand state and received media attention as devastation of Holy place of Kedarnath and clogged Char Dham Yatra in Uttarakhand. Due to media coverage on Kedarnath, Badrinath and other holy places, the people in remote villages were left unattended, unsheltered for many days after disaster.

### 3. Lessons from these events

Analysing a natural disaster is a very complex and risky business due to deficiency of precise information. Many times, a natural

disaster and its human impacts are a result of multiple things occurred simultaneously. Also disasters highlight the stark anthropogenic reasons which contribute towards causing the disaster as well as increasing its impacts. The recent floods and landslides in Uttarakhand have been a rude reminder for India of its historical disasters. These disasters have had proved to be overwhelmingly intimidating for the country, and also pointed at its incompetence to tackle such catastrophes on a massive scale. This trend is likely to increase in future as the activities like pilgrimage, tourism, infrastructure development will increase. Apprehending the tendency of increasing urbanization due to increase in the number of pilgrims, tourists and other developmental activities in the area, selection of safe land use locations would be a daunting task to accomplish.

A major natural adversity is often an initiate of revolution. The systematic efforts to develop the state-of-art of landslide warning system and active disaster management of monitoring system in India for such a rain induced havocs. The disaster response and preparedness measures need to be strengthen in helping the communities in crisis and emergencies. It is utmost require to forecast, accomplish and familiarise these challenging hazard in the near future. The site specific detailed mapping and modelling of landslide prone areas and its reactivation probability methodology needs to be developed in the furry Himalayan terrain.

### References

- Dobhal, D.P., Gupta, A.K., Mehta, M., Khandelwal, D.D. (2013) Kedarnath Disaster- Facts and Plausible Causes, *Current Science*, Vol. 105, No. 2, pp. 7-8.
- Sharda, Y.P., (2007) *Landslide Studies in India, Glimpses of Geoscience Research in India*, pp. 98-101.
- Srinivasan, J. (2013) Kedarnath disaster: facts and plausible causes, *Current Science*, Vol. 105, No. 1, pp. 171-174.

## Web Based Rapid Mapping of Disaster Areas using Satellite Images, Web Processing Service, Web Mapping Service, Frequency Based Change Detection Algorithm and J-iView

Joel Bandibas<sup>a</sup> and Shinji Takarada<sup>a</sup>

<sup>a</sup>Geological Survey of Japan, AIST, Site 7, 1-1-1 Higashi, Tsukuba, Ibaraki 305-8567, Japan, joel.bandibas@aist.go.jp

### 1. Introduction

Earthquakes, tsunamis and volcanic eruptions are the most destructive natural phenomena frequently occurring in most countries located along the Pacific Rim. Timely identification of areas affected by the occurrence of these phenomena is very important for a successful rescue and effective emergency relief efforts. This research focuses on the development of a cost effective and efficient system of identifying areas affected by natural disasters, and the efficient distribution of the information. The developed system is composed of 3 modules which are the Web Processing Service (WPS), Web Map Service (WMS) and the user interface provided by J-iView (fig. 1). WPS is an online system that provides computation, storage and data access services. In this study, the WPS module provides online access of the software implementing the developed algorithm for land cover change detection. It also sends GetMap requests to WMS servers to get remotely sensed

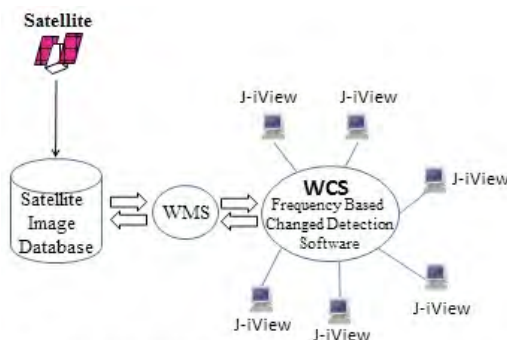


Fig. 1. Web Computing Service (WCS) for detecting land cover change using satellite images provided by a WMS server, a frequency based change detection algorithm and J-iView.

data to be used in the computation. WMS is a standard protocol that provides a simple HTTP interface for requesting geo-registered map images from one or more distributed geospatial

databases. In this research, the WMS component provides remote access of the satellite images which are used as inputs for land cover change detection. The user interface in this system is provided by J-iView, which is an online mapping system developed at the Geological Survey of Japan (GSJ) (fig. 2).

Change detection using multi-temporal remotely sensed data could be divided into two broad types: pre-classification and post-classification (Mettemicht, 1999). Post-classification method involves the separate classification of remotely sensed data sets from individual dates. Changes could be determined by the change in land cover types between dates. This method would indicate the areas that undergo change and how they change (e.g. from corn field to residential). Pre-classification methods on the other hand detect changes due to the variations in the brightness or spectral signatures in the images compared. In this method, areas could just be labeled to have “changed” or “not changed”, not the type of change. There are several pre-classification methods for detecting land cover change using multi-temporal remote sensing data sets. Image differencing is the most common and straightforward method. It is simply the subtraction of the pixel digital values of an image recorded at one date from the corresponding pixel values of the image at the second date (Hayes and Sader, 2001). The output of image differencing indicates that values close to the mean represent areas of ‘no change’ and magnitude close to  $\pm 255$  depicts

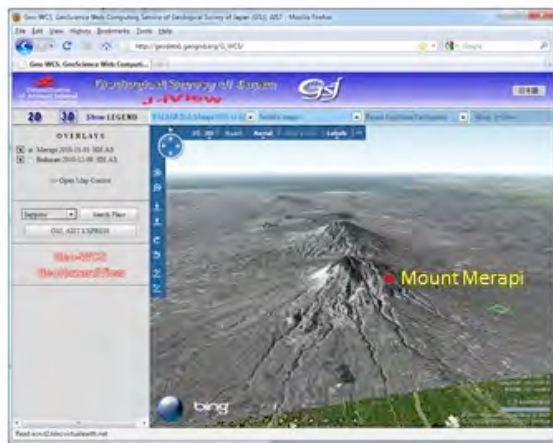


Fig. 2. PALSAR image (HHAs) of Merapi volcano taken on November 1, 2010. The image is displayed using J-iView.

areas of change (Mettemicht, 1999). Image differencing involves the processing of one band of the digital images at a time. Other methods use multiple bands of data for change detection.

These include image differencing using bands ratios like vegetation indices and principal component analysis (PCA). In the temporal change detection using PCA, both the surface proportion and the magnitude of the changed area in an image determine which principal component images will contain change information. It is the relative amount of variance between the change area and the unchanged part in an image that determine which particular PCs contain change information (Sing, 1986).

The pre-classification method of detecting land cover change is the more appropriate procedure for mapping areas affected by natural disasters, because identifying damaged areas would not require information about the type of land cover change. Identifying damaged areas involves the determination of the spectral and spatial changes in satellite images taken before and after the occurrence of the disaster. Areas that sustained significant damage should show significant change in the spectral and spatial characteristics. The conventional pre-classification change detection algorithms described above are pixel by pixel based methods of identifying changes of land cover using multi-temporal remotely sensed data sets. However, changes in pixel values between two images are sometimes not good indicator of land

cover change. Indeed in many instances, a particular pixel's brightness covering a damaged area would not significantly change. The indications that it covers a damaged area are the changes in the brightness of the surrounding pixels. In many cases, changes in texture are more important in identifying damaged areas than the absolute changes in brightness in images. Delineating damaged areas often involves identifying regions in the image whose texture significantly change in the multi-temporal data sets.

## 2. Land Cover Change Detection Algorithm

Several algorithms were developed to determine the spatial signature of pixels in satellite images. One of the earliest spatial signature based algorithms is the contextual identification of pixels or spatial correlation (Khazenie and Crawford, 1989; Alonso and Soria, 1989). A similar method developed by Peddle and Franklin (1989) termed this spatial correlation procedure as gray level-spatial dependency co-occurrence. Gong and Howarth (1992) formulated the frequency based contextual classifier wherein the identity of a pixel is defined by the frequency of occurrence of the different spectral classes of its surrounding pixels. The land cover change detection algorithm used in this study is based on the contextual method to represent pixel's spatial signature, to detect change in multi-temporal data sets covering areas affected by natural disasters. The unsupervised frequency based changed detection algorithm developed in this study involves 3 stages: 1) the classification of the two images into 15 spectral classes, 2) spatial signature generation using the spectral class occurrence frequency method, and 3) change detection. The first stage is the segmentation of the two satellite images into 15 spectral classes using the moving averages clustering algorithm described by Richards (1987). The first image was first segmented into 15 spectral classes. The 15 means of the cluster centers of the first image were then used

to classify the second image into similar 15 spectral classes. If the two images are exactly the same, the aforementioned clustering sequence should generate two identical clustered images. In the second stage, window centered at  $(i,j)$ . The window has a square shape with side length  $l$ . Spectral classes were labeled from 1 to  $v$ , where  $v$  is the total number of spectral classes. Detecting the difference between the spectral class frequency  $f_1(i,j,c)$  of the first image and the frequency  $f_2(i,j,c)$  of the second image centering on the same location  $(i,j)$ , was carried out by determining the Euclidean distance between the two window frequencies. The pixel window was moved pixel by pixel over the clustered images and the frequency occurrence for each spectral class within the window was computed to generate two frequency tables. The distance between the two frequency tables was computed using the formula

$$d(i,j) = \sqrt{\sum_{c=1}^v (f_1(i,j,c) - f_2(i,j,c))^2}$$

where  $d(i,j)$  is the distance between the two frequencies at pixel location  $(i,j)$ . If the two frequency tables are the same, the distance should be 0. The greater is the distance the

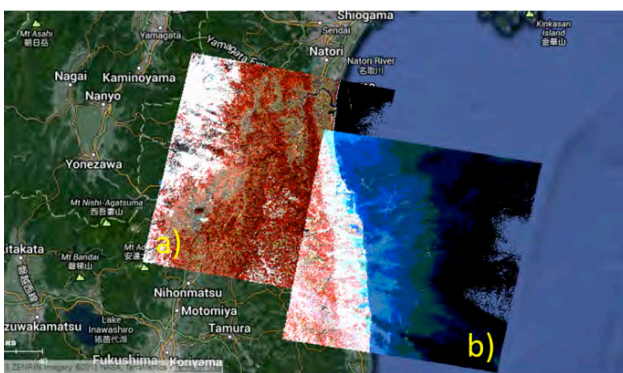


Fig. 3. ASTER images covering Fukushima coastline taken before and after the March 11, 2011 Tohoku Earthquake. a) ASTER image taken on Feb. 24, 2011. b) ASTER image taken on March 14, 2011.



Fig. 4. PALSAR images covering Merapi volcano in Java island, Indonesia before and after the Nov. 2010 eruptions. a) PALSAR image taken on Oct. 16, 2010. b) PALSAR image taken on Nov. 1, 2010.

greater is the difference between the spatial signatures of the pixels from the two images. In this study, the distance threshold was set at 0.70 after several test runs. Distance values greater than the threshold signify change while values below the threshold means no change. The size of the pixel window used is an important factor in a frequency classifier. If the pixel window is too small, insufficient spatial information is included to characterize a specific land-cover class. If the pixel window is too large, it will result to the inclusion of too much spatial information from the other land-cover classes (Gong and Howarth, 1992). After some preliminary experiments, a 5 x 5 pixel window showed optimum change detection accuracy. This window size was used in the experiment.

## Study Area

The areas damaged by the March 11, 2011 Tohoku tsunami and the November 2010 eruptions of Merapi volcano were chosen as test sites of the developed system. ASTER satellite images before and after the March 11, 2013 Tokoku earthquake were used to map the areas damaged by the tsunami (fig. 3 ). On the other hand, PALSAR images were used to map the areas damaged by ash falls and pyroclastic flows from the eruptions of Merapi volcano (fig. 4 ).

## Results

This study successfully developed a cheap and efficient system of identifying areas damaged by natural disasters. The WPS and WMS make it possible to map areas affected by the disaster using a WEB browser. It also shows that satellite images obtained through WMS's GetMap requests are sufficient inputs for the developed algorithm to identify damaged areas. The frequency based change detection algorithm developed in this study successfully delineated areas damaged by the March 11, 2011 tsunami in Honshu Island, Japan (fig. 5). I also successfully mapped the areas damaged by ash falls and pyroclastic flows during the November

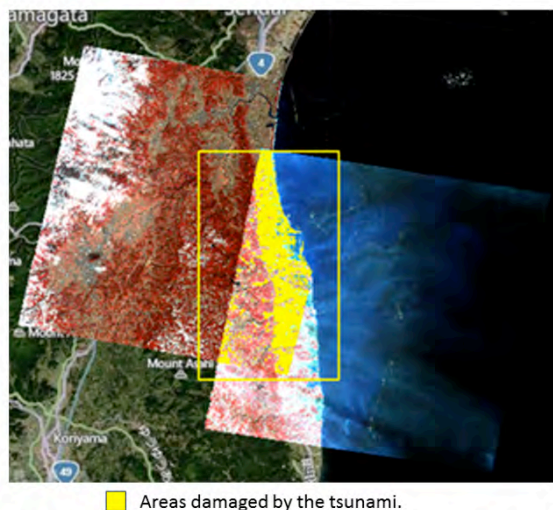


Fig. 5. Map showing some areas damaged by the March 11, 2011 tsunami in Honshu island, Japan.

2010 eruptions of Merapi volcano in Java, Indonesia (Fig. 6). The accuracy of the algorithm in detecting areas damaged by the tsunami is around 85 %. This was determined using aerial photographs and high resolution satellite images. The accuracy of the system in identifying areas damaged by ash falls and pyroclastic flows was validated by comparing the results obtained using the established low level feature extraction method as shown in fig. 6. The damaged areas identified by the developed algorithm are 86% correlated to the results obtained using the low level feature extraction method (fig. 6a). Higher correlation could be observed in areas covered by volcanic ash shown in thin yellow shades in the maps. However, some discrepancies could be clearly observed in areas covered by pyroclastic flows which are shown in thicker yellow shades.

More robust method of determining the accuracies in the identification of the areas damaged by volcanic eruptions would be done later when sufficient field data are already available.

## References

Alonso, F.G., Soria, S.L., 1989. Classification of satellite images using contextual classifiers. Proceedings, 12th Canadian Symposium on Remote Sensing, Vancouver, Canada, July 10-14, 1989. 2, 645-646.

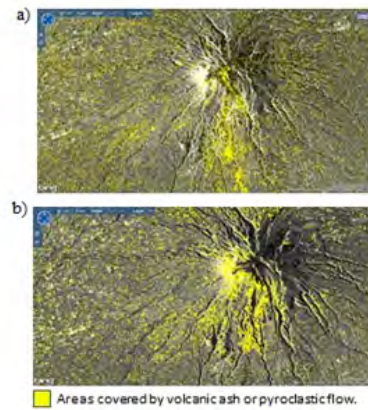


Fig. 6. Maps showing the areas affected by the November 2010 Merapi Eruptions. a) Map generated using low level feature extraction. b) Map generated using the frequency based land cover change detection algorithm.

- Gong, P., Howarth, P.J., 1992. Frequency-based contextual classification and gray-level vector reduction for land-use identification. *Photogrammetric Engineering and Remote Sensing* 58(4), 423-437.
- Hayes, D.J., Sader, S.A., 2001. Comparison of change-detection techniques for monitoring tropical forest clearing and vegetation regrowth in a time series. *Photogrammetric Engineering and Remote Sensing* 67(9), 1067-1075.
- Khazenie, N., Crawford, M., 1989. Spatial-temporal autocorrelated model for contextual classification of satellite imagery. Proceedings, 12th Canadian Symposium on Remote Sensing, Vancouver, Canada, July 10-14, 1989. 2, 497-502.
- Mettemicht, G., 1999. Change detection assessment using fuzzy sets and remotely sensed data: an application of topographic map revision. *ISPRS Journal of Photogrammetry and Remote Sensing* 54(4), 221-233.
- Peddle, D.R., Franklin, S.E., 1989. High resolution satellite image texture for moderate terrain analysis. Proceedings, 12th Canadian Symposium on Remote Sensing, Vancouver, Canada, July 10-14, 1989. 2, 653-654.
- Sing, A., 1986. Change detection in the tropical forest environment of northeastern India using Landsat. *Remote Sensing and Tropical Land Management*. John Wiley and Sons, New York, N.Y. 365 pp.

## Geoethical elements in risk communication

Jose Luis González García<sup>a</sup>, Jesús Martínez-Frías<sup>b</sup> and Niichi Nishiwaki<sup>c</sup>

<sup>a</sup>National Security Department. Complejo de la Moncloa. Avda. Puerta de Hierro s/n, 28071, Madrid, Spain, E-mail: jlgonzalez@dsn.presidencia.gob.es

<sup>b</sup>Geosciences Institute, IGEO (CSIC-UCM) Facultad de Ciencias Geológicas C/Jose Antonio Novais, 2 Ciudad Universitaria 28040 Madrid, Spain, E-mail: j.m.frias@igeo.ucm-csic.es

<sup>c</sup>Faculty of Social Research, Nara University, 1500 Misasagicho, Nara City, 631-8502 Japan, E-mail: niichi@daibutsu.nara-u.ac.jp

### 1. Introduction

Geoethics was born at a junction of geology and ethics (Nemec, 1992), and has developed for last two decades by extending its application to many fields of geosciences (s.l.) including planetary geology (Martínez-Frías et al, 2011; González and Martínez-Frías, 2011). The AGID Working Group for Geoethics issued the International Declaration on Geoethics (AGID WG on Geoethics, 2011), in which the following recommendations are included.

- (1) To emphasize the significance of geoethics in the context of facing extraordinary natural hazards and disasters in the course of recent years.
- (2) To incorporate a geoethical approach to needed new legal aspects (including insurance policy) and to an ethical way of thinking.
- (3) To strengthen the links of geoethics with the new aspects of the geosciences education.
- (4) To recommend the inclusion of geoethical subjects into deontological codes.
- (5) To emphasize the liaison with the mining engineers activities.
- (6) To remark a need of searching new priorities for the 3rd Millenium fitting the World Millenium Goals.
- (7) To recommend links for incorporating geoethics into any activity related with the abiotic world.

Geoethics is clearly defined as follows in the main website of the International Association for Geoethics (IAGETH) (<http://tierra.rediris.es/IAGETH/>).

*“Geoethics is an interdisciplinary field*

*between Geosciences and Ethics, dealing with the way of human thinking and acting in relation to the significance of the Earth as a system and as a model. It includes not only scientific but also educational, technological, methodological and social-cultural aspects, such as sustainability, development, geodiversity and geoheritage, prudent consumption of mineral resources, appropriate measures for predictability and mitigation of natural hazards, geoscience communication, museology, and others.”*

In recent years, serious natural hazards have attacked the world, and the interest to the natural hazards is increasing in human societies. Geoethical elements in the risk assessment of natural hazards are discussed in this paper.

### 2. Geoscience information on natural hazards

The geosciences information is very important before the natural hazard to construct the safeguard system to prevent and reduce the damage. Also it is important after the hazard to rescue the suffered persons, recover and revive the damaged area.

The primary responsibility of geoscientists is to obtain detailed and advanced information through continuous scientific research on natural hazards.

Geoscientists should open the obtained information for the utilization in the human societies. As the information is very important and sensitive, its accuracy, reliability, speedy, simplicity, acceptance and other characteristics should be examined before dispatching. It is

also necessary to prepare the guidelines in advance who and how to decide the content, direction, level, method, timing and others for dispatching the information on time and on site of the natural hazard (Nishiwaki, 2011).

### **3. Duties relating natural hazards**

Geoscientists have not only scientific but also legal, social and ethical responsibility on their activities. Relating natural hazards, the duties will be summarized as follows.

Geoscientists should provide their knowledge and skills in risk mitigation to the society, which have been obtained by their own researches and/or through previous references.

Geoscientists should cooperate with public authorities in crisis and disaster, by giving advices from scientific view points.

Also geoscientists should assist in the transmission of information to society, by synthesizing and explaining the original information.

### **4. General principle of ethical elements in risk communication**

Geoscientists have both the rights and duties to keep independence and impartiality in risk communication. They should deal with interferences from outside in serious and humble manner, distinguish clearly own and outside interests, and reject improper pressures and demand if necessary.

It is their social responsibility to make professional decisions in accordance with public interests on safety, health and environment of citizens and area in the crisis.

Cooperation with others is a principal of risk communication, and ethical dimension and legal obligation should be kept in the process.

### **5. Relations between scientists**

It is essential to obtain the scientific consensus in public communication, by learning to work with other professionals. The mutual agreement should be made in advance for the cooperation to practice scientific procedures in

crisis.

Open and tolerant attitude to external scientific vision is helpful for the constructive cooperation with other professionals.

### **6. Relations with public authorities**

Effective dialogue (even from a geoeducational perspective) should be realized with public authorities, and the attitude for team work is essentially required for the communication.

It is also important to transfer the concept of probability to public authorities, which is involved in the risk assessment of natural hazard.

Geoscientists are requested to make scientific decisions in a limited time in crisis of natural hazard, and they should learn and trained to work under time pressure.

Geoscientists are asked to cooperate with public authorities in crisis, but they are scientists, not the crisis managers. It is necessary to recognize the difference of standpoints.

### **7. Relations with public and mass media**

Geoscientists will be interviewed by various media on the natural hazards and its risk assessment, especially in the crisis. In that case, it is essential to use accurate language in the explanation, avoid distorted facts from the contents, and prevent contradictory statements with other professionals.

The education for the media and common citizens is important for exact understanding of natural hazards, it is better to publish their opinions at ordinal times when peoples can listen calmly and objectively.

It is also necessary to have the empathy with the local culture, with which peoples will accept the opinions/proposals by the outsiders.

### **8. New threats in risk communication**

In the information age, people can easily access to massive and variety of information, though it is necessary to evaluate/verify the

information by the user himself. On the other hand, there are new types of threats.

Increasing of information manipulation is serious problem, as it is dangerous to leading citizens to wrong way in crisis.

In a hyper connected world, the digital wildfire (or flaming) is easily invoked, regardless whether intentionally or accidentally. Such fire in crisis is dangerous to lead to a panic and riot.

### **9. New challenges of risk communication**

In the recent years the theory and techniques of risk assessment have been developed, and it becomes possible to assess more types and range of natural hazard. It is, however, necessary to introduce new perspectives.

It is necessary to enlarge the range of assessment, and include the High-impact Low-frequency (HILF) events (High-Impact Low-Frequency Event Steering Committee, 2010). Though the HILF has much complexity and uncertainty, it should be studied and assessed because of its tremendous damage. Until the complete assessment is available, it is necessary to learn to say “we don’t know”.

It is also necessary to break our common sense and to introduce new ways of thinking, as the black swan theory (Taleb, 2007). An event with catastrophic effects, which had been believed a rare and unexpected event, may be identified as a common event when new evidence has been found. Then, a new model should be developed outside of current theories.

Many security challenges associated with rapid changes occur in a society increasingly interconnected. These changes and resulting crisis can be unpredictable. However, risks are expected to be connected with the fragility of the economic system and, consequently, monitoring threats is not enough. We should strengthen the analysis of the vulnerabilities and interdependencies among the different kinds of risks, as well as identify the crisis scenarios (González, 2013).

Crisis analysis should include the study of

unusual or surprising events in order to improve risk communication planning. These scenarios are plausible futures that violate one of the assumptions that underlie a crisis response plan. The specific purpose is to help planners develop signposts for keeping a flexible preparedness framework (Deward, 2002).

### **10. Conclusion**

It is the fundamental role of science to clarify and forecast the natural hazard, and the risk assessment should be discussed from scientific and technological view point on information processing, hazard modeling and forecasting, disaster alarming and mitigation, etc. In addition it is strongly required to publish the resulted information timely and properly to be utilized for disaster mitigation, and it is necessary to improve the communication process of resulted information.

The communication process contains not only scientific but also ethical elements. Scientific elements have been well discussed, and there are significant developments of communication systems. On the other hand, ethical elements, in spite of its wide and complex contents, have been discussed only in recent years, and the more systematic and detailed discussion is necessary to be generally accepted by human societies.

### **References**

- AGID WG for Geoethics (2011) International Declaration on Geoethics. (Příbram, Czech Republic, October 2011) [http://tierra.rediris.es/Geoethics\\_Planetary\\_Protection/AGID\\_Geoethics\\_International\\_Declaration.htm](http://tierra.rediris.es/Geoethics_Planetary_Protection/AGID_Geoethics_International_Declaration.htm)
- Deward, J.A. (2002) Assumption-based planning: A tool for reducing avoidable surprises. Cambridge University Press, p. 268.
- González, J. L. and Martínez-Frías, J. (2011) Geoética: un reto para la deontología profesional. *Tierra y Tecnología*, no. 40, pp. 10-14.
- González, J.L. (2013) Aspectos civiles de la

- gestión de crisis. En “Situación de crisis en la UE, conducción de crisis y reforma del sector de la seguridad”. Documento de Seguridad y Defensa, no. 57, CESEDEN, abril 2013, pp. 47-73.
- High-Impact Low-Frequency Event Steering Committee (2010) High-Impact, Low-Frequency Event Risk to the North American Bulk Power System. A Jointly-Commissioned Summary Report of the North American Electric Reliability Corporation and the U.S. Department of Energy’s November 2009 Workshop. NERC, p. 118.
- Martínez-Frías, j., González, J. L. and Pérez, F. R. (2011) Geoethics and Deontology: From fundamentals to applications in Planetary Protection. Episodes Vol. 34, no. 4, pp. 257-262.
- Nemec, V. (1992) Ethical Geology in the Education Process. 29<sup>th</sup> International Geological Congress, Kyoto, Japan, 24 August-3 September 1992. section II-24-1 «New ideas and techniques in geological education», vol.. 3, no. 3. Abstract/Paper 06.
- Nishiwaki, N. (2011) Geoethical importance of information management before/after natural hazards. Abst. Mining Pribram Symp., pp. G5.1-4.
- Taleb, N. N., 2007, The Black Swan: The Impact of the Highly Improbable.